Integrating practical and computational approaches to understand morphogenesis of the vertebrate limb

Sahdia Tabassum Raja

Thesis Presented for the Degree of Doctor of Philosophy

University of Edinburgh

2006

Declaration

I declare,

(a) that this thesis is composed by myself,

(b) that this work is my own except where otherwise stated, and

(c) that this work has not been submitted for any other degree or professional qualification.

Sahdia Raja

September 2006

Acknowledgements

If any of us honestly reflects on who we are, how we got here and what we think we might do in the future, we discover a debt to others that spans our life histories. I believe it is appropriate to acknowledge all of these people, whether they are some 'unknown' working in the background or an individual whom we know to have directly shaped our lives and work. Unfortunately, as many know, I do not have the best of memories and so I may miss mentioning someone for which I ask their forgiveness.

Let me begin by thanking God for having allowed me to get further than I ever thought possible.

Many thanks to my wonderful supervisors, James Sharpe and Bob Hill, for having steered me through this PhD and for having provided valuable feedback and suggestions to improve the quality of this thesis. They deserve a great deal of praise for having had the patience to wade through my thoughts in order to understand my underlying logic and reasoning. I must further thank James Sharpe for his invaluable support in helping me to see and meet my potential during the couse of this PhD.

Thanks to Robert Watson, Carlo DeAngelis and Laura Lettice for their help and advice during the early days of my PhD and for their continued support. Thanks also to the Sharpe Lab for their cheery faces and funny jokes which, unfortunately, were often at the expense of my appalling memory. I would paticularly like to thank Jim Swoger from the Sharpe Lab for his help and guidance with respect to the latter half of my PhD.

Many thanks to the ladies at MRCT for their help and patience; the computing boys for always retrieving my 'accidently' deleted files; Paul Perry for teaching me how to use nearly all of the microscopes and visual software available in the HGU; Sandy and Douglas for there support and help when needed; the chaps and chappettes in Mouse Atlas for just being there; the HGU technical staff; and all the remaining staff in the HGU for their support over the years.

A PhD can be one of the most difficult and yet one of the most rewarding experiences -but only with the encouragement and support of those behind the scenes. These people include, first and foremost, my Mum and Bro. for having been my strength, support and comfort throughout; and further includes my loving extended family. The next people to thank are my friends who saw me through the lows and highs: Julie, Dafni, Saima, Arsala, Nazim, Sis. J., Sumaiya, Nasteha, Reema, Jokha, Asmae, Mariam and all the others whom I cannot mention as the list would be endless. There is also one person who came on to the scene quite late but quickly became my rock; my grounding force, and thus deserves my thanks - Thank you Khurom.

Finally, I would like to thank the people who could not see the completion of this thesis but who touched my life and helped me to be the person that I am today. These people include my Father, Grandfather, Uncle Saadat Mahmood, Aunt Rafia, Aunt Ruqiyah, and my friend Shehnaz. May you all find peace.

Abstract

The vertebrate limb has been used and continues to be used as a model system for the study of many developmental and evolutionary processes. More often than not, studies have involved intensive laboratory work. However, as early as 30 years ago researchers such as Wilby and Ede (1975) recognised the potential of computational tools in providing a deeper understanding of the development of the vertebrate limb. Towards this end, the goal of this thesis was to integrate practical and computational approaches for the investigation and analysis of vertebrate limb morphogenesis.

Before a complete picture of vertebrate limb development can be formed the relevant components of the system require thorough analysis. One important component is the changing spatial distribution of cellular proliferation throughout the limb bud tissue during morphogenesis. To date, all of the proliferation studies completed on the vertebrate limb are not truly quantitative or comprehensive. It was with this limitation in mind that a new approach was sought to capture this information. This new approach involved both optimisation of the experimental technique (BrdU-IddU double-staining) and development of new computational tools to estimate cell cycle times in the early vertebrate limb. These developments have allowed, for the first time, a comprehensive spatio-temporal map of quantitative cell cycle times in the early vertebrate limb.

A second key question of limb morphogenesis is how genes create the digit pattern. An example of such a gene is Sox9, which is an early marker of chondrogenesis and is, therefore, assumed to follow a pattern similar to early stages of digit patterning. Classical chondrogenic experiments, suggest digital regions are patterned by the intermediate formation of a "digital arch" from which the digits arise in a posterior to anterior order. In contrast, a thorough analysis of a large number of Sox9 *in situs* revealed digital regions 1, 2 and 3 branch from a region reminiscent of the tibia (anterior zeugopod) and digital regions 4 and 5 branch from a fibula-like region (posterior zeugopod). Moreover, the Sox9 pattern first arises in digital regions 2, 3 and 4, followed by digital regions 5 and 1. The Sox9 *in situ* analysis was achieved using newly developed software for the 3D analysis of optical projection tomographic (OPT) images at a very high spatial resolution.

These studies have highlighted the importance of integrating practical and computational tools in order to close the gaps in our knowledge and understanding of limb development, and developmental processes as a whole. The computational tools generated for the proliferation studies are valuable in offering a thorough means of analysis of cell cycle times and the new OPT software will be invaluable for the study of both weak and strong gene expression patterns in whole embryos. In the future, the proliferation data and 3D Sox9 *in situ* data can be incorporated into simulation software, the results of which should shed light upon the interactive effects of different factors upon the process of limb morphogenesis.

Table of Contents

Declaration i

Acknowledgements ii

Abstract iii

Table of Contents v

List of Figures xiii

List of Tables xvi

List of Abbreviations xvii

Chapter 1 – Introduction 1

1.1 The limb as a model system 2

1.2 Development of the vertebrate limb bud 3

1.2.1 Structure of the limb bud 3

1.2.2 Patterning along 3 axes: 4

1.2.2.1 AP development 7

1.2.2.1.1 AP patterning 7

1.2.2.1.2 The ZPA 7

1.2.2.1.3 Sonic hedgehog 7

1.2.2.1.3.1 Sonic hedgehog regulation 10

1.2.2.1.4 Models for pattern formation along the AP axis 10

1.2.2.1.4.1 Reaction-diffusion model 12

1.2.2.1.4.2 Gradient-threshold model 13

1.2.2.2 DV development 15

1.2.2.2.1 DV patterning 16

1.2.2.3 PD development 17

1.2.2.3.1 The AER 17

1.2.2.3.2 Proximal distal patterning and the progress zone model 19

1.2.3 Outgrowth of the limb bud 20

1.2.3.1 The AER and limb outgrowth 20

1.2.3.2 Cellular proliferation in the limb 22

1.2.3.3 Possible confusion between the progress zone model and the concept of "proliferative zone" 24

1.3 Evolution and skeletal patterning of the vertebrate limb **25**
1.3.1 The origin of the vertebrate limb 25
1.3.1.1 The position and identity of the limbs along the body axis: fore limb or hind limb? 27
1.3.2 Skeletal patterning 28
1.3.3 Skeletal patterns of branching in limb evolution and development 30
1.3.4 Sox9 – The earliest molecular marker for skeletal pattern? 31
1.4 Goals of the PhD **33**
1.4.1 Technical goals 33
1.4.2 Biological goals 34

Chapter 2 - Sox9 **35**
2.1 Introduction **36**
2.1.1 Studying evolutionary morphology 36
2.1.2 Models of limb patterning and the 'digital arch' 37
2.1.3 The origin of birds 38
2.1.4 The origins of the vertebrate limb and the metapterygial axis 41
2.1.5 Studying chondrogenic events versus pre-chondrogenic events 42
2.1.1 Aim 44
2.2 Results **46**
2.2.1 Analysing *in situ* data 46
2.2.1.1 A new visualisation technique for 3D gene expression patterns 46
2.2.1.2 Generating the data and acquiring the region of interest 48
2.2.2 Sox9 gene expression patterns 49
2.2.3 Dorso-ventral patterning 60
2.2.4 The timing of Sox9 expression 63
2.3 Discussion **64**
2.3.1 Newly developed computational tools 64
2.3.2 Does Sox9 expression presage dynamic changes in the cartilage pattern and thus complement histological data of cartilage development? 64
2.33 Do Sox9 expression 'events' conform to Alberch and Shubin's (1986) sequence of events describing limb patterning? 65

2.3.4 Creation of a digital pattern, the "Digital Arch Model" and the "Metapterygial Axis" 65
2.3.5 Digit identity and digit order 66
2.3.6 A new view on skeletal patterning 68
2.3.7 Sox9 - a patterning gene ? 70
2.4 Future Work **71**

Chapter 3 – Generating tools for the quantitative analysis of cell cycle time in the limb **73**
3.1 Introduction **74**
3. 1.1 Cellular proliferation and tissue expansion 75
3.1.2 Measuring cellular proliferation 75
3.1.2.1 Proliferation studies 76
3.1.2.2 Relative proliferation studies 76
3.1.2.3 Determining cell-cycle parameters 79
3.1.12.3.1 IddU/BrdU double-labelling studies 80
3.1.3 Aim 85
3.2 Results **86**
3.2.1 Optimisation of the 3-colour staining technique 86
3.2.2 Checking for antibody cross-reactivity 90
3.2.3 Automatic localisation of every cell on a section 92
3.2.4 Nucleus-based normalisation 93
3.2.5 Determination of whether each cell is positively labelled or not 95
3.2.5.1 Region sizes 95
3.2.5.2 Extracting histograms from tissue regions 98
3.2.5.3 Histogram alignment I: Coping with different intensities across the section 98
3.2.5.4 Histogram aligment II: Coping with difficult histograms 101
3.2.6 Calculating cell cycle time 108
3.2.7 Using the same set of tools for H3 staining 108
3.2.8 Calculating cell density 109
3.3 Discussion **111**
3.4 Future Work **112**

Chapter 4 – Cell cycle time and cell density in the embryonic limb 113

4. 1 Introduction 114

4. 1. 1 Cellular proliferation in the embryonic limb 114

4. 1. 2 Cell densities in the embryonic limb 118

4. 1. 3 Cellular proliferation and cell density 118

4. 1. 4 Aims 119

4. 2 Results 120

4. 2. 1 Comprehensive quantitative analysis of cellular proliferation in the limb 120

4. 2. 1. 1 Mouse embryo hind limbs 120

4. 2. 1. 2 Variability within embryos 120

4. 2. 1. 3 Variability between embryos 130

4. 2. 1. 4 Overall trends and the first quantitative Tc values 131

4. 2. 2 Relating cell cycle time (Tc) to cell density 133

4. 2. 2. 1 Cell density 133

4. 2. 2. 2 Is there a clear relationship between cell cycle time and cell density? 133

4.2.3 Relating cell cycle time (Tc) and cell density to Sox9 expression 135

4.2.4 Iddu/BrdU double labelling vs Phosphohistone H3 single labelling 137

4. 3 Discussion 142

4. 3. 1 Cell cycle time 142

4. 3. 2 Cell cycle time, cell density and Sox9 expression 143

4. 3. 3 IddU/BrdU vs Phosphohistone H3 144

4. 4 Future work 146

4. 4. 1 Comprehensive spatial and temporal study of proliferation and cell density in the mouse limb 146

4. 4. 2 Are all cells dividing? 146

Chapter 5 – Attempting to reduce Shh expression in the mouse limb 147

5.1 Introduction 148

5.1.1 The control of digit number and digit identity by Shh 148

5.1.2 Controlling Shh expression 151

5.1.3 Artificially regulating gene expression by using siRNA technology 153
5.1.4 Aim 156
5.2 Results **157**
5.2.1 The generation of the pDECAP-Shh construct 157
5.2.2 The generation of transgenic embryos with no discernably abnormal phenotype 160
5.3 Discussion 162
5.4 Future Work 164

Chapter 6 - Concluding Remarks **166**
6.1 Scientific and technological advances **168**
6.1.1 A comprehensive analysis of Sox9 expression 168
6.1.2 A core dogma about skeletal patterning is not true 168
6.1.3 Generation of computational tools for the analysis of cellular proliferation and cell density 169
6.1.4 Proliferation rates appear to be extremely high 169
6.1.5 No proximal-distal gradient of proliferation and no "proliferative zone" 170
6.1.6 Limb growth is due to the combinatorial effect of a number of factors 171
6.1.7 The threshold effect of Sox9 expression on cellular condensation 171
6.1.8 Phosphohistone H3 labelling is uninformative 172
6.2 One small limb for man one giant leap for mankind **172**

Chapter 7 - Materials and Methods 173

7.1 Manipulation of nucleic acids 174

7.1.1 General molecular biology reagents 174

7.1.1.1 DEPC-treatment of solutions 175

7.1.2 Restriction enzyme digestion 175

7.1.3 Agarose Gel Electrophoresis 175

7.1.4 DNA quantification 176

7.1.5 DNA purification 177

7.1.5.1 Agarose gel purification 177

7.1.5.2 Phenol-chloroform purification 177

7.1.6 Ligations 178

7.2 Microbiology 178

7.2.1 Growth media for bacterial cultures 178

7.2.1.1 Antibiotic selection 179

7.2.1.2 Xgal/IPTG indicator plates 179

7.2.2 Transformations 179

7.2.3 Isolation of Plasmid DNA 180

7.3 Polymerase chain reaction (PCR) 181

7.3.1 Reagents 181

7.3.2 PCR programmes 183

7.3.3 Molecular cloning 184

7.3.3.1 Sub-cloning via T-Easy vector (Promega) 184

7.3.3.1.2 Screening for transformants 185

7.3.3.2 Cloning via pDECAP 185

7.3.3.2.1 Screening for pDECAP vectors with inverted repeats 185

7.4 Sequencing 186

7.5 Animal husbandry 187

7.5.1 Harvesting of postimplantation embryos 187

7.5.2 Genotyping of transgenic embryos 187

7.5.3 Visual Assessment of the Shh mutation 188

7.5.4 Staging embryos using a computational staging system 188
7.6 Production of transgenic mice 188
7.6.1 Preparation of linearised recombinant DNA for microinjection into fertilised oocytes 188
7.6.2 Microinjection of recombinant DNA and oviductal transfers 189
7.7 Detection of gene expression 189
7.7.1 RNA *in situ* hybridisation 189
7.7.1.1 Preparation of labelled riboprobes 189
7.7.1.2 Wholemount NBT/fluorescent *in situ* hybridisation 190
7.7.1.2.1 Solutions for wholemount *in situ* hybridisation 191
7.7.1.2.2 Procedure for wholemount *in situ* hybridisation 193
7.7.1.2.3 Solutions for fluorescent *in situ* hybridisation 194
7.7.1.2.4 Procedure for fluorescent wholemount *in situ* hybridisation 195
7.8 Histology 198
7.8.1 Unmounting OPT imaged embryos for histological processing 198
7.8.1.1 Agarose embedding 199
7.8.1.2 Vibratome sectioning and immunohistochemistry 199
7.8.2 Wax embedding 199
7.8.2.1 Microtome sectioning 200
7.8.3 Immunohistochemistry of microtome sections 200
7.9 Optical projection tomography (OPT) analysis 201
7.9.1 Preparation of samples for OPT scanning 201
7.9.2 OPT scanning and data analysis 202
7.10 Microscopy 202
7.10.1 Stereo fluorescence microscope 202
7.10.2 Two colour confocal microscope 203
7.10.3 Three colour fluorescence microscope 203
7.11 Statistical Analysis 203
7.12 Programming environments 204
7.12.1 Hardware and software used for C programming and simulations 204
7.12.2 Hardware and software used for IPLab scripting and simulations 204
7.12.3 Hardware and software used for MATLAB programming and simulations 204

7.13 Bioinformatics 204

Appendix A - Sox9 Expression Patterns 205

Appendix B – Statistical analysis of proliferation and cell density data from E10.5 and E11.5 limb buds 214

References 218

List of Figures

1.1 Early stages of embryo limb development 5
1.2 Antero-posterior differences in the limb at an early and later stage of development 6
1.3 Models for pattern formation along the Antero-posterior axis 14
1.4 The apical ectodermal ridge (AER) 18
1.5 The AER and the Progress Zone model 21
1.6 Mitotic index along the proximal-distal limb axis at different stages 23
1.7 FGF10 and Hox gene expression 26
1.8 Skeletal elements and chondrogenesis 29

2.1 Growth of cartilage condensation and branching patterns for different tetrapods 39
2.2 Theories relating to the origins of vertebrate limbs 40
2.3 Imaging and documenting the Sox9 gene expression pattern 47
2.4 The processing of OPT images of Sox9 expression patterns 50
2.5 Formation of the femur and the Y-shape pattern 53
2.6 Formation of the "loop" 54
2.7 The earliest signs of digital positions – Digits II and III come from the anterior zeugopod and digit IV comes from the posterior zeugopod 55
2.8 Continuation into the "digital arch" pattern 58
2.9 The real digit position pattern 59
2.10 Continuation into the phalanges with joint-like regions 61
2.11 Doro-ventral patterning 62
2.12 Schematic of a mouse hind-limb, with the metaptyrigial axis passing through the femur, fibula and finally into digital region4 67
2.13 Views on skeletal patterning 69

3.1 The mitotic cell cycle, an example of tissue expansion and single-labelling of proliferating cells 77-78
3.2 IddU/BrdU double labelling 81

3.3 A diagram of expected primary and secondary antibody reactivity 82
3.4 Dapi and IddU/BrdU staining optimisation 87
3.5 Controls for antibody cross-reactivity 88
3.6 A diagram of antibody cross-reactivity 89
3.7 Localaisation of every cell on a section 91
3.8 Cell based normalisation of sections 94
3.9 Splitting a limb-bud into sub-regions for analysis 96
3.10 Deciding whether a cell is stained green or red 97
3.11 Analysing sections with variations in staining intensity 99
3.12 Examples of "good" and"bad" sub-region histograms for both the green and red colours 102
3.13 Calculating the cut-off point from the intersection of two possible underlying distributions of "on" and "off" cells 103
3.14 Comparing the hypothetical cut-off where the two underlying graphs intersect and the chosen cut-off 104
3.15 Range of red intensity histograms 105
3.16 Range of green intensity histograms 106
3.17 An overview of cell proliferation and cell density results generated by the newly developed software 110

4.1 Single-labelling studies of cellular proliferation in the limb 115
4.2 Density with respect to position along the proximo-distal axis for stages 18-25 of the chick limb (Summerbell and Wolpert, 1972) 116
4.3 Cell proliferation and cell density in the limb 117
4.4 Newly developed software was used to analyse two embryos from two distinct developmental stages 121
4.5 Quantitative proliferation results and cell denisty results of two E10.5 embryos and two E11.5 embryo hind-limb buds 122-128
4.6 Stochastic variation is present in patterns of cellular proliferation in the limb 129

4.7 Variability within and between embryos can be seen plots of cell cycle time and cell density 132
4.8 Developmental stage and embryonic location has an effect on cell density and cell cycle times 134
4.9 Comparing Sox9 expression patterns to patterns of cell cycle time and cell density in the limb 136
4.10 IddU/BrdU staining is more informative than phosphohistone H3 staining 139
4.11 Maps of proliferation rates derived from IddU/BrdU labelled sections and phoshohistone H3 labelled sections of E11.5 embryos 140
4.12 Serial sections stained with phosphohistone H3 of an E10.5 and E11.5 mouse limb bud, with their corresponding maps of proliferation (red:blue ratio map) 141

5.1 Shh expression and patterning in the limb 150
5.2 Interspecies analysis of intron 5 of the Lmbr1 gene and b-galactosidase expression driven by different regions of intron 5 152
5.3 Different contructs of pDECAP 154
5.4 Shh sequence used to produce the inverted repeats in the pDECAP vector 158
5.5 Wild type and transgenic mouse embryos had a normal phenotype 159

List of Tables

1.1 Two simple examples of hierarchical and emergent systems 11

2.1 List of Embryos successfully stained for Sox9 gene expression 51

Abbreviations

^{O}C	degrees centigrade
βgal	β-galactosidase
bp	base pairs
BrdU	bromodeoxyuridine
BSA	bovine serum albumin
cDNA	complementary deoxyribonucleic acid
CMV	cytomegalovirus
DAPI	4'6-diamidino-2-phenylindole-2HCl
DEPC	diethyl pyrocarbonate
dH_2O	distilled water
DNA	deoxyribonucleic acid
dNTP	dinucleotide triphosphate
ds	double stranded
E	embryonic day
ECM	extracellular matrix
E. coli	Escherichia coli
EDTA	ethyldiaminetetra-acetic acid di-sodium salt
g	gram
HCl	hydrochloric acid
Hs	histone H3
IddU	Iododeoxyuridine
IP	intraperitoneal
kb	kilobase pairs
l	litre
lacZ	β-galactosidase gene
M	molar
m	prefix *milli*
μ	prefix *micro*
mRNA	messenger RNA
n	prefix *nano*

ORF	open reading frame
PBS	phosphate buffered saline
PCR	polymerase chain reaction
PFA	paraformaldehyde
pH3	phospho-histone H3
pmoles	pico moles
RNA	ribonucleic acid
rpm	revolutions per minute
ss	single stranded
TAE	tris, acetic acid, EDTA
TBE	tris, boric acid, EDTA
TE	tris, EDTA
xgal	5-bromo-4-chloro-3-indolyl-β-D-galactosidase

Chapter 1 – Introduction

1.1 The limb as a model system for developmental biology

The limb is an external organ that develops relatively independently of the main embryo body, making it amenable to various classical manipulation techniques, especially in the chick. Moreover, many genes associated with limb patterning and differentiation, such as Sonic hedgehog (Shh) and Sox9, are also expressed in other organs during embryonic development (Roberts *et al*, 1995; Chuang & Kornberg, 2000; Wright *et al*, 1995). The fact, that the limb is an external organ makes it is easier to screen for mutational effects in this organ compared to internal organs. The exploitation of these characteristics led to the discovery of a number of developmental principles that are applicable to various developmental systems, such as patterning based upon positional information; that is, cells acquire positional identities with respect to boundaries due to a gradient in a morphogen (Wolpert, 1969; Summerbell *et al*, 1973). Therefore, the limb is an ideal model system for the study of many genetic and molecular processes.

The limb is also a good evolutionary model as a great deal of information can be derived from molecular and genetic experiments as well as the fossil records. The fact that the limb is an external organ means that it is influenced by external factors. Therefore, limb studies provide a great insight into the relationship between form and function leading to evolutionary adaptation. Further to this, the limb is also under the influences of internal constraints, such as conserved developmental mechanisms, which can be described in genetic terms or vice versa, that place "a bias on the production of variant phenotypes caused by the structure, character, composition, or dynamics of the developmental system" (Maynard-Smith *et al*, 1985). Thus, the conservation of many developmental genes allows for the study of conserved gene function and developmental principles across vertebrate species (Gellon and McGinnis, 1998; Ingham and McMahon, 2001; Levin & Mercola, 1998; Mercader *et al.*, 1999; Sagai *et el*, 2004).

Finally, the limb is a good model system to study changes resulting from abnormal development. In humans, limb malformations occur in approximately one in a thousand neonates (Manouvrier-Hanu *et al*, 1999). Although, individual skeletal disorders are rare, they are of clinical relevance because they are usually associated with syndromes, some of which are lethal. For example, Campomelic dysplasia (CD; MIM 114290) is a rare neonatal human chondrodysplasia. Two of the phenotypic characteristics of this disorder are bowing and angulations of the long bones, and abnormalities of the vertebral column with a decreased number of ribs (Olney *et al*, 1999; Wunderle *et al*, 1998). Most affected babies die prior to reaching late stages of infancy due to respiratory difficulties (Foster *et al*, 1994; Wagner *et al*, 1994; Olney *et al*, 1999; Kornak & Mundlos, 2003). Analysis of a mutated version of the human homologue of Sox9 in mice showed it to have a limb phenotype similar to CD patients and was identified as the gene mutated in the skeletal dysmorphology syndrome (Foster *et al*, 1994; Wagner *et al*, 1994).

The limb has been the subject of intensive study, which has yielded a wealth of information. Thus, the mouse limb is one of the most well understood vertebrate developmental model systems. In the remainder of this chapter, I shall introduce and discuss the structure, patterning, outgrowth and evolution of the vertebrate limb bud. During this discussion I shall cover topics related to Shh expression, cellular proliferation and Sox9 expression.

1.2 Development of the vertebrate limb bud

1.2.1 Structure of the mouse limb bud

The first sign of the development of the mouse limb bud are thickenings of the lateral plate mesoderm in specific positions in the flank of the embryo. After a short period of development this region begins to further protrude from the flank of the embryo (E10.5,

fig. 1.1a), at which point it consists of a mass of morphologically homogenous mesenchymal cells surrounded by a layer of ectodermal cells. The limb bud then continues to elongate away from the body wall, with its shape changing as it does so from a semi-circle to a paddle-like structure (E12, fig. 1.1b) and then finally into a limb with digital regions (E14, fig. 1.1c; Wanek 1989; Davidson, 2001).

During the development of the limb bud mesenchymal cells begin to differentiate forming the internal structures of the limb including bones and cartilage. This differentiation begins close to the body wall and proceeds all the way to the tip of the embryo, resulting in a fully developed limb. The fact that different tissues develop in distinct locations constitutes a 'spatial pattern' across the organ. Therefore, the mechanisms leading to the patterning of this organ are of concern to developmental biologists.

1.2.2 Patterning along 3 axes:

Patterning of the limb bud can be considered along three main axes: the antero-posterior (AP), the dorso-ventral (DV) and the proximo-distal (PD) axes (fig. 1.1d, e). During limb bud outgrowth cells within the limb are patterned and differentiate under the control of two signalling centres known as the zone of polarising activity (ZPA) and the apical ectodermal ridge (AER), which will be discussed in more detail in later sections (fig 1.1e). Two well studied signalling proteins that emanate from the ZPA and AER respectively, are Sonic hedgehog (SHH; Riddle *et al*, 1993) and FGF-8 (Ros *et al*, 1996). These are just two examples of proteins that exhibit dynamic temporal and spatial distributions across the limb bud and their direct or indirect interactions with each other result in the patterning and differentiation of cells within the limb (Niswander 2003; Laufer *et al*, 1994; Bueno, 1996, Zuniga 1999, Niswander, 2003).

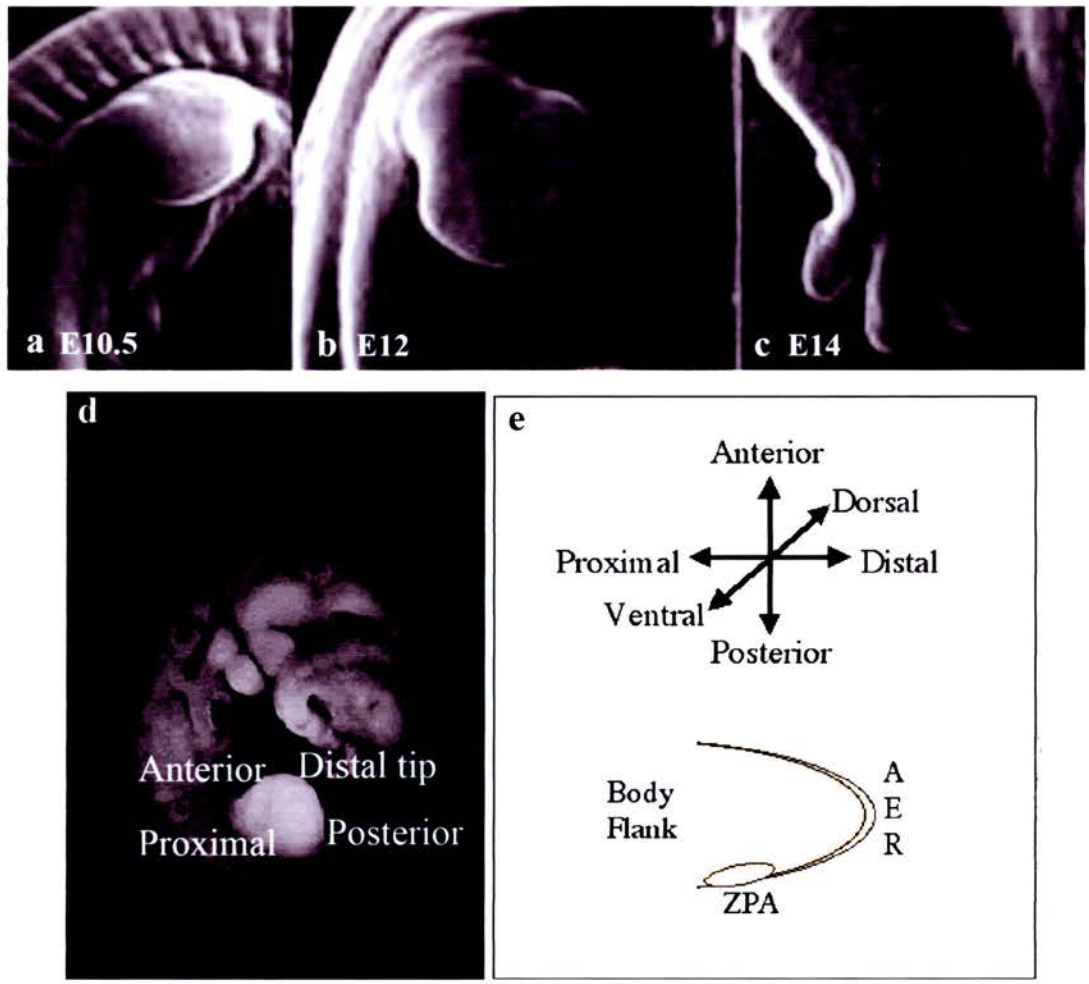

Figure 1.1 Early stages of embryo limb development. (a) Protrusion of the limb bud from the body wall. (b) Development of the limb bud into a paddle-like structure. (c) Further development of the limb leading to the formation of digital regions. (d) Two axes of development of the embryo limb. (e) The limb bud with the AER marked at the distal tip and the ZPA marked at the posterior magin of the limb bud.

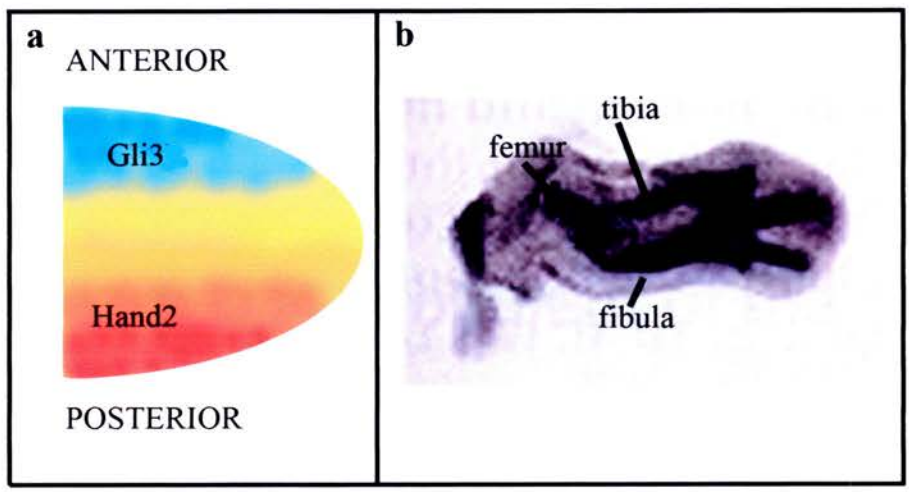

Figure 1.2 Antero-posterior differences in the limb at an early and later stage of development.
Gene expression patterns are the first signs of the establishment of the anterior posterior axis. Gli3 and Hand2 are examples of genes which show anterior-posterior polarity in their patterns of expression, with Gli3 expression localised to the anterior and Hand2 expression localised to the posterior of the limb bud. (b) Anterior-posterior differences can also be seen at later stages of development. For example, a clear difference can be seen in the size of the two zeugopodial elements (tibia and fibula) that branch from the femur.

1.2.2.1 AP development

1.2.2.1.1 AP patterning

Localised gene expression patterns can be seen as early as E9-E9.5 and are the first molecular signs of anterior-posterior patterning. For example, Gli3 gene expression is localised to the anterior half of the limb bud and Hand2 gene expression is localised to the posterior half (fig 1.2a, Welscher *et al*, 2002; Benoit and Yvan, 2006). Anterior-posterior differences at later stages of development can be seen in the skeletal pattern with the bifurcation of the single stylopodium (humerus or femur) branching into two distinct zeugopodal elements (fig 1.2b; radius/ulna or tibia/fibula). The way in which these anterior-posterior differences are established is attributed to signals coming from the ZPA (Tickle *et al*, 1975; Tickle *et al*, 1981).

1.2.2.1.2 The ZPA

Research by Saunders and Gasseling (1968) identified a group of cells at the posterior margin of the chick limb that was able to induce supernumerary digits when implanted into the anterior margin of a host limb bud. The posterior margin, or zone, is best known as the zone of polarising activity (ZPA) with which, many years later, the Sonic hedgehog morphogen was found to co-localise (Riddle *et al*, 1993). *Shh* is now known to be involved in the antero-posterior patterning of the limb as its absence severely compromises the development of many embryonic structures (Chiang *et al*, 1996). In the case of the limb, all digits are lost except for digit 1, the formation of which seems to be independent of Shh expression (Ros *et al*, 2003; Chiang *et al*, 2001; Kraus *et al*, 2001).

1.2.2.1.3 Sonic hedgehog

Shh is activated in the posterior mesenchyme at E9.5; thereafter expression levels increase from E9.5 to E10.5 and decline by E11.5 (Lewis *et al*, 2001). Its confined

pattern of expression is under the control of HOX proteins encoded by gene members of both the HoxA and HoxD clusters (Charite et al, 1994; Zakany, 2004; Kmita *et al,* 2005). Tarchini, Duboule and Kmita (2006) used a set of partial deletions to show that the last four Hox paralogy groups, whose expression is excluded from the most anterior limb cells, elicit this response. This led the group to suggest that the limb AP polarity is produced as a collateral effect of Hox gene collinearity.

Shh protein is first detected between E9.5-9.75 at the posterior margin of the limb bud (Lewis *et al*, 2001). At E10.5 a gradient of SHH protein can be detected beyond the site of SHH biosynthesis, which is confined to the posterior of the limb (Gritli-Linde *et al*, 2001). Analysis of the Shh protein has revealed that Shh signalling can be long- and short-range, time dependent and concentration dependent. Here I shall give a brief overview of Shh signalling activity in the limb, which will be discussed in more detail in chapter 5.

The *Sonic Hedgehog (Shh)* gene is a member of the hedgehog family of intercellular signalling molecules, which have essential functions in patterning vertebrate embryos (Shimeld, 1999). The Shh gene encodes a 45-kDa protein that undergoes autocatalytic cleavage to yield an N-terminal and C-terminal peptide, with signalling capacities confined to the N-terminal (Gritli-Linde *et al*, 2001). Furthermore, N-Shh peptides is present in both cholesterol modified or unmodified forms, however the two forms are said to have similar biological activity (Lewis *et al*, 2001). Cholesterol modification of Shh involves the covalent binding of cholesterol to the C-terminus (N-Shh_p), which results in the tethering of N-Shh_p to the cell membrane (Lee *et al*, 1994, Bumcrot *et al*, 1995, Marti *et al*, 1995, Porter, 1995). Analysis of the distribution of activity of N-Shh, a form that lacks cholesterol, and N-Shh_p, a form that carries cholesterol, revealed that N-Shh is posteriorly restricted whereas N-Shh_p expression acts over a few hundred microns (Lewis *et al*, 2001). Thus, Shh signalling is both long- and a short-range.

Limb manipulation experiments have shown that ectopic presentation of Shh in the anterior of the limb bud induces additional digits in a dose-dependent manner, higher levels of Shh activity inducing progressively more digits of more posterior character (Yang *et al*, 1997). This together, with the finding that loss of Shh expression in the limb results in the absence of all digits except digit 1 (Ros *et al*, 2003; Chiang *et al*, 2001; Kraus *et al*, 2001) clearly indicates that Shh concentration plays a significant role in anterior-posterior patterning, specifically that of the digital patterning in the limb.

In a recent study Harfe and associates (2004) generated transgenic mice with a gene that encodes a gfpcre fusion protein in the Shh locus in order to fate map cells that have expressed Shh in the mouse limb. The insertion of the gfpcre cassette resulted in the production of GFP in cells that normally expressed Shh mRNA. Moreover, CRE-mediated recombination in Shhgfpcre cells expressing R26R reporter allele marked the cells and their descendents through the production of β-galactosidase. Analysis of the transgenic mice revealed that at E17.5 all cells of digits 5 and 4, and a subset of digit 3 were descendents of ZPA cells. To identify which population of Shh-positive cells contributed to each digit, a tamoxifen-inducible cre reporter cassette was knocked into the Shh locus to create a ShhcreER^{T2} allele. CRE was produced in all cells which normally expressed Shh mRNA but cytoplasmically sequestered CREER^{T2} protein was incapable of instigating a recombination event at the R26R reporter locus until the injection of tamoxifen. When embryos were exposed to tamoxifen at E9.5, LacZ labelled cells were present throughout digits 4 and 5, as well as a subset of digit 3. Injection of tamoxifen at E10.5, resulted in the presence of LacZ labelled cells in digit 5 and the posterior half of digit 4. Finally, injection of tamoxifen at E11.5 resulted in labelling of cells only in digit 5. Based upon these results the group suggested that the expansion of the posterior limb bud cell population affects the length of time a digit primordium is within the Shh-expressing domain, which may be critical for the specification of digits 5, 4 and 3. In contrast, the specification of digits 2 and 1 may rely solely on Shh concentration, and in the case of digit 1 may be independent of Shh signalling.

1.2.2.1.3.1 Sonic hedgehog regulation

The expression of Shh is driven by a regulatory element, termed the ZPA regulatory sequence (ZRS; Lettice *et al*, 2003), which is located within intron 5 of the Lmbr1 gene approximately 1Mb upstream of the *Shh* gene (Lettice *et al*, 2002). The regulatory element was located using Sasquatch (*Ssq*) mutants that were produced via the random insertion of a transgene into intron 5 of the Lmbr1 gene (Sharpe *et al* 1999). The transgenic insertion carried the human placental alkaline phosphatase (HPAP) reporter gene (Sharpe *et al* 1999), the expression of which was found in the ZPA of the limb bud and in the anterior limb margin overlapping the ectopic Shh expression responsible for generating the polydactyly phenotype in *Ssq* mutants (Lettice *et al*, 2002). The results suggested the possible existence of a regulatory element that directs a pattern of HPAP expression similar to the expression pattern of *Shh*. In order to determine if a regulatory sequence truly resided near the Ssq insertion site a 1.7Kb fragment of highly conserved mouse sequence from this region was incorporated into transgenic constructs containing the heterologous β-globin promoter and LacZ reporter gene (Lettice *et al*, 2003). Transgenic embryos produced using this construct showed similar β-gal staining patterns at the posterior margin of both the fore- and hind-limbs reminiscent of Shh expression in the limb (Lettice *et al*, 2003). Furthermore, cis-trans genetic tests revealed that the *Ssq* mutation only influenced the expression of chromosomally linked *Shh* (Lettice *et al*, 2002). Therefore, the inserted transgene in the *Ssq* genome marked a cis-regulator that drives normal *Shh* expression (Hill *et al*, 2003).

1.2.2.1.4 Models for pattern formation along the AP axis

Two of the most prominent models used to explain the patterning of the vertebrate limb are the reaction-diffusion model and the gradient-threshold model, also known as the positional information model. However, the two models are fundamentally different. One of the main differences is that the reaction-diffusion model is an example of an emergent system, whereas the gradient-threshold model is an example of a hierarchical

Hierarchical	Emergent
	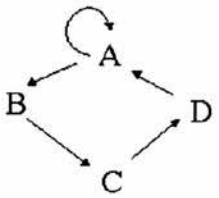
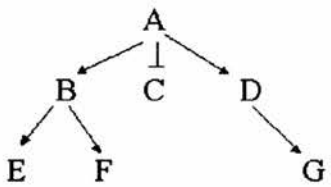	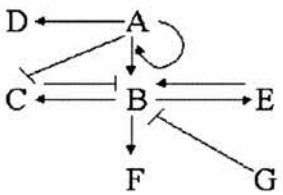

Table 1.1 Two simple examples of hierarchical and emergent systems

The hierarchical systems exhibit unidirectional relationships between genes. The emergent systems show feedback between genes. Note, letters denote genes, and arrows and 'dead-end' lines denote activation and inhibition interactions, respectively.

system (Table 1). Hierarchical networks are those in which a morphogen is never affected, directly or indirectly, by the genes under its influence. All interactions are unidirectional or hierarchical by nature. By contrast, emergent systems can have a morphogen that indirectly activates the same morphogen in a neighbouring cell by interacting with its cellular receptor. An essential feature of these systems is feedback. This means that, unlike hierarchical systems, emergent systems have no 'master' gene regulating all other genes.

1.2.2.1.4.1 Reaction-diffusion model

The reaction-diffusion model is an example of an emergent system, which can be said to be a generic process as it is broadly applicable to living and non-living things (Newman & Comper, 1990). This is because the components of the reaction-diffusion model can range from gene products in a chick to gas concentrations in space (hence living and non-living). This contrasts with the positional information systems, as they are generally too complicated to occur within 'simple' non-living cases. It is assumed that genetic networks are one of the few natural systems of the complexity required to encode a positional information system.

Turing's original reaction-diffusion model consisted of two molecules (morphogens) A and B, where A is the activator and B is an inhibitor (fig. 1.3a; Kondo & Asai, 1995). Initially both A and B diffuse over a continuous domain producing a constant homogenous situation. However, with time, instability driven by diffusion gives rise to spatially heterogeneous concentrations. The feedback that exists within this system acts like a lateral inhibition system in which peaks of concentration inhibit the formation of other peaks near by, which can result in the formation of a periodic pattern (fig. 1.3b). In terms of the limb, the pattern of molecules would directly correlate with the patterning of the mesenchymal cells in the limb – that is to say, no interpretation of a global molecular signal is involved. Thus, development and pattern generating mechanisms

may be under genetic control but genes do not create pattern as such, a point well appreciated by Turing who thought of genes as catalysts (Murray, 1990).

Due to the spontaneous nature of reaction-diffusion systems they can allow for the formation of multiple patterns for a given set of parameters. However, different types of patterns are sensitive to different initial conditions (Arcuri and Murray, 1986). Thus precise control of the initial conditions and equation parameters is required to ensure the selection of a specific pattern. This is a generic feature of global (emergent) pattern generators such as the reaction-diffusion model (Crampin *et al*, 1999).

1.2.2.1.4.2 Gradient-threshold model

Some authors have concluded that global emergent pattern formation mechanisms alone cannot result in reliable spatial pattern under normal biological variation due to the sensitivity mentioned above. Therefore, other proposed frameworks for morphogenesis and pattern formation have de-emphasised generic emergent effects while placing more of a burden on the effect of hierarchical genetic 'programs' that arise through mutation and selective evolution. The most well studied example of hierarchical systems is the gradient-threshold model. According to the model cells in a developing system acquire 'positional information': that is, identity or positional value along a length of cells. It is this, positional information that largely determines the nature of molecular differentiation the cell will undergo and consequently the morphogenetic patterning that will result. The assignment of positional information is thought to be brought about by a concentration gradient of a particular molecule: a morphogen (Turing, 1952). Cells interpret the local concentration of the morphogen according to pre-programmed threshold constraints (predetermined genetic program) resulting in their differentiated states. This system of patterning was described using the analogy of the french flag (fig. 1.3c), where each cell has the potential to develop as blue, white or red. The cells are exposed to a concentration gradient and the position of each cell within the flag is defined by the concentration at that point. This information is then interpreted in terms

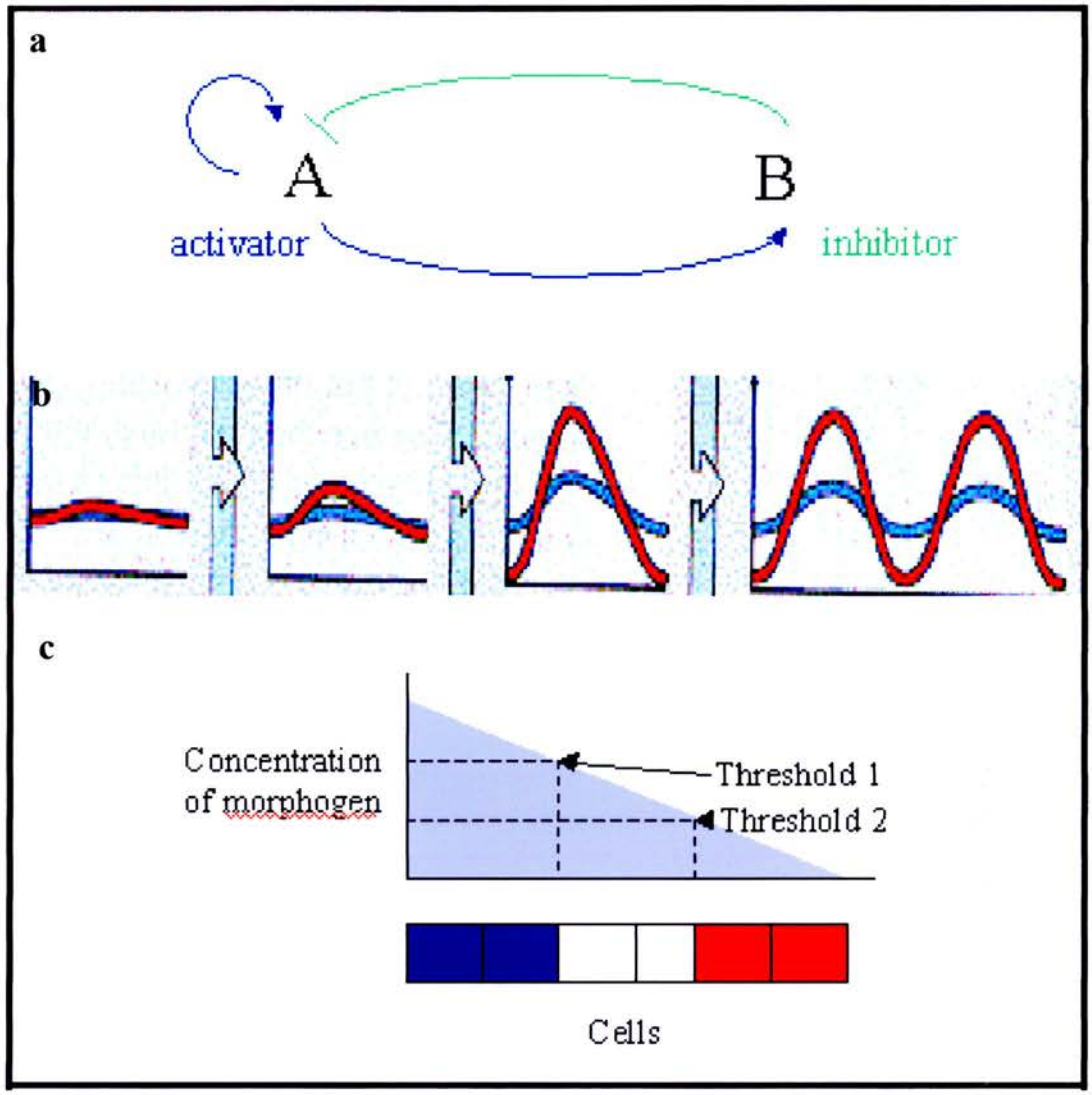

Figure 1.3 Models for pattern formation along the Antero-posterior axis
(a) Diagram of the activation and inhibition relationships between molecules A and B from Turing's reaction diffusion model. (b) Diagram of the steps involved in spontaneous pattern generation due to a reaction-diffusion mechanism. The initial distribution of the molecules is uniform, but over time the system forms wave-like patterns (Wolpert *et al.*, 1998). (c)Wolpert (1969) put forward the French flag model as a means of explaining the gradient-threshold model. In the system each cell in a line of cells has the potential to develop as blue, white or red. The line of cells is exposed to a concentration gradient of some substance and each cell acquires a positional value defined by the concentration at that point. Each cell then interprets the positional value it has acquired and differentiates into blue, white or red, according to a predetermined genetic program, thus forming the French flag pattern (Wolpert et al, 1998).

of a cells genetic constitution leading it to differentiate into blue, white or red, thus forming the french flag pattern (Wolpert, 1969).

In the field of limb development, there has been a long running debate as to whether, "Shh functions as a diffusible morphogen, as suggested by the gradient model of ZPA function?....." (Johnson and Tabin, 1997). As mentioned earlier, the elimination of the Shh signal results in the formation of a single digit whereas ectopic Shh expression leads to the formation of extra digits (Riddle *et al*, 1993), providing strong evidence that Shh plays a role in antero-posterior patterning. In 1997, Yang and associates demonstrated that there is a relationship between dose, distance and time of Shh exposure with anterior-posterior polarity, thus adding another level of complexity to the question of whether Shh concentration determines digit identity. Recent findings by Harfe and associates (2004), suggest that the most anterior digits are concentration dependent whereas the identity of the most posterior digits is dependent upon the length of exposure time to Shh. Thus, the role and mechanism by which Shh regulates digit number and digit identity is still not fully understood and requires further analysis, as was attempted in chapter 5 of this thesis.

1.2.2.2 DV development

Growth of the limb bud is significantly less along the DV axis compared to either the PD or AP axes (Stark and Searls, 1974). The differential rates of growth along the axes results in the limb bud looking elliptical and flattened dorso-ventrally early in development. The dorso-ventral flattening becomes even more pronounced when the autopod is formed and the digits develop (Maini and Solursh, 1991).

Differences along the DV axis are apparent in many vertebrate species. For example, in humans the palm of the hand is the ventral side and the back of the hand is the dorsal side. The differences that are found along the DV axis are attributed to signalling

between the mesenchymal cells and the ectoderm during development (MacCabe *et al*, 1974).

1.2.2.2.1 DV patterning

At the onset of limb development, the mesenchyme transmits dorso-ventral information to the ectoderm that enables it to control the patterning of the limb along the DV axis (Geduspan and MacCabe, 1986, 1987, 1989). Thus, when the ectodermal layer is surgically manipulated and is rotated 180° relative to the mesenchyme, mesenchymal structures such as the skeletal elements, cartilage and musculature are inverted corresponding to the polarity of the ectoderm (MacCabe *et al*, 1974).

Wnt7a, which encodes a secreted factor, is expressed by cells in the dorsal ectoderm (Dealy *et al.*, 1993; Parr *et al*, 1993), and induces Lmx1 expression in the dorsal mesenchymal necessary for the cells to adopt a dorsal character (Riddle *et al.*, 1995). The homeobox containing transcription factor Engrailed1 (En1) is expressed solely in the ventral ectoderm (Loomis *et al.*, 1996). Either Lmx-1 or Wnt-7a can dorsalize the ventral mesoderm in the distal portion of the limb bud (Riddle *et al.*,1995; Vogel *et al.*, 1995). In the absence of Wnt7a, the dorsal patterns of distal structures of the autopod are not formed and the limb appears bi-ventral (Parr and McMahon,1995) whereas the absence of En1 results in the absence of distal ventral structures and the limb appears bi-dorsal (Loomis *et al*, 1996). En1 expression is itself found to be induced in the ventral ectoderm by bone morphogenetic protein (BMP) signalling through the type 1 receptor (BMPr1a). Thus, loss of BMP signalling via loss of the BMPr1a receptor also results in a bi-dorsal limb phenotype (Ahn *et al.*, 2001).

Although many details are known about DV patterning, the developmental picture is not yet complete. The problem of how and when DV polarity actually originates in the early limb remains a matter of controversy (Chen and Johnson, 1999). Moreover, although limb experiments performed by Geduspan and MacCabe (1989) suggest that the

mesenchyme already contains information about DV polarity which it then confers to the ectoderm, other results suggest that inductive signals from the somites are equally as significant (Michaud *et al*, 1997).

1.2.2.3 PD development

1.2.2.3.1 The AER

The apical ectodermal ridge is a thickening of the ectoderm at the distal tip of the limb, marking the dorsal-ventral boundary (fig 1.4a, b) (AER; Saunders, 1948; Todt and Fallon, 1984). It is composed of a group of tightly packed epithelial cells separated from the underlying mesenchyme by a basement membrane (Kelly and Fallon, 1976). The grafting of stage 12-17 chick limb mesoderm into host flank induced AER formation demonstrating that AER formation is dependent upon signals from the underlying limb mesoderm (Saunders and Reus, 1974). In the chick, Fibroblast growth factor 10 (*Fgf10*) was determined to be important in the initiation of limb bud outgrowth based upon its early expression within the limb field mesoderm (fig. 1.7a) (Ohuchi *et al*, 1997). Further data suggests that FGF-10 activates *Wnt-3a* in the overlying ectoderm and that WNT-3A then signals through the β-catenin pathway to activate *Fgf-8* expression resulting in the formation of the apical ectodermal ridge at about stage 18 of chick limb development (fig 1.4c) (Kengaku *et al.*, 1998; Kawakami *et al*, 2001, Todt and Fallon, 1984). In mouse, Wnt/-catenin signaling is also necessary and sufficient for AER induction, and *Wnt3* is critical for this process (Galceran *et al.*, 1999; Barrow *et al.*, 2003). Furthermore, Bmp molecules, together with regulating DV development, regulate AER formation through the induction of *En1* and *Fgf8* expression (Ahn *et al.*, 2001; Pizette *et al.*, 2001). Disruption of the transcription factor *En1* results in ventral expansion of the AER and in some cases ectopic AER formation (Loomis *et al*, 1996, 1998). Associated with AER expansion, the dorsal factor *Wnt7a* (Riddle *et al.*, 1995; Parr and McMahon, 1995) becomes misexpressed in the ventral ectoderm, and removal of *Wnt7a* in *En1* mutants rescues the abnormal AER morphology (Cygan *et al.*, 1998; Loomis *et al.*, 1998). Thus,

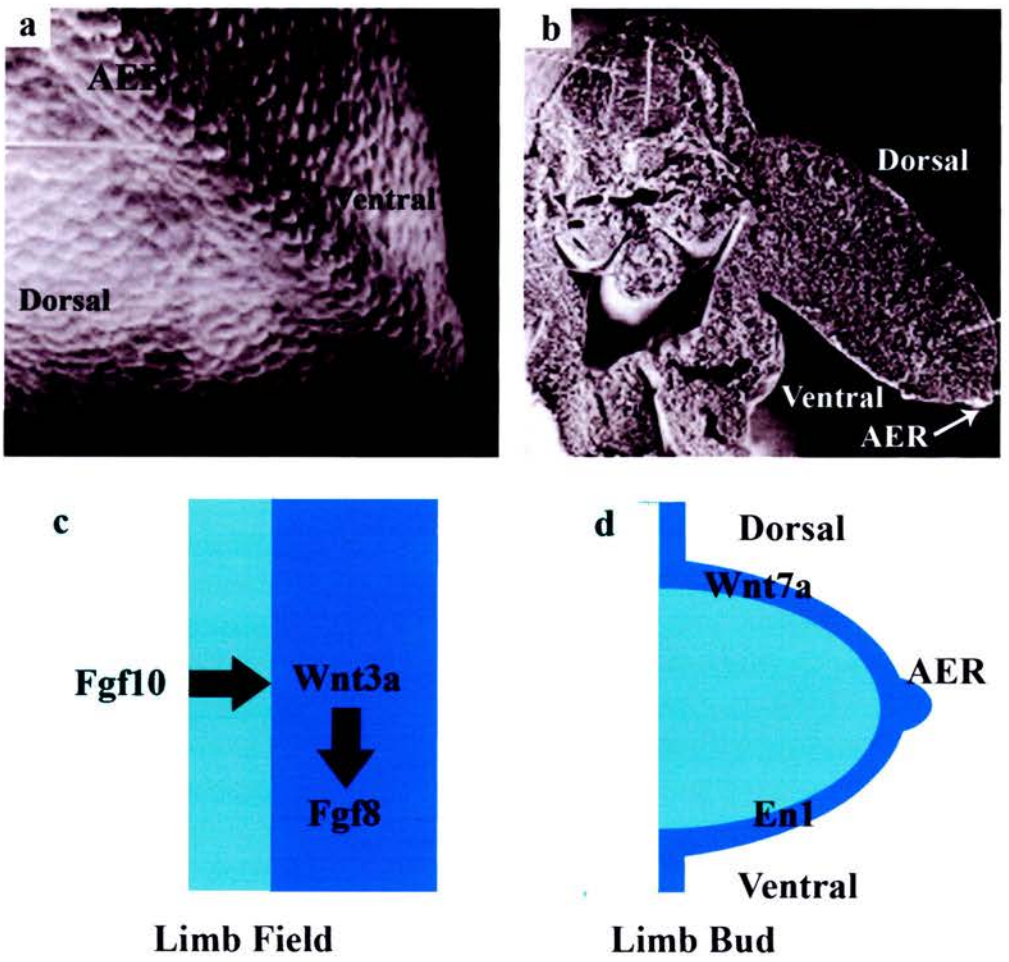

Figure 1.4 The apical ectodermal ridge (AER)
(a) Scanning electron micrograph of an early chick fore-limb, with the AER in the foreground as a thickening of the ectodermal layer. (b) Section through the hind limb bud of a 24-25 somite chick embryo, with the AER at the dorsal ventral boundary of the limb. (c) Formation of the AER is dependent on FGF signals from the underlying mesoderm. Fgf10 signals Wnt3a in the overlying ectoderm, which activates Fgf8 resulting in the formation of the AER. (d) The positioning of the AER is under the control of a number of genes, two of which are Wnt7a and En1 whose expression originates from the dorsal and ventral ectoderms, respectively.

Wnt7a and *En1* seem to play a role in not only DV development but also AER formation (a diagram of their origins of expression is given in fig 1.4d).

In the chick the AER forms soon after the limb bud begins to protrude from the body, however in the mouse the AER does not form until limb outgrowth is well underway (Wanek *et al*, 1989). In this thesis I have used the chick and mouse limb as paradigms for AER development in the tetrapod limb.

1.2.2.3.2 Proximo-distal patterning and the progress zone model

The progress zone model (PZ model; fig. 1.5a) suggests that signals from the AER maintain an underlying region of mesenchymal cells in an undifferentiated state, which is known as the progress zone. Summerbell, Lewis and Wolpert (1973) first introduced the idea of the progress zone to explain the patterning of the limb bud along the proximal-distal axis. The model states that progressive proximal-distal specification depends on the AER in which proximal fate is specified first, followed by more distal specification. As the limb grows, cells are forced out of the progress zone at which point their positional value that they acquired within the progress zone is fixed. Thus, cells that leave the progress zone first produce more proximal structures and as development proceeds exiting cells will be specified to form more distal structures.

The model was originally based upon experiments in which the replacement of a distal tip for an older tip generated only distal structures and replacement with a young tip generated all proximal-distal structures. This was interpreted as cells undergoing progressive changes in specification under the control of the distal tip, specifically the AER. Although many experiments have been performed since the proposal of the 'progress zone model' none have clearly disproved the model although the results of some can fit easily with other ideas. For example, X-irradiation ablation of mesenchymal cells before condensation results in skeletal loss and a reduction of limb elements (Wolpert *et al*, 1979). These results could be explained in terms of the progress

zone model, where cells within the progress zone were ablated resulting in the lack of more distal structures. However, it could also be said that the ablated cells were already patterned and segregated in the early limb and that a sufficient population of cells could not be re-established to form appropriate size condensations (Niswander, 2003). A second example can be taken from the work of Dudley *et al* (2002) who found that the removal of the ridge resulted in limb truncation and attributed this to significant cell death in the underlying region to the AER rather than loss of the progress zone. However, this argument did not account for truncations in the autopod, as at that later stage they saw no cell death (Wolpert, 2002). Therefore, much work still needs to be done in order to fully understand the proximal-distal patterning of the limb bud under the influence of the AER.

1.2.3 Outgrowth of the limb bud

1.2.3.1 The AER and limb outgrowth

Outgrowth of the limb bud arises from the presumptive limb region and results in the initial protrusion of the limb bud from the body wall. Continued growth along the proximal-distal axis results in limb elongation. It has been suggested that limb elongation may be due to high rates of cellular proliferation within the limb field and lower rates of proliferation within regions flanking the future limb bud (Searls and Janners, 1971). The overall control of limb bud outgrowth is thought to be under the influence of the AER. In a classical experiment, Saunders (1948) showed that the removal of the AER resulted in the truncation of the limb bud, resulting in the loss of distal structures. Moreover, removal of the AER at progressively earlier stages resulted in increased limb truncation, beginning with the most distal elements (fig. 1.5b, Saunders, 1948; Summerbell, 1974, Dudley *et al*, 2002). However, the removal of the AER produces only a transient reduction in mitotic index, which, after 24 hours, returns to a level observed prior to AER removal (Janners and Searls, 1971; Summerbell, 1977).

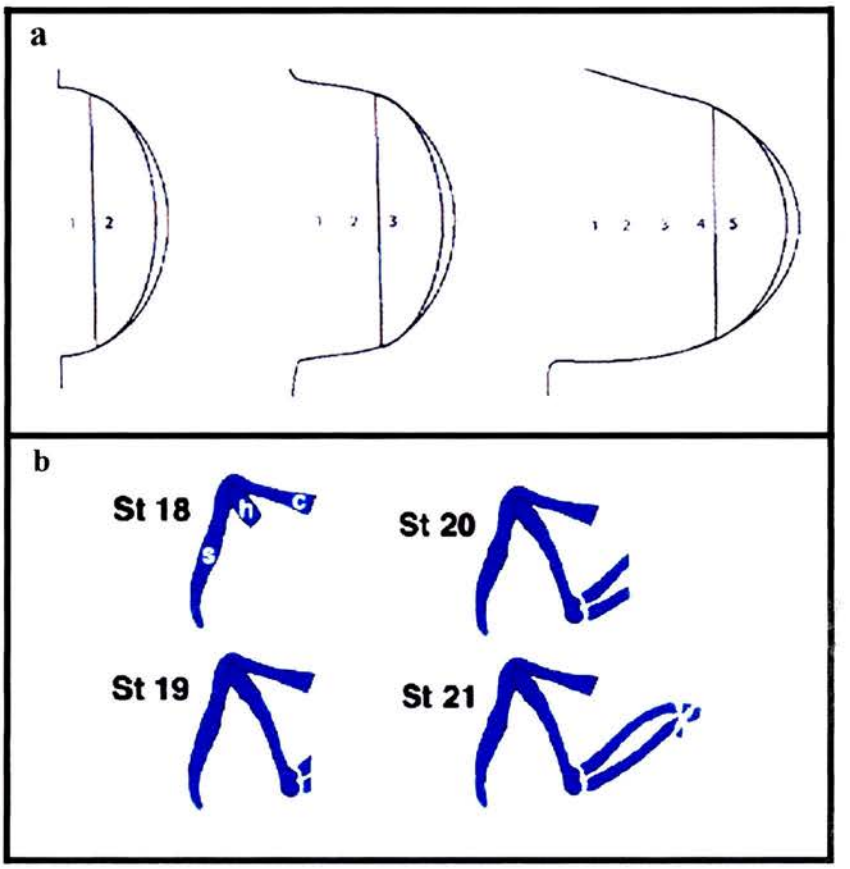

Figure 1.5 The AER and the Progress Zone model
(a) Progress zone model for the patterning of the limb. Numbers represent positional values along the proximal distal axis. In the progress zone model, these values are generated as cells leave the progress zone (shaded) at the tip of the limb bud (Tickle, 2003) (b) Removal of the AER effects the growth of the limb. Removal at progressively later stages of development results in less limb truncation. Shoulder girdle and wing skeletal parts formed after the excision of the AER at successively later stages of development of the chick wing bud, c, coracoid; s, scapula; h,humerus (Saunders, 2002 derived from work by Dudley et al, 2002).

Moreover, limb budding has been shown to occur in the absence of the AER in *limbless* mutants (Ros *et al*, 1996). Therefore, the evidence suggests that the regulation of cell proliferation and the control of limb elongation by the AER can be disassociated from each other.

The activity of the AER is thought to be mediated by fibroblast growth factor (FGF) proteins, as shown in experiments where ectopically applied FGF induced distal elongation of amputated limbs (Taylor *et al*, 1994; Kostakopoulou *et al*, 1996). Four members of the FGF family show AER-specific expression - Fgf4, Fgf8, Fgf9 and Fgf17 (Niswander and Martin, 1993; Ohuchi *et al*, 1994; Martin, 1998; Sun *et al*, 2000). Individual loss of function of Fgf4 (Sun *et al*, 2000), Fgf9 (Colvin *et al*, 2001) or Fgf17 (Xu *et al*, 2000) has no effect on limb development whereas loss of Fgf8 results in hypoplasia (Lewandoski *et al*, 2000; Moon *et al*, 2000). Thus it was suggested that FGF8 is most relevant for AER mediated limb outgrowth (Ohuchi *et al* 1994; Moon *et al*, 2000). However, the complete absence of Fgf4 and Fgf8 in the limb, results in the complete absence of the mouse hind-limb and severe truncation of the fore-limb (Sun *et al*, 2002), indicating a combinatorial effect. These results reveal complex signalling involving the FGF proteins during limb development – signalling which has yet to be finely dissected.

1.2.3.2 Cellular proliferation in the limb

Cellular proliferation is believed to be critical to limb outgrowth under the influence of the AER (Searles and Janners, 1971). However, our understanding of the regulation of cellular proliferation in the limb goes little beyond simplistic descriptions of patterns of proliferation and development, which I shall discuss here.

Patterns of mesenchymal cell proliferation are relatively uniform at early stages of chick development (Hamburger-Hamilton stages 18-23; Hornbruch and Wolpert, 1970, Sun *et al*, 2002). Only after significant elongation is a proximal-distal gradient of proliferation

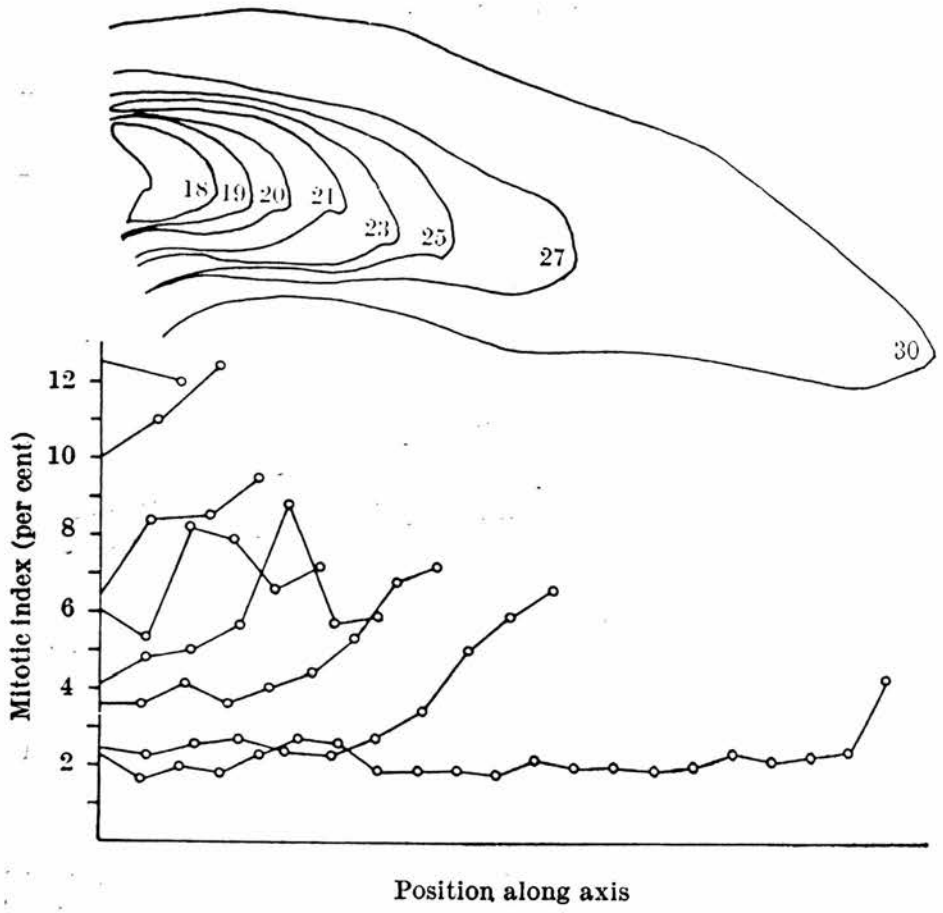

Figure 1.6 Mitotic index along the proximal-distal limb axis at different stages, with a significant decrease in proximal regions compared to distal regions from stages 23-27. The upper drawings give the outline of the limb at the appropriate stages (Hornbruch and Wolpert, 1970).

rates observed (Hornbruch and Wolpert, 1970; Summerbell and Wolpert, 1972) with a significant decrease in the mitotic index in proximal regions compared to distal regions (fig. 1.6, Hornbruch and Wolpert, 1970). At these same stages, there are high rates of proliferation not only at the distal tip but also at the proximal-dorsal and proximal-ventral boundaries of the limb bud, with a low rate of proliferation at the centre of the limb bud (Summerbell and Wolpert, 1972).

Although a number of proliferation studies have been completed using the chick limb (Hornbruch and Wolpert, 1970; Summerbell and Wolpert, 1972; Cooke and Summerbell, 1980) there has been no quantitative study of cellular proliferation in the mouse limb. To date, mouse limb proliferation studies have been qualitative in nature, the most recent study was published by Fernandez-Teran *et al*, (2006), providing information about patterns of proliferation but not about cell cycle times. However the development of new techniques has allowed for the study of absolute cell cycle parameters (Nowakowski *et al*, 1989, Shibui *et al*, 1989) and thus, can provide greater insight into the development of an organ or system. For example, Martynoga and associates (2005) implemented these techniques in order to quantitatively analyse cellular proliferation in the mouse telencephalon. The use of similar techniques for the analysis of limb development will be discussed in detail in chapter 4 and 5.

1.2.3.3 Possible confusion between the progress zone model and the concept of "proliferative zone"

"...the ridge signals the mesenchyme immediately underlying it, termed the progress or proliferative zone, to proliferate, resulting in directed proximodistal outgrowth."
Niswander *et al* (1993)

The quote above highlights the fact that although, the progress zone model (Summerbell, Lewis and Wolpert; 1973) has been around for over 30 years, some researchers continue to confuse the progress zone model with the idea of a "proliferative zone"; in other

words failing to distinguish between questions of PD patterning versus the mechanics of outgrowth. In the progress zone model the AER is said to influence cells in the distal tip of the limb bud to form the progress zone (Wolpert, 2002), which is a theoretical zone of fixed size within which cells are believed to undergo a progressive change from a more proximal to a more distal fate according to the time within the zone. Further to this, the AER is known to be essential to outgrowth of the limb bud as a whole. However, it is by no means clear that this is achieved through an AER-induced "proliferative zone", nor is it clear that limb bud outgrowth is achieved through controlling proliferation per se. This has instead become an implied assumption in certain descriptions of limb development, and is one of the questions I have sought to explore in this thesis.

1.3 Evolution and skeletal patterning of the vertebrate limb

1.3.1 The origin of the vertebrate limb

The 'fin fold theory' suggests that paired appendages (fins) arose within a paired but continuous set of ventrolateral folds in the body wall that were stiffened by a transverse series of endoskeletal pterygiophores (Kardong, K. V., 1998). Analysis of the fossil record has led to the suggestion that the transition from fins to limbs occurred in the Devonian period, with the fins of Sarcopterygian (lobe-finned) fishes, such as Panderichthys, as ancestral forms of the tetrapod limbs (Janvier, 1996). In tetrapods there are two pairs of appendages (limbs): the fore- and hind-limbs (Coates, 1994). However, not all vertebrates have limbs, of which snakes are a good example, such vertebrates have lost the ability to form limbs during the course of evolution (Cohn & Tickle, 1999).

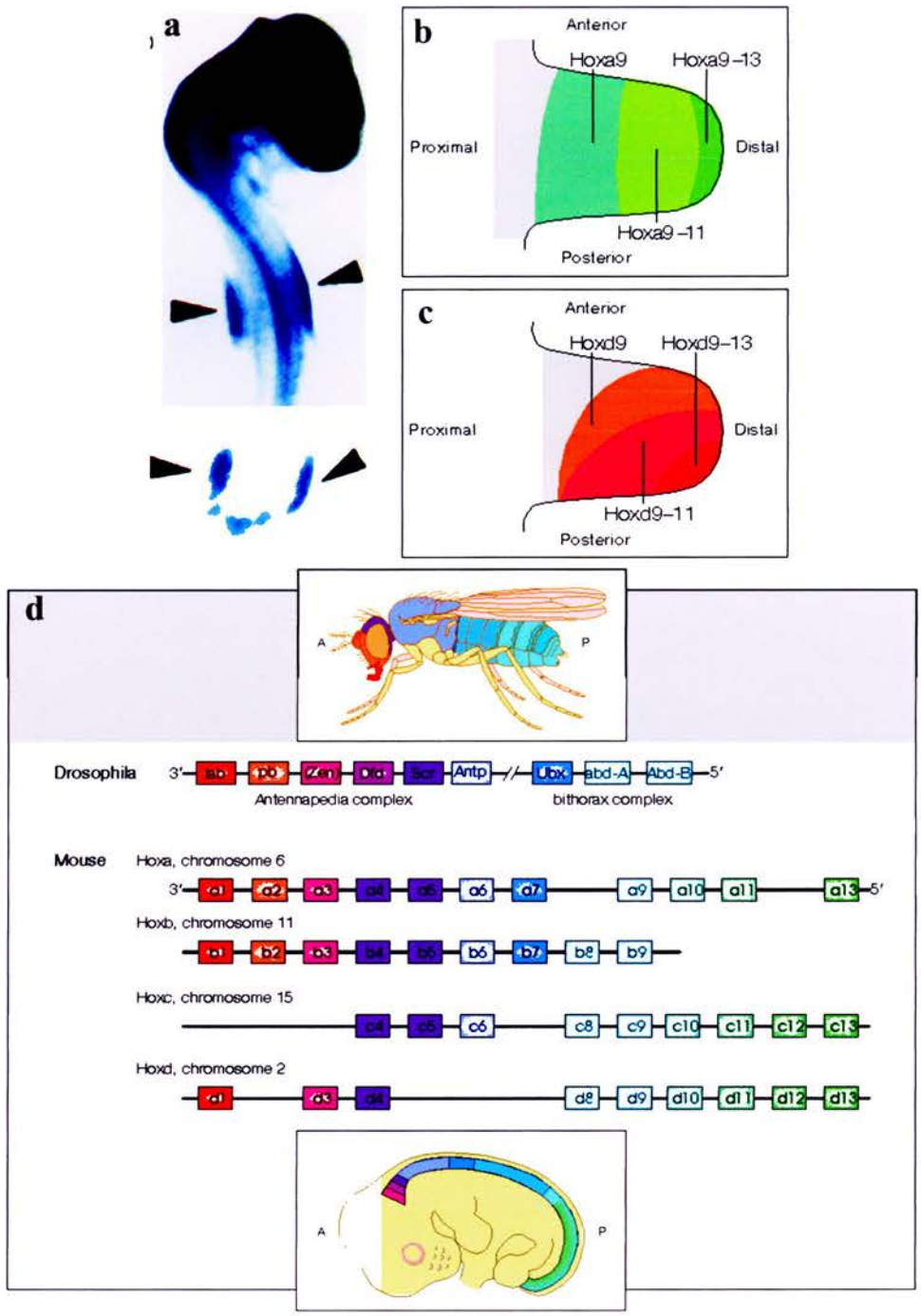

Figure 1.7 FGF10 and Hox gene expression
(a) FGF10 expression marking the developing chick limb fields of future fore and hind-limbs (Ohuchi *et al,* 1997). (b,c) Patterns of Hox gene expression within the chick fore (top) and hind limbs (bottom; Wolpert et al, 1998). (d) Patterns of Hox gene expression along the drosophila (top) and mouse (bottom) body axes (Wolpert et al, 1998).

1.3.1.1 The position and identity of the limbs along the body axis: fore limb or hind limb?

Pairs of limb fields are present on either side of the embryonic body axis, which give rise to the forelimbs and hindlimbs (fig. 1.7a). The positioning of limb fields is attributed to the spatial cues provided by the Hox genes, which encode homeodomain transcription factors. The Hox genes are evolutionary conserved between invertebrates and vertebrates in terms of their ordered spatial expression patterns along the embryonic body axis (fig. 1.7d; Duboule, 1994; Deschamps *et al*, 1999; McGinnis & Krumlauf, 1992; Wolpert *et al*, 1998). In vertebrates Hox genes also illustrate conservation in terms of their role in the positioning of the limb (Nelson, 1996; Scott, 1997; Kmita, 2002). For example, the expression boundaries of Hoxc6 are found to exactly correlate with the forelimb position in diverse vertebrate species (Nelson *et al*, 1996; Khan, 1999). Furthermore, it has been shown in the chick that flank cells can be induced to form either a wing or a leg, and that induction of these ectopic limbs is accompanied by specific changes in expression of three Hox genes (Hoxb9, Hoxc9 and Hoxd9) in lateral plate mesoderm (Cohn *et al*, 1997). Analysis has shown that Hoxa and Hoxd gene clusters (fig. 1.7b, c) are expressed in both the fore- and hind-limbs, whereas the expression of Hoxb and Hoxc gene clusters is restricted to either the fore- or hind-limb (Wolpert *et al*, 1998).

After the locations of the forelimbs and hindlimbs have been specified, limb bud outgrowth occurs. The molecular mechanisms that control forelimb and hind limb bud outgrowth are similar but not identical. Both the forelimbs and hindlimbs develop in a sequential manner but there are apparent temporal differences (forelimb buds appear – Theiler's stage 15, 9.5-10.25 days, 21-29 somites; hind limb buds appear – Theiler's stage 16, 10.25-10.75, 30-34 somites). The differences in forelimb and hind limb temporal emergence (Theiler, 1989) and development mean that comparative developmental studies between the forelimb and hind limb can only be relative in nature.

1.3.2 Skeletal patterning

During limb bud outgrowth the cells within the limb are patterned and differentiate into skeletal precursors, this process is known as chondrogenesis (Goldring *et al*, 2006). The initial stages involve the outgrowth of the limb bud along the proximo-distal axis (Maini and Solursh, 1991) during which time mesenchymal begin to condense (Goldring *et al*, 2006) leading to the formation of the first chondrogenic element, the stylopodium segment; humerus or femur (Shubin and Alberch, 1986). This is followed by antero-posterior development involving the condensation and branching (segmental bifurcation) of mesenchymal cells from the humerus or femur forming the zeugopodium segment consisting of two bones; radius and ulna, or tibia and fibula (Shubin and Alberch, 1986). Additional branching events generate the autopodium (hand or foot), consisting of the carpal-tarsal elements, the metacarpal-metatarsal elements and the digits, which develop at specific locations and are morphologically distinct from one another (Shubin and Alberch, 1986). Figure 1.8a (Cummings, 2001) is an example of the final skeletal structure of a vertebrate limb. The example given is of a human hind-limb but essentially all vertebrate species have one stylopodal element, two zeugopodal elements and an autopod consisting of a varied number of skeletal elements.

The initial mass of homogenous mesenchymal cells that constitute the limb bud, can be identified as being pre-chondrogenic through the presence of type-1 collagen (Pacifici *et al*, 2000; Lizarraga *et al*, 2002). Bone formation begins with the condensation of mesenchymal cells (fig. 1.8bI), which can be recognised through the closer packing of cells (Thorogood & Hinchcliffe, 1975), resulting in regions of high cell density (Tsonis and Goetinck, 1990), or by binding peanut agglutinin lectin to the cell surface molecules of condensed cells (Miyake *et al*, 1996; Zschabitz, 1998). Post condensation, cells differentiate into cartilage forming chondrocytes; cells at the border of condensations form a perichondrium. Chondrocytes can be characterised by their spherical shape (fig 1.8bII) and the secretion of extracellular matrix proteins, predominantly type-2 collagen

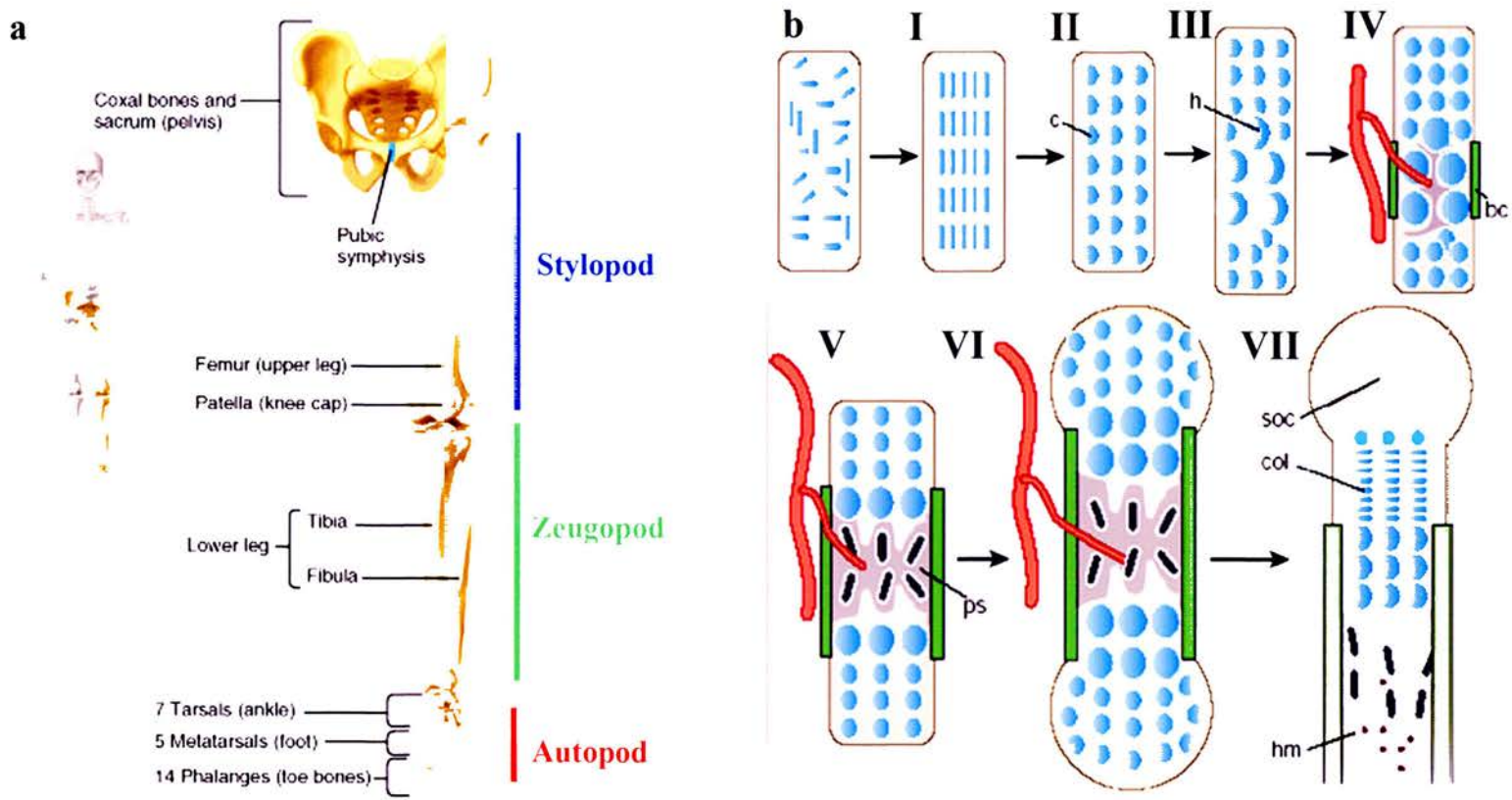

Figure 1.8 Sketal elements and chondrogenesis.
(a) Human hind-limb skeleton (modified from Cummings, 2001) (b) Steps involved in endochondral bone formation (Kronenberg, 2003).

(Pacifici *et al*, 2000; Lizarraga *et al*, 2002) and aggrecan, which can be stained using alcian blue (Gotz *et al*, 1995). The cartilage enlarges as chondrocytes proliferate (fig. 1.8bIII), eventually, those at the centre of the cartilaginous element stop proliferating and become hypertrophic. Perichondrial cells adjacent to hypertrophic cells become osteoblasts, forming a bone collar (fig. 1.8IV). After the apoptosis of the hypertrophic chondrocytes the osteoblasts proceed to invade the space once inhabited by the hypertrophic chondrocytes (fig. 1.8bV). The proliferation of remaining chondrocytes results in the lengthening of bone (fig. 1.8VI) and the production of secondary sites of ossification at the ends of the bones (fig. 1.8bVII).

1.3.3 Skeletal patterns of branching in limb evolution and development

Explanations for the evolution and development of the limb are improving as biologists increasingly combine molecular and fossil record data in order to determine mechanisms of evolution and development. In the early days of evolutionary studies, the majority of theories were based upon adult and fossil limbs. In recent times, we have seen an improvement in embryonic manipulation and analysis techniques, providing embryonic developmental data that has supported or refuted previous theories of development and evolution.

The definitive skeletal structure of fins and limbs has been explained using a theoretical axis of development, known as the metapterygial axis, which I shall briefly introduce here and discuss further in chapter 2. The theoretical axis is thought to have been present in ancestral species and retained in tetrapods where it runs through the ulna/fibula and distally through the distal carpals/tarsals as the "digital arch" (Shubin and Alberch, 1986; Coates, 1995). The carpals/tarsals and the metacarpals/metatarsals are suggested to arise from the digital arch by a process of branching. This was supported by Shubin and Alberch's (1986) work, in which they analysed the chondrogenic patterns of numerous vertebrate species.

Although Shubin and Alberch's work provides a good model for skeletal development it must be noted that the pre-skeletal pattern is not necessarily a reflection of early patterning events. Moreover, Oster and colleagues (1988) argue that explanations of developmental processes lie within the details of genetic regulation of patterning and morphogenesis, and not in physical-mechanical models. Therefore, it is essential that in this age of molecular and genetic studies, that the issues such as the development of skeletal elements be analysed from an early developmental perspective to see if underlying mechanisms of development are comparable between vertebrate species.

1.3.4 Sox9 – The earliest molecular marker for the skeletal pattern?

The Sox9 gene has been described as the earliest chondrogenic marker as it is expressed in the chick limb bud in a dynamic pattern that prefigures the appearance of chondrogenic condensations (Chimal-Monroy *et al*, 2003). At stage 22, equivalent to E10.5 in the mouse, Sox9 expression is seen as two domains running proximo-distally marking the future position of the zeugopodial cartilages (Chimal-Monroy *et al*, 2003). This dynamic pattern of expression is shared by Sox5 and Sox6, however Sox9 expression precedes the expression of both these genes (Chimal-Monroy *et al*, 2003).

Sox9 is from the Sox protein family, which consists of a group of proteins that have strong amino acid similarity (usually above 50 %) to the HMG domain of Sry, which is also known as the Sry box (Wegner, 1999). The protein also contains a transactivation domain at the C terminus, suggesting it to act as a transcription activator (Sudbeck *et al*, 1996; Ng *et al*, 1997). In fact, it is proposed to be a differentiation factor expressed in cells that have already been patterned, rather than a patterning molecule (Akiyama, 2002). Sox proteins, and particularly Sox9 (Marshall and Harley, 2000), are well conserved throughout the vertebrates indicating a conservation of function.

The Sox9 gene is known to play a role in a number of developmental processes including chondrogenesis, sex determination and Sertoli cell differentiation, hence its expression can be found in a number of different cell types including mesenchymal condensations and chondrocytes, the genital ridge and adult testis, the notochord and ventricular CNS cells (Wegner, 1999). Moreover, studies of SOX9 knockout chimeras have shown that mesenchymal cells that do not carry SOX9 do not differentiate into cartilage forming chondrocytes (Bi, 1999). In the mouse forelimb mesenchyme, Sox9 expression can be found as early as 9dpc (Ng *et al*, 1997) and is seen as a smear across the limb tissue.

1.4 Goals of the PhD

The goal of this PhD thesis is to further our understanding of limb development. In the past, scientists have analysed and attempted to understand the development of the limb using either laboratory techniques or computational tools. In recent times, scientists have begun to realise that combining the two would be more fruitful. In this thesis, I aimed to develop and use a variety of techniques and new computational tools to revisit certain issues more accurately, and in more detail than has been done before. Moreover, I aimed to generate two comprehensive sets of spatial and temporal data – one of Sox9 expression and the other of cell cycle times in the limb - which would help in answering a number of questions related to the patterning of the limb bud.

1.4.1 Technical Goals

I aimed to participate in generating two sets of computational tools. The first set of tools would be used in the analysis of 3D gene expression patterns that are imaged and recorded using optical projection tomography (OPT) software. The tools would be designed to allow for the easy dissection of gene expression patterns with respect to the different staining intensities within a specimen. The second, more sophisticated, set of tools would be for the purpose of analysing 2D sections of proliferating cells doubly-labelled with IddU/BrdU or singly labelled for phosphohistone H3. The tools would be designed to automatically and efficiently locate, count and analyse cells within images, in order to generate proliferation and cell density maps of sections. Two different types of proliferation maps would be generated - cell cycle time maps for doubly labelled sections and labelling-ratio maps for singly labelled sections.

1.4.2 Biological Goals

There are many genes involved in the development of the limb bud, one such gene is Sox9, which is considered to be the earliest known marker of chondrogenesis. One of my goals was to analyse the spatial and temporal expression pattern of Sox9 in greater detail than has been done before, in order to see whether the current description of its function is accurate i.e. differentiation rather than patterning. More specifically, I aimed to address a couple of questions related to the process of chondrogenesis, including,

- whether early gene expression patterns are a reflection of later chondrogenic patterns and,
- whether Sox9 expression patterns support the hypothesis that all the digits are derived from the posterior half of the limb bud.

Alongside the expression of genes, cellular proliferation plays a significant role in the morphogenesis of the limb. Therefore, I aimed to analyse proliferation rates in the early mouse limb bud in more detail that has been done before. It was envisaged that the analysed proliferation data would allow me to,

- determine quantitative values of cell cycle time (Tc);
- determine patterns of Tc across the limb bud;
- compare patterns of Tc to the findings of qualitative proliferation studies in the literature;
- find a relationship between quantitative Tc values obtained using IddU/BrdU staining and qualitative proliferation rates derived from phosphohistone H3 staining and
- determine whether regions of high cell density have low cell cycle times, as suggested in the literature.

Chapter 2 - Sox9 expression in a developmental and evolutionary context

2.1 Introduction

The evolution of the vertebrate limb is believed to have occurred approximately 200 million years after the establishment of the chordate body plan (Newman and Muller, 2005). The invariant stability of the vertebrate limb phenotype has resulted in this characteristic being perpetuated over time and can today be found in the majority of vertebrate species. Moreover, close examination of the vertebrate limb highlights a highly conserved skeletal pattern. The existence of conservation and the non-existence of imaginable phenotypes seems to cry out for evolutionary and developmental explanations. In fact, emerging limb skeletal patterns have led to many important evolutionary debates. For example, how do we assign identity to bird digits? Whether they are assigned as digits I-II-III or II-III-IV is not about semantics but relates to whether birds are believed to have followed the digital reduction pattern of other amniotes and whether the identification of bird digits provides evidence for the digits of Archaeopteryx (Hinchliffe and Hecht, 1984). Another example of an evolutionary question under debate, is from where the digits arise? Do they arise from a presumptive digital region, known as the digital arch (Shubin and Alberch, 1986), which is analogous to the primitive metapterygial axis? (Shubin *et al*, 1997) The debate related to bird digits and the digital arch will be discussed in more detail later in this introduction.

2.1.1 Studying evolutionary morphology

Within the biological community, evolutionary morphology has been studied in two main ways –the first can be traced to Darwinian theory of evolution and the second can be traced to pre-Darwinian times (Shubin and Alberch, 1986). The former involves the study of adaptive change, where there are clear relationships between form and function leading to morphological adaptation. The latter involves the analysis of non-adaptive change; in other words, looking at morphogenetic similarity irrespective of functional or adaptive differences between species, which was the methodology adopted by Shubin

and Alberch (1986) in order to dissect and understand the evolution and development of the vertebrate limb skeleton.

2.1.2 Models of limb patterning and the 'digital arch'

Shubin and Alberch (1986) completed a study in which they looked at histological sections and whole-mount specimens from a representative group of tetrapods. From the specimens they were able to analyse the skeletal patterns found in various tetrapods, including *Mus musculus* (mammal), *Ambystoma* (urodelan amphibian) and *Struthio australis* (bird) (fig. 2.1 a, b and c, respectively). Moreover, it was through their analysis that a model for a sequence of hierarchical branching events to describe limb patterning was developed, which are:

1. *De novo* condensation - An element may appear *de novo,* its mesenchymal condensation unconnected to any other (fig. 2.1di).

2. Branching - There may be a Y-shaped branching of a single element into two (fig. 2.1diii).

3. Segmentation - A single element may give rise to a single distal condensation. This can involve either the budding of a new condensation from a single existing one or the formation of a continuous rod of precartilage that subsequently breaks up into two separate elements (fig 2.1 div).

The general pattern of events was found to occur in a proximal-distal direction, in all analysed tetrapods. The first event is the *de novo* condensation of the proximal element (humerus/femur) after which a bifurcation branching event at the distal end of the element results in the formation of the tibia and fibula or the radius and ulna (fig 2.1a, first step in series). It is at this point that an asymmetry is said to arise, whereby the anterior side segments elements and the posterior side gives rise to the 'digital arch' (fig. 2.1a) (Milaire, 1978; Shubin and Alberch, 1986, Hinchliffe, 2002); the digital arch being the presumptive embryonic structure from which the digits arise.

It is proposed that before the appearance of the digital arch development occurs in a proximo-distal direction however, the digital arch adds another orientation of development to this scheme, namely the antero-posterior axis of development (Shubin and Alberch, 1986). The digital arch is said to first appear as a single continuous condensation (Hinchliffe, 2002), which then segments its early embryonic connections to form skeletal elements of the autopod, however there is always an exception to the rule and this is the case in the bird wing where the digital arch does not segment, leaving a single fused mass (Shubin and Alberch, 1986; fig. 2.1c). Finally, according to the digital arch model the metatarsals/metacarpals and distal tarsals/carpals form through a process of branching and segmentation (Shubin and Alberch, 1986). The order in which the digits arise differs slightly from one tetrapod class to the other. For example, in the fore-limb of Mus musculus, representative of mammals, the digits arise in an order where digits 3, 4 and 5 arise together followed by digit 2 and then by digit 1, summarised as (3-4-5)-2-1 (fig 2.1a); in *Ambystoma*, representative of Urodelan Amphibians, the digits arise in an order of (2-1)-3-4 (fig. 2.1b) and in birds the digital sequence is 4-5-3-2 (fig. 2.1c). Irrespective of these slight variations, the consensus is that, in the majority of tetrapods, digit formation occurs in a posterior to anterior sequence, beginning with digit 4 (Shubin and Alberch, 1986; Hinchliffe, 2002) and in virtually all mammals this ends with the development of the 1st and 5th digits (Hecht and Heebt, 1994).

2.1.3 The origin of birds

The study of the digits has led to many evolutionary questions being posed, one such question is whether birds originate from dinosaurs. It is difficult to answer this question by analysing the development of bird wing digits because the wing is a highly specialised form of the tetrapod limb with only three digits, which makes it difficult to clearly identify them. Nonetheless, both paleontologists and embryologists have attempted to identify the digits of the bird wing. Paleontological studies have focussed

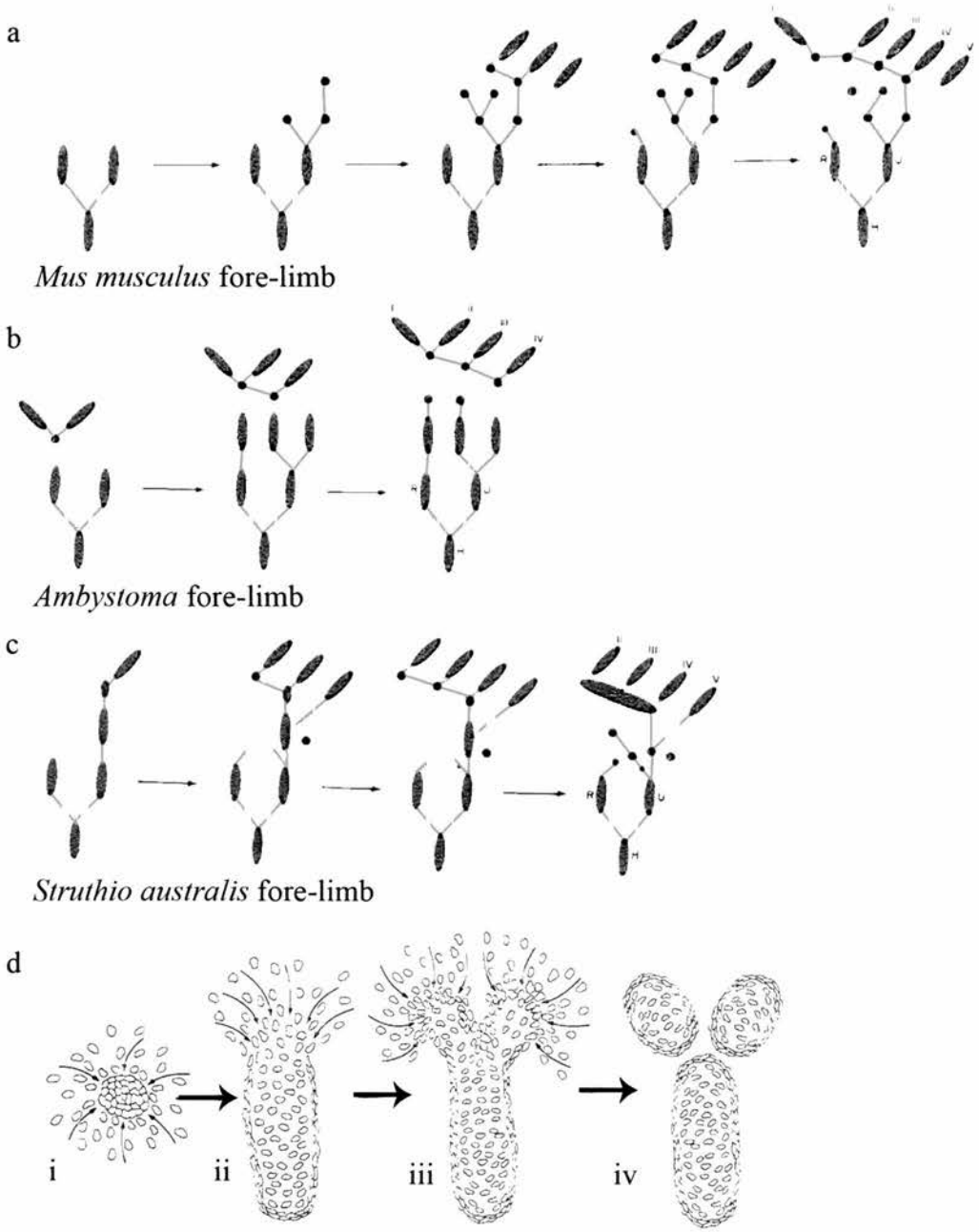

Figure 2.1 Growth of cartilage condensations and branching patterns for different tetrapods,
including (a) Mus musculus fore-limb (b) Ambystoma fore-limb and (c) Struthio australis fore-limb (H= Humerus, R=Radius, U=Ulna, Roman Numerals represent digits, grey lines represent patterns of connectivity among chondrogenic condensations). (d) Growth of a cartilage condensation, from an early stage at which a *de novo* cndensation is formed (i) through to its extension (ii) branching forming a Y-shaped structure (iii) and when a single branched element breaks up into seperate elements (modified from Shubin and Alberch, 1986).

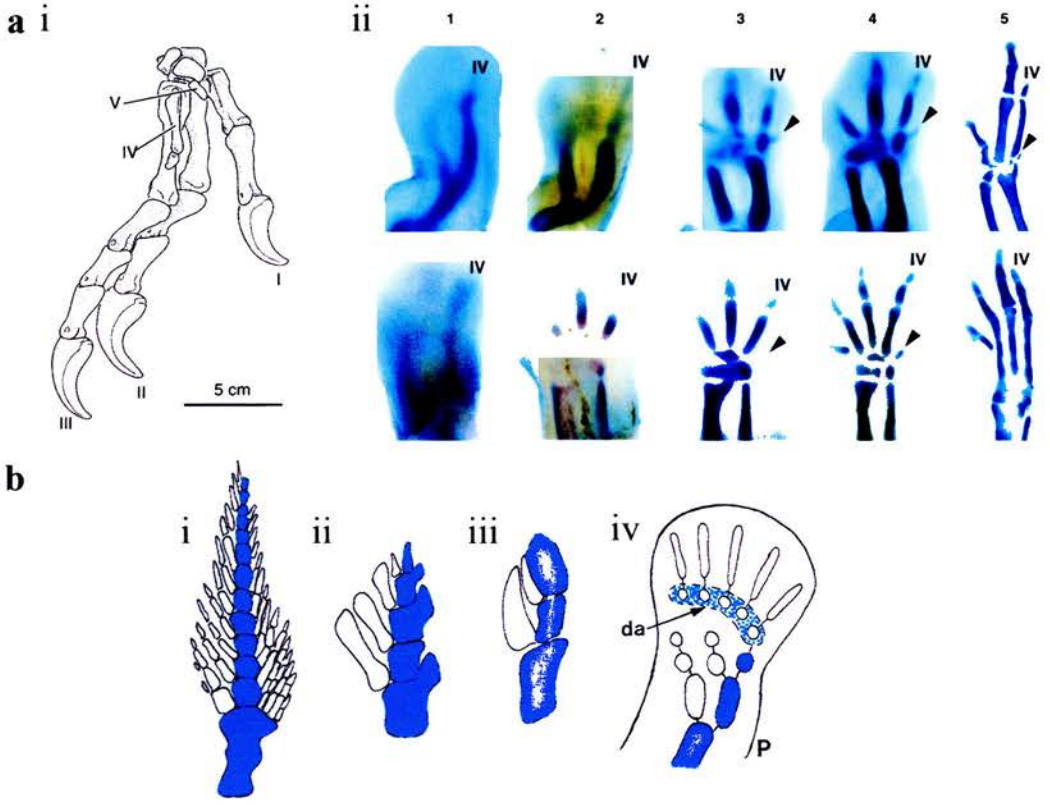

Figure 2.2 Theories relating to the origins of vertebrate limbs
(a) Competing theories about the origin of the bird limb. (ai) Digits I-II-III are prominent on the earliest known theropod Herrerasaurus, ventrolateral view; (aii) Digits II-III-IV are clearly visible during the development of the chicken right manus (top row) and pes(bottom row) (Burke an Feduccia, 1997). (b)Definitive paired anterior fin and limb skeleton patterns in Sarcopterygian's (bi) Neoceratodus (dipnoan); (bii) Eusthenopteron (osteolepiform) and (biii) Panderichthys; and (biv) a generalised pentadactyl limb showing the Shubin-Alberch (1986) development skeletal bauplan. The hypothetical metapterygial axis is marked in blue for i-iii. In iv, the metapterygial axis runs post-axially supposedly continueing as the digital arch (da; posterior, P; Hinchliffe, 2002).

on comparing the bird wing to dinosaur fossils, such as that of the earliest known theropod, *Herrerasaurus,* which has three prominent digits assigned as I-II-III and two extremely reduced manual digits believed to correspond to digits IV and V (fig. 2.2ai; Sereno, 1993). Paleontologists claim that the pattern and identity of the prominent digits in this dinosaur species is comparable to the digits found in todays bird species (Ostrom, 1976), and thus birds have a digit identity of I-II-III originating from ancenstral dinosaurs. This notion was further supported by molecular data provided by Vargas and Fallon (2005) who found similar patterns of Hox gene expression in the chicken foot and mouse hand and foot; digit I in the developing limbs did not express Hoxd12 but expressed Hoxd13. This result was interpreted to mean that the most anterior digit in bird wings is homologous to digit I. In contrast, the majority of embryologists claim that bird digit identity is II-III-IV (Hamilton, 1965; Romanoff, 1960; Hinchliffe and Hecht, 1984; Burke and Feduccia, 1997; Larsson and Wagner, 2002; Feduccia and Nowicki, 2002; Galis *et al*, 2005). This convention is the result of studies in which Holmgren (1955) claimed to have found all five archetypal condensations of the metacarpal region, with the metacarpal of the first digit present transiently in the preaxial position. Thus, the general pattern in amniotes of digital reduction by loss of metacarpals 1 and 5 and digits 1 and 5 seen in some lizards and mammals (Morse, 1872; Underwood, 1977) suggests that a similar reduction happens in birds and that the remaining digits in birds are digits II-III-IV. Moreover, patterns of cartilage condensation which follow through from the humerus into digit IV, together with serial homologous elements being identified in the bird hind-limb (fig. 2.2aii; Burke and Feduccia, 1997) supports the notion that homology exists between birds and other amniotes.

2.1.4 The origins of the vertebrate limb and the metapterygial axis

Another area of speculation is the evolutionary origins of the limb as a whole. Homology between early tetrapods and their lobe-fin (sarcopterygii e.g *Neoceratodus, Eusthenopteron* and *Panderichthys*) fish ancestors is apparent in the proximal regions

including the stylopod, zeugopod and intermedium (Vorbeyeva and Hinchliffe, 1996). This homology is used to support the theory of fin to limb evolutionary transition (fig. 2.2b). Furthermore, it is hypothesised that the digital arch is derived from the metapterygial axis, which is the main axis of osteolepiforms such as *Eusthenopteron* (Hinchliffe, 2002). According to Shubin and Alberch's (1986) developmental bauplan the radial branching and the metapterygial axis are retained in tetrapods as the radius/fibula plus proximal carpals/tarsals, and the ulna plus the digital arch. However, the idea that the metapterygial axis extends into the digital arch remains theoretical as the more distal parts, specifically the digits, are not believed to be homologous with the radials of paired lobe-fin fish (Hinchliffe and Vorbeyeva, 1999) rather, digits are believed to be newly evolved in the tetrapods (Hinchliffe, 2002).

More recently, the 'digital arch model' itself, rather than its evolution, has come into question as experimental findings suggest that the presence of proximal elements, such as the ulna, are not essential for the formation of the digits (Cohn *et al*, 2002). Moreover, Wagner and Chiu (2001) highlight the fact that digital elements are not solely derived from the posterior zeugopod, rather there are some examples, such as that of the anuran foot, where one digit arises from the anterior zeugopod. These findings would suggest that digital arch model does not fully explain digit formation, and that further investigation into digital patterning is required.

2.1.5 Studying chondrogenic events versus pre-chondrogenic events

Here I have discussed a number of evolutionary models that have come about as a result of studies completed on patterns of chondrogenic and final skeletal elements. However, as shown in the case of birds, it can sometimes be difficult to assign identity to a region (e.g bone) when working on the assumption of shared inheritance based upon morphogenetic similarity. Moreover, the final product of a patterning mechanism, such as chondrogenic regions and skeletal elements may not predict the original mechanism.

Therefore, it is necessary to look at a more fundamental level of development in order to gain a greater insight into patterning mechanisms and consequently, evolutionary homologies. This is because early developmental events, such as Sox9 expression, may set the stage for later ones, where alteration of the early process may disrupt later development. Thus early processes are likely to be the subject of stabilising selection, and early developmental stages would display less evolutionary change than later ones. The result being von Baers law (1828) that the features more common to a more inclusive taxon, such as a group of vertebrate species, often appear in development before the specific characters of lower-level taxa. This earlier similarity would provide for easier and more justifiable conclusions with regards to evolutionary homology.

2.1.1 Aim

In contrast to previous research, I aimed to gain a greater insight into skeletal patterning by analysing a gene that could be a good candidate for a pre-pattern i.e. primary gene expression patterns, rather than later defined skeletal patterns. An example of such a gene is Sox9, which is generally described as the earliest known marker for cartilage differentiation (Akiyama, 2002; Chimal-Monroy, 2003). Therefore, the focus of my study was the Sox9 gene expression pattern rather than condensation patterns or cartilage formation. As mentioned in chapter 1, Sox9 expression presages the known cartilage pattern (Lefebvre *et al*, 1998; Smits *et al*, 2001) and it is therefore assumed that dynamic changes in Sox9 expression also presage dynamic changes in the cartilage pattern. However, previous analysis has been on only a few time points of Sox9 expression, meaning that some interesting patterns of expression may have been overlooked and that this assumption could not be truly tested.

Here I aimed to analyse the Sox9 expression pattern at a higher temporal and spatial resolution than done before. It was envisaged that the completion of a comprehensive 3D Sox9 expression data set would allow me to address a number of issues including:

- whether Sox9 expression presages dynamic changes in the cartilage pattern and thus complement histological data cited in the literature;
- whether Sox9 expression 'events' conform to Alberch and Shubin's (1986) sequence of events describing limb patterning, which was based upon chondrogenic events;
- whether the Sox9 expression pattern would support or refute the digital arch model (Alberch and Shubin, 1986) and the proposed order of digit formation in a posterior to anterior sequence, beginning with digit 4 (Hinchliffe, 2002);
- whether Sox9 expression patterns enforce the proposal that it is simply a down-stream differentiation factor expressed in cells that have already been patterned, rather than a patterning molecule (Akiyama, 2002).

In order to address the issues listed, a comprehensive data set of Sox9 expression patterns was required. Therefore, I endeavoured to produce a comprehensive set of spatio-temporal Sox9 *in situs* of the *Mus musculus* hind-limb from early day 11 – late day 13 (Appendix A). Although, hind limb development lags behind that of the fore limb, the final skeletal pattern of both limb types consists of a single stylopod, two zeugopod elements and an autopod that has five digital elements. Therefore, it was assumed that the general pattern of Sox9 expression found in the *Mus musculus* hind limb would be comparable to that of the fore limb. Moreover, any mechanisms derived from the analysis of the *Mus musculus* hind limb would be useful in understanding the development of the mammalian limb, as a whole.

Currently, gene expression data is analysed and, more often than not, presented as either 2D images of section and whole-mounts (fig 2.3ai and 2.3aii). However, certain details of connectivity may be lost from a 2D analysis, so I wished to re-assess the Sox9 pattern in 3D. I aimed to do this by using optical projection tomography (OPT; Sharpe *et al*, 2002). OPT is a microscopy technique developed to produce high-resolution 3D images of both fluorescent and nonfluorescent biological specimens with a thickness of up to 15 millimeters. OPT microscopy would allow for rapid and accurate mapping Sox9 RNA distribution in the mouse limb. Interestingly, Sox9 expression was recently analysed in 3D in the chick (Welten, *et al*, 2005), however for reasons explained later they did not reach the same conclusions as this thesis. This chapter will further serve to summarise the development of computational tools used in the 3D analysis of Sox9 *in situ* data allowing for the analysis of different levels (intensities) of staining together with the virtual sectioning of embryological material.

2.2 Results

2.2.1 Analysing *in situ* data

2D expression data establishes the general pattern of expression but in the case of whole mounts it can be limited by the extent of light penetrance through the embryonic sample. Recently, *in situ* data has been presented in the form of 3D reconstructions, which can be derived from either whole mounts or sections. 3D reconstructions of serial sections can present problems as they depict discontinuous disjointed patterns with a 'lumpy' appearance (fig. 2.3aiii and 2.3aiv). However, 3D reconstructions of whole mounts using OPT produces a clear image of an embryo with the internal gene expression pattern clearly visible.

2.2.1.1 A new visualisation technique for 3D gene expression patterns

During the course of my research I set about analysing Sox9 *in situ* data using a new approach, which involves the imaging of the embryos using OPT and the analysis of generated image files using newly developed computational tools. I first explored the computational tools that were designed to display 3D surface images of different levels of staining, which I believe to be synonymous with levels of gene expression. The opaque nature of surface images meant that only the outer surface (the lowest level of expression, fig 2.3bi, darkest blue surface; 3ci darkest red surface) could be seen. Therefore, a virtual section through a sample was used in an attempt to see all levels of expression (fig. 2.3bi). However, the fact that a virtual section could only be performed in a flat plane meant that only some regions of expression could be seen after sectioning (fig 2.3bi). For example, as a limb bud develops it bends resulting in the sectioning of only a few levels of expression in some regions of the limb bud (fig. 2.3cii). In order, to obtain images of all regions of high expression it would have been necessary to perform many virtual sections. As a result of these early tests computational tools were

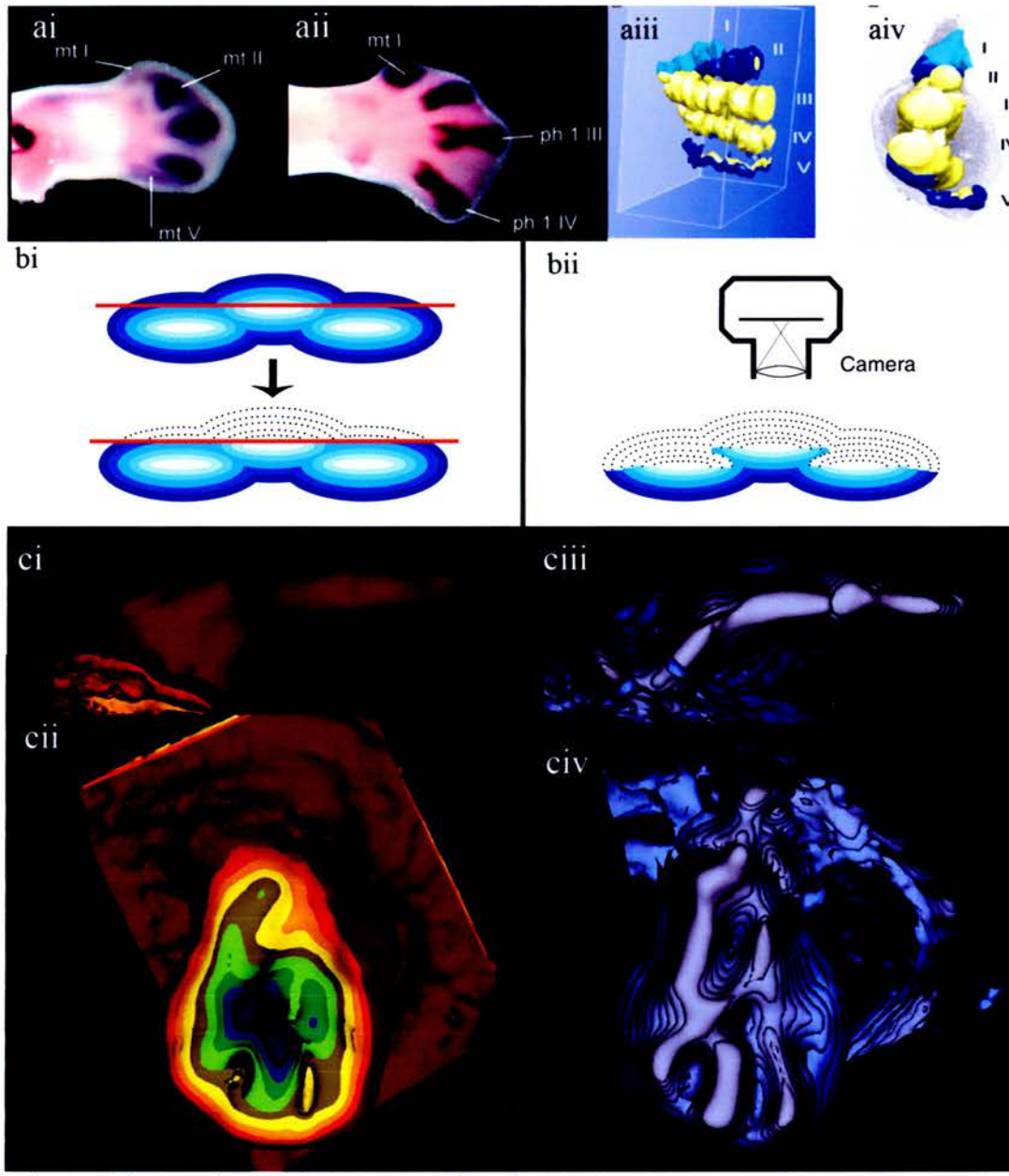

Figure 2.3 Imaging and documenting the Sox9 gene expression pattern.
(a) Previous attempts to document the Sox9 pattern. 2D photographs of left chicken hindlimbs hybridised with a Sox9 insitu probe, at stage (i)27 and (ii)30. Roman numerals, digit and metacarpal number; mt, metacarpal; ph, phalanx. (iii) 3D reconstruction of a specimen (yellow, cartilage; dark blue and light blue, Sox9 expression) Anterior is to the top, ventral aspect (iv) proximal aspect (Welten et al, 2005). (b) Diagramatic representations of virtual sections through regions of Sox9 expression. (i) LO_MultiPlaneCut.py removes all contours to one side of the red sectioning line (ii) LO_CustomPlaneAlignment.py removes the upper surface of each contour (those closest to the camera).(c) Sox9 expression in an E11.5 mouse embryo limb. Analysis using LO_MultiPlaneCut.py only reveals some of the Sox9 expression pattern (i) anterior view, distal left (ii) dorsal view, anterior right, whereas analysis completed using LO_CustomPlaneAlignment.py reveals all of the Sox9 expression pattern at different levels of expression (iii) anterior view, distal left (iv) dorsal view, anterior right.

developed to overcome the limitation brought about by virtual sectioning allowing for 3D images to be displayed so that all layers of expression can be seen without the need for virtual sectioning (fig. 2.3bii).

In summary, the first version of computational tools only allowed for a few graded levels of gene expression to be visualised after virtual sectioning, and only then if the region of interest coincided with the cutting plane (fig. 2.3ci and 2.3cii). The second version of computational tools surpassed expectations and allowed for the visualisation of all graded levels of gene expression, irrespective of the position or orientation of the biological sample (fig. 2.3ciii and 2.3civ).

2.2.1.2 Generating the data and acquiring the region of interest

I stained and imaged whole embryos using OPT. The embryo body provided information not only about the body surface (fig. 2.4a) but, more importantly, information about the many intricate regions of gene expression present within the embryo at a given stage of development (fig 2.4b). In some cases, it can be difficult to analyse a region of expression because of other overlapping regions obscuring the overall view, as shown in figure 2.4c and 2.4d. In such cases it was possible to use MA3Dview, a computational tool developed by the MRC Mouse Atlas group, to virtually dissect (crop) the limb from the embryo (fig. 2.4b). I then processed the limb bud image in order to generate new visualisation files that could be 'overlayed' to display different levels of gene expression (fig. 2.4d).

In some cases, the cropping of the limb bud from the embryo body was not successful in eliminating all elements obscuring the gene expression pattern (fig. 2.4c and 2.4d). Hence, further sectioning was required along certain planes of orientation, which is not possible using MA3Dview. After much deliberation, it was realised that the 'virtual sectioning' functionality of the newly developed software could be used to 'clean-up' cropped limb images, as the sectioning line could be orientated at any angle along any

plane (fig. 2.4e). Thus, producing a cropped image of a limb bud, which can be orientated in any direction in order to view the Sox9 gene expression pattern (fig. 2.4f).

2.2.2 Sox9 gene expression patterns

A total of 39 embryos, ranging from those harvested early on day 11 to late on day 14 were successfully stained with a Sox9 *in situ* probe, of which 23 were stained using the visible marker BCIP/NBT protocol and 16 were stained with fluorescent labels (Table 2.1). I originally began using fluorescent labels however, they were found to be unreliable and with time limitations in mind I decided to use the more reliable BCIP/NBT staining protocol.

After staining, the embryos were imaged using OPT and processed using existing and newly developed computational tools, as described previously. The presence of blood in 5 samples made it extremely difficult to distinguish the Sox9 expression pattern from auto-fluorescing blood; therefore these samples were not used to derive any further conclusions but have been included in Appendix A; a compendium of all successfully stained embryos.

Below is a list of the distinct patterning events observed from the analysis of Sox9 expression, which I shall later discuss in more detail:

- Formation of the femur and the Y-shape pattern;
- Formation of the "loop";
- Appearance of earliest signs of digital positions – Digits II and III come from the anterior zeugopod and digit IV comes from the posterior zeugopod;
- Appearance of the "digital arch" pattern;
- Appearance of the real digit position pattern;
- Appearance of the presumptive knee joint;
- Loss of Sox9 expression in proximal and posterior regions;
- Appearance of the phalanges with joint-like regions;

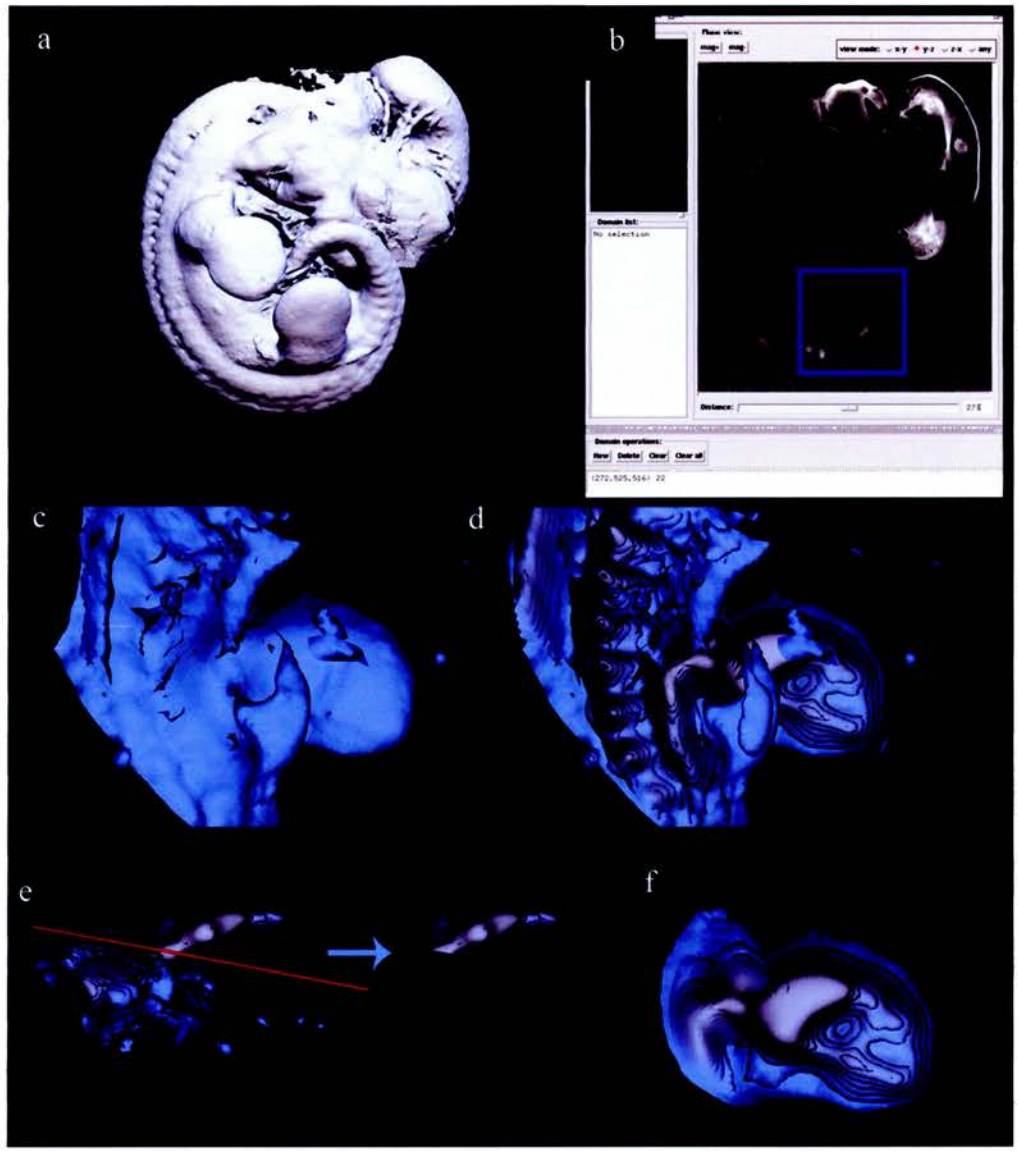

Figure 2.4 The processing of OPT images of Sox9 expression patterns
(a) OPT image of a whole E11.5 embryo. (b) 2D section of embryo with virtual cropping box visible (blue box) around one limb bud. The image is seen using the program MA3DView. (c) 3D view of cropped limb bud with the body obscuring the view of the limb bud. (d) 3D contours of Sox9 expression are generated using GeneratePattern and displayed using LO_Customplanealignment. (e) The body is cut away using the cutting line (red) in LO_Customplanealignment, allowing for a clear view of the Sox9 expression pattern in the limb bud (f).

Embryo	Harvested on Embryonic Day	Stain Type
19_2	11	Fluorescent
9_3	11	Fluorescent
5A3	11	Fluorescent
12_5	11	Fluorescent
12_4	11	NBT/BCIP
19_4	11	NBT/BCIP
51_2	12	NBT/BCIP
53_1	12	NBT/BCIP
33_3	12	Fluorescent
52_3	12	NBT/BCIP
33_5	12	NBT/BCIP
50_1	12	NBT/BCIP
11_5	12	Fluorescent
56_1	12	NBT/BCIP
17_2	12	Fluorescent
50_4	12	NBT/BCIP
16_1	12	NBT/BCIP
10_5	12	NBT/BCIP
34_3	12	NBT/BCIP
30_4	12	Fluorescent
57_1	12	NBT/BCIP
20_11	12	NBT/BCIP
21_1	12	NBT/BCIP
55_1	12	NBT/BCIP
55_2	12	NBT/BCIP
E429	12	Fluorescent
10_7	12	Fluorescent
16_3	12	Fluorescent
54_2	12	NBT/BCIP
4A1	12	Fluorescent
23_2	12	Fluorescent
21_3	12	Fluorescent
35_2	13	NBT/BCIP
36_2	13	Fluorescent
36_4	13	NBT/BCIP
14_1	13	Fluorescent
37_1	14	NBT/BCIP
40_1	14	NBT/BCIP
59_2	14	NBT/BCIP

Table 2.1 List of Embryos successfully stained for Sox9 gene expression.

Details of the day embryos were harvested is given in the second column and the staining technique used on each embryo is given in the last column. A total of 39 embryos were successfully stained; 6 embryos were harvested on day 11, 26 on day 12, 4 on day 13 and 3 on day 14. 23 embryos were stained using the NBT/BCIP procedure and the other 16 were stained using a fluorescent marker.

Figure 5 - Formation of the femur and the Y-shape pattern

The first sign of Sox9 expression was seen in day 11 (~E10.5) mouse embryos (fig. 2.5a), where there was *de novo* expression unconnected to any other. The expression pattern then extended distally and formed a definitive shape, the proximal of which likely reflected early stages of femur patterning (fig 2.5c, d). A bulb of expression resided at the distal end of the presumptive femur that then formed a fork like structure. In other words, the first signs of two distal elements, namely the tibia and fibula, were formed on day 11(fig 2.5e) through the branching of the presumptive femur, forming a continuous Y-shape, demonstrating the existence of a patterning bifurcation. Also, interestingly, the presumptive femur pattern arose before the hip pattern and began to develop distally prior to any sign of Sox9 expression in the hip region (fig 2.5e).

Figure 6 - Formation of the "loop"

The Y-shaped bifurcation extended distally (fig. 2.6), with Sox9 expression continuing in a region joining the developing pattern of the two zeugopodial elements resulting in a "loop" pattern (fig. 2.6c, d). The loop pattern persisted even when the posterior zeugopodal region (fibula region) had extended further than the anterior zegopodial region (tibia region; fig. 2.6e).

Figure 7 - Appearance of earliest signs of digital positions – Digits II and III come from the anterior zeugopod and digit IV comes from the posterior zeugopod

The Sox9 expression pattern continued to extend distally over day 12 resulting in the extension of the tibia and fibula regions of expression (fig 2.7). At this stage, the high intensity of expression in the connecting region between the femur and zeugopodial elements was observed to extend distally along the tibia (fig 2.7) at the same time Sox9 expression extended distally along the fibula culminating in high region of expression at

Figure 2.5 - Formation of the femur and the Y-shape pattern.
A series of Sox9 expression patterns from different day 11 mouse embryos, showing a small region of expression extending and beginning to form a more defined Y-shaped pattern.

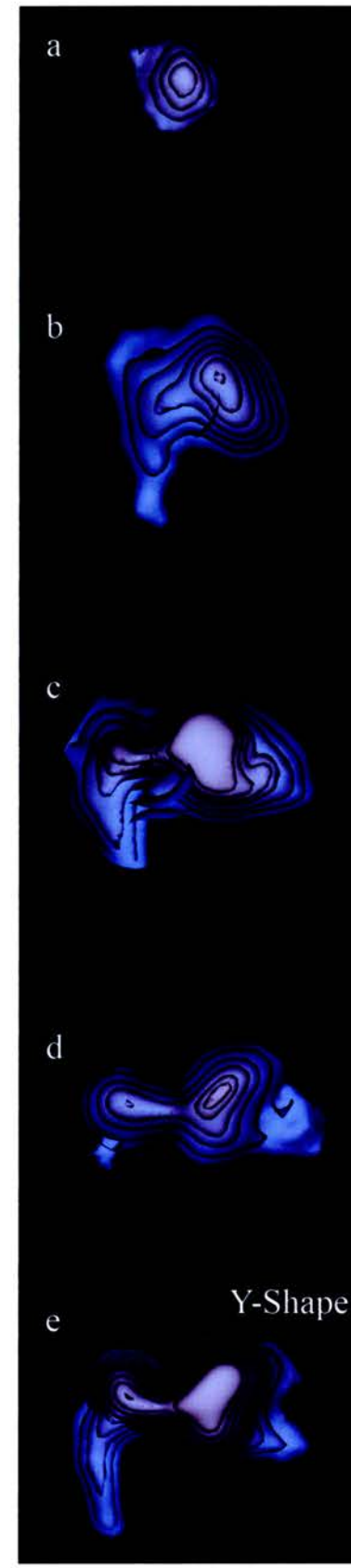

Figure 2.6 - Formation of the "loop" Sox9 expression series illustrating a Y-shaped pattern extending to form a "loop" of expression, whose extension leads on to form the tibia (t) and fibula (f).

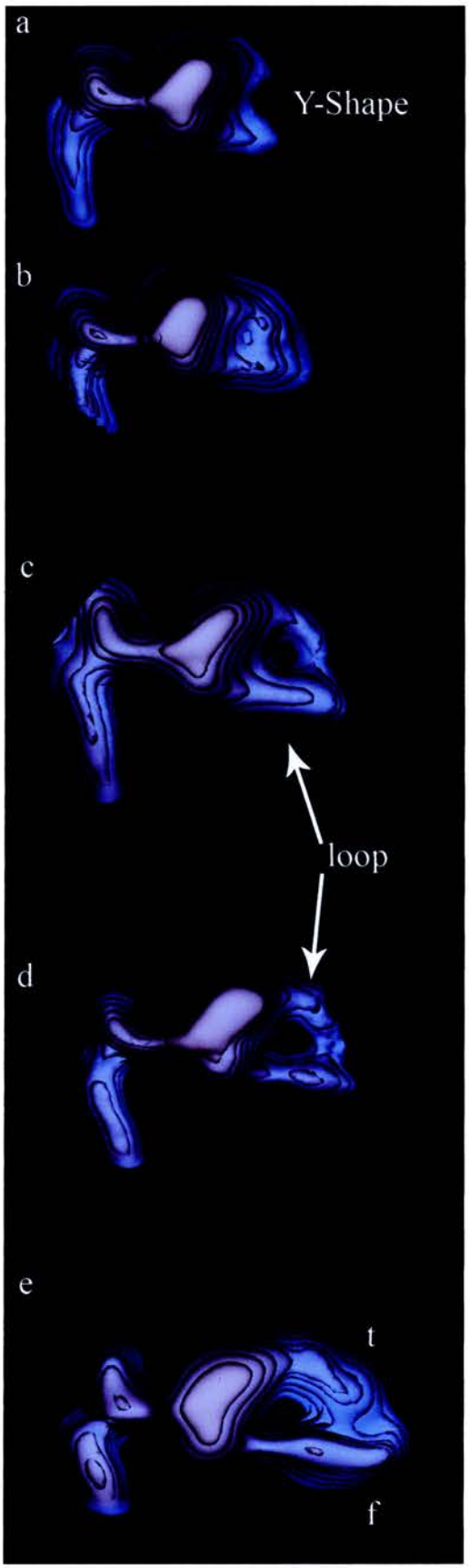

Figure 2.7 The earliest signs of digital positions – Digits II and III come from the anterior zeugopod and digit IV comes from the posterior zeugopod

The Sox9 pattern extends from the femur to form the tibia and fibula, and then leads on to the earliest sign of digit positions IV-(II-III).

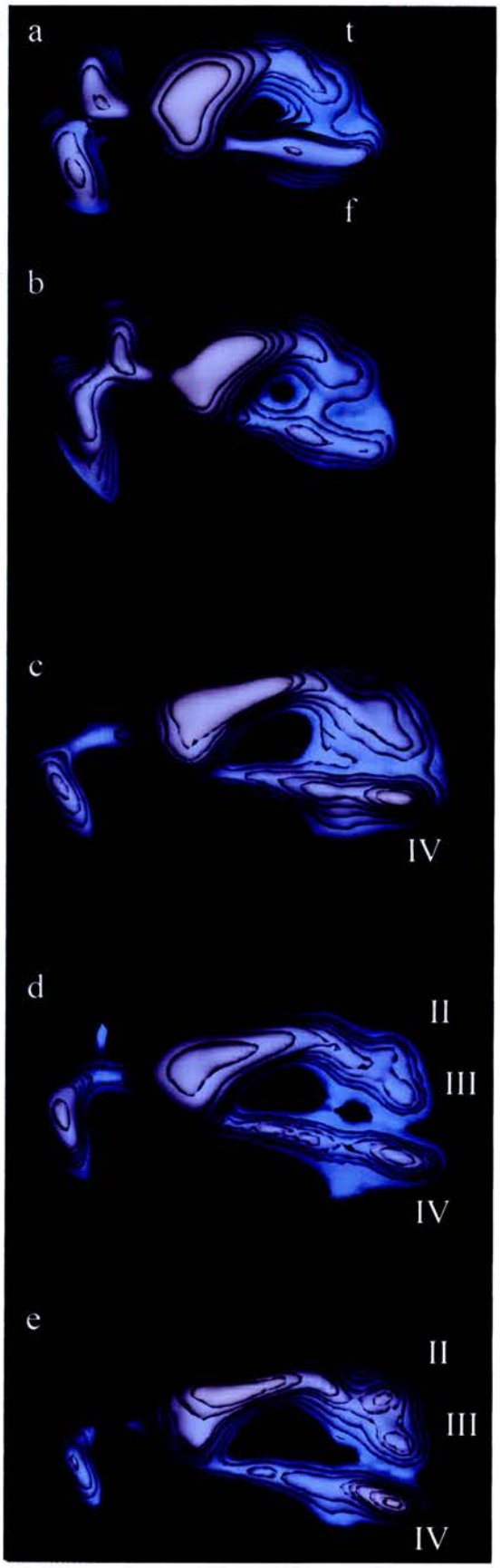

the distal tip. This expression is interpreted as the first sign of digital region IV (fig 2.7c), which becomes apparent in the analysis of later stages of Sox9 expression in the limb (discussed below).

According to the "digital arch" model digital region IV is the first to arise from the posterior zeugopod (Hinchliffe, 2002) and is shortly followed by other digital regions through a process of branching and extension. Surprisingly, this was not observed. Instead, the distal tip of the tibia region began to branch and extend into two presumptive digital regions (fig. 2.7d, 7e). The two digital regions have been classified as digital regions II and III based upon the fact that digital region I forms more anteriorly, at a later stage of development. Therefore, all of the digital regions of Sox9 expression did not arise from the posterior zeugopod, which illustrates that the Sox9 expression pattern does not conform to the "digital arch" model. This will be further discussed in the next section.

Figure 8 – Appearance of the "digital arch" pattern

Early development of the digital expression pattern does not conform to the "digital arch" model, in that digital regions II and III arise from the anterior zeugopod and digital region IV is connected to the posterior zeugopod. However, as the limb develops the Sox9 expression pattern changes and can be interpreted in accordance with the digital arch model. Initially, the digital regions elongated and extended distally, all the while a low level of Sox9 expression connected the distal anterior and distal posterior digital-regions of expression to one another, which could mistakenly be interpreted as the digital arch from which digits arise (fig. 2.8a, b). Gradually, Sox9 expression intensity increased in the connecting region proximal to digital regions II and III, resulting in a distinct region of expression connecting the distal end of the fibula region to the base of digital regions II and III (fig. 2.8c, d). If we gave no regard to previous stages of expression it would seem that digital regions II and III are connected and thus arose from the fibula. The expression of Sox9 at a slightly later stage of development, enforces

the notion that digital regions II and III arose from branching of the fibula as the connection to the tibia is lost, whereas there is a remnant of a branch coming from the fibula region (fig. 2.8e). In essence, if we had not analysed previous stages of expression, the results would suggest that Sox9 expression follows the digital arch model, for it could be understood that digital regions II and III have arisen through the branching and extension of the posterior zeugopod, however our analysis reveals this to be untrue.

Figure 9 – Appearance of the real digit position pattern

By day 13 digital regions I and V began to bud off from the anterior and posterior zeugopodal regions, respectively (fig. 2.9). Digital region I extended in an anterior direction, whereas digital region V extended in a distal direction (fig. 2.9b). The expression pattern of digital region V compared to digital region I was considerably larger (fig. 2.9c), this difference in size continued on through development and is reflected in a comparable difference in size in the final skeletal elements of digital region V and digital region I.

Figure 9 – Appearance of the presumptive knee joint

At around the time digital regions I and V are formed so too is the presumptive knee region (fig. 2.9b). A pattern of the knee joint emerges from the connecting region between the femur and the two zeugopodial regions of expression. Initially, the proximal ends of the tibia and fibula are connected by a low region of Sox9 expression. At this point the proximal ends of the tibia and fibula look bulb-like in shape, with a relatively flat side facing the femoral region. The flat side of the tibia and fibula regions looks very much like the adult tibia and fibula plateau with which the femur would connect. The definition of the presumptive knee joint is enhanced when Sox9 expression is lost between the zeugopodial elements, but then expression within the presumptive knee joint is also then quickly lost.

Figure 2.8 Continuation into the "digital arch" pattern
The Sox9 pattern continues on from an early II, III, IV digit-like pattern to one which is reminiscent of a "digital arch" pattern, and small protrusions marking digits 1 and 5 can be seen.

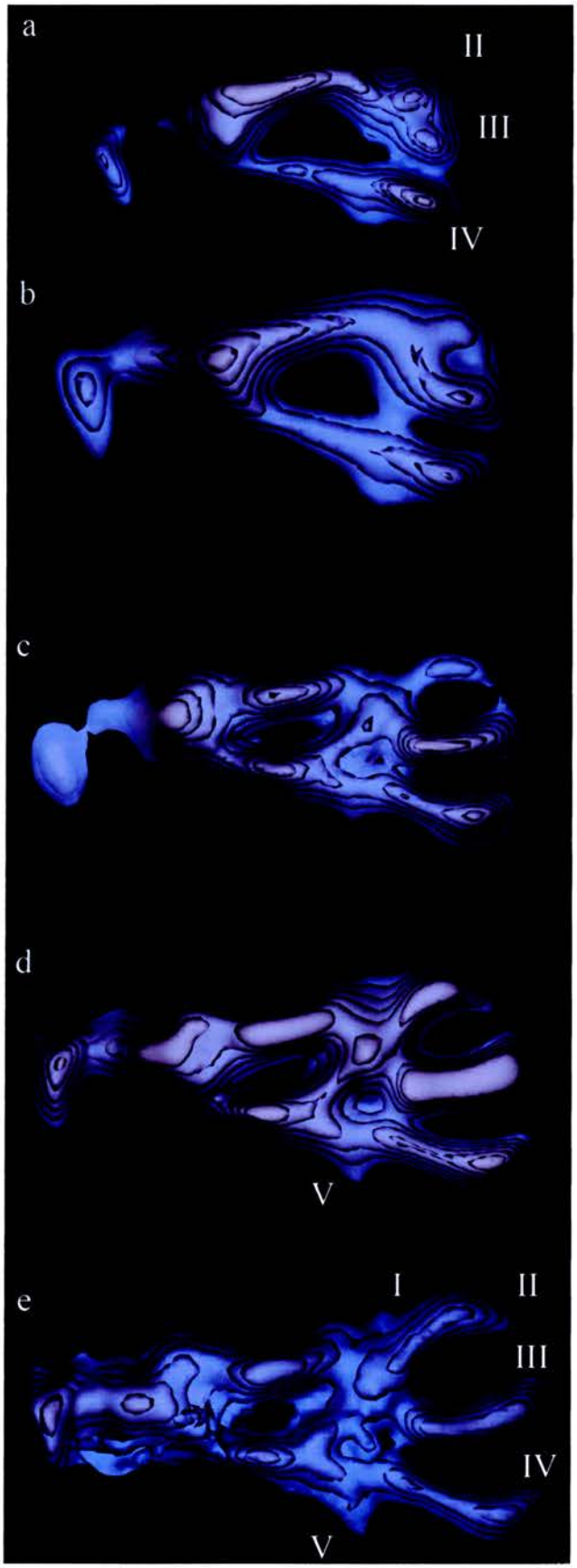

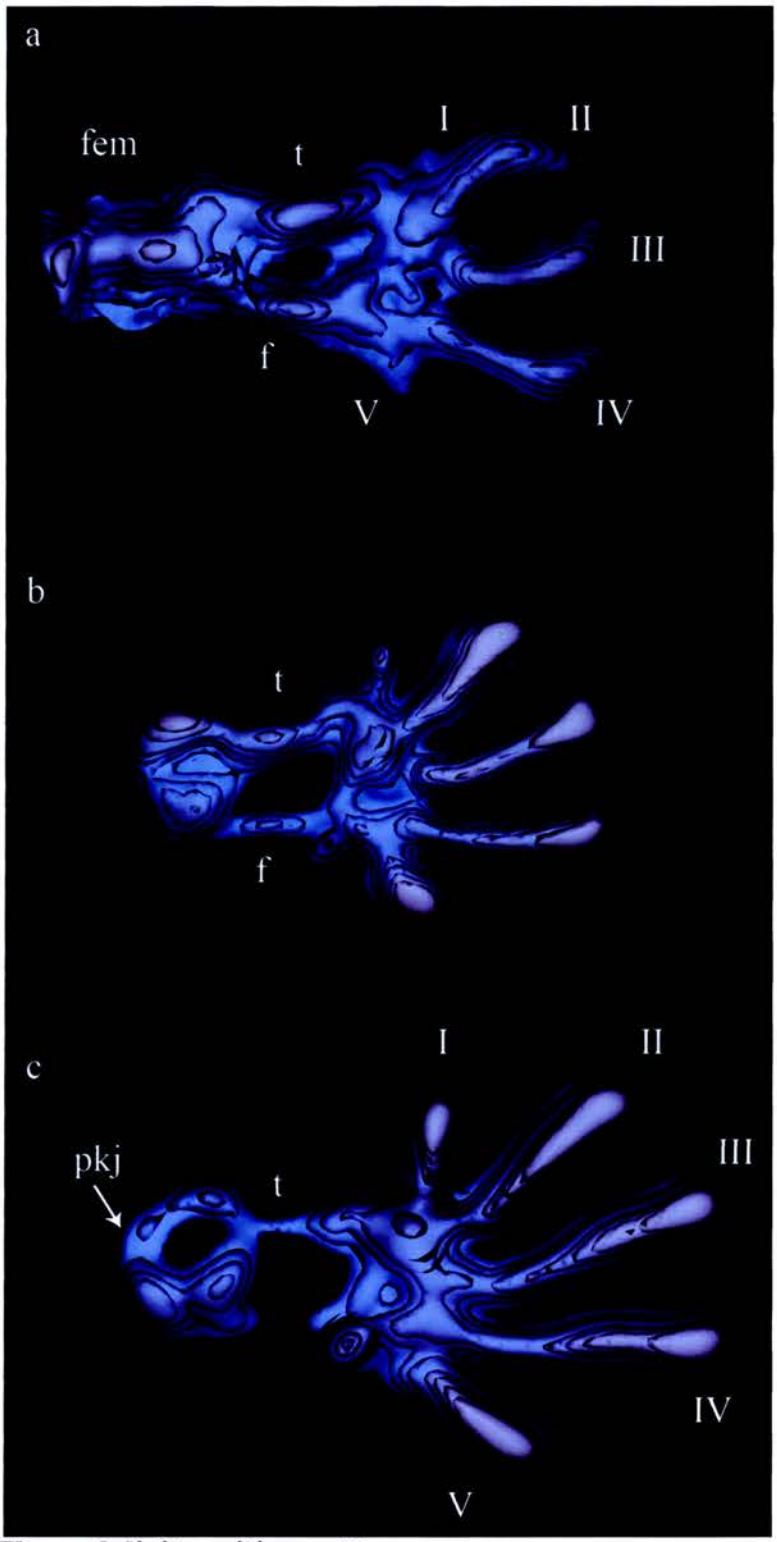

Figure 2.9 The real digit position pattern
Sox9 expression develops in digits I and V, while expression in digits II, III, and IV continues to extend distally. Sox9 expression is lost in some proximal structures, including the femur (fem), followed by the fibula (f), tibia (t) and presumptive knee region (pkj).

Figure 9 and 10 - Loss of Sox9 expression in proximal and posterior regions

The gradual loss of Sox9 expression is seen in a proximo-distal order. The first clear example of this is in the femur, where Sox9 expression is completely absent by the time digital regions I and V are clearly apparent (fig. 2.9b). Further to this, Sox9 expression is lost in the fibula region, shortly followed by the tibia and the knee joint but expression can still be seen in the digital regions (fig. 2.10b).

Figure 10 – Appearance of the phalanges with joint-like regions

Sox9 expression extended distally in the phalanges with the greatest intensity of expression being detected at the distal tips (fig 2.10b). Once the region of expression had extended as far as possible, reflecting the final skeletal pattern, it began to be refined. Higher levels of Sox9 expression were seen in the presumptive proximal, middle and distal phalanges, with less expression between the phalanges marking future joints (fig 2.10c).

2.2.3 Dorso-ventral patterning

The analysis of the Sox9 expression pattern, and any other expression pattern, from more than one perspective allows for a greater number of observations to be made and theories to be formed. For example, the earliest identifiable region of Sox9 expression, which is the presumptive knee joint (pkj) can be clearly identified only when we look at a series of Sox9 expression patterns from a posterior view as marked in fig. 2.11. Surprisingly, the size of this region along the dorso-ventral axis remains relatively constant throughout development, although it may look larger or smaller in relation to other regions of Sox9 expression. Moreover, the general pattern of Sox9 expression from the knee joint to the distal tip is relatively straight with little deviation from the proximo-distal axis. This suggests that any bending seen in the limb during this period of

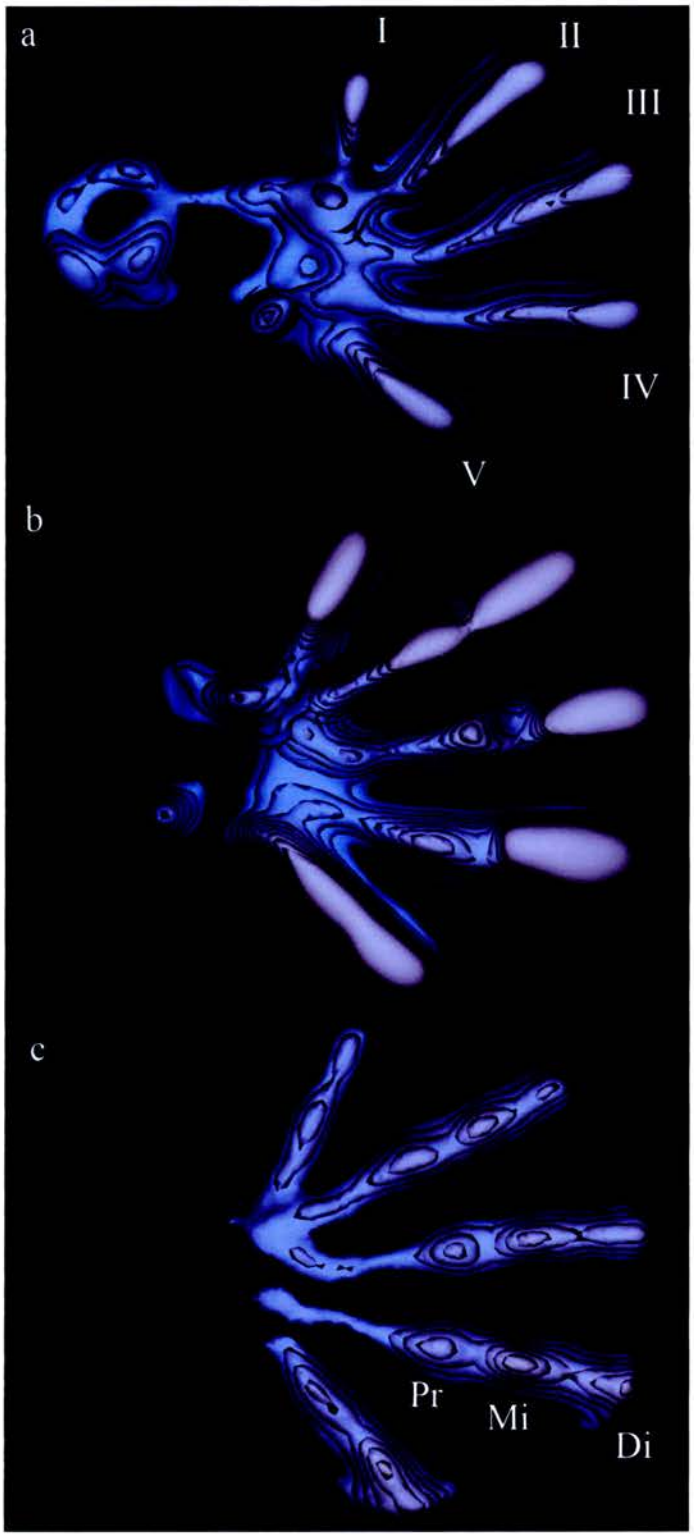

Figure 2.10 Continuation into the phalanges with joint-like regions
Sox9 expression is lost in proximal regions but becomes defined in distal regions, including the proximal (Pr), middle (Mi) and distal (Di) phalanges.

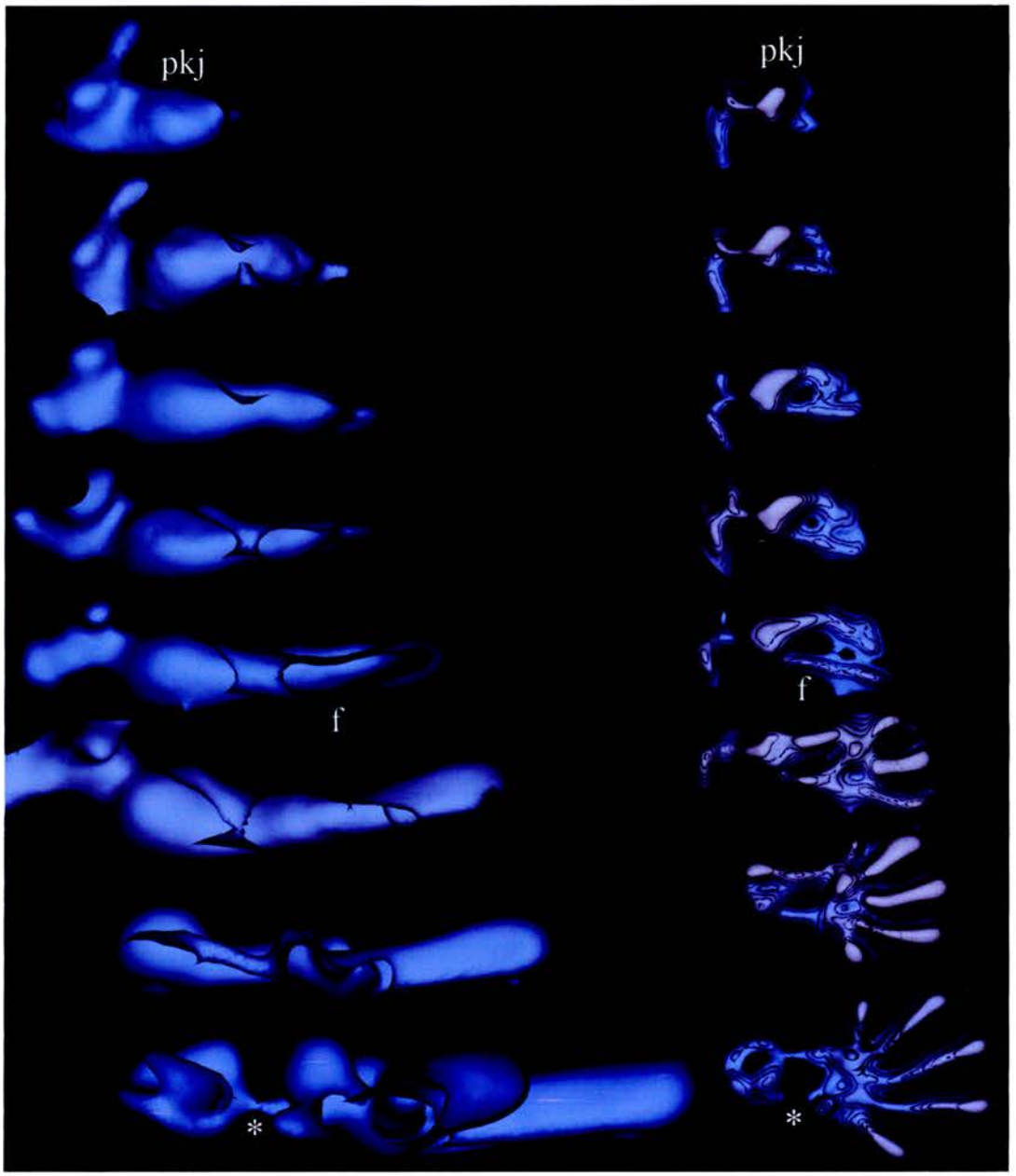

Figure 2.11 Dorso-ventral patterning
Time course series illustrating the dorso-ventral (left) Sox9 pattern in the Mus musculus hind limb (posterior views; distal-right, fibula-front). The time course begins on day 11 with a 'Y shape' pattern and continues until day 13 when the fibula (f) dissapears and the digital regions have extended distally. The prospective knee joint (pkj) begins as an amorphous lump that protrudes along the dorso-ventral axis. Over time, the knee joint grows smaller in relation to the other regions of Sox9 expression. Moreover, the knee joint pattern becomes more defined and continues to remain after fibula (*) expression has dissapeared.

development does not affect these regions rather, it correlates with regions proximal to the presumptive knee joint (fig. 2.11).

2.2.4 The timing of Sox9 expression

Sox9 expression can be seen early on day 11 as a smear across the central region of the *Mus musculus* hind-limb and can be detected until late on day 14, prior to bone formation, when expression is localised to the phalangial regions. Although Sox9 expression was detected over a period of 4 days the majority of patterning events occurred on day 12. The first event observed on day 12 was the formation of a defined region of expression in the proximal half of the limb which became the femur-like region that later branched to form the two zeugopodial regions, which in turn branched to form the digital regions. The last pattern of Sox9 expression on day 12 consisted of the femur, tibia, fibula, digits II, III and IV and the beginnings of digits I and IV. Thus the majority of the skeletal structures were patterned over a space of ~ 24 hours. After day 12 the Sox9 began to disappear in the order that it had appeared; in a mainly proximo-distal order.

2.3 Discussion

The generation and analysis of a comprehensive data set of Sox9 limb expression patterns has been described. The advantage of this data over previously collated data, is that of a much higher temporal resolution and it covers all stages of expression from when Sox9 first begins to be expressed in the hind-limb to when its expression becomes defined within the phalangeal regions. Moreover, a bank of the original data files as well as those generated after computational analysis can be made available for use by the wider scientific community.

2.3.1 Newly developed computational tools

Computational tools used in the 3D analysis of Sox9 *in situ* data allowed for the unprecedented analysis of different levels of gene expression within one sample. In this way, the newly developed computational tools facilitated a semi-quantitative analysis of gene expression.

2.3.2 Does Sox9 expression presages dynamic changes in the cartilage pattern and thus complement histological data of cartilage development?

Early stages of Sox9 expression were comparable to later patterns of cartilage development, as described in the literature. Sox9 expression began in a region representative of the femur, which branched to form regions of expression in the tibia and fibula regions of the limb bud. These two events; the first being de novo expression and the second being Y-shaped branching, have been summarised by Shubin and Alberch (1986) as two of three generalised patterns present during the development of

the tetrapod limb. The third pattern is that of a single element extending to form a single distal element, such as the formation of digital region IV from the fibula-like region.

2.3.3 Do Sox9 expression 'events' conform to Alberch and Shubin's (1986) sequence of events describing limb patterning?

The summary of developmental events produced by Shubin and Alberch (1986), was based on histological evidence of condensation and cartilage formation in a genre of tetrapods. Surprisingly, this same summary is found to be applicable to the dynamic development of Sox9 expression although the gene is known to be expressed prior to any signs of chondrogenesis. This highlights the fact that both prechondrogenic events and the formation of the final cartilage pattern are produced through a similar mechanism in which a de novo pattern is formed that then extends and branches and finally segments into individual segments.

2.3.4 Creation of a digital pattern, the "Digital Arch Model" and the "Metapterygial Axis"

Further analysis of the Sox9 expression pattern revealed that a similar mechanism of development between Sox9 expression and condensation formation, did not translate into an identical dynamic pattern of development. This is most apparent when Sox9 begins to be expressed in the digital regions.

According to the "digital arch model" all digital regions branch off from the posterior zeugopod via an intermediary structure known as the digital arch. The model follows the idea that digital arch is an extension of the metapterygial axis, which runs through the fibula. Although late patterns of Sox9 expression depict a structure connecting digital regions VI, III and II to the posterior zeugopod, the analysis of a slightly earlier stage of development reveals that, in fact, digital regions II and III arise through the branching of

the anterior zeugopod. Thus, all digital regions do not branch off from the intermediary digital arch structure and nor do they all arise from the posterior zeugopod as suggested by the digital arch model (therefore, the prechondrogenic results of Sox9 expression do not support the digital arch model). However, the results do support the idea that the metapterygial axis runs through the fibula. I suggest that in Mus musculus, and probably other mammalian species, the metapterygial axis runs through the femur and the ulnar/fibula and finally through digit IV (fig. 2.12). The suggested end point of the metapterygial axis is supported by the finding that Sox9 expression is seen in the fibula region and then in an extension of the fibula into digital region IV. Moreover, Sox9 expression in digital region IV occurs prior to expression in any other digital region, which concurs with Hinchliffe's (2002) proposal that digit formation begins with digit 4 (Hinchliffe, 2002). However, these results bring into question the importance of the metapterygial axis if not all digits derived from it.

2.3.5 Digit Identity and Digit Order

Development of the digital regions progressed in a largely postero-anterior order, as previously suggested by Hinchliffe (2002), beginning with digital region IV, even in the absence of a digital arch. The last digital regions to form were V and I, with an overall order of digital region development of IV-(III-II)-(V-I). Therefore, the outer two digital regions were the last to form. This digital sequence is in accordance with 'Morse's law of digital reduction' that contrasts the stability of inner digits III and IV with the lability of outer digits I, II and V (Morse, E. 1872; Shubin, Tabin and Carroll, 1997); where the outer digits are first to be lost during experimental manipulations performed on Mus musculus (Holder, 1983) and other tetrapods, such as *Ambystoma* (Oster, 1988). Moreover, the formation of the earliest digital regions IV-(III-II) is reminiscent of that found in the bird manus by developmental biologists (Burke and Feduccia, 1997) elucidating to developmental homology between mammals and birds, providing further argument against the palaentological idea that birds originate from dinosaur ancestors.

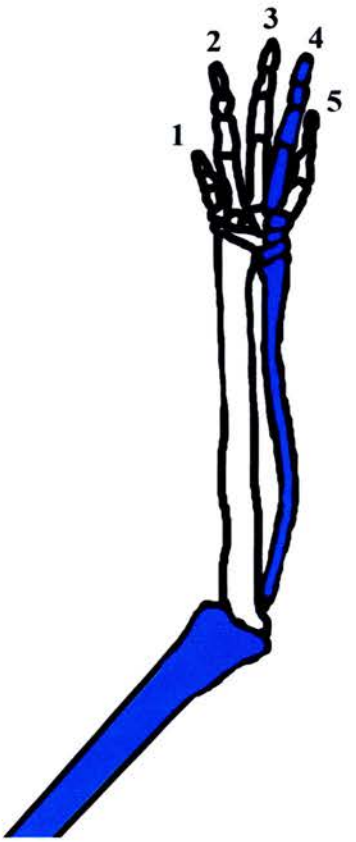

Figure 2.12 Schematic of a mouse hind-limb, with the metaptyrigial axis passing through the femur, fibula and finally into digital region 4.

2.3.6 A new view on skeletal patterning

Here I propose a new view on mammalian skeletal development, the schematic for which is depicted alongside a schematic derived from histological studies of condensation events (Shubin and Alberch, 1986) in figure 2.13. Since, the skeletal development of the *Mus musculus* hind limb is mechanistically comparable to that of the fore limb (personal observation), I have assumed the hind limb to be representative of the mammalian limb. The schematic from the literature only draws on information from studies of the fore-limb, and is also used as a representation of the mammalian limb. I recognise that comparison of the two schemata may be limited, as they are derived from different limb types, but this limitation can be eliminated which will be discussed in section 2.4.

According to our new view on skeletal patterning the stem of the mammalian limb is the result of a series of proximo-distal extension, bifurcation and segmentation events. Bifurcation of the stylopod gives rise to the two zeugopodial regions. The stem then continues through the extension of the posterior zeugopod to form digital region IV, while branching of the anterior zeugopod forms digital regions II and III. This is followed by branching from the base of the digital region connected to the posterior zeugopod resulting in digital region V, and branching from the base of the digital region connected to the anterior zeugopod resulting in digital region I. The resolution and segmentation of all of these regions culminates in the final skeletal pattern.

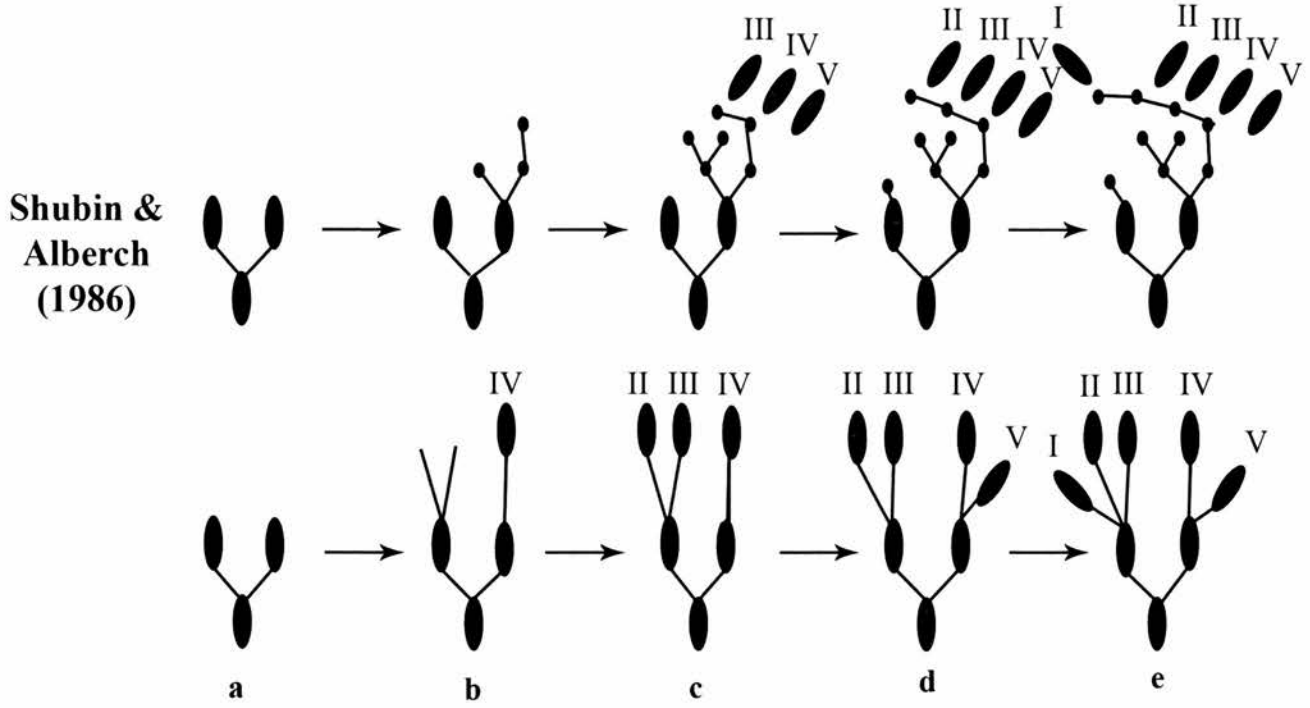

Figure 2.13 Views on skeletal patterning.
According to Shubin and Alberch (1986) digital elements develop from the posterior zeugopod, via the branchial arch (top). However, in accordance with Sox9 expression data digital elements I, II and III branch from the anterior zeugopod and digital elements IV and V branch from the posterior zeugopod (bottom).

2.3.7 Sox9 - a patterning gene ?

Our new view on skeletal patterning based upon the Sox9 expression pattern could be seen as a prepattern model, in the sense that,

'chemical heterogeneity in which the embryonic field is divided into regions of high concentration of chemical substances (morphogens) surrounded by valleys of low concentration',

(Shubin and Alberch, 1986)

is a general reflection of a later histological pattern (cited in the literature). Moreover, early broad patterns of Sox9 expression were found to slowly resolve over time into patterns reflecting skeletal elements. For example, at the base of digital regions Sox9 expression began as a smear with no defined shape, however, over time the expression pattern began to resemble metatarsal elements (fig. 2.10). A further example of Sox9 pattern resolution was seen in the presumptive joint regions (fig. 2.11), where early expression in the form of a continuous rod resolved into distinct skeletal-like elements, between which there were presumptive joint regions. The dynamic nature of the Sox9 expression pattern, suggests that there is not simply a progressive commitment of different regions to a chondrogenic fate but something more regulative. Moreover Sox9 does not seem to simply be a down-stream differentiation factor expressed in cells that have already been patterned (Akiyama, 2002) rather I would suggest that Sox9 may also be a patterning gene. The developmental fate of a cell being initiated as a response to the concentration of the gene, and the cells position within the prepattern (Wolpert 1969).

2.4 Future Work

Does Sox9 have the same pattern of expression in the mouse fore- and hind-limb?

Analysis of Sox9 expression in the *Mus musculus* fore limb bud is necessary to validate the assumption that skeletal patterning in the hind limb bud is comparable to that of the fore limb bud. Only after this analysis has been completed can we assess whether the schematic representation of mammalian skeletal development derived from the hind limb bud, would be applicable to the fore limb bud. Most importantly, it is only then that we can definitively say that the Sox9 expression pattern in the *Mus musculus* limb does not follow the "digital arch" model.

Studying Sox9 expression in other vertebrate species

The completion of Sox9 expression studies in other vertebrate species would be significant in highlighting comparable findings. Importantly, the analysis of Sox9 expression patterns in the chick fore-limb may provide evidence supporting or refuting the proposal that bird digit identity is II-III-IV (Burke and Feduccia, 1997). Moreover, Sox9 expression patterns may provide information into the existence of five archetypal metacarpal regions in the chick limb of which I and V are lost through digital reduction, as claimed by Holmgren (1955). Based upon the idea that the tetrapod metapterygial axis runs through the ulna and digit IV and that digits I and V are lost through digital reduction, I hypothesis that Sox9 expression patterns will support the proposal that bird digit identity is II-III-IV.

Do the anterior digits truly arise from the anterior zeugopod independent of the posterior zeugopod?

Furthermore, experimental manipulation of the chick limb will allow us to test the digital model proposed in this thesis that anterior digits arise from the anterior zeugopod independent of the posterior zeugopod. It is proposed that the removal of the anterior half of the limb prior to the formation of the anterior zeugopod would result in the

formation of only the posterior digit. If a similar experiment were performed *in vitro* on the mouse limb bud then, according to the model of digit development, only digits IV and V should form.

Analysing Sox9 pattern refinement and resolution with respect to the process of chondrogenesis

The observed refinement and resolution of the Sox9 expression pattern could occur through a number of possible mechanisms. One possibility is the migration of Sox9 expressing cells into cartilage forming regions and/or cell death of Sox9 expressing cells in non-cartilage forming regions. A second possibility is that Sox9 expression is down-regulated in non-skeletal regions, such as the presumptive joint, and up-regulated in skeletal-forming regions. To assess the existence of either of these situations I could directly aim to identify the fates of Sox9-expressing cells in the mouse limb by constructing a mouse line that expresses CRE recombinase in all cells in which Sox9 is normally expressed. This may be accomplished by inserting a gfpcre fusion cassette into the Sox9 locus. A similar technique was used by Harfe and associates (2004) to fate map cells that expressed Shh. The groups gfpcre cassette contained a nuclear localization signal and was inserted at the ATG site of Shh, as could be done for Sox9. ES cells in which the gfpcre cassette is correctly targeted can then be used to generate transgenic mice. The insertion of the gfpcre cassette at the ATG of Sox9 should result in the production of GFP cells that normally express Sox9 mRNA. Furthermore, CRE-mediated recombination in Sox9gfpcre cells expressing R26R reporter allele would mark the cells and their descendents by the production of ß-galactosidase (Mao et al, 1999). Thus, Sox9-expressing cells and their descendents can be irreversibly be marked and followed through development. This together with alcian blue staining of condensing cells would allow us to assess the time-points and relative positions Sox9-expressing cells enter the process of chondrogenesis and begin to condense. We would also be able to assess whether all Sox9-expressing cells enter into the chondrogenic pathway. The results, should provide further evidence to support or refute the proposal that Sox9 is simply a differentiation factor (Akiyama, 2002).

Chapter 3 – Generating tools for the quantitative analysis of cell cycle time in the limb

3. 1 Introduction

We are exploring the ways in which cell behaviours combine with various physical models of tissue to generate observed shape changes in the limb. In particular, it has become clear from early modelling results that explaining phenomena as to why the limb bud does not expand like a baloon, may be more complicated than expected (unpublished data). A finite-element model has been created by engineers to explore various parameters related to the growth of the limb. An essential aspect of this project is that empirically measured biological data is combined within the simulation. One essential piece of biological information relates to patterns of cellular proliferation and cell cycle time in the limb.

Cellular proliferation is recognised as playing a crucial role in the growth and patterning of the limb. However, confusion concerning the relationship between cellular proliferation and morphogenesis is rife, possibly due to the emphasis placed on local proliferative zones. For example, outgrowth is occasionally attributed to a group of cells at the distal tip of the limb bud, otherwise known as the proliferative zone, which are thought to be under the control of the AER (Niswander *et al*; 1993). In terms of patterning, local differences in rates and patterns of proliferation are associated with the appearance of new cell types, such as myogenic and chondrogenic precursors (Stockdale and Holtzer, 1961; Marchok and Hermann, 1967; Akiyama *et al*, 2006) however the temporal and spatial development of these local differences has never been fully analysed. Thus, precise control of rates and 'global' patterns of cellular proliferation must be essential for normal limb development but as to how these develop over space and time is still a mystery.

3.1.1 Cellular proliferation and tissue expansion

Cellular proliferation results in the expansion of tissue and ultimately leads to cells occupying different regions within a developing system (fig. 3.1b, Vargesson *et al*, 1997). Thus the study of cellular expansion would give us an insight into rates of cellular division within different temporal and spatial regions of the limb bud, and vice versa. For example, a greater cellular expansion in one region compared to another would indicate that the cells are proliferating at a much higher rate. In fact a recent study into the developmental mechanisms underlying polydactyly in the mouse mutant *Doublefoot* revealed that cell proliferation plays a significant role (Crick *et al*, 2003). In *Doublefoot* mouse mutants abnormal expansion of the autopod along the anteroposterior axis is associated with tissue expansion, which is concomitant with the extension of posterior high cellular proliferation rates. The analysis of this mutant highlights the importance of patterns of cellular proliferation, and thus we can say that the analysis of such patterns in the limb can provide insight into the expansion and growth of the limb bud.

3.1.2 Measuring cellular proliferation

Cellular proliferation is the division of cells resulting in an overall increase in cell number. Proliferating cells proceed through the mitotic cell cycle (fig. 3.1a), which is composed of four phases. The first phase is known as the Gap 1 (G1) phase, during which a cell grows, next is the Synthesis (S) phase when chromosome duplication occurs, after which a cell proceeds through to the Gap 2 (G2) phase and finally divides into two daughter cells during Mitosis (M).

3. 1.2.1 Proliferation studies

Studies on live whole embryonic organs and tissues have been used to follow cell fate and to discover cell lineage. In contrast, the study of how fast groups of cells divide has been completed on groups of homogenised cells using flow-cytometry. However, for the purpose of examining patterns of heterogeneity across a tissue or between tissues, methods such as immunohistochemistry, that preserve the spatial arrangement of the tissue are essential.

3.1.2.2 Relative proliferation studies

Studies of rates of proliferation have involved the use of single labelling techniques. This involves the use of radiolabels, *in situ* hybridisation assays and, more recently, immunohistochemistry using antibodies against single markers of the cell cycle, such as phospho-histone H3 (M phase marker; Scott, 2003; Shibata and Ajiro, 1993). Single labelling allows for relative comparisons to be made between different tissues (e.g. proximal and distal regions of the limb; wild type and mutants; fig. 3.1c, 3.1d). For example, a greater proportion of labelled cells in one population (fig 3.1d, Ihh^{fl}/Ihh^{fl}) compared to another (fig. 3.1d, Col2α1-cre; Ihh^{d}/Ihh^{d}) indicate a greater rate of proliferation. This is illustrated in the diagram in Figure 3.1c where two proliferating cell populations are single-labelled for an S-phase marker. S-phase is the same length in both populations but a shorter cell cycle time for population A compared to population B results in a greater proportion of cells being labelled, indicating that population A is proliferating faster than population B. However, single labelling only allows for the measurement of the ratio between one stage of the cell cycle, such as S-phase, and other stages of the cell cycle. Therefore, an absolute value of cell cycle time (Tc) cannot be calculated using single labelling.

Figure 3.1 The mitotic cell cycle, an example of tissue expansion and single-labelling of proliferating cells.

(a) Stages of the cell cycle. In the first phase (G1) the cell grows. When it has reached a certain size it enters the phase of DNA-synthesis (S) where the chromosomes are duplicated. During the next phase (G2) the cell prepares itself for division. During mitosis (M) the chromosomes are separated and segregated to the daughter cells, which thereby get exactly the same chromosome set up. The cells are then back in G1 and the cell cycle is completed. (b) Fatemap of DiI labelled mesenchymal cells in the chick wing bud at somite stage 18. Proximal mesenchyme injection mid-way in the limb bud (500 μm from somites). Labelled cells expand and occupy the prospective forearm region (Vargesson et al, 1997) (c) Two proliferating cell populations singly-labelled for an S-phase marker. S-phase is the same length in both populations, however a shorter cell cycle time for population A compared to population B results in a greater proportion of cells being labelled. The proportion of labelled cells provides no information about cell cycle time. (d) Differences in the proportions of cells are useful in assessing obvious differences. Chondrocyte proliferation is markedly reduced in Col2α1-cre; Ihh^{d}/Ihh^{d} compared to Ihh^{fl}/Ihh^{fl} littermates at E16.5, with the proportion of BrdU postive nuclei (dark purple) being significantly less in the former compared to the latter (Razzaque et al, 2005).

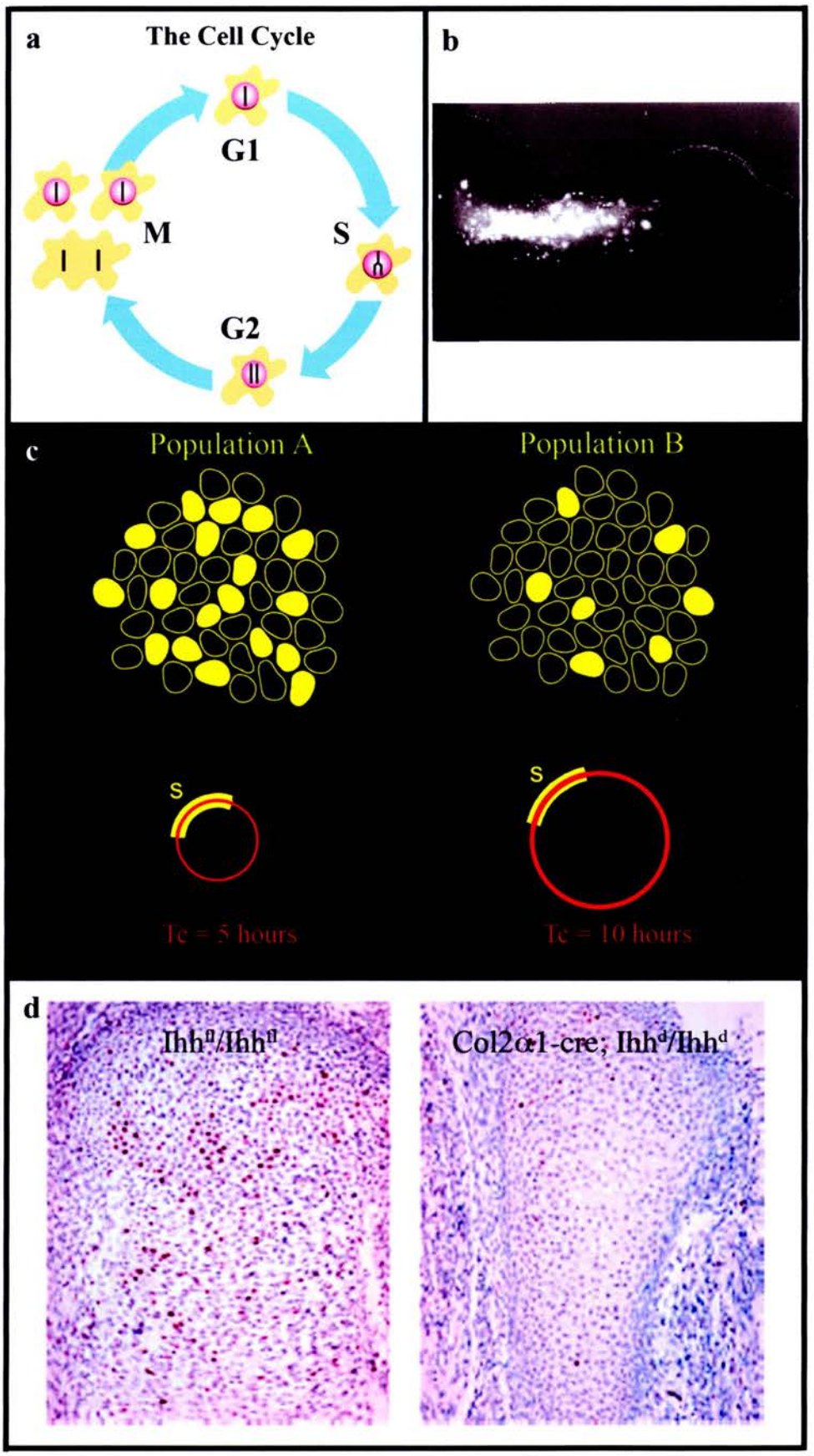
a
The Cell Cycle
G1
S
G2
M
b
c
Population A
Population B
S
S
Tc = 5 hours
Tc = 10 hours
d
Ihh^fl/Ihh^fl
Col2α1-cre; Ihh^d/Ihh^d

3.1.2.3 Determining cell-cycle parameters

A number of antibody markers can be used to deduce absolute cell cycle times, including proliferating cell nuclear antigen (PCNA), Ki67 $_{MIB-1,}$ phospho-histone H3, bromodeoxyuridine (BrdU) and Iododeoxyuridine (IddU). Both PCNA and Ki67 $_{MIB-1}$ antibodies label proliferating cells (Bravo, 1987; Gerdes, 1984), phospho-histone H3 is a M-phase marker (Scott, 2003) and BrdU and IddU label cells in the S-phase of the cell cycle (Shibui, 1989). Samples can be analysed using both tissue sections and flow cytometry.

Flow cytometric anlysis can be performed on synchronously dividing cells (Kubbies *et al*, 1985; Rabinovitch *et al*, 1988; Cai *et al*, 1997) and asynchronously dividing cells (Hui *et al*, 2003; Ormerod, 2004). A study was performed by Hui and associates (2003) in which they analysed samples using BrdU labelling followed by flow cytometry, together with immunohistochemical staining for BrdU and Ki67. From the flow cytometric (FCM) analysis, Ts (S-phase duration in hours) and FCM-labelling index (LI) were obtained and potential doubling time (Tpot) was calculated. From immunohistochemical staining and histological study, histological labelling-index (H-LI) and Ki67 were estimated and combined histological (H-Tpot) was calculated. FCM-LI was found to be strongly correlated with H-LI ($r=0.671$, $p<0.001$), while Tpot was strongly correlated with H-Tpot ($r=0.703$, $p<0.001$), reflecting good agreement between FCM anf histological data. Both FCM-LI and H-LI were positively correlated with Ki67, and Tpot and H-Tpot were both negatively correlated with Ki67. The group deduced that the results of FCM analysis, histological determination and immunohistochemical Ki67 were generally consistent and indicated good validity of various kinetic parameters.

BrdU labelling can not only be used to determine the length of S-phase (Ts) but also cell cycling time (Tc). An early technique that involved the cumulative labelling of

proliferating cells using bromodeoxyuridine (BrdU) followed by immunohistochemistry allowed for the determination of:

1) the proportion of cells that comprise the proliferating population;

2) the length of the cell cycle, and

3) the length of the DNA-synthetic phase (S-phase).

(Nowakowski *et al*, 1989).

The group was able to show that BrdU immunohistochemistry provides a method for the *in situ* analysis of cell cycle parameters for defined proliferative populations. Furthermore, BrdU has been used in concert with other cell cycle markers in double-labelling protocols, providing information about various parameters of the cell cycle (Takahashi *et al* 1992, 1993). Double-labelling studies have been completed using a combination of bromodeoxyuridine (BrdU) and iododeoxyuridine (IddU), which are both thymidine analogues (Shibui *et al*, 1989; Martynoga *et al*, 2005).

3.1.2.3.1 IddU/BrdU double-labelling studies

Briefly, the IddU/BrdU double-labelling technique involves the sequential interperitoneal administration of IddU to a pregnant mouse, followed by BrdU after a defined inter-injection interval (Ti). After a short interval embryos are harvested and fixed. After wax sectioning of the samples, labelled cells are identified with two monoclonal antibodies, one is BrdU specific and the other binds to both IddU and BrdU, as shown in figure 3.2a and figure 3.3. By using the two different fluorescent secondary antibodies and 4',6-diamidino-2-phenylindole (DAPI) staining, three cell populations can be identified; IddU only labelled cells that left S-phase during Ti, BrdU/IddU doubly labelled cells that were in S-phase and DAPI-only labelled cells that did not enter S-phase during the labelling periods (fig. 3.2b, c).

BrdU and IddU are incorporated into newly synthesised DNA during S-phase (Shibui, 1989, Ohta & Ichimura, 2000). For BrdU (and therefore probably IddU) the loading time needed to label an S-phase cell to detectability is estimated at <0.2h shortly after

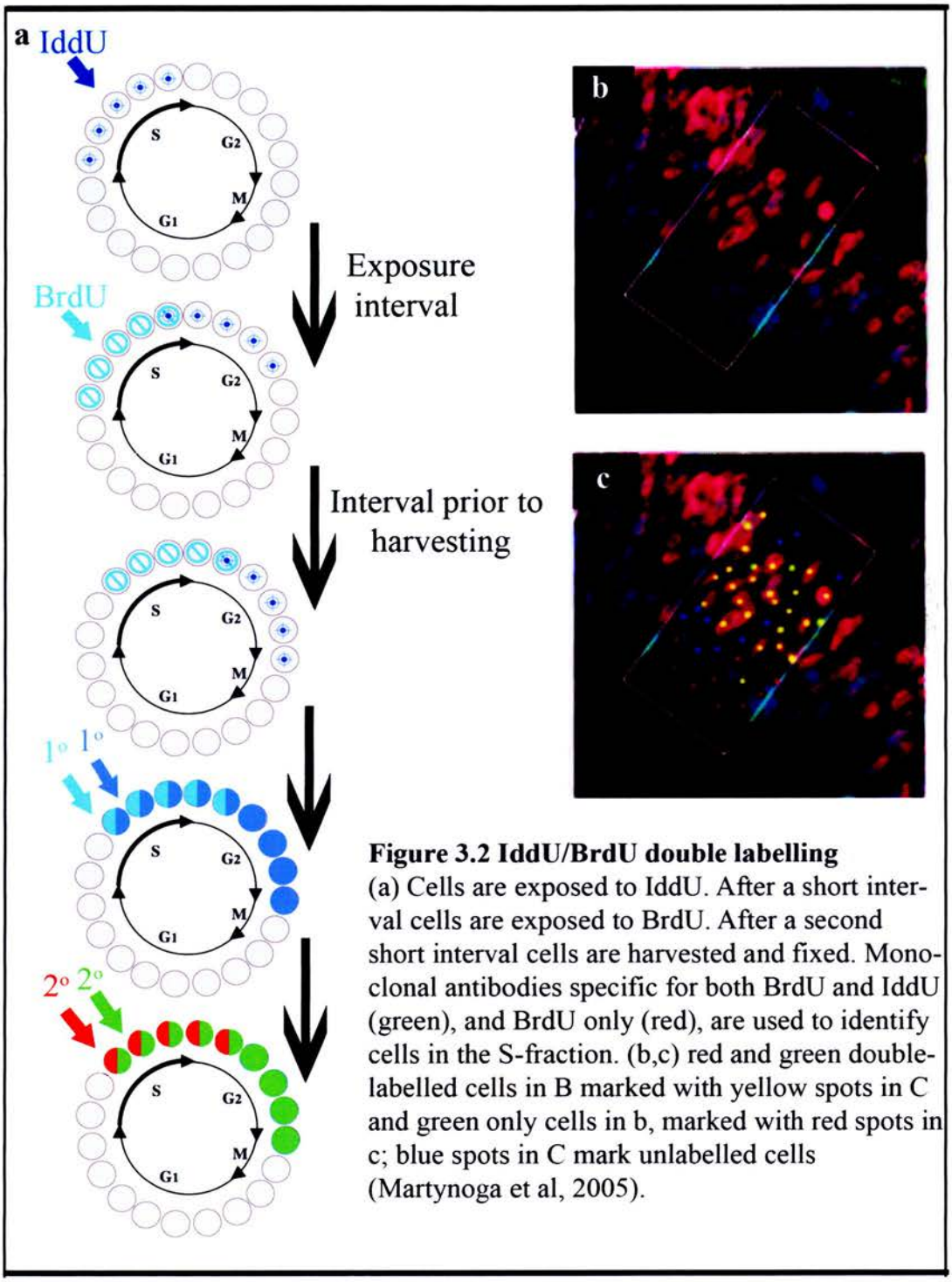

Figure 3.2 IddU/BrdU double labelling
(a) Cells are exposed to IddU. After a short interval cells are exposed to BrdU. After a second short interval cells are harvested and fixed. Monoclonal antibodies specific for both BrdU and IddU (green), and BrdU only (red), are used to identify cells in the S-fraction. (b,c) red and green double-labelled cells in B marked with yellow spots in C and green only cells in b, marked with red spots in c; blue spots in C mark unlabelled cells (Martynoga et al, 2005).

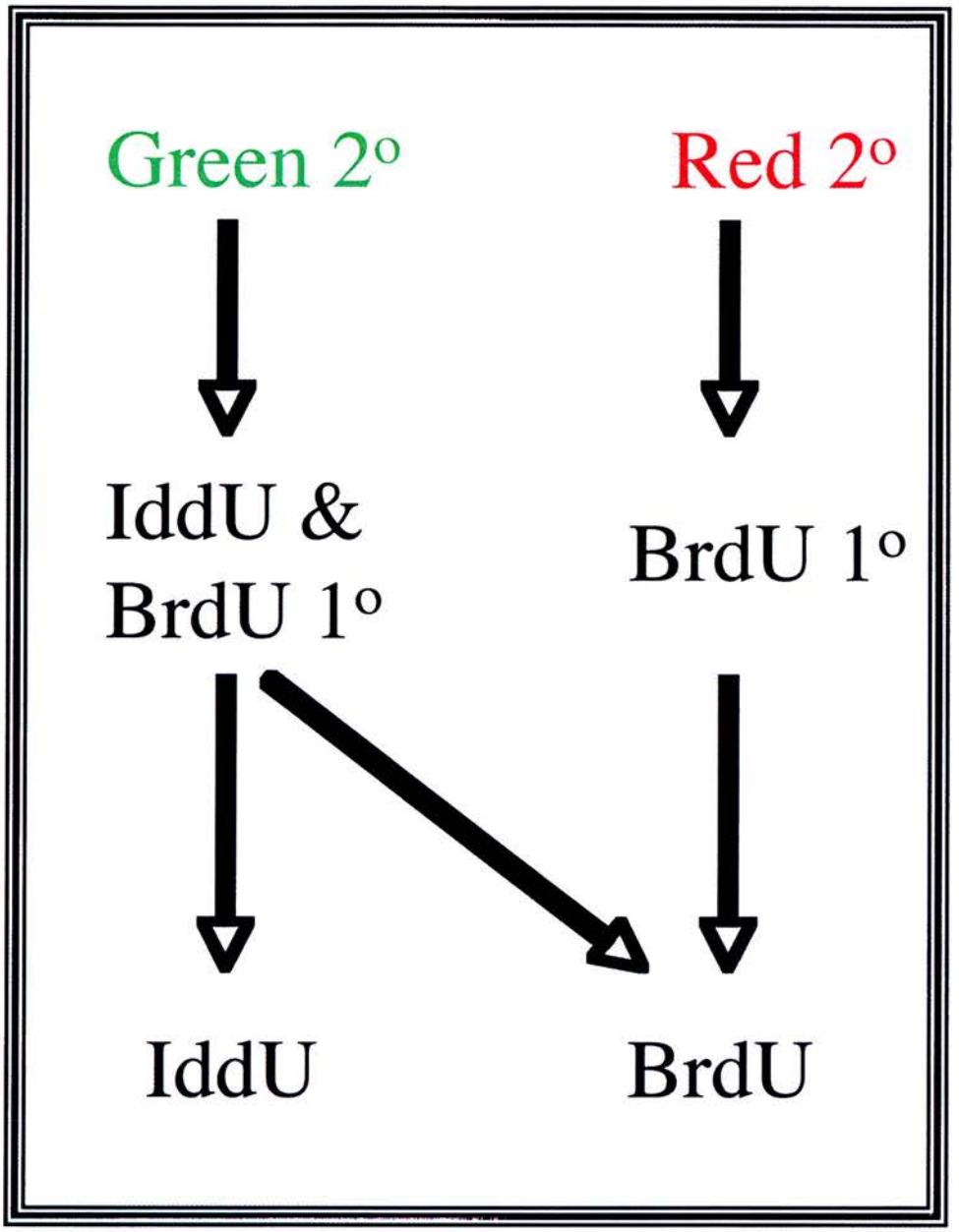

Figure 3.3 A diagram of expected primary and secondary antibody reactivity.

injection of the label, thereafter, cells that enter the S-phase continue to become detectably labelled for approximately 5-6hrs (Hayes and Nowakowski, 2000). The administration of BrdU and IddU at known intervals and their detection using immunohistochemistry techniques together with a total cell count makes it possible to determine quantitative parameters of the cell-cycle including the length of S-phase (Ts) and cell cycle time (Tc), as shown below. Therefore, the Iddu/BrdU double labelling technique allows for a quantitative analysis of proliferation.

$Ti / Ts = Lcells / Scells \quad \therefore Ts = Ti/(Lcells / Scells)$

where $Lcells = IddU^{+} / BrdU^{-}$ and $Scells = IddU^{+} / BrdU^{+}$

$Ts / Tc = Scells / Pcells \quad \therefore Tc = Ts/(Scells / Pcells)$

where Pcells is the total number of proliferating cells in the sampling area.

(Martynoga *et al*, 2005)

The above equation, rests on two main assumptions the first is that all cells are proliferating asynchronously and the second is that the cells consist of a single proliferating population with the same cycling kinetics (Martynoga *et al,* 2005). If either assumption were untrue then the formulae would not produce a trusted result.

The IddU/BrdU double labelling technique has, so far, involved the human scoring and counting of labelled cells and is therefore, prone to human error. Figures 3.2b and 3.2c show an example of IddU/BrdU data, which has to be categorised by eye. Although strongly pink or strongly green cells are obvious, many cells show an intermediate level of staining for one or both fluorescent markers. In fact, all imaging techniques suffer from an intrinsic problem of background. Therefore in practice, the scorer must decide what would constitute a realistic background level for each individual cell. The hope of this project, was that this error could be significantly reduced using computational tools. Moreover, computational tools can comprehensively and rapidly analyse a large amount of data, providing a complete set of information about patterns of cellular proliferation.

Some groups have acknowledged this fact and have used computational tools in analysing important cellular processes and morphogenetic patterns in the limb (Salas-Vidal *et al*, 2001). However, to date, no group has developed and used computational tools to complete a comprehensive quantitative 4D study of cell cycle times in the limb bud.

3.1.3 Aim

I aimed to use the IddU/BrdU double labelling technique to determine absolute values for cell cycle parameters in the mouse limb bud. I hoped to avoid the subjective choice of analysing specific regions of the limb bud and by taking the data set as a whole to create a comprehensive map of cell cycle times using histological sections spanning the entire limb bud. Moreover, we aimed to develop computational tools that would analyse real data that has variations in staining and examples of histological misdemeanours, such as cracks in the tissue. The generated program would be designed to remove the subjective determination of labelled and unlabelled cells. The steps necessary to develop the complete technique are listed here and their individual development is explained fully in the next section.

- Optimisation of three colour staining, which means to make sure that both IddU/BrdU and DAPI staining work successfully on the same limb bud section.
- Checking for antibody cross reactivity to ensure that the staining we see on a section is a reflection of the expected antibody interactions.
- Automatic localisation and measurement of every cell on a section as the manual localisation of cells upon a section is subjective and can bring about human error. Moreover, a computer program can be designed to count and localise the cells on a section at a fraction of the time it would take a human. This makes a significant difference to processing time when there are many cells per section and many sections to analyse.
- Cell based normalisation of staining intensities so that the staining of one cell becomes comparable to the staining of another cell on a section. Therefore, the size and thus the uptake of stain should not make a considerable difference to staining intensity across a section.
- Determination of whether each cell is positively labelled or not, with respect to the staining intensity of the other cells on a section.
- The calculation of regional cell cycle times across an entire section using a computational algorithm.

3. 2 Results

3.2.1 Optimisation of the 3-colour staining technique

In order to analyse cell number an effective nuclear staining technique was required. The nuclear DAPI stain was used however, initial attempts at staining proved problematic. DAPI staining looked smeary across a section, making it difficult to differentiate one cell from the next, as shown in figure 3.4a. A reduction in the amount of DAPI stain used on sections resulted in an improved result with cells easily distinguishable form one another. However, a new problem arose in that individual nucleoli were intensely stained, thus a single cell was marked by a number of intensely stained nucleoli as shown in figure 3.4b. The cell counting algorithm could not successfully segment images of such groups of cells into individual cells as it works on the assumption that a nucleus is uniformly stained with DAPI. In terms of a blue staining intensity distribution a uniformly stained section (fig 3.4c) would produce a distribution of smooth peaks and troughs as in figure 3.4di where each peak represents a cell, and can be segmented and counted as such. However, with a speckled image (fig 3.4b) the blue intensity distribution is irregular and does not reflect cell positions (fig. 3.4dii), where the intense staining of nucleoli can be represented as peaks in the distribution, thus a single cell can be represented by more than one peak. The analysis of such a section would result in a cell being segmented a number of times and counted as more than one cell. Therefore, it was necessary to prevent the occurrence of a speckled DAPI staining pattern. After some analysis it was found the further reduction of DAPI staining and keeping a slide constantly moist during staining prevented the 'speckled' effect producing clear DAPI staining (fig. 3.4c).

A section of cells can be classified as successfully stained when both the DAPI staining and the IddU/BrdU staining have been successful. Therefore, after DAPI optimisation it was necessary to ensure successful IddU/BrdU staining. In some cases DAPI staining

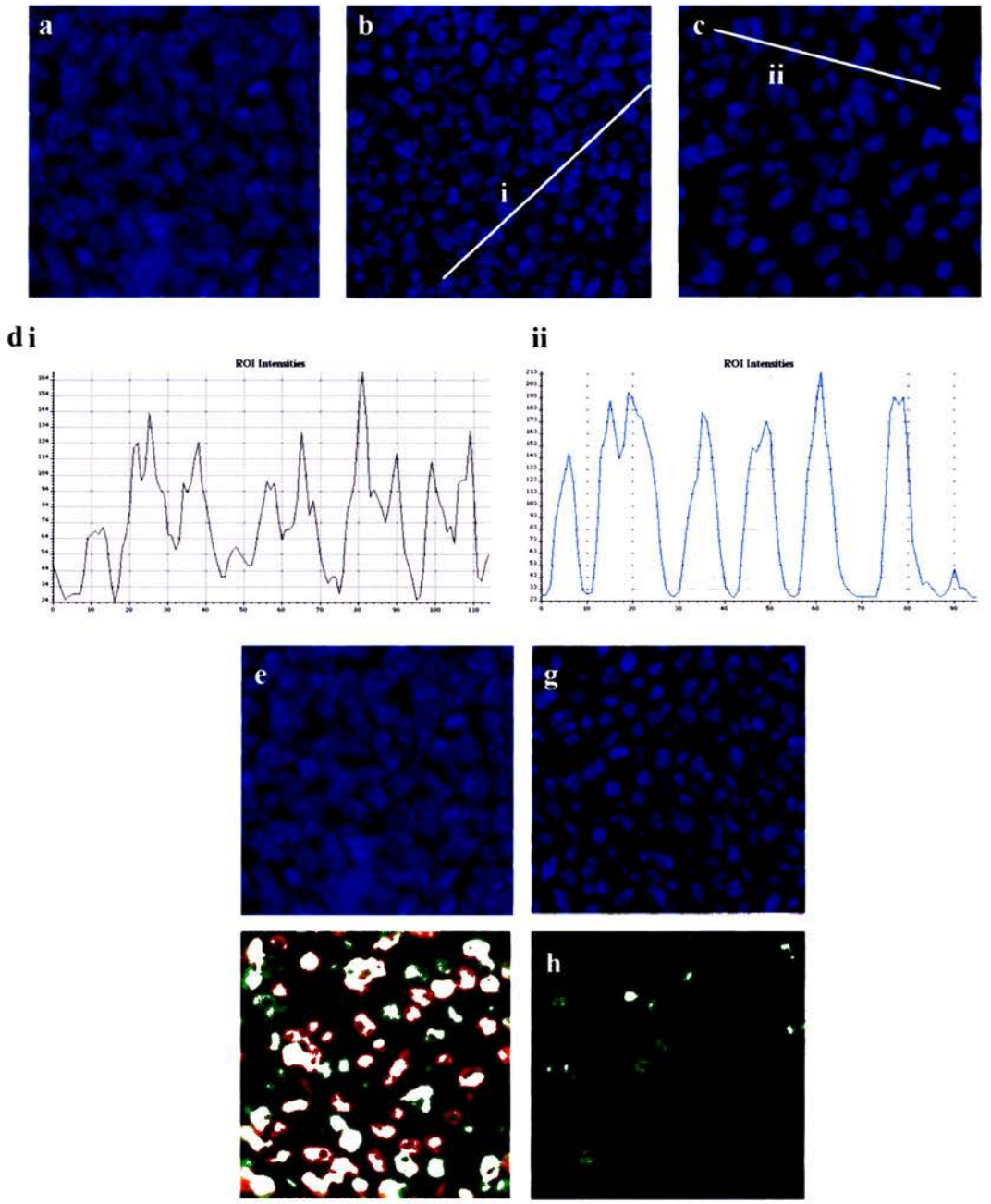

Figure 3.4 DAPI and IddU/BrdU staining optimisation.
(a) Blurred DAPI staining (b) Intense DAPI staining of nucleoli resulting in a speckled effect. (c) Optimal DAPI staining with cell nuclei clearly visible. (d) Plots of blue intensity along a line of cells from b and c. In the case that the staining is speckled, clear peaks are not formed, which means that the computer finds it difficult to determine where each nucleus ends (i). In the case, that we have clear blue staining it is also possible to obtain a clear histogram of blue intensity, with each peak representing a cell nucleus.Section with Blurred DAPI staining (e) and clear BrdU/IddU staining (f) (IddU-only labelled cells are stained green and BrdU or Doubly IddU/BrdU labelled cells are stained red/yellow). Section with clear DAPI staining of cell nuclei (g) and unsuccessful BrdU/IddU staining (h).

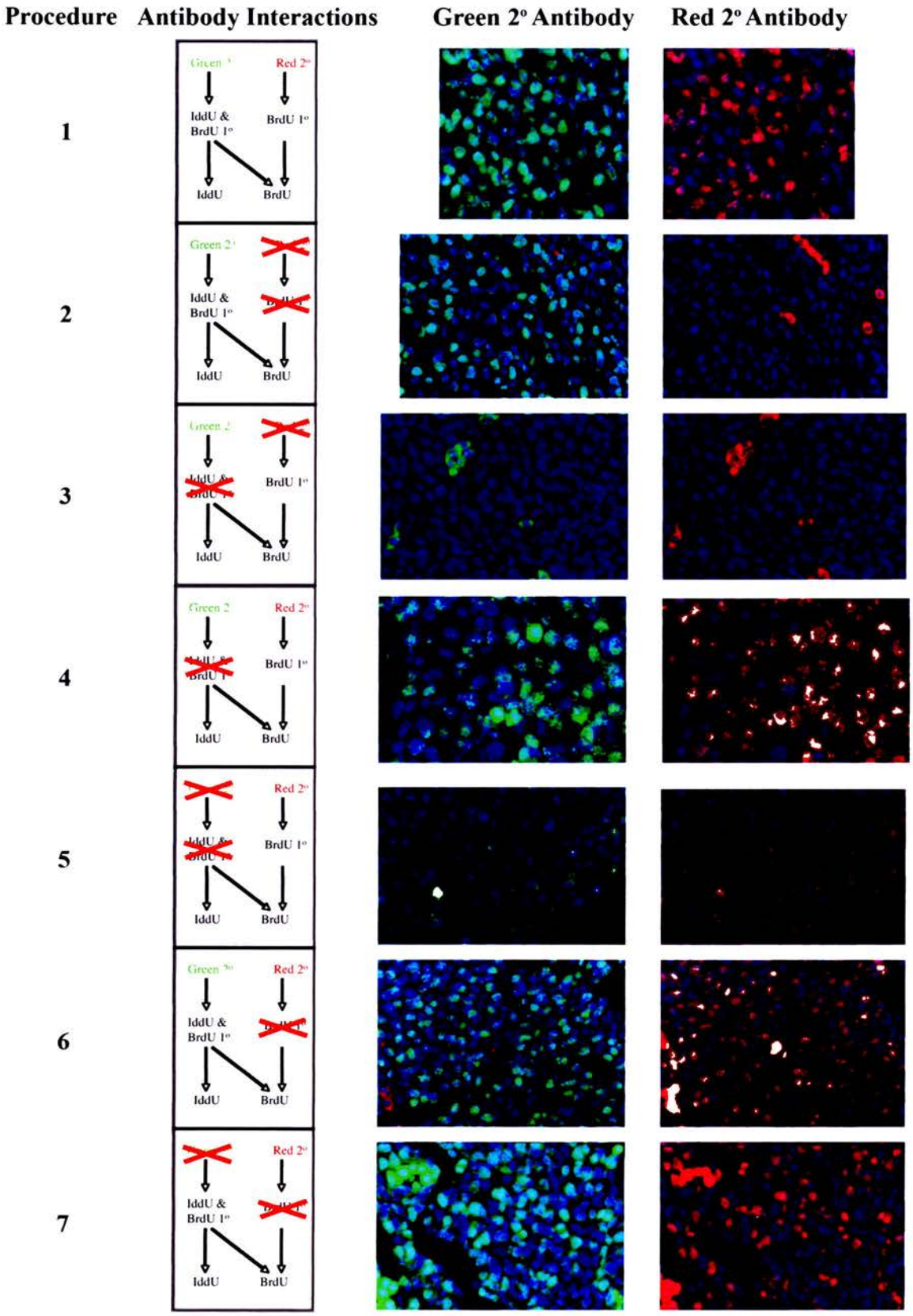

Figure 3.5 Controls for antibody cross-reactivity. Antibodies used on a control section are shown in an interaction diagram in the first column. The second column is of green staining results and the third column is of red staining results. Blue DAPI staining is shown in an all sections. Autofluorescing red blood cells can be seen as brightly stained cells, as in sections in the third row.

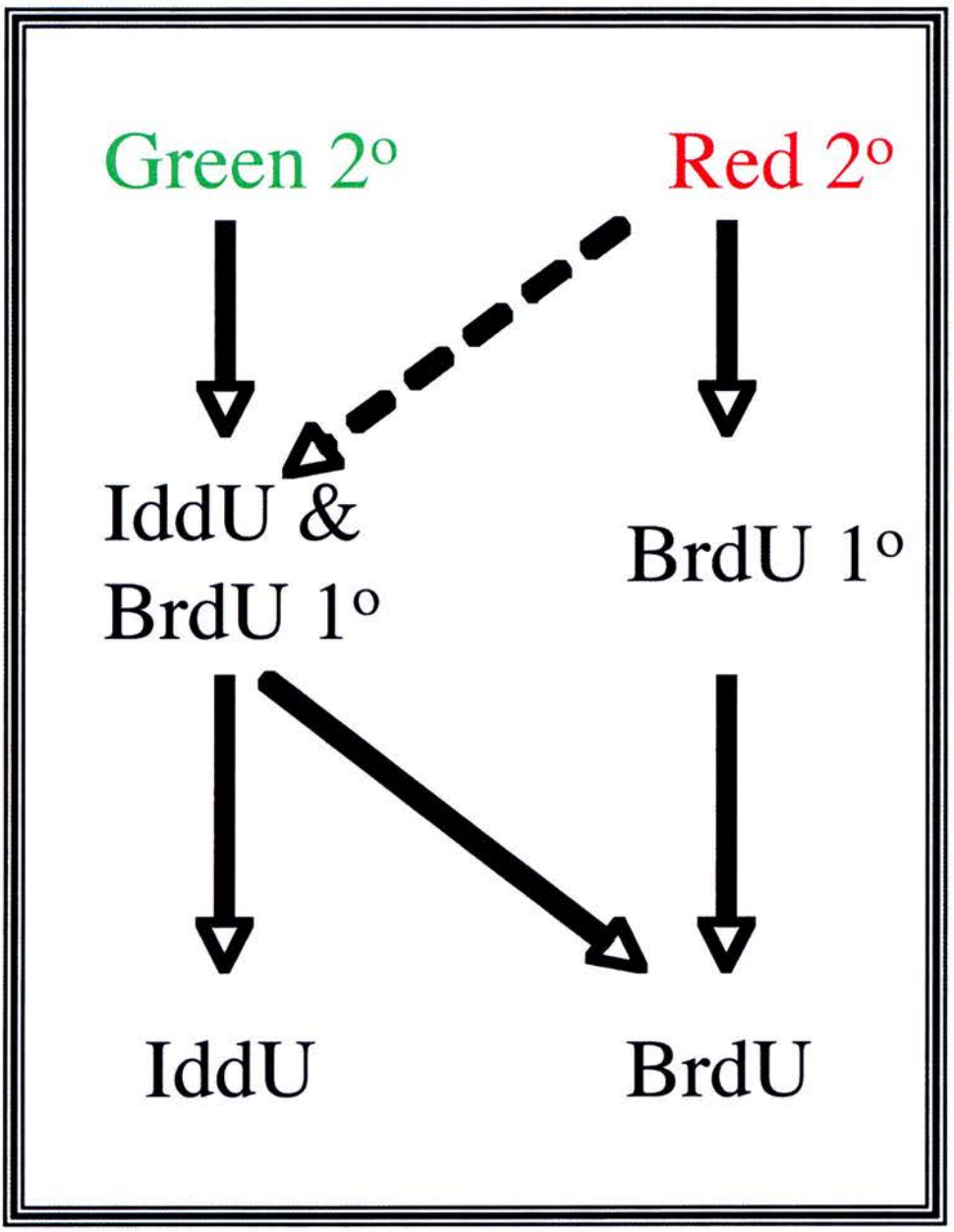

Figure 3.6 A diagram of antibody cross-reactivity.
Solid arrows depict currently known interactions. Dotted arrow depicts a new interaction discovered through the completion of control experiments.

was unsuccessful (fig. 3.4e) with successful IddU/BrdU staining (fig. 3.4f) and in other cases the reverse was observed, suggesting there may be some conflict between the two staining procedure (fig. 3.4g, h). Unsuccessful IddU/BrdU staining could either be attributed to an unsuccessful injection of either IddU or BrdU into the pregnant female or poor staining. Both the former and later were optimised resulting in an overall staining efficiency of over 95%.

3.2.2 Checking for antibody cross-reactivity

Since the aim of this study was to produce an accurate a set of data as possible I wished to verify that the combination of the four antibodies (two primary and two secondary) was working correctly. Therefore, before proceeding with the study, I completed an extensive panel of controls.

The application of all primary and secondary antibodies (fig. 3.5, procedure 1) resulted in cells being stained either red and green or only green. This revealed that the majority of cells were labelled with IddU and BrdU or only IddU, which was expected from what we knew of the reactivity of the antibodies. As expected the green secondary antibody did not cross react with the IddU primary antibody (fig. 3.5, procedure 3) and green fluorescence did not bleed through to the red channel (fig. 3.5, procedure 2).

Upon further inspection, we found that in the presence of only the IddU/BrdU primary antibody, identical staining patterns were obtained for the red secondary antibody and the green secondary antibody (fig. 3.5, procedure 6). Thus, the red secondary antibody did cross-react with the IddU/BrdU primary antibody, represented by a dashed line in figure 3.6. Moreover, in the presence of the IddU/BrdU primary antibody and only the red secondary antibody (procedure 7) identical staining patterns were seen using the red and green fluorescence channels, reminiscent of a pattern of proliferating cells. This result meant that cells labelled with only IddU (and so should only be stained green) would have some red background fluorescence. The occurrence of antibody cross-

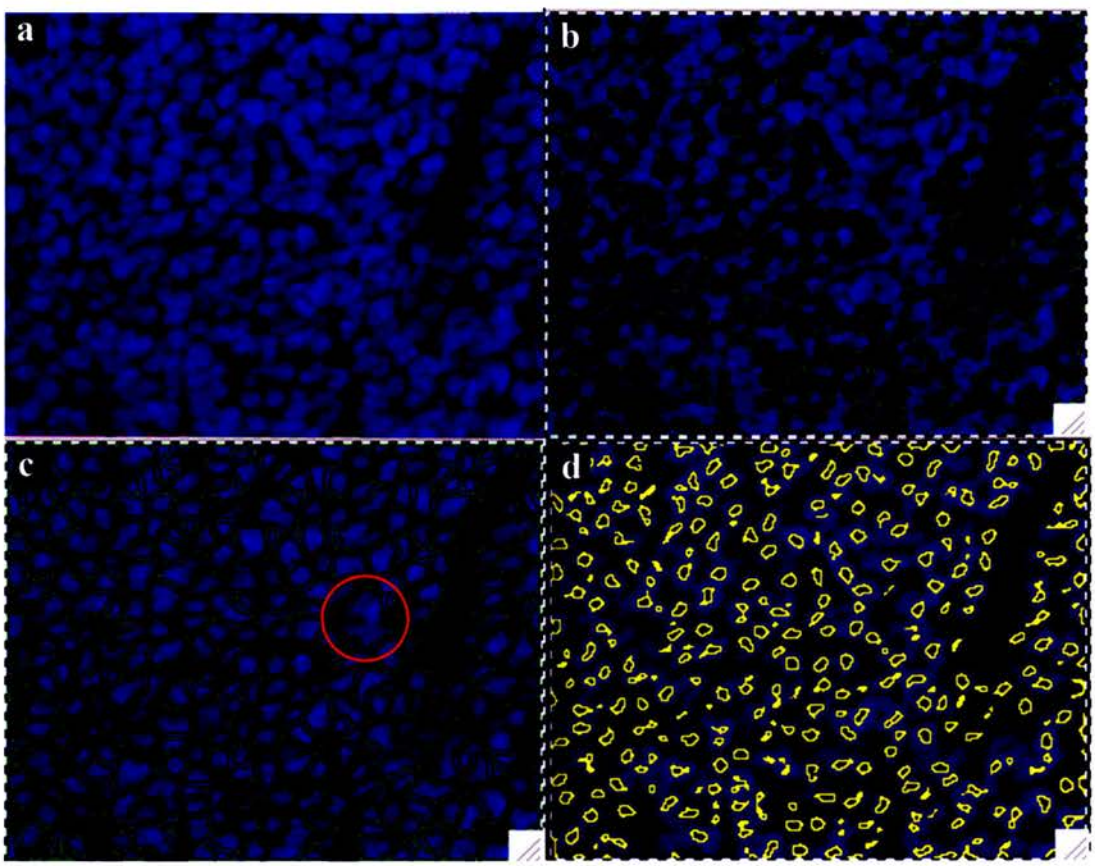

Figure 3.7 Localisation of every cell on a section
Cells are localised by the DAPI staining of their nuclei (a). Inbuilt IPLAB segmentation algorithms produce poor results; classifying groups of cells as a single cell (b). Optimisation of inbuilt alogorithms improves cell-localisation results but some groups of cells are still classified as a single cell (example marked in red) (c). Optimum segmentation results are obtained using our newly generated algorithm (d).

reactivity is quite significant, as the calculation of cell cycle time relies on accurate staining of cells as being either red and green, or only green. Due to the cross-reactivity a higher proportion of cells would look like they are stained both red and green, rather than just green, which would effect calculated values of Tc. When performing the computational analysis we took this finding into account by selecting a staining threshold, above which cells were classified as labelled and below which cells were classified as unlabelled. In other words, cells with intense red staining were classified as labelled for the marker, whereas other cells were classified as unlabelled for the red marker.

A second unexpected phenomenon associated with the red-secondary antibody was that its fluorescence was found to 'bleed' through to the green channel. This meant that red-stained cells could be visualised using both the red and green channels (fig. 3.5, procedures 4, 5 and 7). However, this finding had no significant effect upon our analysis, as all cells stained red should, by default, be stained green.

3.2.3 Automatic localisation of every cell on a section

Commercially available software, such as IPLab can be used to analyse images of cells. IPLab has inbuilt functions, such as 'Autosegment', that can segment an image into its composite units, for example, an image of a tissue can be segmented into individual cells. The program works on the assumption that each cell represents a region of high colour intensity and that there are regions of low staining intensity between cells. However, we found that the inbuilt functionality of IPLab was unable to localise individual cells within a limb section composed of thousands of closely packed cells (fig. 3.7b). The software grouped regions of cells as a single unit instead of locating individual cells. Attempts at optimising the function improved results but some groups of cells were still segmented as a single cell (fig. 3.7c). We realised that even the improved DAPI staining approach (discussed in section 4.2.1) could result in non-uniform DAPI staining, which was posing a problem for the inbuilt function of IPLab.

The program worked on the assumption that all cells had a similar level of staining and that the staining was above a given threshold. In reality, some cells have very low staining intensities whereas others have high staining intensities. Therefore, no amount of optimisation of the inbuilt IPLab functions would result in the successful processing of our section images.

The second phase of the analysis involved the development of my own image processing scripts. The main objective of the scripts was to deal with non-uniform DAPI staining. The scripts were designed to do this by first seeking out cells with low blue intensity and gradually moving on to seek out cells with higher blue intensity, thus all cells, irrespective of their staining intensity, were picked out. Further to this, the average area of a single cell was incorporated into the scripts so that groups of cells were not marked as a single cell. The final result was the successful segmentation of an image with respect to its cellular composition (fig. 3.7d). Finally, the scripts recorded the positions and colour intensities of cells in a text table for the analysis and determination of cell cycle time across a region of cells.

3.2.4 Nucleus-based normalisation

In order to be able to perform 2D analysis on each section using fluorescence microscopes the sections had to be relatively thin (7μm). However, this introduced further problems. A proportion of cells were cut in half and so had incomplete nuclei. Whole nuclei (red square in fig. 3.8a) naturally take up a greater amount of stain than partial nuclei (yellow circle in fig. 3.8a) and therefore, a whole nucleus gives a stronger staining intensity (fig. 3.8b). The difference in staining of different cell nuclei can lead to incorrectly classifying incomplete nuclei as unlabelled nuclei. However, this problem can be overcome by determining the size of a nucleus by analysing the blue image of a section (fig. 3.8c). The red and green staining intensity of a nucleus can then be normalised with respect to the blue intensity of the nucleus (fig. 3.8d and e). Ultimately, the normalisation of nucleus colour intensities across a section allows for the intensities

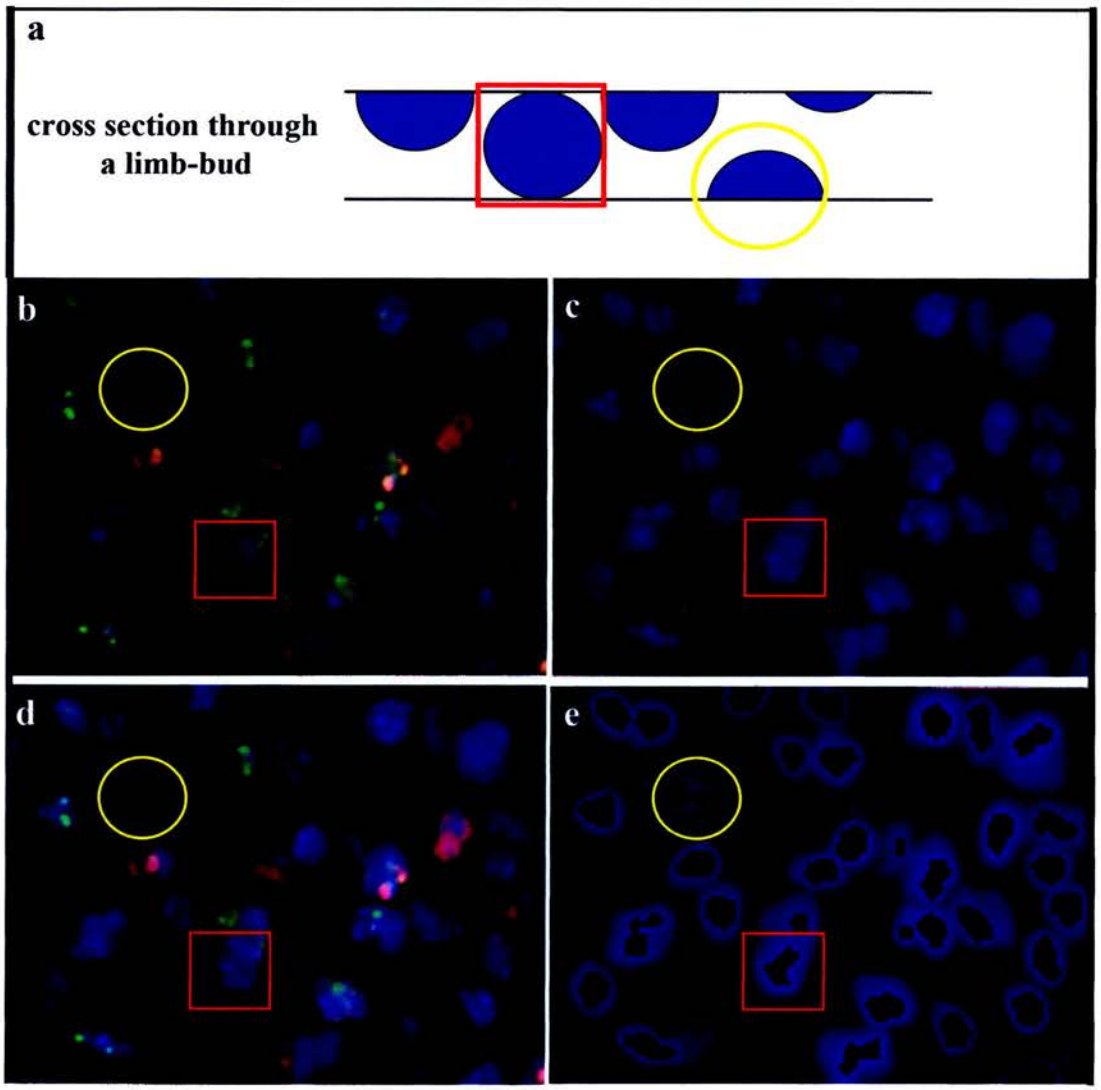

Figure 3.8 Cell based normalisation of sections
A complete cell may have high DAPI staining intensity (cell in red square in a, b and c) and an incomplete cell may have low staining intensity (cell in yellow circle in a, b and c), as there is less of a nucleus to stain. Cells may also have low IddU/BrdU staining intensity (cell circled in yellow in b) or they can have high staining intensity (cell in red square in b). Our alogorithm corrects for cell-based differences by normalising the green and red intensity with respect to the blue DAPI intensity (d, 3-colour image of section; e, blue colour image of section).

to be corrected for the size of a nucleus and helps to prevent labelled nuclei from being classified as unlabelled nuclei.

3.2.5 Determination of whether each cell is positively labelled or not

3.2.5.1 Region sizes

The analysis of a single cell only tells us about the most recent state of the cell, such as S-phase. Therefore, it is not possible to determine the length of the cell cycle (Tc) for a single cell. However, as previous research has shown, it is possible to determine Tc for a group of homogenous cells by using a formula that takes into the account the ratio of IddU/BrdU labelled and unlabelled cells.

Previous limb proliferation studies have involved the subdivision of the limb into regions of arbitrary sizes. For example, a section from the middle of a limb-bud may be subdivided into the proximal region connected to the body, the progress zone at the tip of the limb bud, the dorsal and ventral regions and a central region (fig. 3.9a). By changing the sizes and shapes of these sub-regions it is theoretically possible to produce a wide range of proliferation results and thus come to a varied set of conclusions.

James Sharpe, James Swoger and I attempted to bypass the problems associated with arbitrarily sub-dividing a limb bud by analysing fixed-size, over-lapping regions across whole limb sections. This allowed us to determine local cell cycle times and successfully construct maps of spatial patterns of proliferation. The circular sub-regions were centrally weighted, so that cells at the edge of a circle would have less of an effect upon the overall proliferation rate of a sub-region (fig. 3.9b). The use of small overlapping sub-regions overcame the limitations of arbitrarily sub-dividing a limb bud section and provided a complete view of patterns of proliferation across a limb bud.

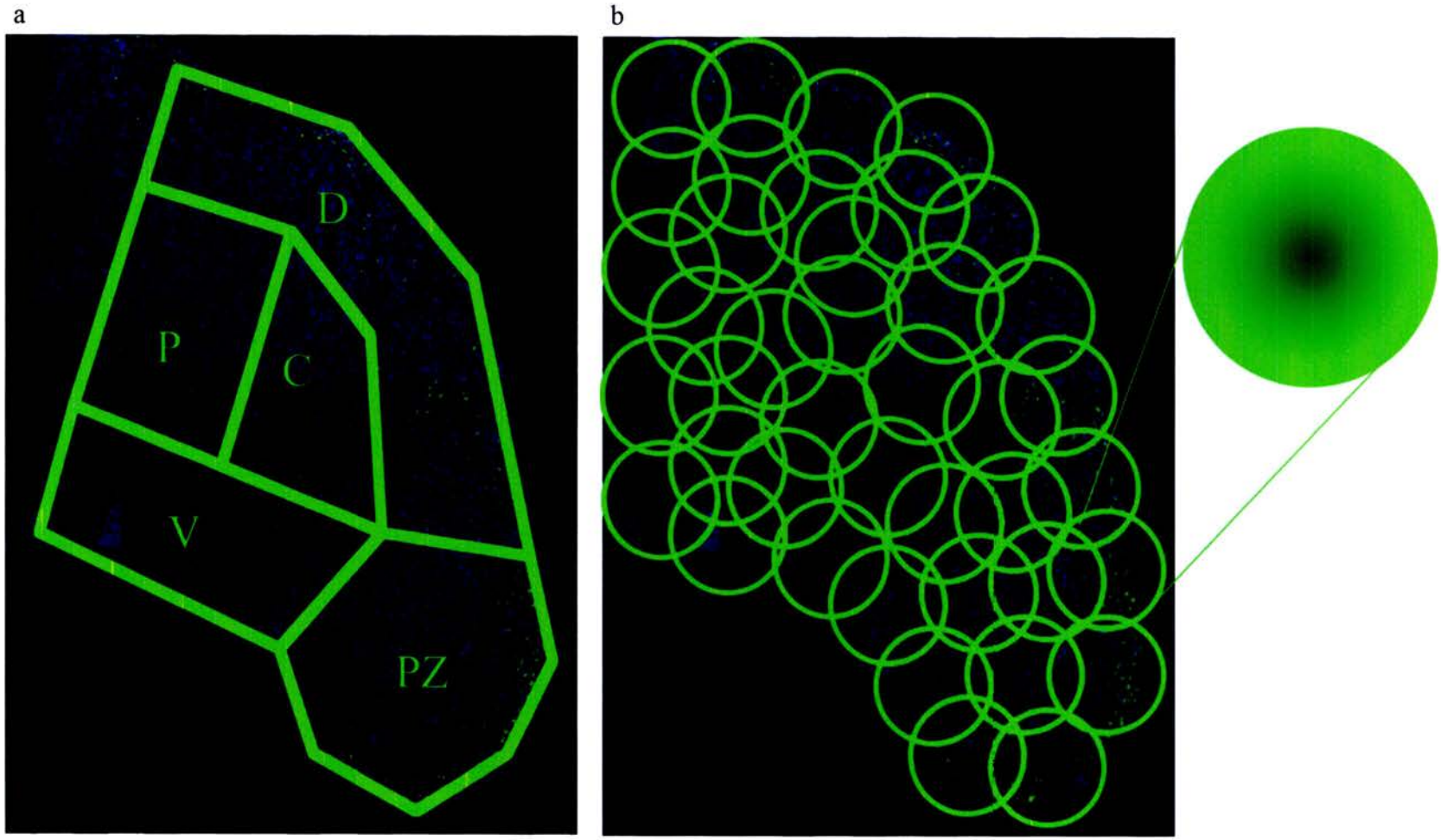

Figure 3.9 Splitting a limb-bud into sub-regions for analysis

Traditionally the limb-bud is split into specific domains for analysis. Five domains are shown on a horizontal section of a E11.5 limb bud (a; P, proximal; C, central; V, ventral; PZ, porgress zone and D, dorsal). Our algorithm analyses small over-lapping sub-regions across the whole limb-bud. The analysis of a sub-region is centrally weighted (green circle), meaning that cells in the centre of a cicle have a greater effect upon the final result of a sub-region than those on the edge (b).

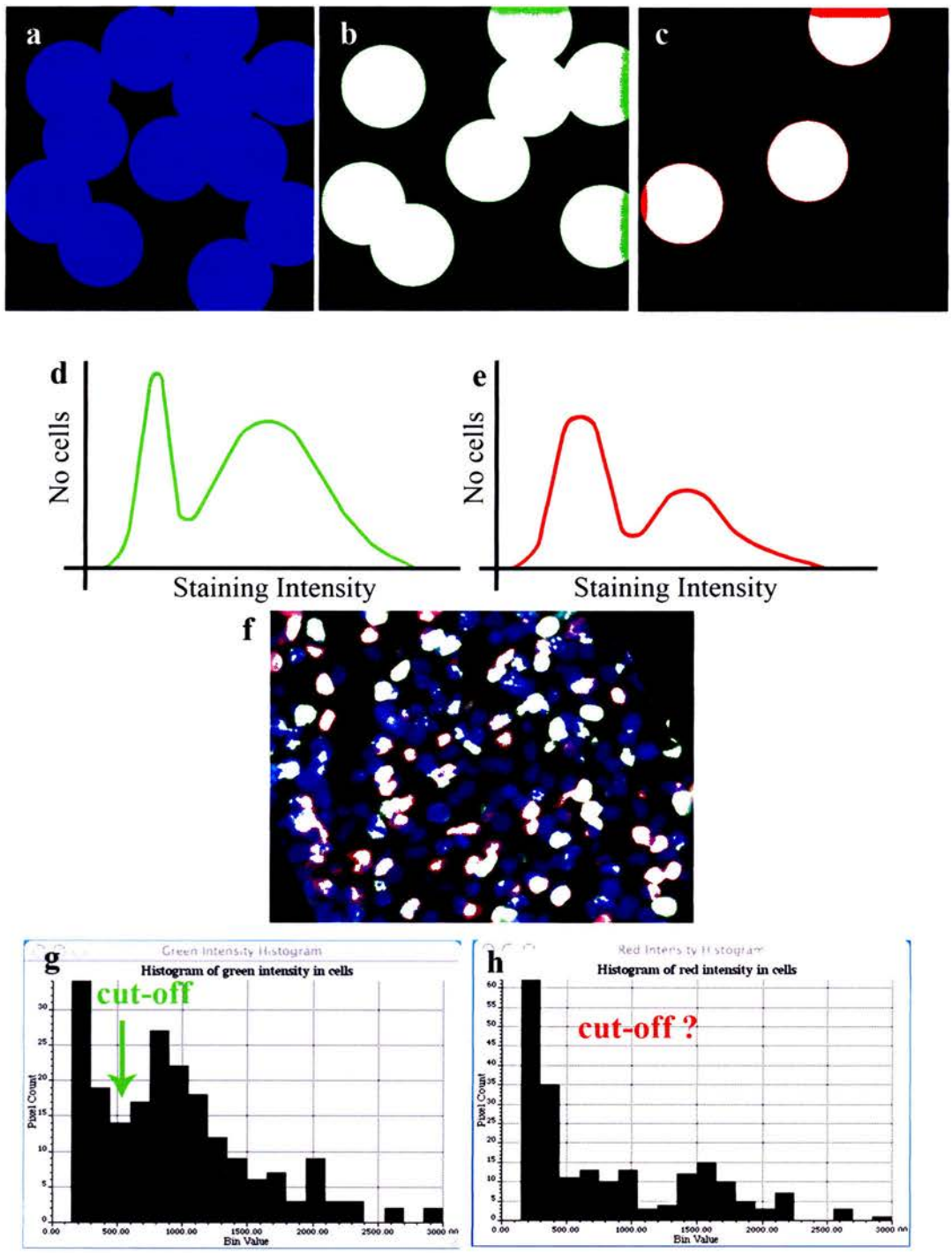

Figure 3.10 Deciding whether a cell is stained green or red

All cell nuclei stain blue with DAPI (a). Ideally some nuclei also stain green (b) and some stain red (c), so if we were to plot red and green staining intensity across a section, we would obtained a bimodal distribution (d and e). The peak to the left would represent cells that have not stained and the peak to the right representing cells that have stained. A real section that has been stained red, green and blue (f) sometimes produces the ideal intensity distribution (g) and so it is easy to select a cut-off to the left of which cell nuclei are classified as being unstained. In some cases an ideal distribution is not produced and a cut-off is more difficult to determine (h).

3.2.5.2 Extracting histograms from tissue regions

In order to complete a calculation for cell cycle time it is necessary to know the numbers of cells stained red, green, or blue. In an ideal cell population, all cells would be stained blue (fig 3.10a), of the blue stained cells some would also be stained green (fig. 3.10b), and of the cells stained green some would also be stained red (fig. 3.10c). If we were to plot the green and red staining intensities of the ideal cell population the resulting histogram would be bimodal. The first peak would represent unstained cells and the second peak would represent stained cells (fig. 3.10d and e). Thus, the trough of the histogram would represent a threshold cut-off – where the left of the cut-off represents a cell colour intensity that is classified as 'off' and the right of the cut-off represents a cell colour intensity that is classified as 'on'. In reality, a section that may seem as though it could be counted manually (fig. 3.10f) can produce both a bimodal and a non-bimodal distribution (fig. 3.10g and h).

Therefore, we needed to develop an algorithm that made a sensible and consistent choice of cut-off thresholds for all analysed sub-regions, irrespective of the presence of a bimodal distribution. Moreover, the algorithm was designed with the intention that it would be able to cope with variations in embryo age, proliferation rates and experimental variation, such as different staining intensities and background staining. However, this was made difficult by the issues to be discussed in the next two sections.

3.2.5.3 Histogram alignment I: Coping with different intensities across the section

In some cases we found uneven staining across the section, which meant that sub-regions of the same section had different staining intensities (fig. 3.11a). Thus two sub-regions may have had similar proliferation rates but because of the difference in staining the calculated Tc value may be different for the two regions. This is because the

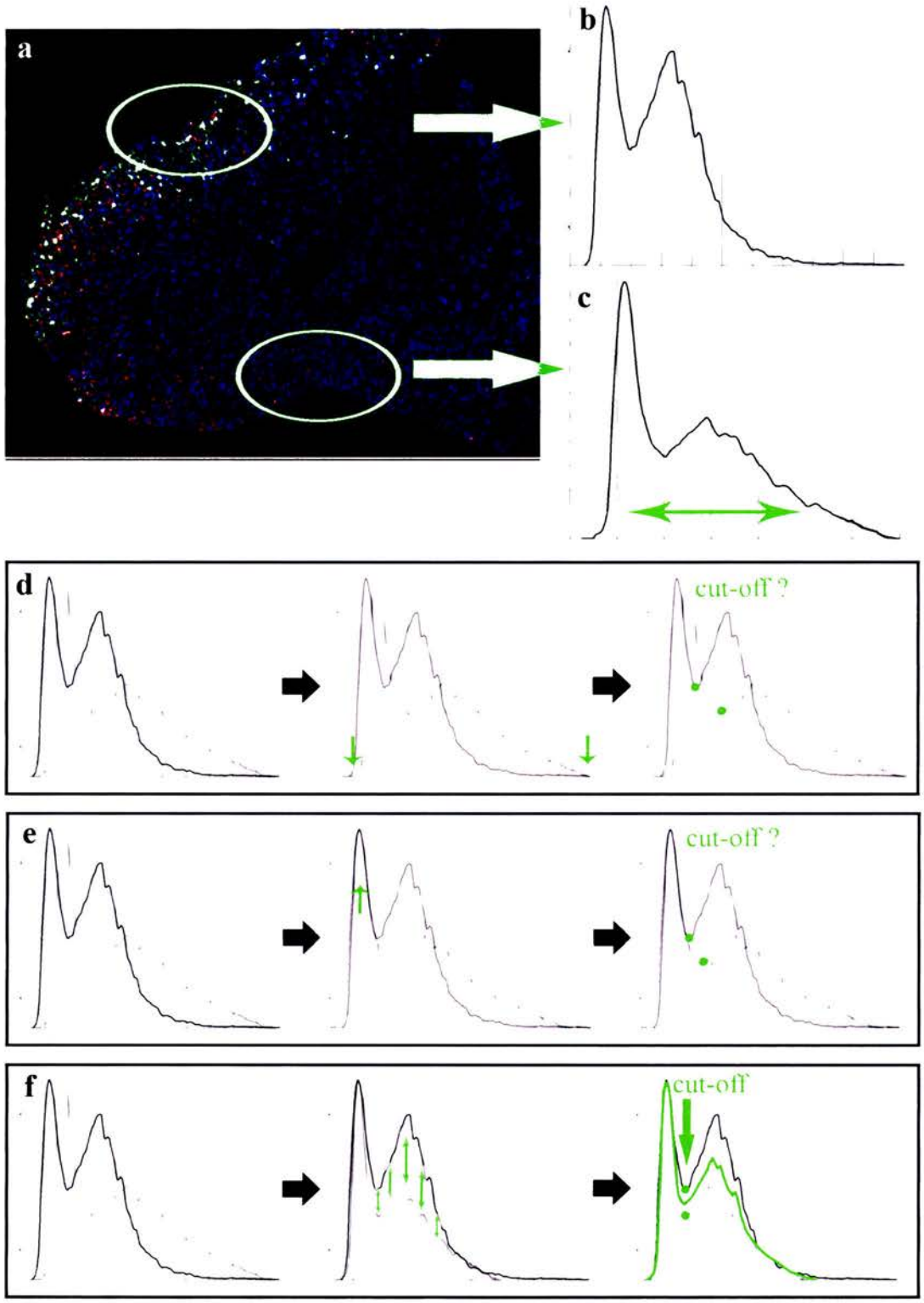

Figure 3.11 Analysing sections with variations in staining intensity
Variations in staining intensities across a section (a) have an effect upon sub-region intensity histograms (a theoretical representation of this effect is shown in b and c). To obtain a cut-off for a section the various sub-regions histograms must be aligned with one another. Aligning histograms by their minimum and maximum value along the x-axis was unsuccessful in pinpointing a single cut-off for all graphs (d). Aligning histograms by their first peak was also unsuccessful (e). Fitting sub-region histograms by using a method of least squares difference produced an average histogram, which had a cut-off that could be applied to sub-region istograms (f).

intensity histogram for one region may have a wider intensity distribution compared to another region, as shown in figures 3.11b and 3.11c, resulting in a different threshold cut-off for each histogram and a different proportion of cells classified as "on". This is true for both green and red staining. Therefore, a consistent cut-off threshold could only be found by independently applying a correction to the red and green intensity histograms derived from the sub-regions of a section.

To overcome the observed variation in intensities we tried to align the intensity histograms for all sub-regions with one another. The successful alignment of the histograms would mean that a single intensity correction and a single cut-off threshold could be chosen for all sub-regions. This would be equivalent to carefully brightening or darkening the red or green channel for each sub-region so that all regions end up looking similar in colour intensity. This is possible as long as each sub-region has at least one positive intensely labelled cell to define the upper limit of the regional histogram. Initially we attempted to align histograms by the minimum and maximum of the distribution along the x-axis, which was ineffective (fig. 3.11d). Some histograms aligned better without this correction. A second strategy that was employed involved aligning the first peak (i.e. the off peak, fig. 3.11e) however, the first peak may be very small and difficult for the program to distinguish within an intensity distribution. Therefore, there were a number of examples where the alignment of the histograms was unsuccessful. Our third and final strategy was to align histograms by using a method of least squares difference between histogram distributions (fig. 3.11f). Sub-region histograms were scaled with respect to one another, without shifting along the x-axis in order to reduce the difference between them. This strategy proved to be relatively successful and allowed for a single cut-off threshold to be determined for the sub-regions of a section for both the red and green intensity.

3.2.5.4 Histogram alignment II: Coping with difficult histograms

Although the alignment protocol within the computational algorithm was quite successful it was not able to cope with some extreme intensity distributions, which are deemed to be 'bad' distributions (fig. 3.12). The extreme distributions were a product of extreme proliferation rates and the sampling of a small section with few cells, resulting in only a few sub-region histograms per section ('bad' distributions in fig. 3.12). It was found that although large sections may also have extreme proliferation rates the high number of cells present on the section (>1000) resulted in the generation of many sub-region histograms and a better alignment (e.g. 'good' green histogram farthest right).

On any given histogram there is an apparent cut-off point. However, to understand where the "real" cut-off should be for a given histogram I explored hypothetical uni-modal "on" and "off" distributions that could be combined to create a realistic bimodal intensity distribution, for which step-by-step instructions are given in fig. 3.13. The underlying assumption of this analysis was that the two uni-modal populations were independent of one another and that both had a certain level of noise effecting their distributions. My exploration involved selecting a range of bimodal intensity distributions and then sub-dividing them into their two unimodal constituent distributions. In theory, the number of "off" cells is the total number of cells to the left of this cut-off point. This sum was used to calculate where the cut-off should be on the bimodal histograms. In all cases, the calculated cut-off was at the same point at which the uni-modal histograms intersected.

During the completion of my analysis I realised that a single distribution could be composed of a number of different sets of unimodal distributions (fig. 3.14). In some cases, the intersection of the two unimodal histograms lay directly below the trough of the bimodal histogram (fig. 3.14 middle panel) and thus, the calculated cut-off (fig. 3.14 middle panel, red arrow) matched what we had previously assumed to be a suitable cut-

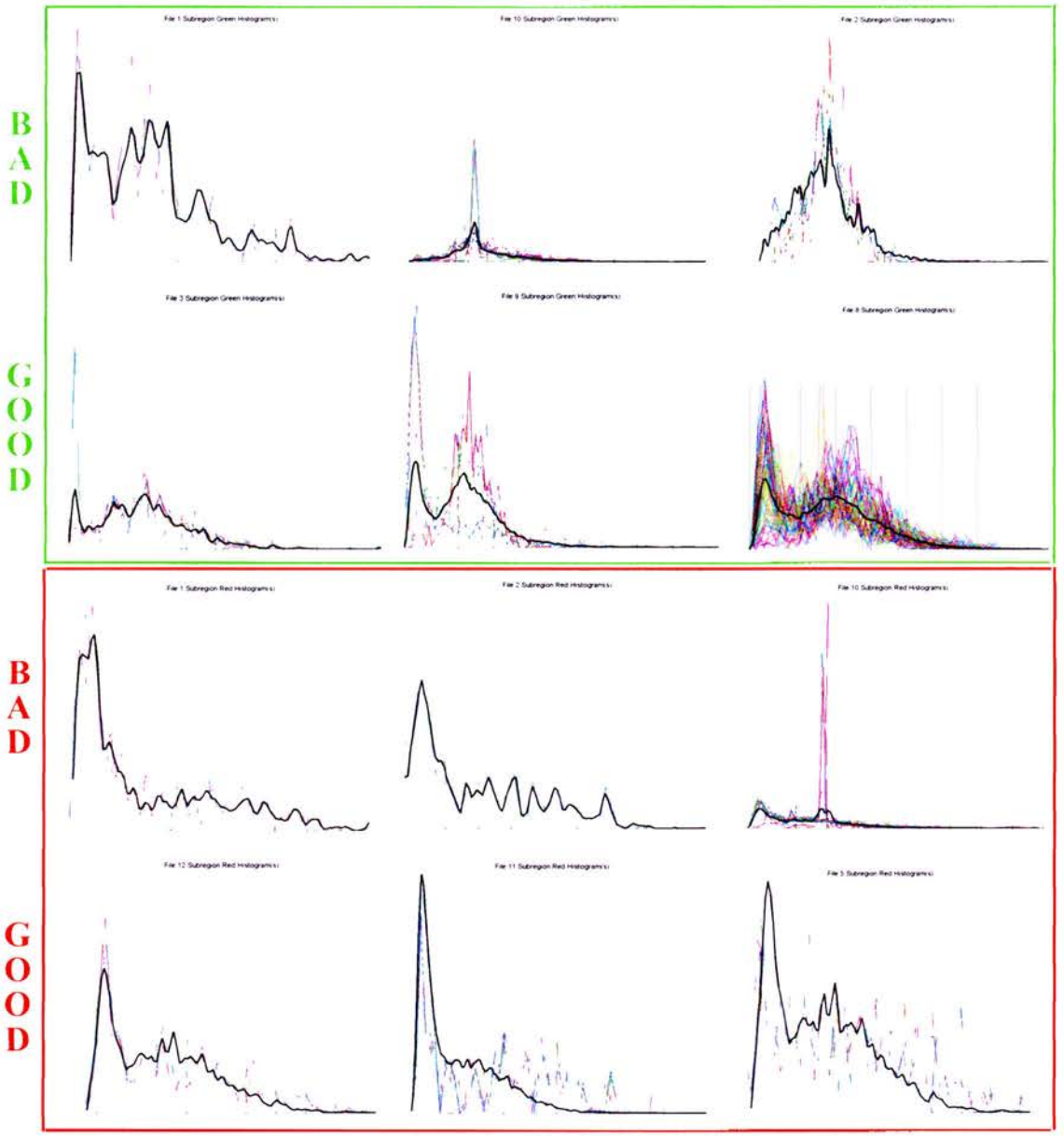

Figure 3.12 Examples of "good" and"bad" sub-region histograms for both the green and red colours

Histograms for which a cut-off can be easily selected are classified as "good" and those for which a cut-off cannot be selected easily are classified as "bad".

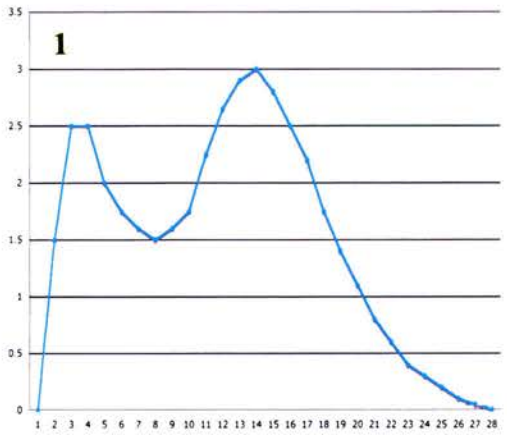

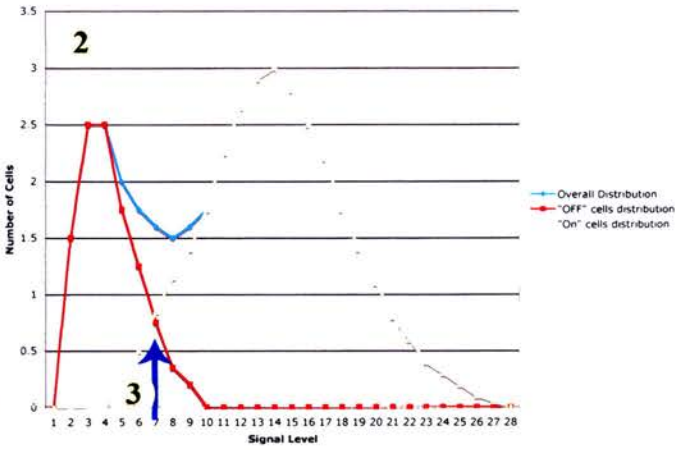

X-axis point	overall	sum overall	"off"	"on"	"off" + "on"
1	0	0	0	0	0
2	1.5	1.5	1.5	0	1.5
3	2.5	4	2.5	0	4
4	2.5	6.5	2.5	0	6.5
5	2	8.5	1.75	0.25	8.5
6	1.75	10.25	1.25	0.5	10.25
7	1.6	11.85	0.75	0.85	11.85
8	1.5	13.35	0.35	1.15	13.35
9	1.6	14.95	0.2	1.4	14.95
10	1.75	16.7	0	1.75	16.7
11	2.25	18.95	0	2.25	18.95
12	2.65	21.6	0	2.65	21.6
13	2.9	24.5	0	2.9	24.5
14	3	27.5	0	3	27.5
15	2.8	30.3	0	2.8	30.3
16	2.5	32.8	0	2.5	32.8
17	2.2	35	0	2.2	35
18	1.75	36.75	0	1.75	36.75
19	1.4	38.15	0	1.4	38.15
20	1.1	39.25	0	1.1	39.25
21	0.8	40.05	0	0.8	40.05
22	0.6	40.65	0	0.6	40.65
23	0.4	41.05	0	0.4	41.05
24	0.3	41.35	0	0.3	41.35
25	0.2	41.55	0	0.2	41.55
26	0.1	41.65	0	0.1	41.65
27	0.05	41.7	0	0.05	41.7
28	0	41.7	0	0	41.7

5

4

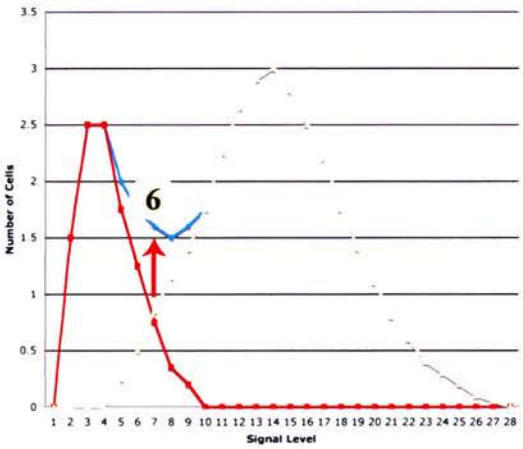

Figure 3.13. Calculating the cut-off point from the intersection of two possible underlying distributions of "on" and "off" cells.

1 - Select a bi-modal histogram

2 - Plot the hypothetical distribution of "on" and "off" cells.

3 - Find the point of intersection of the "on" and "off" histograms.

4 - Calculate the sum of cells to the left of the intersection

(cells to the left of the intersection in the red histogram + cells to the left of the intersection in the yellow histogram)

5 - Calculate the cumulative sum of cells in the bi-modal histogram along the x-axis until the total is equivalent to that calculated in step 4.

6 - The point reached along the x-axis is the calculated cut-off.

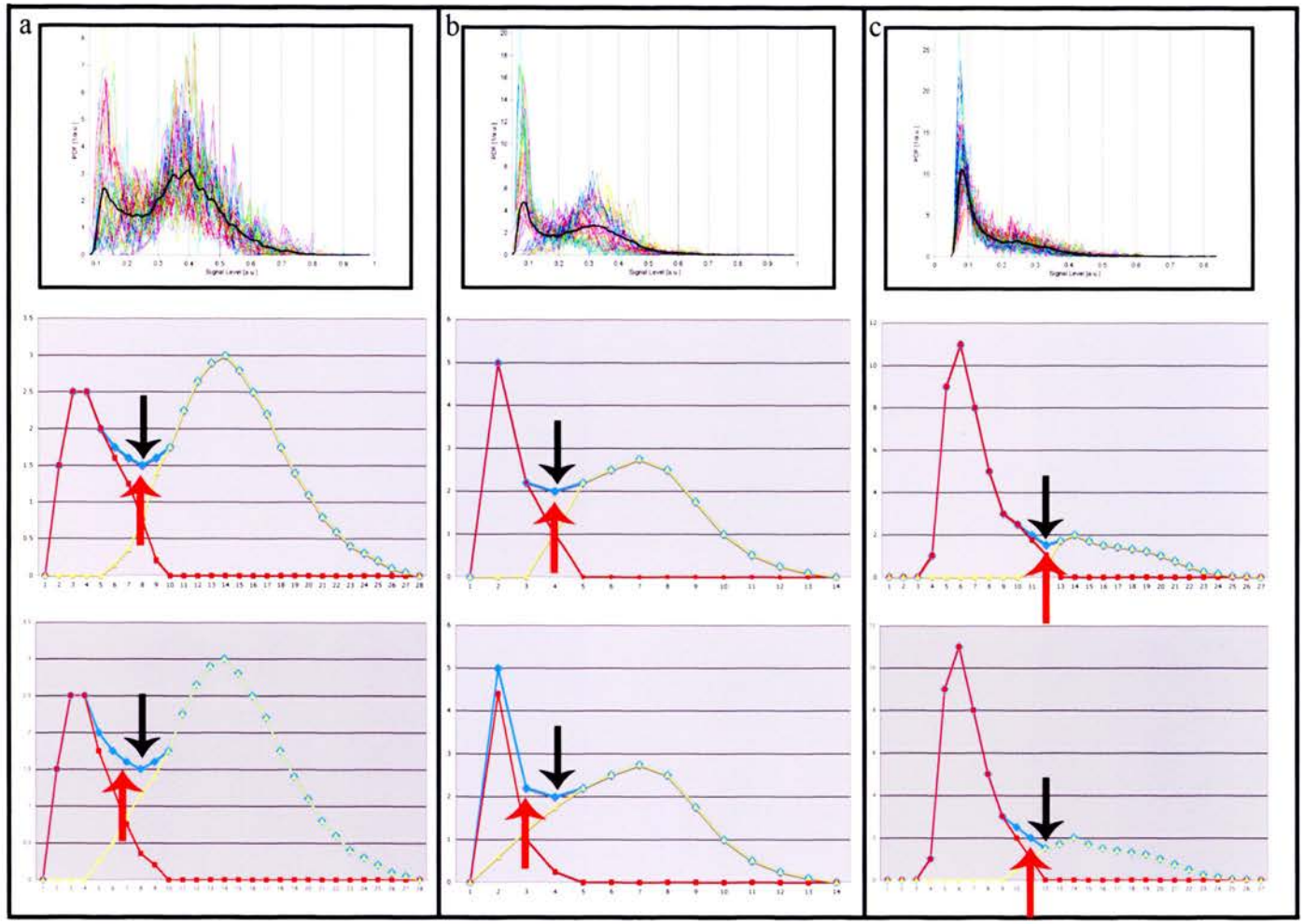

Figure 3.14 Comparing the hypothetical cut-off where the two underlying graphs intersect and the chosen cut-off. Intensity histograms may be the product of two underlying intensity distributions which can be both symmetrical (middle row) or as-symmetrical (bottom row). The chosen cut-off (black arrow) for the overall distribution (blue line) may not lie at the point where the two underlying distributions cross (red arrow) , this is more probable if the hypothetical underlying distributions are assymmetrical.

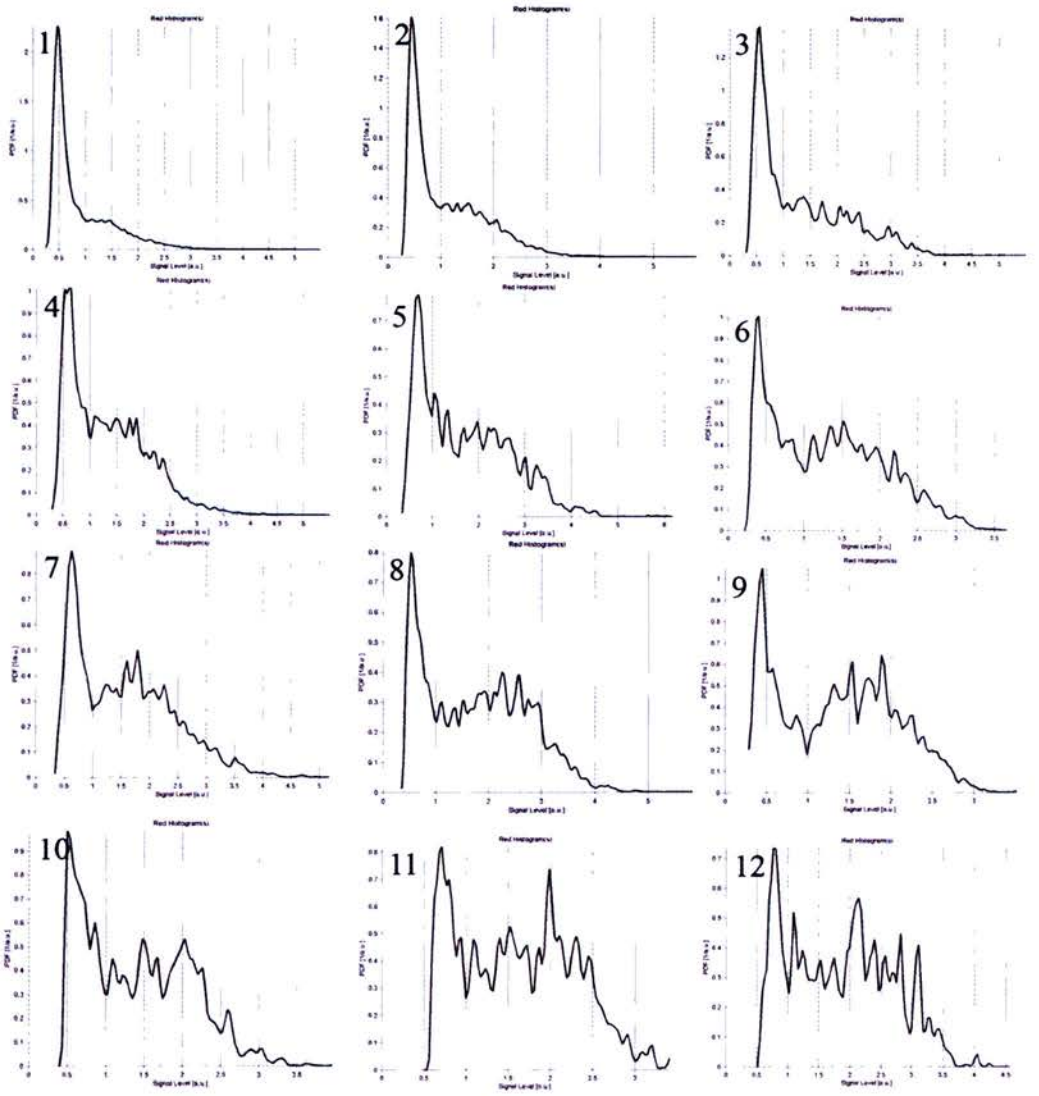

Figure 3.15 Range of red intensity histograms. The value of 1 on the x-axis marks the cut-off point for each of the histograms.

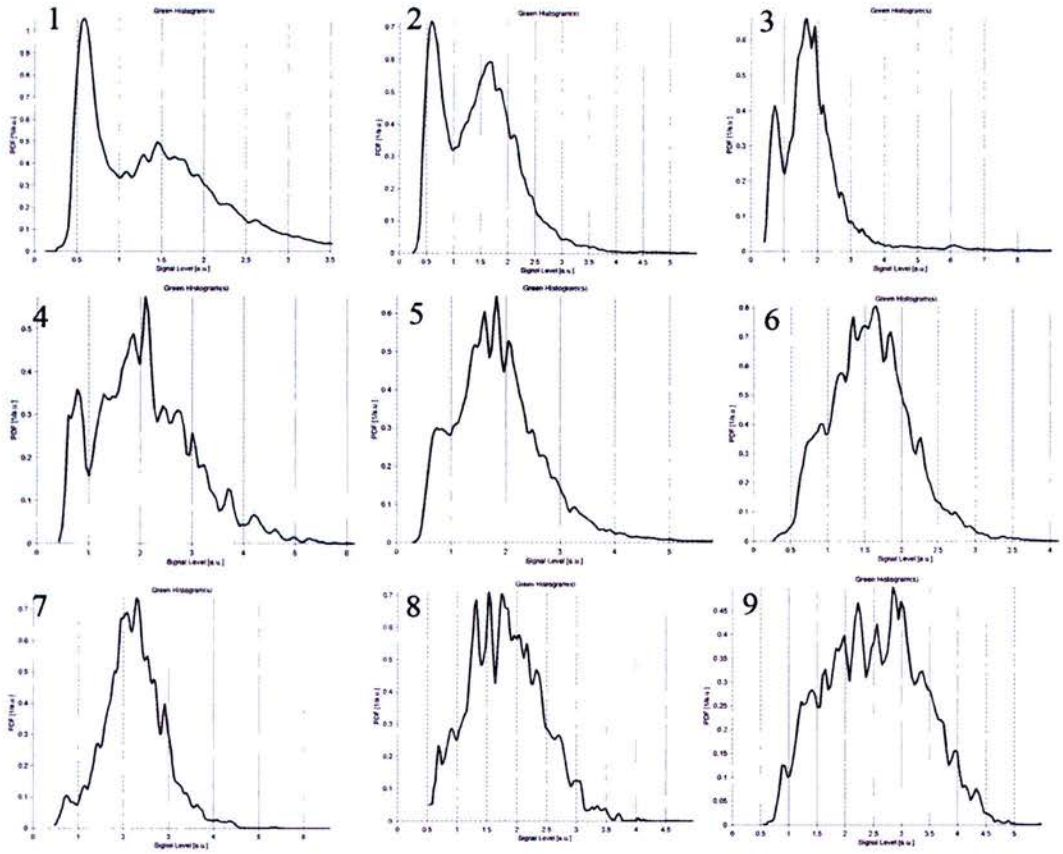

Figure 3.16 Range of green intensity histograms. The value of 1 on the x-axis marks the cut-off point for each of the histograms.

off i.e. the middle of the bimodal trough (fig. 3.14 middle panel, black arrow). In other cases, the intersection of the two unimodal histograms lay to the left of the trough of the bimodal histogram (fig. 3.14 bottom panel). In summary, I found that our assumed cut-off point was justified in some cases but not all. Moreover, this meant that we might, on occasion, slightly over-estimate the number of "off" cells and underestimate the number of "on" cells. Therefore, we should slightly shift our choice of cut-off to the left.

After much analysis I realised that a single histogram could not represent all possible proliferation states and so I explored a wide range of green and red intensity distributions, of which I chose 12 red and 9 green histograms representing a range of intensity distributions (fig. 3.15 and 3.16, respectively). The ranges consist of histograms which are more representative of low proliferation rates to those with higher proliferation rates, which is illustrated by the fact that the first peak becomes smaller and smaller as we move along the range of histograms (i.e. there are fewer unlabelled cells). This spectrum of distributions shows the "easier" (i.e. bimodal) and more difficult distributions that I needed to analyse. However, I was able to choose a suitable threshold for each of the histograms. I was then able to automatically align each newly generated histogram to the histogram with which it fitted best and transferred a suitable threshold to the newly generated histograms of a section. In this way, we have successfully been able to select a cut-off threshold by which we can define whether cells are 'on' or 'off'.

3.2.6 Calculating cell cycle time

Cell cycle time was calculated from the number of cells that had been classified as being 'on' or 'off' for the red, green and blue colour. The formula used in the calculation was:

Tc / No. blue cells = Injection interval / No. green-only cells,

where the number of green only cells is the number of cells that passed out of S-phase during the injection interval, Tc is cell cycle time and the number of blue cells provides for a total cell count.
(modified from Martynoga *et al*, 2005).

3.2.7 Using the same set of tools for H3 staining

The software developed for the analysis of IddU/BrdU labelled cells was adjusted slightly so that it could also be used to analyse sections of limb buds singly labelled for phosphohistone H3. The secondary antibody for phosphohistone H3 was red in colour and blue DAPI staining was used to localise all cells. The first step in processing the images involved the use of the IPLab scripts generated to analyse 48 and 24 bit IddU/BrdU sections. This allowed for the localisation of cells and the generation of a text table that listed their positions as well as their colour intensities. It is worth noting that although the script tries to measure green intensity, there was none to detect and hence the green intensity for every cell was recorded as being zero. The images and the text table were then analysed to produce red: blue ratio plots using the newly generated software. The generated red:blue ratio plots represent the proportion of cells in M-phase of the cell cycle. Regions of high red:blue ratios are regions with high rates of proliferation and regions with low red:blue ratios are regions with low rates of proliferation. Thus, the analysis of the phosphohistone H3 staining provides a qualitative

map of proliferation rates across the limb tissue whereas we can generate quantitative Tc plots using the same software by analysing IddU/BrdU sections (fig 3.17).

3.2.8 Calculating cell density

Previous research has suggested that changes in proliferation rates are inversely related to changes in cell density (Ede *et al*, 1975; Warchol, 2002). Therefore, we developed the analysis software to analyse DAPI stained sections to produce cell-density plots (fig. 3.17). The software could be used to analyse both IddU/BrdU and phosphohistone H3 sections, as both were also stained with DAPI. The cell density plots generated from sections stained with IddU/BrdU and phosphohistone H3 were comparable, thus the different staining procedures had no significant effect upon cell density within a section.

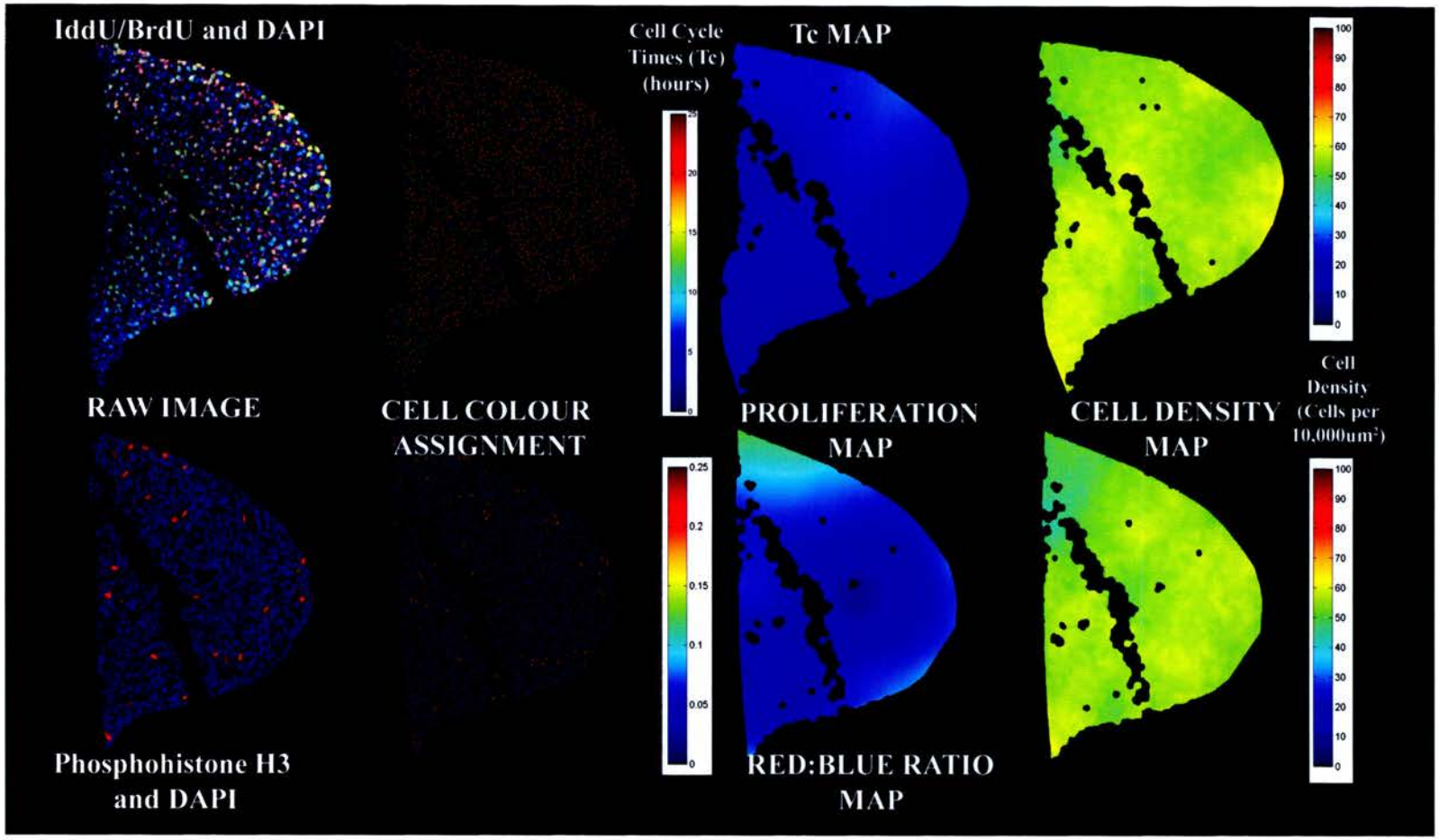

Figure 3.17 An overview of cell proliferation and cell density results generated by the newly developed software.
The newly developed tools can analyse a raw image to generate a plot of cells and assign their correct colour. Maps of cell cycle time (Tc) and cell density can be generated from a plot of cell colours, derived from IddU/BrdU and DAPI data. Maps of red:blue staining ratio and cell density can be generated from a plot of cell colours, derived from phosphohistone H3 and DAPI data.

3.3 Discussion

I optimised the IddU/BrdU double labelling technique for the analysis of cell cycle time in the limb bud. Further to this, we generated computational software that allows for the automated analysis of images. The developed software is in two parts; the first of which may be run within an IPLab environment and the second may be run in the Matlab environment. Together the two pieces of software provide the means by which we can complete a comprehensive and automated analysis of many sections. The first piece of software successfully detects a cells position and records its red, green and blue intensity levels. The second piece of software analyses the information generated by the first script and produces histograms of cell colour intensity across a section image. After many trials and tribulations, we have successfully developed a method by which many intensity histograms can be aligned to determine a single cut-off threshold, ultimately, allowing us to produce quantitative maps of proliferation rates across the section of a limb bud.

Both pieces of software can also be used to analyse sections labelled with phosphohistone H3 and DAPI, producing a red: blue ratio section map. The map indicates the proportion of mitotic cells within a section. Furthermore, the software can be used to generate cell-density plots of sections, providing further insight into the relationship between changes in proliferation rates and cell density.

3.4 Future Work

Although, we believe we can determine the cut-off threshold for any given section we aim to check whether this threshold would change if we were to analyse specimens with alternative injection intervals. If we see no difference then we can be truly confident in our software to produce relatively accurate maps of cell cycle times.

The developed computational software has also laid the grounds for possible automatic stacking of histological sections, and for the identification of cells within a model of embryo limb bud, of which the 4D visualisation needs to be realised. Moreover while, the analysis of limb tissue is most relevant to understanding limb development, it is envisaged that these techniques and software can be used to analyse cell cycle times in other tissue types, such as carcinoma cell masses and the developing gut.

Chapter 4 – Cell cycle time and cell density in the embryonic limb

4. 1 Introduction

The generation of computational tools for proliferation studies was described in the previous chapter. To reiterate, the tools can be used to generate maps of cell cycle times of IddU/BrdU double-stained sections, labelling ratio maps from phosphohistone H3 stained sections and maps of cell density from DAPI stained sections. In this chapter, I shall present proliferation and cell density results as generated by the computational tools for two developmental stages of the mouse embryonic hind limb.

4. 1. 1 Cellular proliferation in the embryonic limb

Studies of cellular proliferation in the vertebrate limb have mainly involved the use of radiolabels such as tritiated thymidine (Kirkwood *et al*, 1989; Goff and Tabin, 1997), haemotoxylin and eosin (Hornbruch and Wolpert, 1970; Summerbell and Wolpert, 1972) or phosphohistone H3 antibody (Sun *et al*, 2002). Studies conducted on relatively young limb buds seem to suggest that in terms of spatial variation the approaches produce equivalent findings. For example, no significant difference was seen in the mitotic index of proximal and distal regions using haemotoxylin and eosin staining ($P < 0.01$; Hornbruch and Wolpert, 1970) and relatively uniform cellular proliferation was found in an equivalent stage of the mouse limb bud (38 somites) using an antibody against phosphohistone H3 (fig. 4.1, 35 somites, Sun *et al*, 2002).

More importantly, all examples of limb proliferation studies have been qualitative and have not provided any absolute quantitative information with regards to cell cycle time. Nonetheless, previous research has highlighted patterns of proliferation in the vertebrate limb, as discussed in chapter 1. To reiterate, at later stages of development (stage 25-30 in chick, Hornbruch and Wolpert, 1970; Summerbell and Wolpert, 1972; which is equivalent to E11.5 – E13 in mouse) the overall rate of limb proliferation decreases and a proximal-distal gradient of proliferation rates is observed (fig. 4.1). Furthermore, high

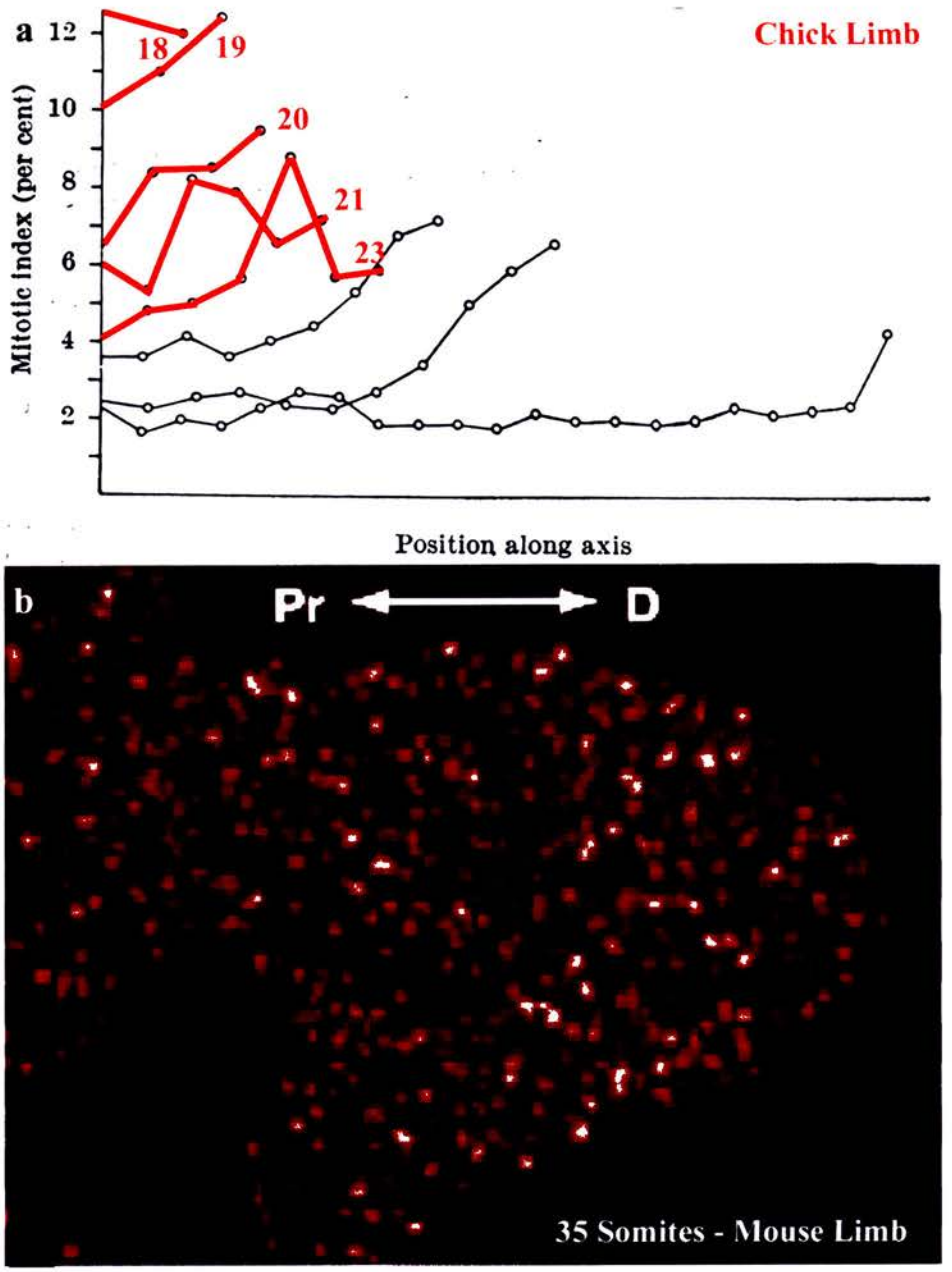

Figure 4.1 Single-labelling studies of cellular proliferation in the limb.

(a) Mitotic index at different points along the proximo-distal axis of the chick limb (Hornbruch and Wolpert, 1970) (b) Transverse section of mouse limb bud at stage indicated, in which phosphorylated histone H3 marks nuclei in cells undergoing mitosis in bright red (Sun et al, 2002).

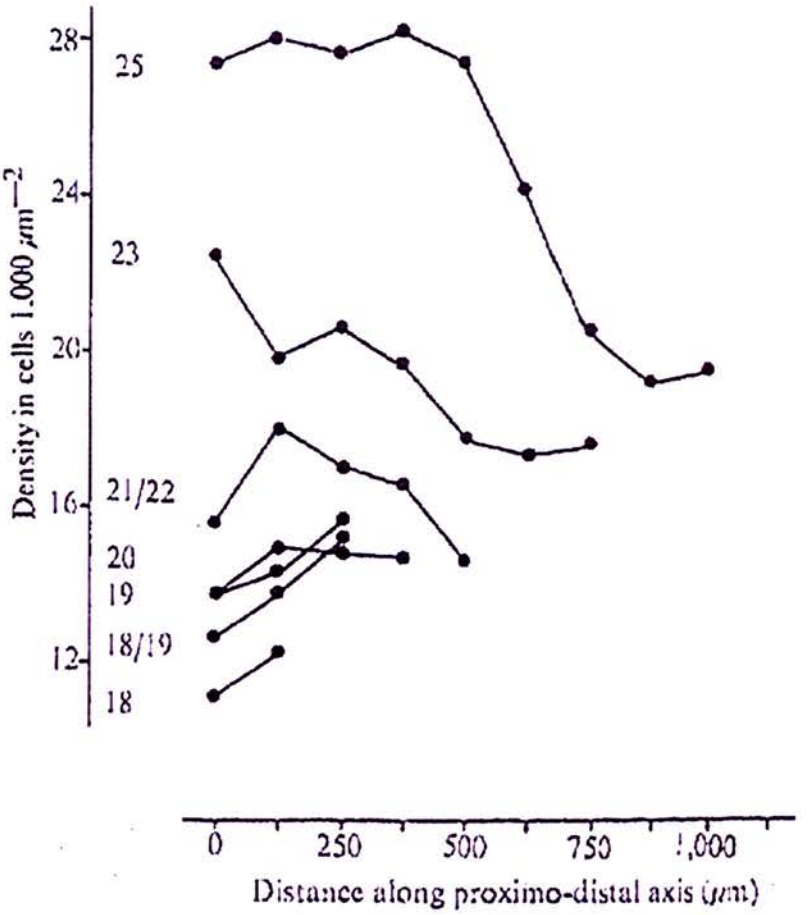

Figure 4.2 Density with respect to position along the proximo-distal axis for stages 18-25 of the chick limb (Summerbell and Wolpert, 1972).

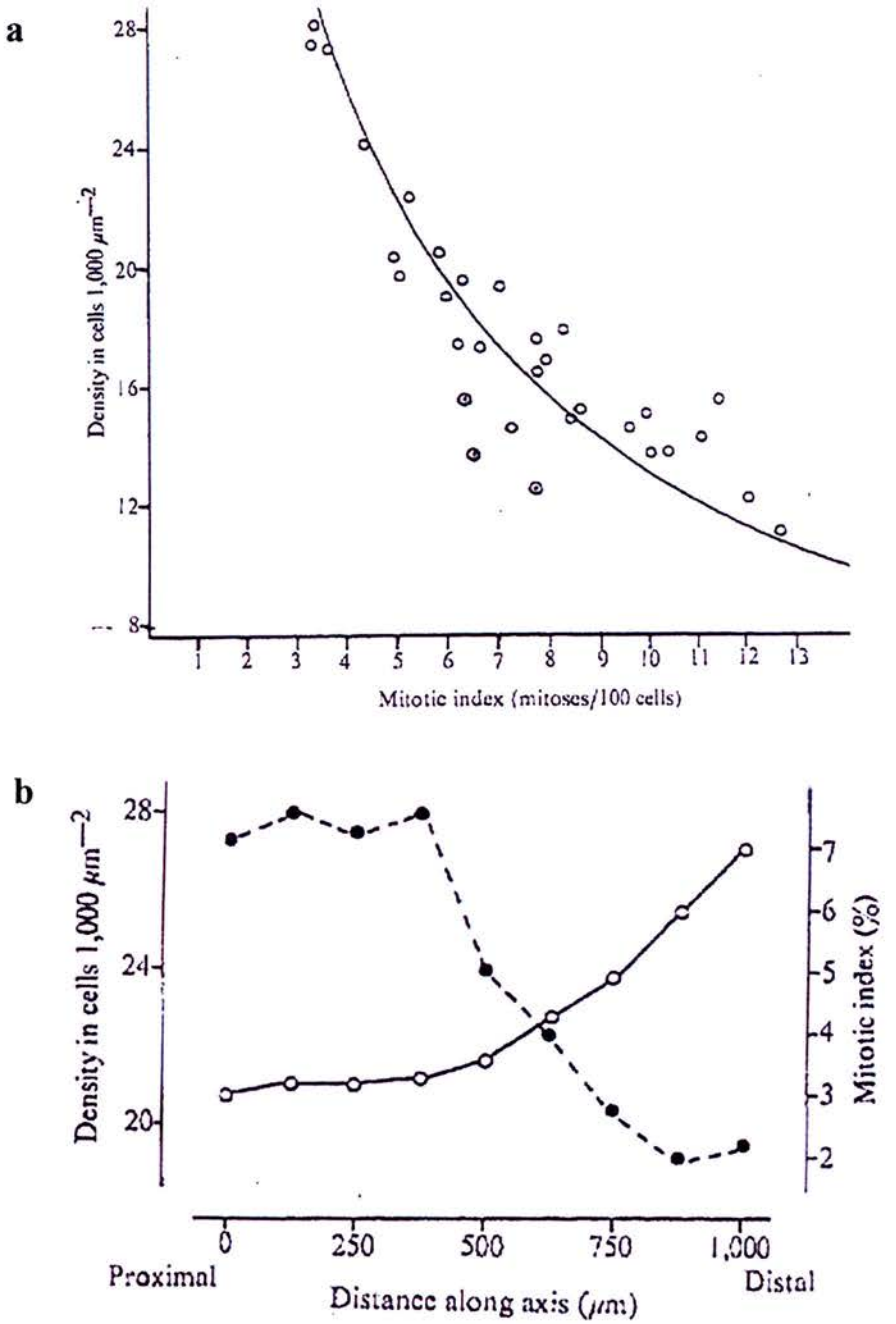

Figure 4.3 Cell proliferation and cell density in the limb.
(a) Correlations between mitotic index and density derived from data gathered from chick limbs of different developmental stages and different positions along sections. (b) Variation in density (dotted line) and mitotic index (solid line) with respect to distance along the proximo-distal axis of a stage 25 chick limb (Summerbell and Wolpert, 1972).

rates of proliferation are observed at the proximal-dorsal and proximal-ventral boundaries of the limb bud, with a low rate of proliferation at the centre of the limb bud (Summerbell and Wolpert, 1972).

4. 1. 2 Cell densities in the embryonic limb

Cell density increases with development and an appropriate proximal-distal gradient of cell-density is established (fig. 4.2, Summerbell and Wolpert, 1972). In the chick limb a clear gradient of cell-density can be seen at stage 25, with high cell density in proximal regions gradually reducing distally along the limb (Summerbell and Wolpert, 1972; equivalent to E11.5 in the mouse limb) at which stage there is a hint of humerus formation in the forelimbs (Martin, 1990). Thus a change in cell density is associated with the differentiation of mesenchymal cells into skeletal precursor cells.

4. 1. 3 Cellular proliferation and cell density

Changes in cell density are said to be closely correlated with changes in cellular proliferation, where "mitotic index is inversely proportional to cell density" (fig. 4.3, Summerbell and Wolpert, 1972). For example, at stage 25 in the chick limb, mitotic index is low in proximal regions and higher nearer the distal tip, whereas cell density is high in proximal regions and gradually reduces nearer to the distal tip (fig. 4.3, Summerbell and Wolpert, 1972).

4. 1. 4 Aims

The overall aims of this chapter are three-fold. Firstly, I aim to assess the success of the newly developed tools in generating proliferation and density results. Secondly, I aim to present the quantitative findings of our study. Under the umbrella of limb development I will:

- present a comprehensive quantitative analysis of limb proliferation, which has never been done before;
- relate limb cell cycle times (Tc) to cell density;
- relate proliferation results obtained from IddU/BrdU stained sections to those obtained from phosphohistone H3 sections and;
- relate patterns of Sox9 expression to patterns of Tc and cell density.

Thirdly, I aim to see how our results relate to the findings of previous studies.

4. 2 Results

4. 2. 1 Comprehensive quantitative analysis of cellular proliferation in the limb

4. 2. 1. 1 Mouse embryo hind limbs

The capabilities of the newly developed software were tested on sections derived from the hind limbs of four embryos – two of embryonic stage E10.5 (L40E2 and L40E5; fig. 4.4) and two of E11.5 (L4E4 and L4E3; fig. 4.4). At stage E10.5 the limbs were small buds protruding from the flank of the body wall. At E11.5 the limbs had extended distally, and the autopod could be distinguished as a paddle-like structure.

Each of the embryos was fixed, wax-embedded and sectioned at 7μm, with 5 sections placed on each slide. Odd numbered slides were stained for IddU/BrdU and DAPI and even numbered slides were stained with the phosphohistone H3 antibody and DAPI. The newly developed computational tools were then used to generate maps of cell cycle time (Tc), cell density and labelling ratios from images of the stained sections. The results for IddU/BrdU stained sections were then put together as a montage and are displayed in figure 4.5.

4. 2. 1. 2 Variability within embryos

Observation of labelling patterns showed a seemingly discontinuous distribution of patterns (fig. 4.6 top row). Analysis of only the first two panels in figure 4.6 gave the impression that there was a trend in the data for a lower labelling ratio at a specific position on the dorsal side (pale blue). However, this region seemed to have shifted ventrally in the third panel. Upon examination of the original images (fig. 4.6 bottom row) it became clear that this pattern could be attributed to stochastic variation in the

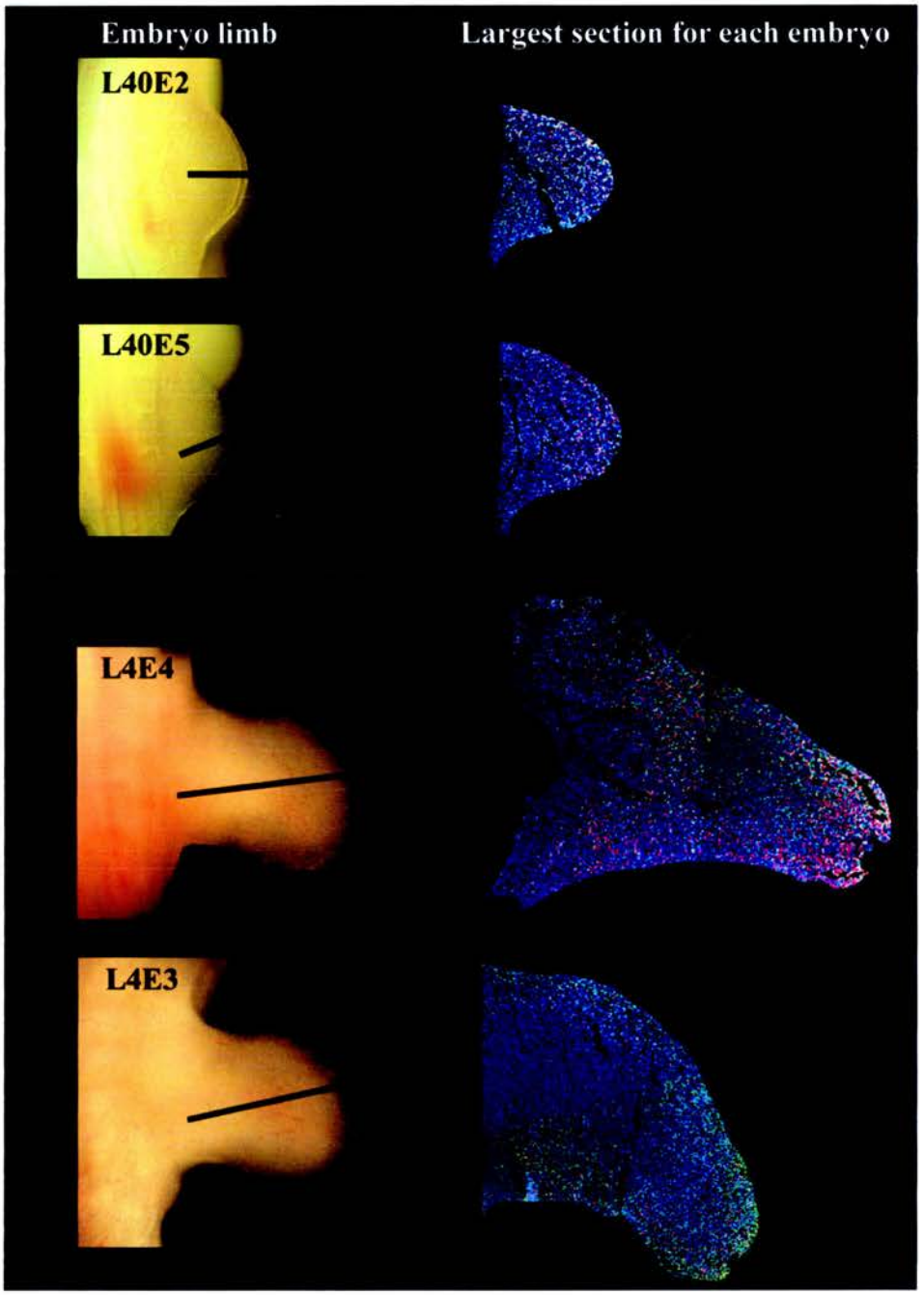

Figure 4.4 Newly developed software was used to analyse two embryos from two distinct developmental stages.

E10.5 (top panel) and E11.5 (bottom panel). The location of each section in relation to the limb bud is marked with a black line.

Figure 4.5 Quantitative proliferation results and cell density results of two E10.5 embryos and two E11.5 embryo hind-limb buds.

In (a) and (b) are raw data images of two E10.5 limb sections stained for IddU/BrdU and Dapi (top row); plots of cell colour assigment made by the newly developed computational tools (second row from top); plots of cell cycle time for each section (third row from top) and plots of cell density for each section (bottom row). Raw data images of limb sections from two E11.5 limb buds stained for IddU/BrdU and Dapi and their plots of cell colour assigment are found in (ci) and (di). The plots of cell cycle time and plots of cell density for the E11.5 limb buds are in (cii) and (dii), respectively. In each figure there is a photo of the sectioned limb bud with markings representing the approximate position of each section.

Figure 4.5a

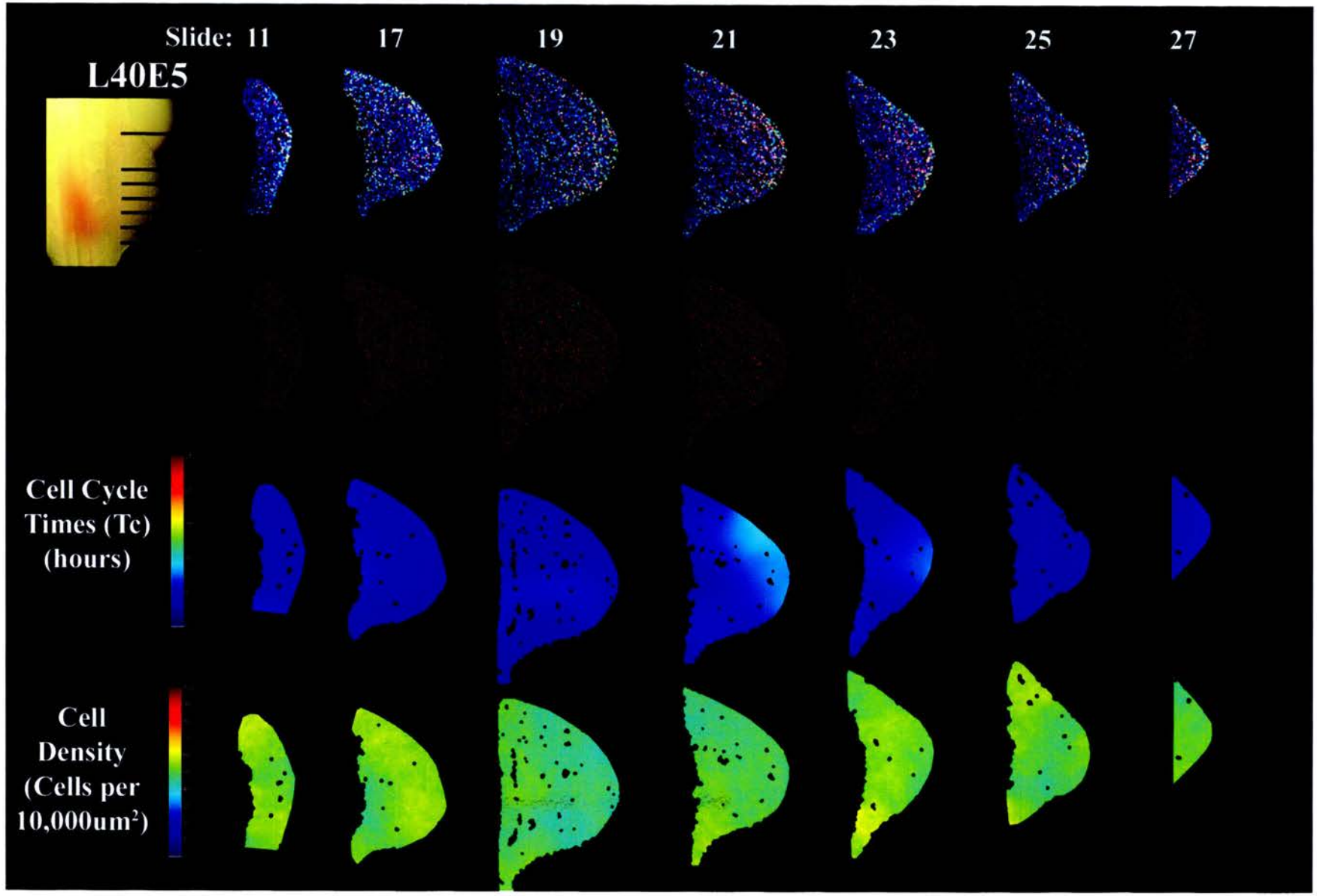
Slide: 11
17
19
21
23
25
27
L40E5
Cell Cycle Times (Tc) (hours)
Cell Density (Cells per 10,000um²)

Figure 4.5b

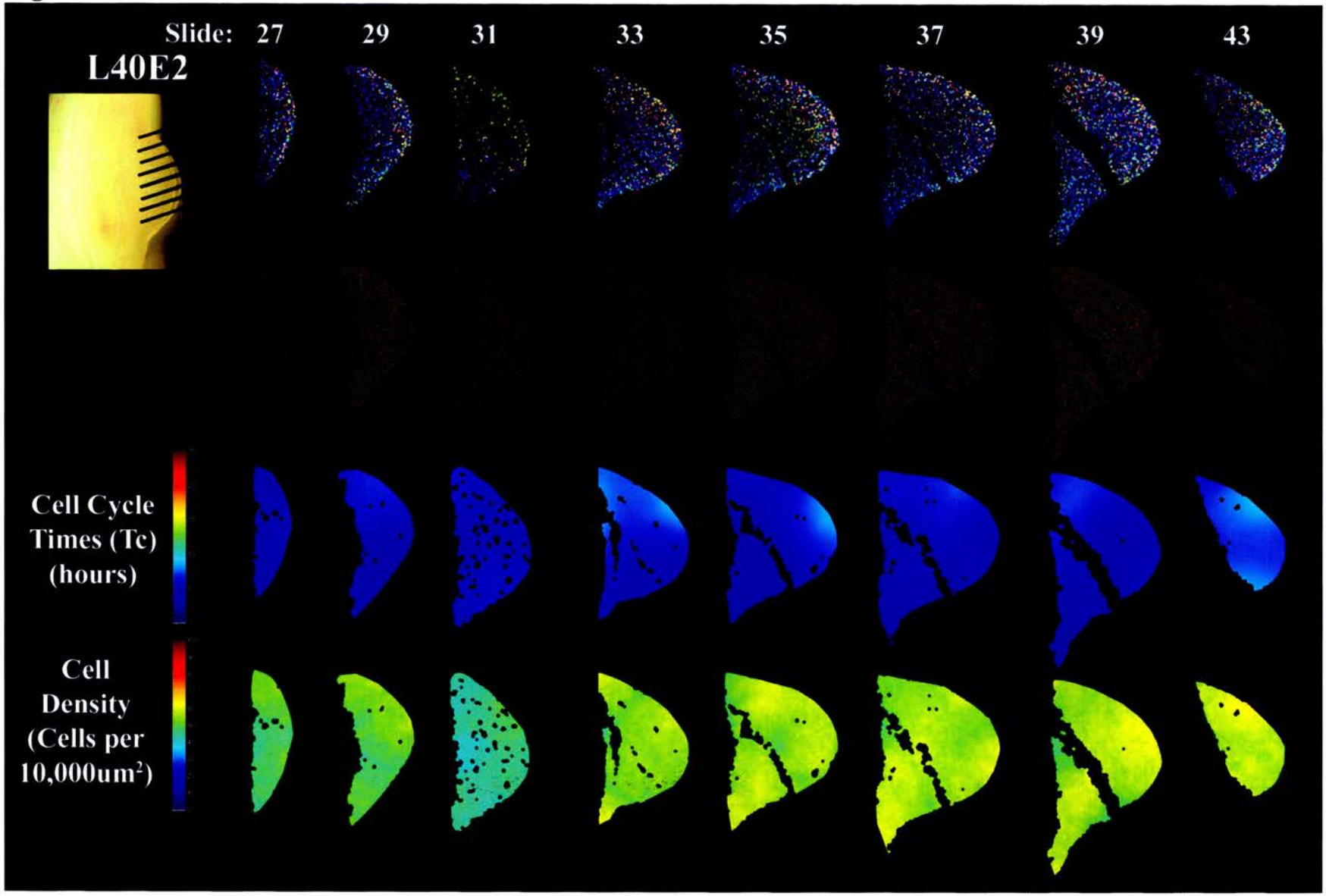
Slide: 27 29 31 33 35 37 39 43
L40E2
Cell Cycle Times (Tc) (hours)
Cell Density (Cells per 10,000um²)

Figure 4.5ci

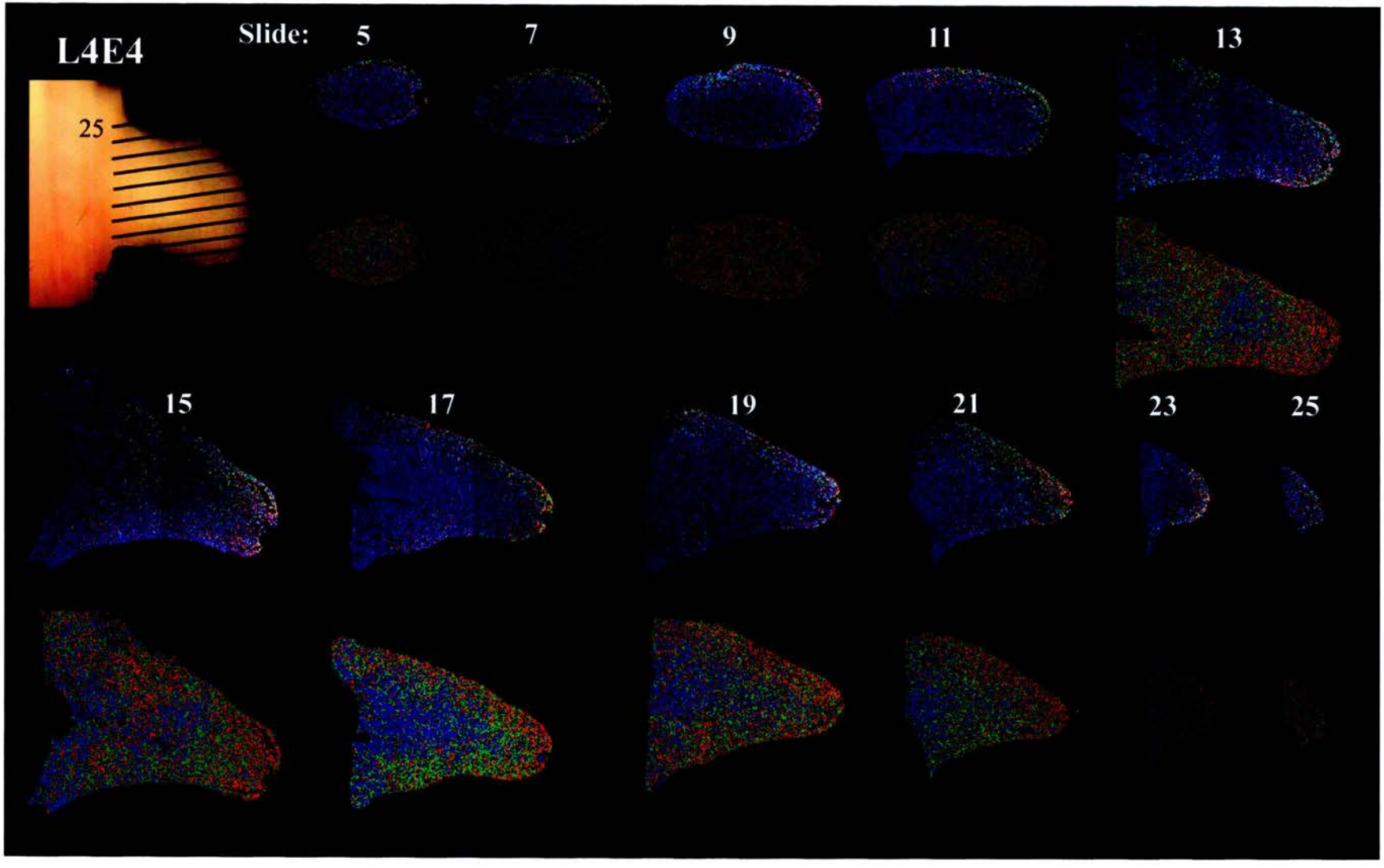

Figure 4.5cii

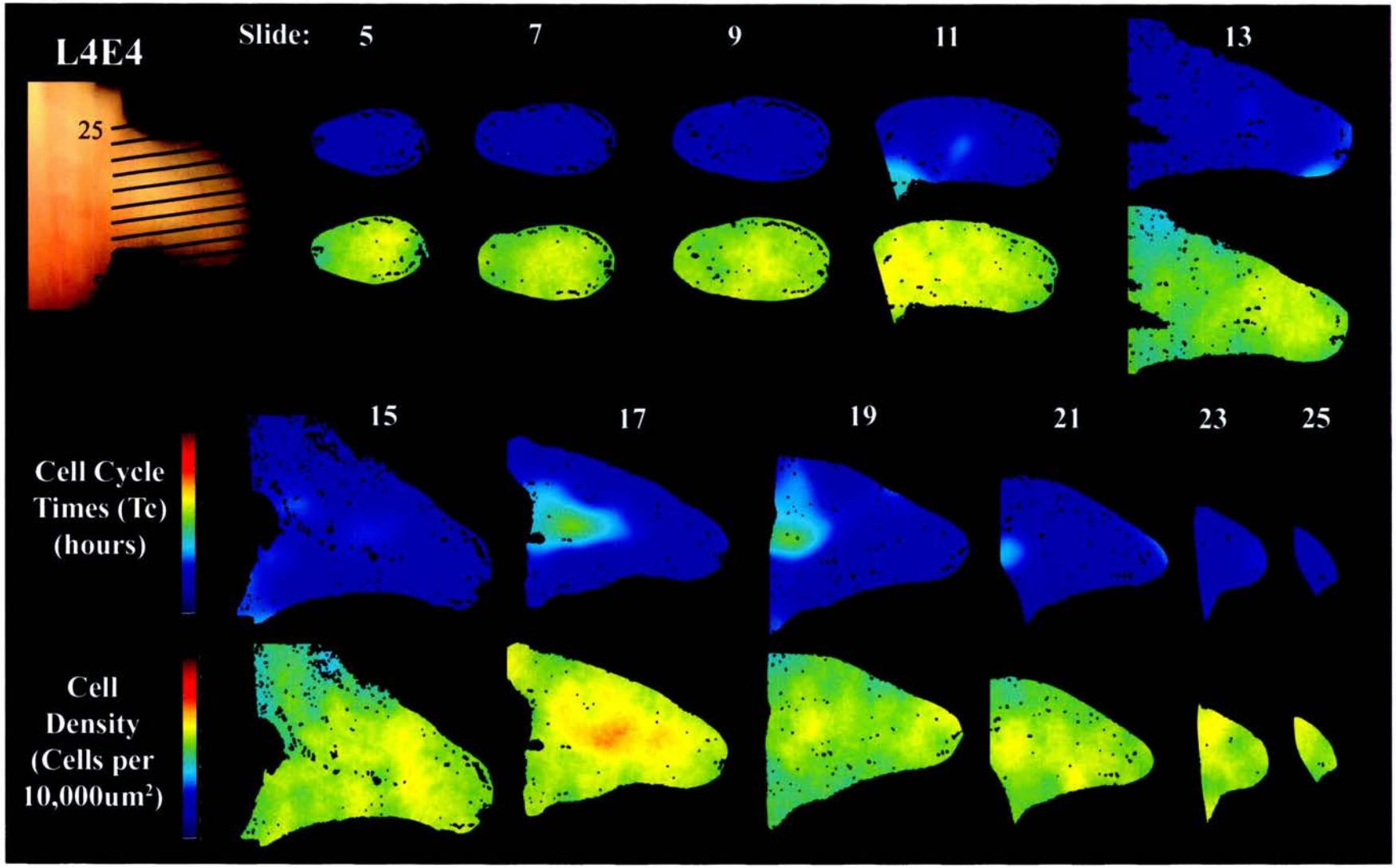

Figure 4.5di

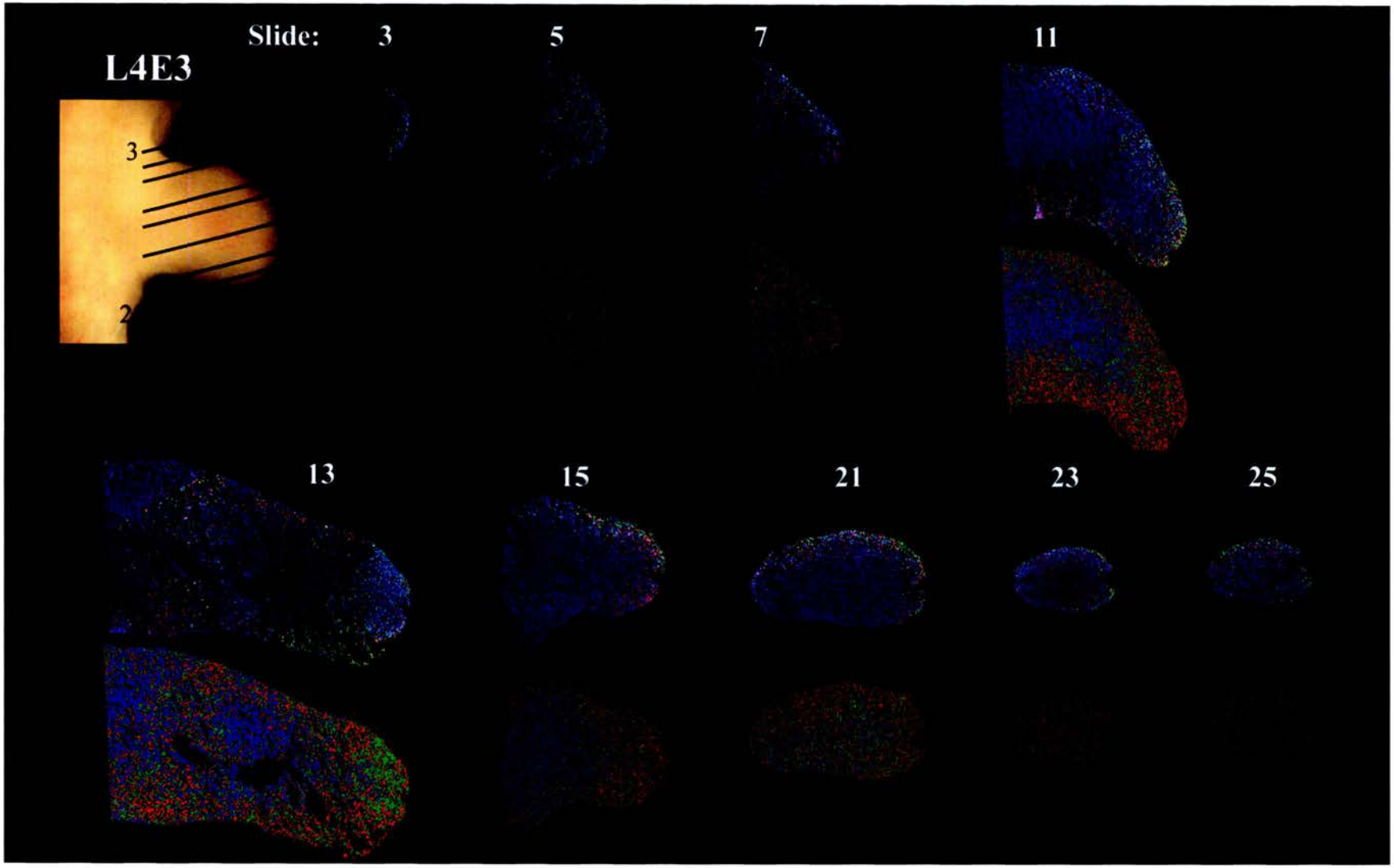

Figure 4.5dii

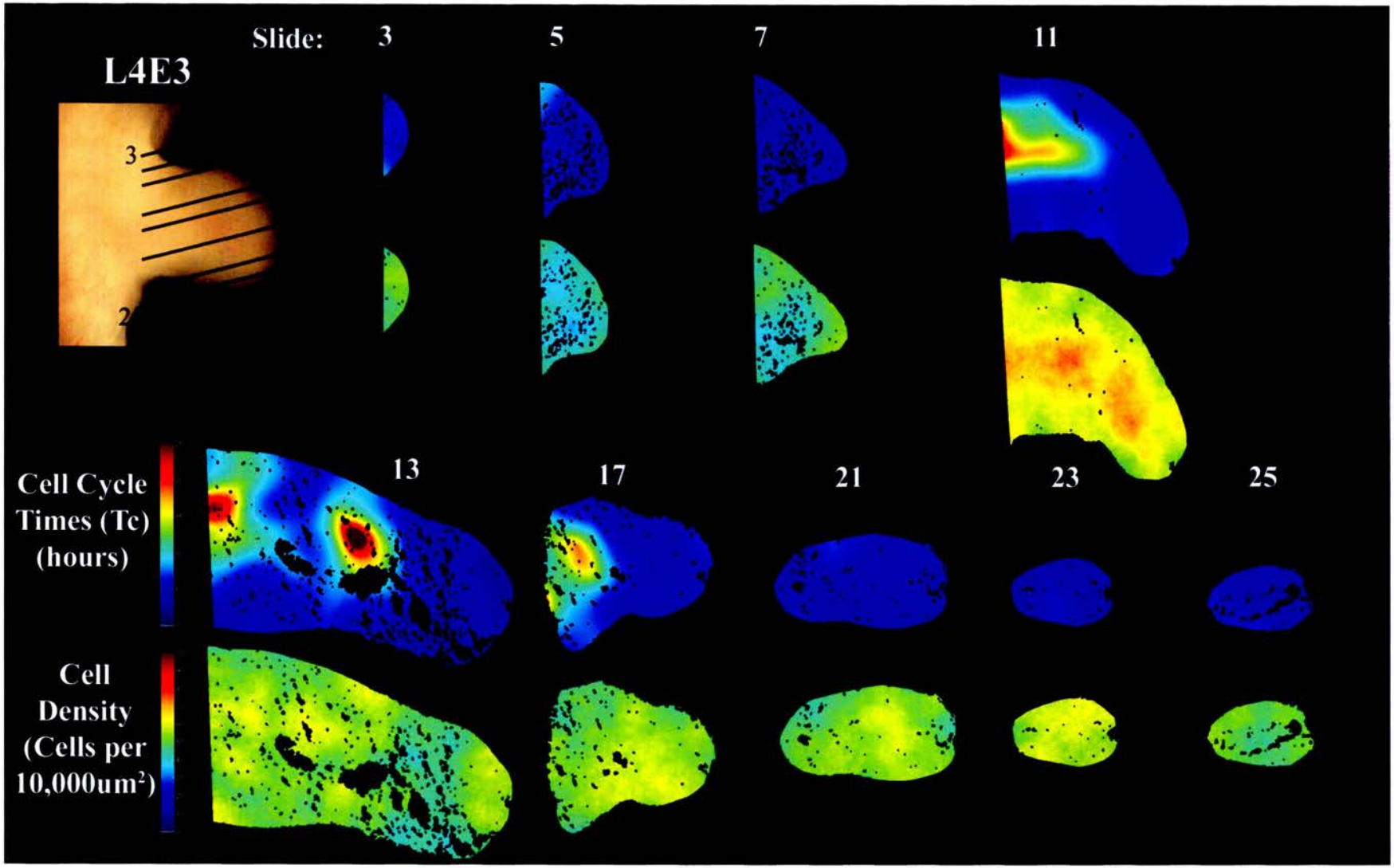

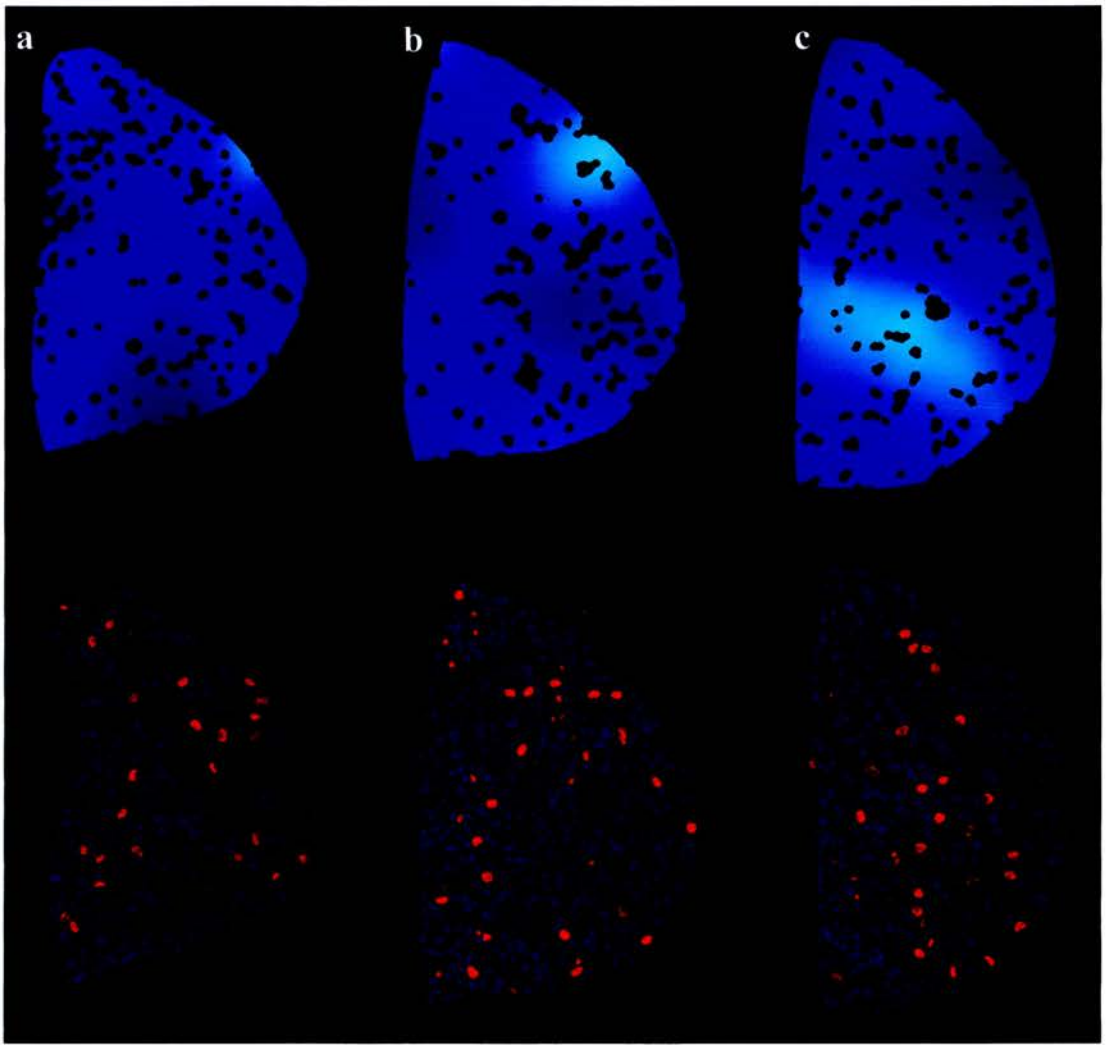

Figure 4.6 Stochastic variation is present in patterns of cellular proliferation in the limb.

A dorsal region with a high labelling ratio (pale blue) in a and b shifts ventrally in c (top row). The raw images of phosphohistone H3 (red) and Dapi (blue) stained sections (bottom row), show that the observed patterns can reflect meaningless noise.

data. The samples analysed consisted of only a few hundred cells of which approximately a tenth were stained. Thus, there was a high probability that the computer program would pick out a stochastic pattern rather than a real pattern of proliferation, as seems to be the case in Figure 4.6. However, if the sample consisted of thousands of cells of which a high proportion were labelled then there would be a lower likelihood of stochastic variation being picked out as a pattern of proliferation.

Stochastic variability could be seen in maps derived from sections stained for phosphohistone H3 (fig. 4.6) as described, and also in sections stained for IddU/BrdU. This was clearly highlighted in cell cycle time maps and cell density maps of the sections (fig. 4.7), where a region of high cell cycle time (pale blue) in one section (fig. 4.7. top row) is not located at the same point in the next section (fig. 4.7. second row down). Thus, the issue of stochastic variability within embryos is equally important for sections stained for IddU/BrdU as it is for sections stained for phosphohistone H3. The observations highlight the importance of averaging values from one section to the next to obtain a clear picture of patterns of proliferation.

4. 2. 1. 3 Variability between embryos

A greater degree of variation was observed between than within embryos. The variation was more obvious in cell density maps than in cell cycle time maps. For example, sections from L40E2 have a cell density of ~60 cells per 10,000μm^2 across the limb tissue whereas sections from L40E5 have ~50, resulting in a difference of ~15-20% in cell density between the embryos at this early stage of development (fig. 4.7). This may be due to slight differences in tissue processing (dehydrating, embedding etc).

Despite the small number of embryos analysed, the extent of the differences would suggest that they are due to some variation from embryo to embryo rather than slight differences in tissue processing (dehydrating, embedding etc) alone. A high rate of proliferation at this stage, could mean that there is a greater degree of variability

between embryos at this early stage than at later stages when proliferation rates are lower overall, resulting in a greater degree of stability and a reduction in stochastic noise between embryos. In order to overcome variability in the results both hind-limbs of a single embryo could be analysed and averaged. Moreover, a greater number of embryos for a given developmental stage could be analysed increasing the likelihood that a common pattern of proliferation can be seen.

4. 2. 1. 4 Overall trends and the first quantitative Tc values

Despite variability between and within embryos we can extract a general picture of proliferation. At a qualitative level, there are no significant spatial asymmetries (i.e. patterns) in the youngest embryos but significant differences can be seen in the older two embryos (fig. 4.7). Visual analysis of the generated maps allows us to see that the quantitative cell cycle time across the youngest embryos is surprisingly rapid, at about 5 hours (fig 4.8, graph of cell cycle times, primary data in Appendix B). The observation of stochastic variability (mentioned above) suggests that we can indeed take an average of the values across each whole section for E10.5 embryos.

In the older two embryos cell cycle times vary from 5 hours to over 20 hours. The high proliferation rate of 5 hours can be seen not only near the distal tip, the so-called "proliferative zone", but also along the dorsal and ventral boundaries. However, higher cell cycle times (i.e. lower rates of proliferation) are localised to the proximal region and central regions (fig. 4.7). The average cell cycle times in the proximal and central regions were ~15 hours and ~10 hours, respectively.

Using two-way ANOVA analysis I found that the differences observed in cell cycle times between older and younger limbs, and different regions at the later stage are statistically significant ($P = 0.001$, and 0.0008 respectively, Appendix B). The Statistical test checks the null hypothesis that the means of different groups are equal. It also

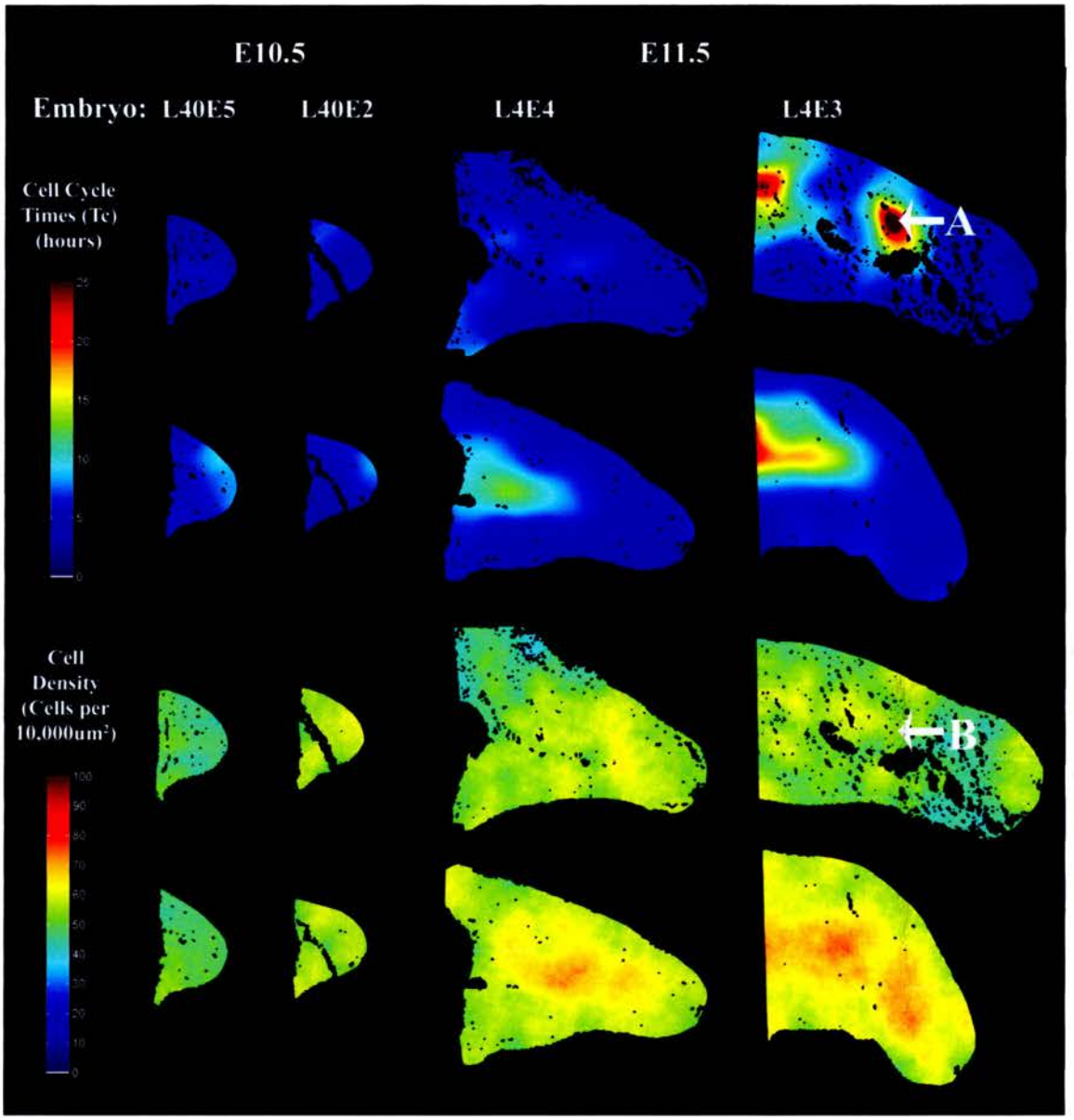

Figure 4.7 Variability within and between embryos can be seen as plots of cell cycle time and cell density.

Two plots of cell cycle times (top) and two plots of cell density (bottom) are shown for four embryos. Examples of variability within embryos can be seen in plots of cell cycle time and cell density in sections for L4E4 and L4E3. Variability between embryos can be seen in cell density plot comparisons between L40E5 and L40E2. A= region of high proliferation rates, B = region without high cell density; Dorsal, top; ventral, bottom; distal, right; and proximal, left.

checks for an interaction between the two factors. The results suggest that embryonic age and limb location have a combinatorial effect upon proliferation rates (P = 0.0005).

4. 2. 2 Relating cell cycle time (Tc) to cell density

4. 2. 2. 1 Cell density

Although, cell density seems to show slight variation between embryos, as discussed in section 4. 2. 1. 3, the overall trend is a small but significant increase across young limb buds at ~50-55 cells per 10,000μm^2 (fig. 4.8, graph of cell density, primary data in Appendix B). The average cell density in older limb buds is slightly higher at ~55-65 cells per 10,000μm^2, with the average cell density in distal, dorsal and ventral regions at ~55-60 cells per 10,000μm^2. Analysis of cell density images of the older limbs shows that cell density can go up to ~70-75 cells per 10,000μm^2 in the proximal and central regions (fig. 4.7). This is an increase of ~ 30-50% from younger to older limb buds. However, the average values for these regions are ~60 and ~65 cells per 10,000μm^2, respectively (fig 4.5), which is a lesser increase of ~10-30 %. Although the difference in cell density between the younger and older limb buds is small it is significant (P = 0.01, Appendix B). However, the statistical test completed does not accord this significant difference to any single region but to the limb bud as a whole.

4. 2. 2. 2 Is there a clear relationship between cell cycle time and cell density?

In E10.5 limb buds there is a uniform pattern of cell cycle time and cell density across the limb sections. In older limb buds (E11.5), cell cycle times and cell densities in the dorsal, ventral and distal regions are comparable in value to those in the younger limb buds at ~5hrs and ~55 per 10,000μm^2, respectively. Thus, the distal, dorsal and ventral

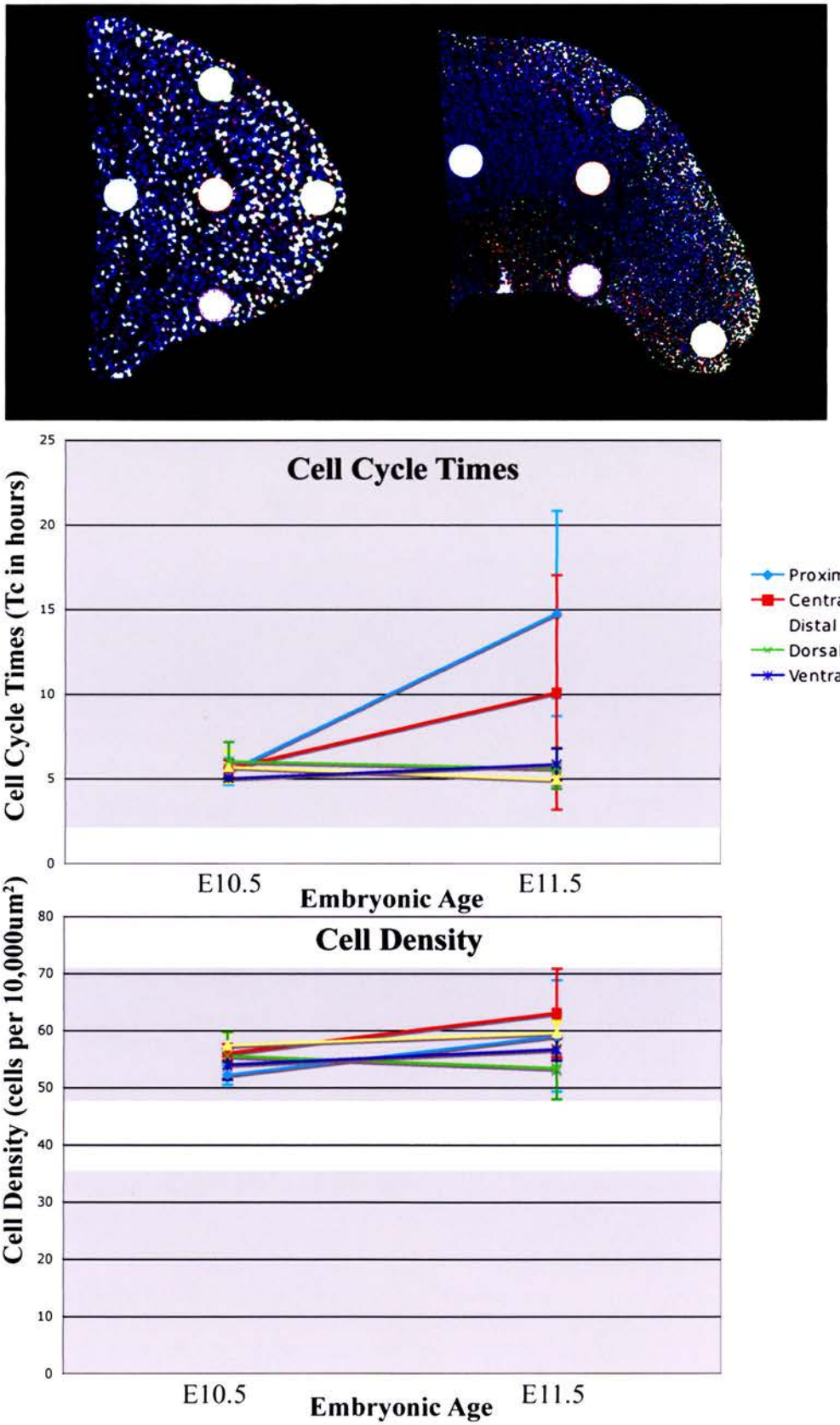

Figure 4.8 Developmental stage and embryonic location has an effect on cell density and cell cycle times.

A significant increase can be seen in cell cycle times in the proximal and central regions from mouse embryonic stage E10.5 to E11.5. There is a slight increase in cell density, in the same regions. Standard deviation of the sample was used as a measure of the error for both cell cycle times and cell density. Little error is seen at E10.5 for cell cycle time and cell density, however at E11.5 error bars are larger for cell density and very large for cell cycle time.

regions seem to be the same for cell proliferation and cell density both spatially and temporally between E10.5 and E11.5 embryos.

A combination of high cell cycle time (i.e. low rate of proliferation) and high cell density is seen in proximal and central regions in the older limb buds, which would suggest that these are pre-chondrogenic regions. However, the results would also suggest that the relationship between cell cycle time and cell density is not as tight as stated in the literature. For example, a comparison of a map of cell cycle time for L4E3 (fig. 4.7, A) with regions of high cell cycle time does not translate into regions of high cell density in equivalent positions (fig. 4.7, B). Further suggestions of why there is not such a tight link between these two factors are discussed in more detail in the next section.

4.2.3 Relating cell cycle time (Tc) and cell density to Sox9 expression

A fast cell cycle time of about 5 hours is observed in the E10.5 limb and the dorsal, ventral and the distal tip of the E11.5 limb (fig. 4.9 aii, bii). The high rate of proliferation corresponds to a low cell density of about 55 cells per 10,000μm^2 in E10.5 limbs and 60 cells per 10,000μm^2 in E11.5 limbs (fig. 4.9 aiii, biii) and there is an absence of Sox9 expression in these regions (fig 4.9 cii, ciii). This would suggest that prior to Sox9 expression there is a high rate of cellular proliferation in the limb and there is no cell aggregation, which is associated with early chondrogenesis.

Low proliferation rates are found in proximal and central regions of the E11.5 limb, with the highest time of above 20 hours found most proximally (fig. 4.9 bii). This pattern of proliferation corresponds with Sox9 expression in the femur region (fig 4.9 cii). At early stages of development Sox9 expression is high in this region but at this stage of development Sox9 expression is considerably less than in other regions of the limb, such as in the anterior zeugopodal region. These factors combined with a high cell density of about 70 cells per 10,000μm^2 (fig. 4.9 biii), suggest that early stages of chondrogenesis,

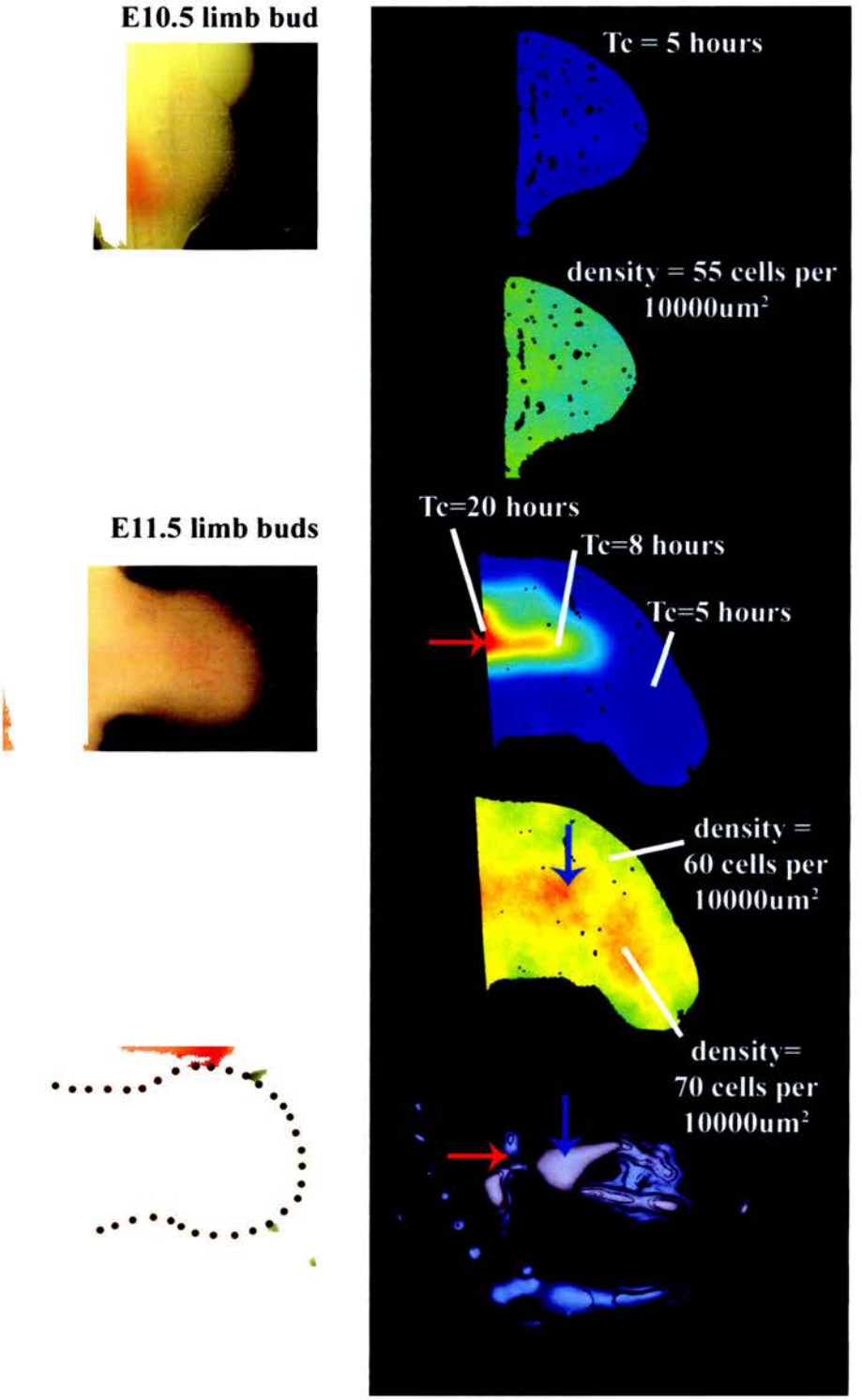

Figure 4.9 Comparing Sox9 expression patterns to patterns of cell cycle time and cell density in the limb.

In the E10.5 limb there is uniformly high cell proliferation and uniform cell density. Regions of high cell density (orange) correspond to regions of high levels of Sox9 expression (grey), marked with a blue arrow. Regions of low cell cycle time correspond to Sox9 expression in the femural region, marked with a red arrow.

at which cells begin to aggregate and differentiate into pre-chondrogenic precursors, has begun.

In the central region where cell cycle time is approximately 8 hours (fig. 4.9 bii), which corresponds to a high Sox9 expression in a connecting region between the anterior and posterior zeugopods (fig 4.9 cii), high cell density is detected equivalent to that seen in the proximal region (fig. 4.9 biii). I suggest that the cells in this region are at a slightly earlier stage of differentiation, hence cell cycle time has not dropped to the level seen in the proximal region.

Overall, the results suggest that a high rate of cellular proliferation in the early limb bud drops in regions corresponding to Sox9 expression. Moreover, I suggest that Sox9 expression initiates changes within cells leading to early signs of chondrogenesis (chapter 2), such as a high cell density in regions of cellular aggregation. This then initiates a reduction in proliferation rates. The data suggests that this process occurs in a proximal to distal direction and occurs as Sox9 expression begins to decline in the same direction, hence high cell density and low Sox9 expression is associated with low proliferation rates in the proximal but not in more distal regions of the E11.5 limb.

4.2.4 Iddu/BrdU double labelling vs. Phosphohistone H3 single labelling

A comparison of staining maps derived from Iddu/BrdU double labelling experiments and phosphohistone H3 single labelling experiments with similar tissue, highlighted a clear difference in the staining patterns picked up by the two techniques. IddU/BrdU staining highlighted a clear spatial pattern of mesenchymal proliferation (fig. 4.10, left column) whereas phosphohistone H3 staining seemed random and did not illustrate any pattern (fig. 4.10, right column). IddU/BrdU proliferation maps highlighted regions of high proliferation in the distal, dorsal and ventral regions and low proliferation in the proximal and central regions (fig. 4.11, left column). However, in proliferation maps derived from sections stained with phosphohistone H3 (fig. 4.11, right column) no such

pattern could be observed. Furthermore, proliferation maps calculated from phosphohistone H3 stained sections were prone to extreme variations from one section to the next for young limb buds (fig. 4.12, top panel) and exhibited random noise in maps of sections for older limb buds (fig. 4.12, bottom panel). Thus, the H3 technique seems incapable of picking up patterns of proliferation and is prone to a high level of noise, unlike IddU/BrdU technique. Further discussion of this issue is in the next section.

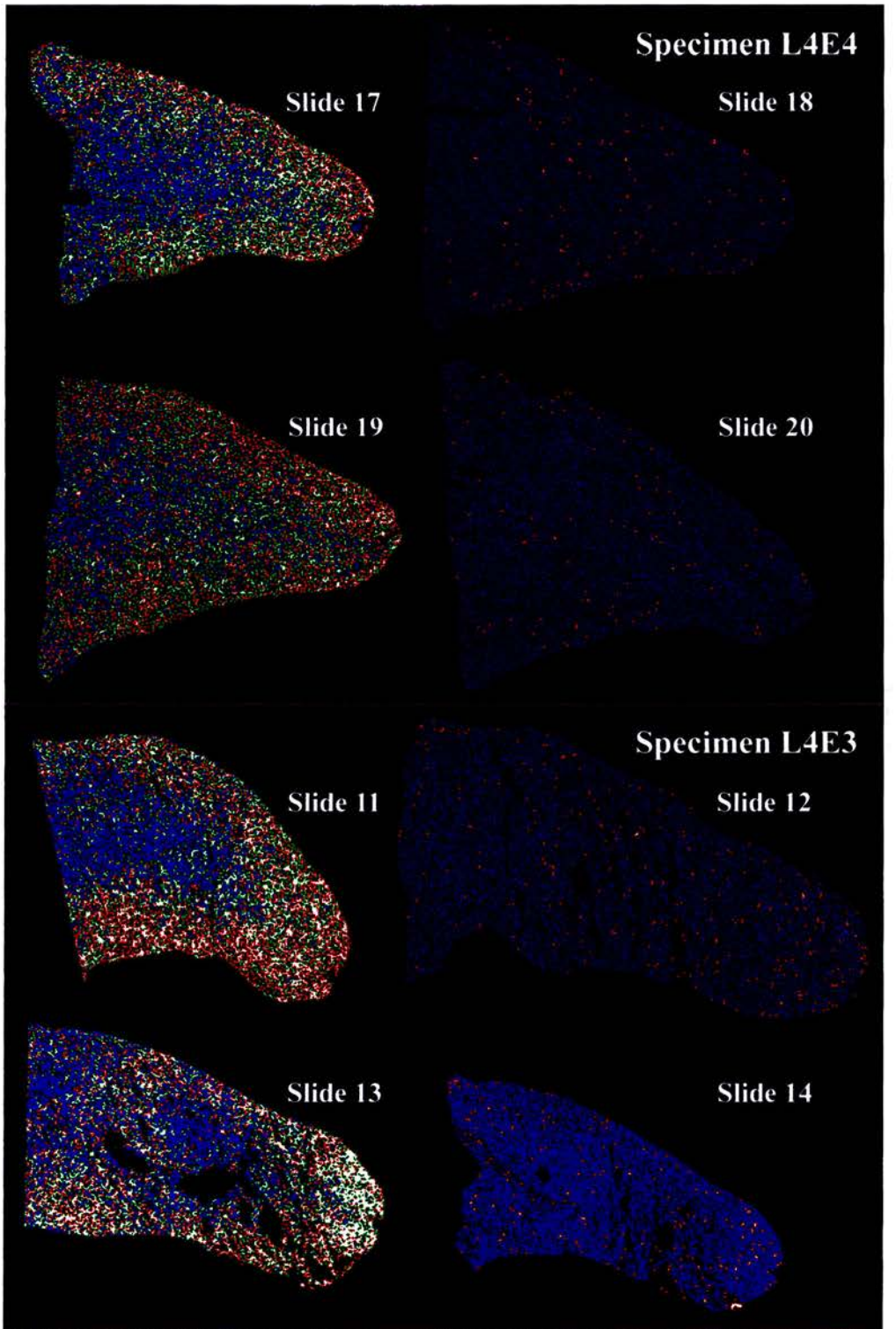

Figure 4.10 IddU/BrdU staining is more informative than phosphohistone H3 staining. IddU/BrdU limb-staining patterns provide information about regions of high and low proliferation; where regions of low proliferation consist of mainly blue cells and regions of high proliferation have many red and green stained cells (first column). Phosphohistone H3 stained sections do not show any obvious staining patterns that reflect patterns of proliferation in the limb (second column).

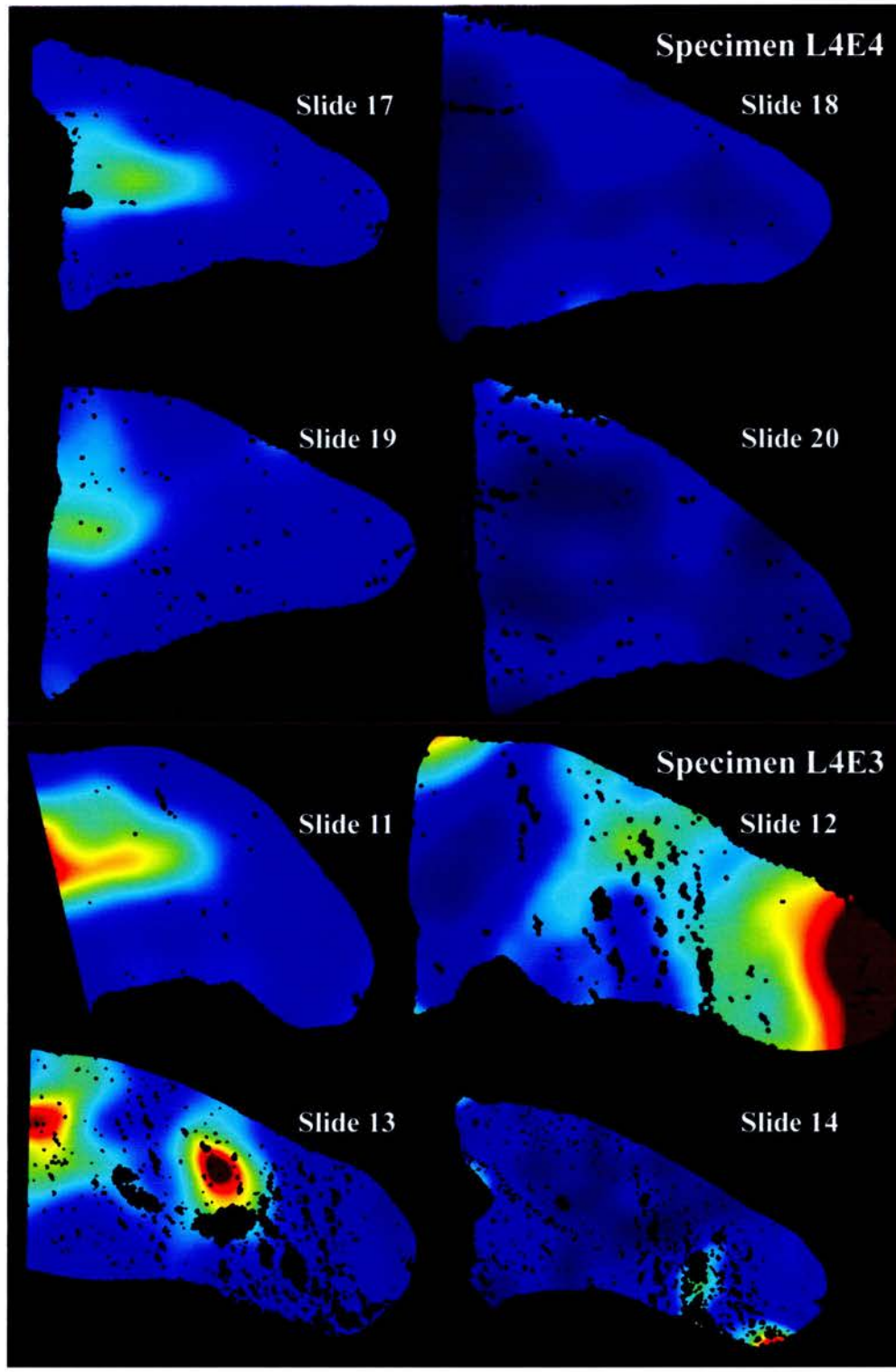

Figure 4.11 Maps of proliferation rates derived from IddU/BrdU labelled sections and phoshohistone H3 labelled sections of E11.5 embryos. A clear pattern of proliferation can be seen in section maps derived from IddU/BrdU stained sections (left coloumn). However, alternate sections stained with phospho-histone H3 do not generate clear patterns of proliferation (right column).

Figure 4.12 Serial sections stained with phosphohistone H3 of an E10.5 and E11.5 mouse limb bud, with their corresponding maps of proliferation (red:blue ratio map).

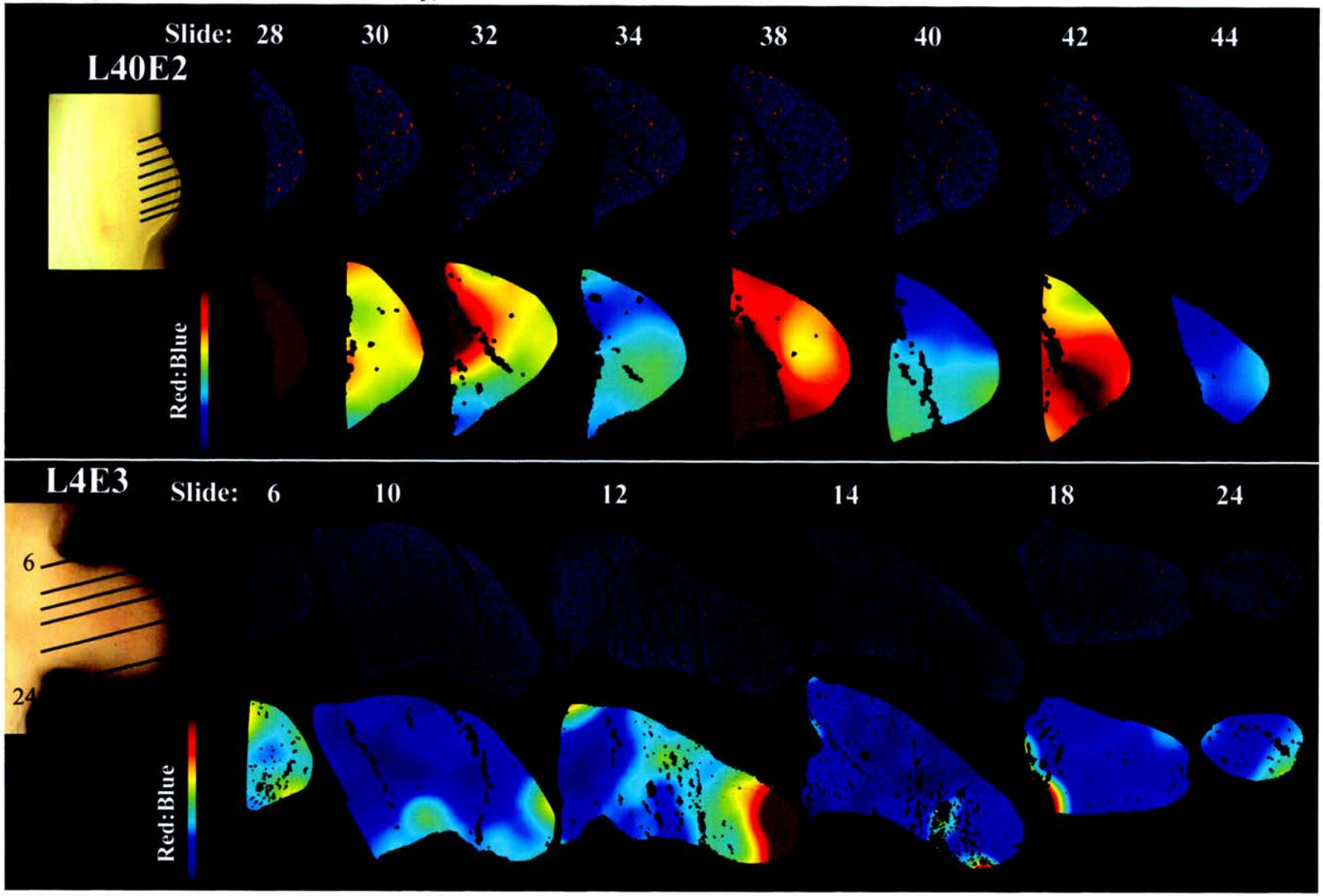

4. 3. Discussion

4. 3. 1 Cell cycle time

These studies show that cell cycle time in an early mouse limb bud (E10.5) is surprisingly short, at 5 hours and relatively uniform across the limb bud. This is comparable to the relatively uniform high mitotic index found in stage 18 chick embryos (Hornbruch and Wolpert; 1970). In our studies we also find that there is a high rate of proliferation in the distal tip of E11.5 embryos, equivalent to that in E10.5 embryos. This is contrary to the findings of Hornbruch and Wolpert (1970) who found that mitotic index is considerably reduced throughout the chick limb bud in subsequent stages of development. The difference in findings may be due to species differences, however I suggest that mitotic index studies may be limited in a similar manner to H3 labelling and cannot highlight a true pattern and rate of proliferation.

The high rate of proliferation in the distal tip of the limb could be attributed to signals emanating from the AER resulting in underlying distal cells remaining in a proliferative state. However, we find that cells in the dorsal and ventral regions are in an equally high state of proliferation with cell cycle times at ~5 hours. This pattern of proliferation is contrary to the prevailing idea that the proliferative zone is located adjacent to the AER (Reiter and Solursh, 1982; Tabin, 1991). Further to this, qualitative results, similar to our findings, have been shown by Summerbell and Wolpert (1972) and Dudley *et al* (2002) but neither of the two groups discussed the significance of the finding. In fact, the second group seemed unaware of this observation as they did not even acknowledge the finding. I suggest that a high rate of proliferation exists in the whole limb bud from an early stage of development (E10.5) to the later stage of development (E11.5), reflecting that the limb bud is a very fast-growing structure at these early stages. It is only a change in cell state leading on to chondrogenesis that results in a reduction in proliferation rates in central and proximal regions. In other words, the zone of proliferation is not isolated

to the distal tip but encompasses the whole limb bud, and local changes in proliferation are found to occur within this zone.

4. 3. 2 Cell cycle time, cell density and Sox9 expression

In the E11.5 mouse limb bud, cell cycle time can range from 5 hours to over 20 hours, depending on the region. The lower rates of proliferation are located in proximal and central regions, and changes in proliferation rates are correlated with a small but significant increase in cell density. In general regions of high cell density give rise to cartilage precursor cells, which matches with early patterns of Sox9 expression seen in the developing limb. Moreover, a later reduction in Sox9 expression is also correlated with a reduction in cellular proliferation rates, as described in section 4.2.3.

My data suggests that changes in cell density may not be tightly linked to changes in proliferation, although the correlation between density and proliferation is thought to have an important role in the growth of cells. Previous research has shown that once a maximum cell density is reached proliferation rates are reduced (Peterson, 1996). This means that some regions may have a high cell density but also a relatively high proliferation rate if the maximum density threshold has not been reached. Moreover, this threshold may be different for different regions of the limb tissue. However, this does not explain our finding of low proliferation rates in the absence of high cell density. Similar spurious outliers were picked up by Summerbell and Wolpert (1972) who attributed the result to the heterogeneity of cells within proximal regions, as it was difficult to make more than an arbitrary division between flank and limb mesenchyme.

In summary, I would suggest that Sox9, although probably not a pure differentiation factor (as discussed in chapter 2) initiates a cascade of chondrogenic events, involving a change in cell density and proliferation rates. Early in development (E10.5) there is a low level of Sox9 expression but this is not correlated with high cell density. As the embryo develops Sox9 expression levels increase and we find that regions of high Sox9

expression correlate with regions of high cell density. Thus, the mere presence of the Sox9 protein does not automatically initiate an increase in cell density (i.e. differentiation). This result suggests that during early development, the Sox9 gene may have a patterning function. Furthermore, high cell density does not automatically translate into low proliferation rates but a correlation is eventually seen, supporting the idea that proliferation rates only begin to decline when a threshold density is reached (Peterson, 1996). It must be noted that the lowest proliferation rates are seen in regions where Sox9 expression is in decline, as to whether this is coincidental or whether a reduction in Sox9 expression is involved in the further reduction of proliferation rates could not be assessed using my data.

4. 3. 3 IddU/BrdU vs. Phosphohistone H3

Finally, it is important to note that a pattern of proliferation can be observed using the IddU/BrdU double labelling technique but it cannot be found using the phosphohistone H3 single labelling technique. It would seem that S-phase constitutes a large proportion of the cell cycle when cells are proliferating quickly and a smaller proportion when they are proliferating slowly. Hence, different numbers of cells are labelled with an S-phase marker in regions of high and low proliferation. In contrast, M-phase seems to change in length. Hypothetically, this means that if M-phase is a tenth of the length of cell cycle time when cells are proliferating slowly then it would still be a tenth of the cell cycle when the cells are proliferating quickly. The consequence of this is that an M-phase marker, such as phosphohistone H3 would label the same ratio of cells in regions of low and high proliferation, showing no difference in proliferation rates in terms of labelling.

The fact that phosphohistone H3 does not resolve patterns of proliferation would suggest that H3 studies are not a good way of monitoring cell proliferation in the limb, especially if we wish to observe their patterns. These results have a significant bearing upon the findings of previous studies, such as those conducted by Sun and associates (2002) on the mouse limb. The group used the technique to examine differences in cell

proliferation between the limbs of normal and Msx2-cre; Fgf4;Fgf8 (double knockout, KO) mice, at 28, 30 and 32 somites. From their analysis they deduced that in double knockout hind-limb buds, labelled cells were evenly distributed throughout the mesenchyme at the same density as in normal hind-limb buds. They therefore concluded that loss of Fgf4 and Fgf8 function in the AER had no detectable effect on cell proliferation in the underlying mesoderm. However, my results would suggest that this conclusion is unreliable when based solely on data gathered from phosphohistone H3 labelling. However, the fact that the group came to the same conclusion using single BrdU labelling, allows for a scope of validity to their argument, as single BrdU labelling is sufficient to highlight changes in rates and patterns of proliferation in the limb.

4. 4 Future work

4. 4. 1 Comprehensive spatial and temporal study of proliferation and cell density in the mouse limb

I have shown that we can establish cell cycle times for E10.5 and E11.5 mouse limb buds. The next step would be to extend this study to cover earlier and later time points. The data can then be used to generate a 4D model of limb proliferation that will help us to address a number of questions. For example, the data should allow us to identify whether cell proliferation remains high in the dorsal and ventral regions, or whether the pattern of proliferation changes in these regions reflecting a pattern of limb bending along the dorso-ventral axis. The 4D proliferation data can also be fed into a computational model of limb development providing further insight into non-intuitive mechanisms involved in limb development.

4. 4. 2 Are all cells dividing?

Here, we have seen a graded distribution of proliferation rates along the proximo-distal axis of the E11.5 mouse limb. However, we do not know if this is a result of the core being a mixture of fast-dividing cells and post-mitotic cells, which have stopped dividing. The only way in which we can establish this is by completing a serial labelling experiment, in which a pregnant female would be injected with IddU at 3 hour intervals for a period of 24 hours. If all of the cells within the core are still in a state of proliferation then they will all be labelled and if not then some of the cells will remain unlabelled.

Chapter 5 – Attempting to reduce Shh expression in the mouse limb

5.1 Introduction

At the beginning of the last century Thomas Hunt Morgan highlighted the importance of gradients in controlling pattern formation; where cellular responses to different thresholds could pattern a system (Wolpert, 1991). Wolpert (1969) expanded upon this idea in his theoretical model of 'positional information', which explained the establishment of differential cell fates in response to morphogen concentrations. A morphogen is defined as a graded signal that is detected by cells and triggers distinct threshold responses, thus specifiying a series of different cell fates. In terms of limb development, cells are assigned positional values along the anterior-posterior axis by a morphogen gradient that originates from the posterior margin of the limb bud (fig. 5.1ai), known as the zone of polarising activity (ZPA; Tickle *et al*, 1975). The diffusible morphogen that originates from the ZPA is the Sonic hedgehog protein (Shh, Echelard *et al*, 1993; Krauss *et al*, 1993; Riddle *et al*, 1993).

5.1.1 The control of digit number and identity by Shh

The Shh protein is attributed with a number of functions in the limb including controlling the number and identity of digits. This was first indicated by work by Saunders and Gasseling (1968) who showed that the grafting of the ZPA from the posterior of one chick limb bud to the anterior of another chick limb bud resulted in a mirror image duplication of digits (fig. 5.1aii). Thus, a chick limb bud which normally has three digits, defined as digits 4, 3 and 2 going from the posterior to the anterior, is transformed into a limb bud of 6 digits, identified as digits 4, 3, 2, 2, 3 and 4. The presence of two signalling centres and two Shh gradients resulting in twice the normal number of digits with mirror image identity.

Grafting a small region of the ZPA rather than the whole region, equates to grafting a smaller number of shh-expressing cells and thus the polarizing signal is reduced, as is

the concentration gradient (fig. 5.1aiii). In such a situation, the limb bud forms few ectopic digits that are more anterior in character (Tickle, 1981). This indicates that high levels of Shh concentration specifies the most posterior digits, whereas low levels of Shh concentration specifies the most anterior digits, excluding digit 1 which forms in the absence of a Shh signal. Thus, it was traditionally thought that only the concentration of the morphogen controls digit identity. However, in 1980, Smith showed that a shorter exposure time to a polarising graft can have the same effect as a smaller number of grafted polarising cells. Furthermore, fate mapping experiments in mice indicate that both Shh concentration and exposure time control digit development (fig. 5.1c, Harfe *et al*, 2004); while specification of the anterior most digits (1, 2 and 3) depends upon differential concentrations of Shh, the specification of the most posterior digits (3, 4 and 5) depends upon the length of time of exposure to Shh (fig 5.1d).

Digit number is related to the size of the limb bud (Alberch and Gale 1985; Lee and Tickle, 1985; Brickell and Tickle, 1989), the growth of which is said to be controlled by signals from the apical ectodermal ridge (AER), as discussed in chapter 1. It has been shown that the expression of the AER signal Fgf4 can be activated by Shh-expressing cells (Niswander *et al*, 1994). It has been reported that the secreted bone morphogenetic protein (BMP) antagonist Gremlin relays the SHH signal from the polarising region to FgF4 in the AER (Zuniga, 1999; Scherz, 2004). Thus, Shh indirectly controls the size of the limb bud through Shh-Fgf4 interaction. Moreover, it has been shown that the complete deletion of Shh expression results in the formation of a single digit in the mouse limb, namely digit 1 (fig. 5.1b; Chiang *et al*, 2001; Kraus *et al*, 2001; Litingtung *et al*, 2002). Together, these results suggest that the Shh gene not only controls the size of the limb bud but also digit number.

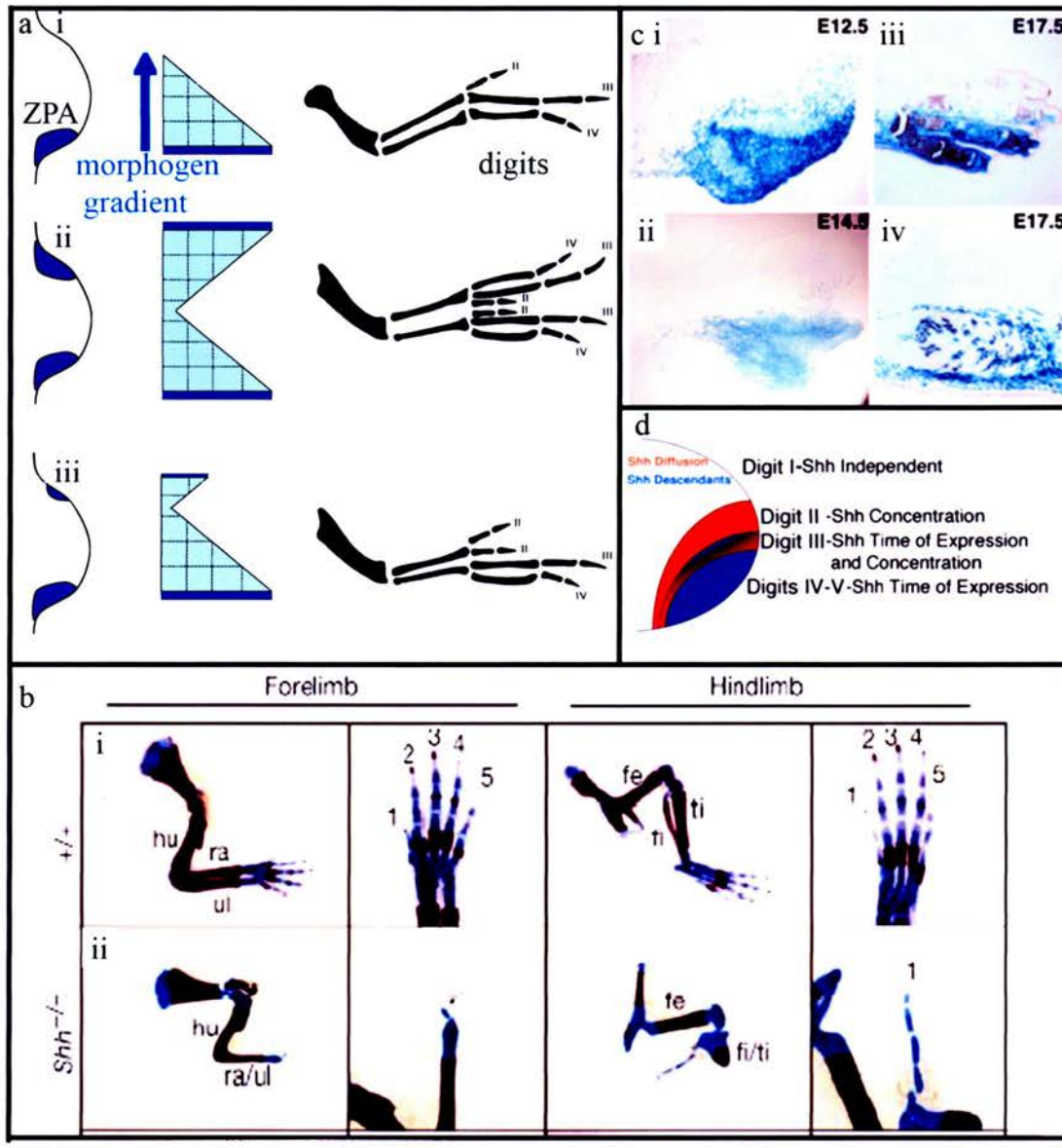

Figure 5.1 Shh expression and pattering in the limb.
(a) Determination of the digits through the effects of the Shh signal eminating from ZPA regions. (i) Normal signal gradient resulting in a normal set of digits (IV-III-II). (ii) Grafting of a ZPA to the anterior of the limb produces a mirror image duplication of digits (IV-III-II-II-III-IV). (iii) Grafting of a small number of ZPA cells to the anterior of the limb produces a chick limb bud with a single extra digit (IV-III-II-II). (Modified from Raff and Kaufman, 1983). (b) skeletal analysis of E16.5 (i) wild type and (ii) Shh -/- mouse limbs (Litingtung et al, 2002). (c) β–galactosidase staining in sections of Shh::GFPCre/+;R26/+ forelimbs show that Shh descendants contribute to digits 3, 4 and 5 at (i)E12.5, (ii)E14.5 and (iii) E17.5 as well as (iv) the posterior zegopod at E17.5 (Harfe et al, 2004). (d) Harfe and colleagues (2004) propose that digit specification depends upon both Shh concentration as well as temporal expression, with different digits being specified by different combinations of Shh concentration and Shh exposure time.

5.1.2 Controlling Shh expression

Many polydactylous mouse mutants have been studied in order to determine the mechanism responsible for the polydactyly phenotype. A significant break through was made when Sharpe *et al* (1999) analysed the sasquatch (Ssq) mouse mutant, which has an ectopic region of Shh expression resulting in the formation of extra digits. The analysis of the mutant (Lettice *et al,* 2002) revealed it to have a transgenic insertion site within intron 5 of the Lmbr1 gene, which resides ~1Mb upstream of Shh. The Ssq transgene was expressed in normal posterior and ectopic anterior sites of Shh expression suggesting that the Ssq locus was involved in the expression of Shh. A further cis-trans test showed that the Ssq phenotype is suppressed in cis by the Shh null mutation. The data supported the hypothesis that long-range disruption of Shh regulation is the mechanism for limb dysgenesis in Ssq mice. Further analysis of the regulatory region showed its deletion leads to the complete loss of limb specific Shh expression resulting in the formation of a single digit in the mouse hind-limb and a stunted skeletal element in place of a digit in the fore-limb (Sagai, 2005), which is comparable to results of Shh deletion in mice (fig. 5.1b; Litingtung *et al*, 2002).

Comparison of genetic sequence between human, mouse, chick and Fugu led to the identification of an ~800bp sequence within intron 5 of the Lmbr1 gene that is near to the Ssq insertion site (fig. 5.2a, Lettice *et al*, 2003). A 445bp fragment of the mouse genome corresponding to this region was used to drive *lacZ* expression in the developing mouse embryo producing an expression pattern reminiscent of ZPA localised expression of the Shh gene in the limb bud. The ~800bp sequence was thus designated the ZPA regulatory sequence (ZRS). Further phylogenetic analysis of the sequence highlighted the presence of a region of ~400bp conserved between all four species. A 305bp sequence from the ~400bp conserved region was found to successfully drive ZPA localised *lacZ* expression. However, as the size of the ZRS region used in constructs was reduced so too was the area and intensity of expression (fig. 5.2b). Thus, in theory, one

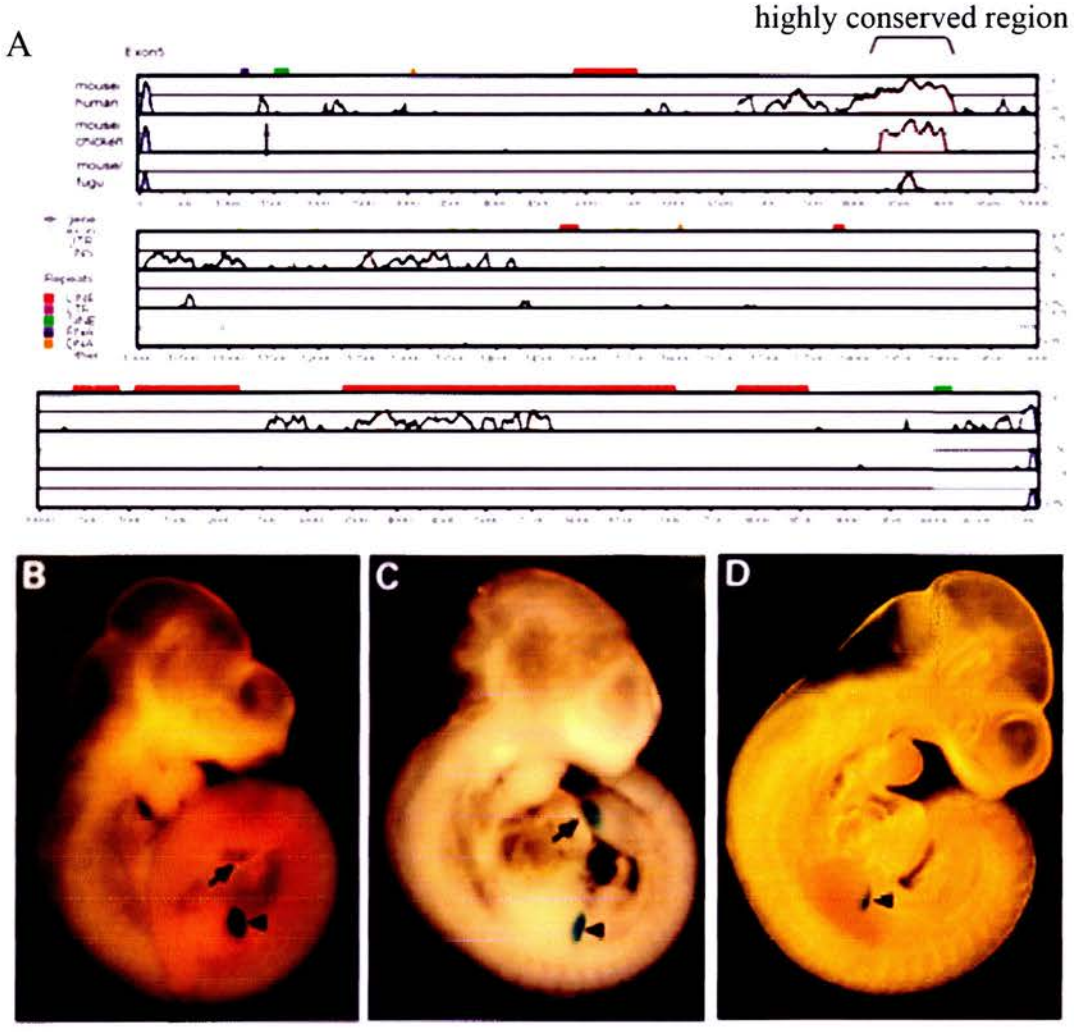

Figure 5.2. Interspecies analysis of intron 5 of the Lmbr1 gene and b-galactosidase expression driven by different regions of intron 5.
(A) interpecies sequence comparision of fourvertebrate species (human, mouse, chick and *Fugu rubripes*) for intron 5 of the Lmbr1 gene. Transgenic embryos showing β–galactosidase expression in E10.5 G0 embryos carrying (B) the 1.7 kb ZRS; (C) the 445 bp mouse construct and (D) the 305 bp fragment. Expression of the reporter gene in the posterior margin of the forelimbs are indicated with arrowheads and hindlimbs with arrows (Lettice et al, 2003).

can achieve an effect of Shh down-regulation in the limb by using different sized regions of the ZRS to drive Shh expression.

5.1.2 Artificially regulating gene expression by using siRNA technology

Over the years many tools and techniques have been developed for gene expression studies, one such tool is siRNA technology. In 2003, Shinagawa and Ishii published a paper detailing a new vector, named pDECAP (fig. 5.3a). The vector was used to knockdown Ski expression resulting in the production of transgenic mouse embryos that were remarkably similar to those of Ski-deficient embryos, with defects of neural tube closure and eye formation.

The pDECAP vector carried a CMV promoter, which was reported to be active in various regions of mouse embryos (Schmidt *et al*, 1990). Shinagawa and Ishii investigated the validity of this statement by generating transgenic mouse embryos containing the ß-galactosidase expression vector driven by the CMV promoter. They found that CMV driven expression was present in almost all embryonic tissues (Shinagawa and Ishii, 2003).

RNA carried by the vector are said to be transcribed using Pol II (Shinigawa and Ishii, 2003), however, Pol II transcripts are transferred immediately to the cytosol, where they induce interferon synthesis (Stark *et al*, 1998) leading to a block in translation and mRNA degradation (Manche *et al*, 1992). In order to prevent an interferon response the vector was designed with a ribozyme cassette that would cut off the m^7G cap structure from the 5'end of the transcript and a MAZ site that would cause Pol II pausing preventing the formation of a 3'poly-A tail. The absence of these two structures would predictably inhibit the transcript from being transported out of the nucleus into the cytoplasm thus preventing an interferon response. Instead, ribonucleases located in the nucleus, such as Dicer (Lee *et al*, 2002) were expected to cleave the transcript into

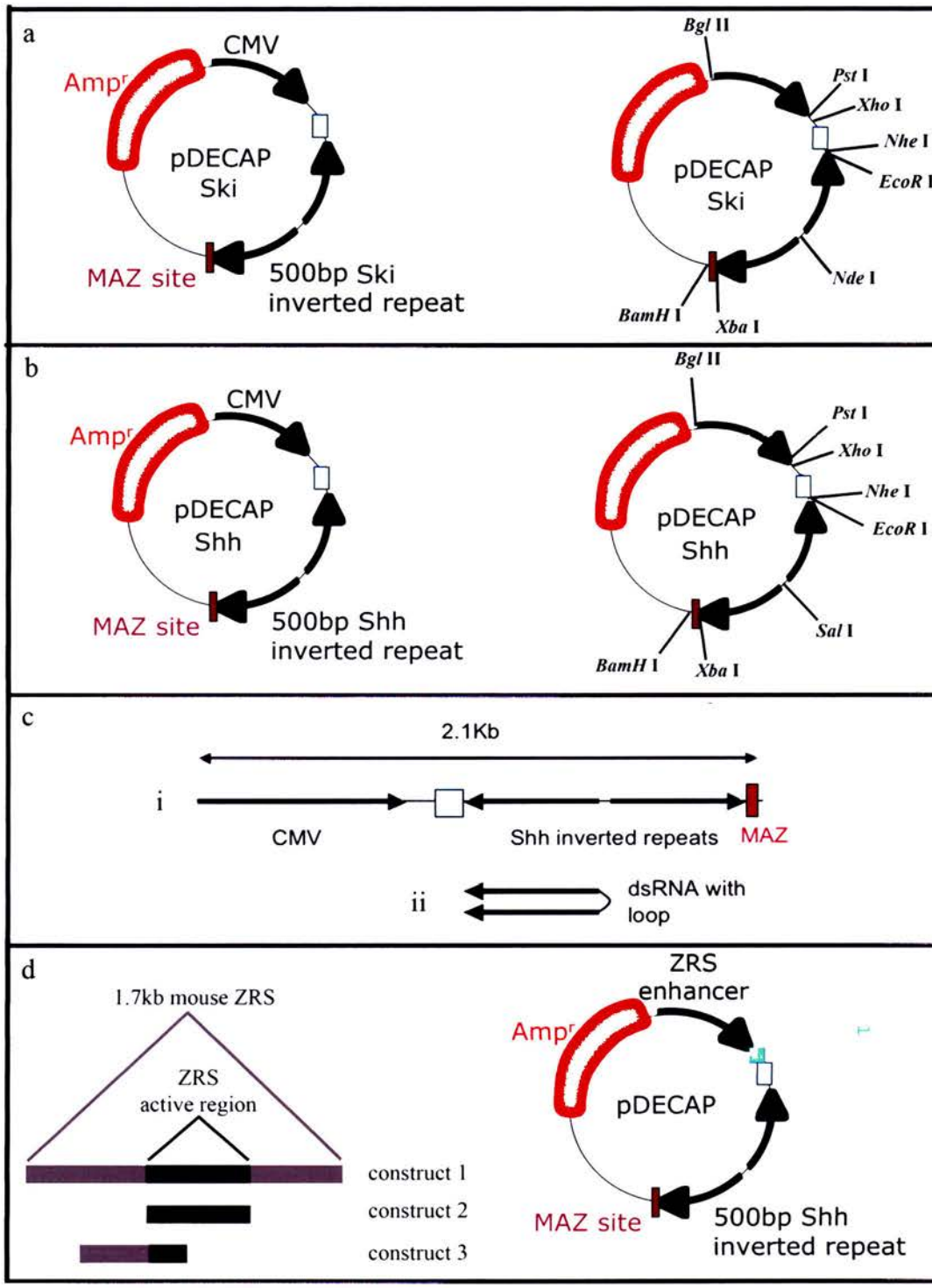

Figure 5.3. Different constructs of pDECAP

(a) pDECAP-Ski construct (Shinagawa et al, 2003). (b) pDECAP-Shh construct. (ci) DNA fragment containing the expression sequence of the 500nt Shh ds-RNA from the pDECAP vector and (cii) the predicted secondary structure of the Shh RNA transcribed from the pDECAP vector. (d) pDECAP-ZRS-βglobin-Shh contruct, with contruct 1 carrying 1.7kb of the mouse ZRS, construct 2 carrying 445bp of the active region of the ZRS and construct 3 carrying 600bp of the ZRS of which 200bp are of the active region.

siRNA which then moves to the cytosol where it would induce the degradation of target mRNA. Moreover, ds-RNA > 400 nt was inserted into the vector and used for knock-down experiments as previous research had shown that ds-RNA > 400 nt is sufficient in effective gene silencing (Hammond *et al*, 2000).

In theory this vector could be used to quickly generate a transgenic mouse with a knockout phenotype. If the CMV promoter is used then this phenotype should be seen in all possible tissues. Slight modification of the vector, in terms of the promoter, could make the vector amenable to tissue specific and knockdown experiments. However, in all cases a number of transgenic animals would need to be generated as even with a CMV promoter the exhibition of a phenotype is at most ~40% in some tissue types of transgenic animals (Shinigawa and Ishii, 2003). Nonetheless, the vector system has the benefit of quickly producing a phenotype whereas other systems such as homologous recombination in embryonic stem cells (Capecchi, 1989) can be time-consuming.

5.1.3 Aim

Although, many experiments have been performed to further understand the control of digit number and identity by Shh none have involved an elegant *in vivo* model of the gradual reduction of Shh expression. Therefore, the effects of reduced levels of endogenous Shh expression on digit number and digit identity have not been directly analysed and understood. Some questions relating to Shh control which remain to be clarified are:

1 – Does a serial reduction in the level of endogenous Shh expression result in a serial reduction in the number of digits in the limb bud?

2 - Does digit identity become more anterior in nature as endogenous Shh expression is reduced?

I aimed to address these questions by generating ZPA-specific Shh knockdown mice using the pDECAP vector carrying a long Shh double-stranded RNA. Three different vectors each one carrying a different length of the ZRS enhancer sequence and a ß - globin promoter (fig 5.3d) were to be created in the hope that they would drive different levels of transcript production in the limb.

However before generating a limb-specific phenotype I felt it prudent to test the efficiency of the vector system and so I aimed to generate a construct carrying a long Shh double-stranded RNA and the CMV promoter (fig. 5.3.b). I expected that the presence of the CMV promoter would drive ubiquitous expression of the transcript resulting in a phenotype similar to Shh -/- mice, where Shh-/- embryos have an overall reduced size that lack distinct fore limb and hind limb structures and exhibit a growth deficit in craniofacial structures (Chiang *et al*, 1996).

5.2 Results

5.2.1 The generation of the pDECAP-Shh construct

The first step in generating the pDECAP construct involved the selection of exonic Shh DNA >400 nt in size, that did not carry restriction sites which would be used for cloning at a later stage. The region selected was 490 nt in length from the 5' end of the Shh gene (fig. 5.4). The forward and reverse double-stranded sequence was amplified using primers which had restriction sites added to the ends of the sequences using the PCR protocol, described in the materials and methods. I was able to amplify both the forward and reverse fragments of the hair-pin at a reasonable concentration of about 100ug per 20ul PCR reaction.

Amplification and gel purification of 1μg of each fragment was then followed by cloning them into an intermediate vector prior to their insertion into the pDECAP vector. Initially, I attempted to use the pGEM11 vector as the intermediate vector. However, after numerous attempts this proved fruitless. It was believed that the fragments may be re-ligating rather than ligating to the vector. After some deliberation, I decided to try and use the pGEM-Teasy vector system, as I knew that a greater level of success is achieved in ligating a DNA sequence to this vector. After a few ligation attempts I was successful in cloning both Shh fragments, which were to form the inverted repeat in the pDECAP vector. I then attempted to sequentially clone each fragment into the pDECAP vector. The cloning of the first fragment proved successful. The annealing of the second fragment proved more difficult. This may have been due to the hairpin secondary structure formed by the inverted repeat sequences, however the pDECAP plasmid was amplified in *E. coli* strain Sure 2 strain (Stratagene), which allows the accurate replication of DNA containing inverted repeats as they are recombination deficient. Sequencing of the fragments revealed that one had base change within a restriction site near the end of the sequence due most likely to a nucleotide change in the primers

>gi|40254618|ref|NM_009170.2| Mus musculus sonic hedgehog (Shh), mRNA
CCTTGCTACCATTTAAAATCAGGCTCTTTTTGTCTTTTAATTGCTGTCTCGAGACCCAACTCCGATGTGT
TCCGTTACCAGCGACCGGCAGCCTGCCATCGCAGCCCCAGTCTGGGTGGGGATCGGAGACAAGTCCCCTG
CAGCAGCGGCAGGCAAGGTTATATAGGAAGAGAAAGAGCCAGGCAGCGCCAGAGGGAACGAACGAGCCGA
GCGAGGAAGGGAGAGCCGAGCGCAAGGAGGAGCGCACACGCACACACCCGCGCGTACCCGCTCGCGCACA
GACAGCGCGGGGACAGCTCACAAGTCCTCAGGTTCCGCGGACGAGATGCTGCTGCTGCTGGCCAGATGTT
TTCTGGTGATCCTTGCTTCCTCGCTGCTGGTGTGCCCCGGGCTGGCCTGTGGGCCCGGCAGGGGGTTTGG
AAAGAGGCGGCACCCCAAAAAGCTGACCCCTTTAGCCTACAAGCAGTTTATTCCCAACGTAGCCGAGAAG
ACCCTAGGGGCCAGCGGCAGATATGAAGGGAAGATCACAAGAAACTCCGAACGATTTAAGGAACTCACCC
CCAATTACAACCCCGACATCATATTTAAGGATGAGGAAAACACGGGAGCAGACCGGCTGATGACTCAGAG
GTGCAAAGACAAGTTAAATGCCTTGGCCATCTCTGTGATGAACCAGTGGCCTGGAGTGAAGCTGCGAGTG
ACCGAGGGCTGGGATGAGGACGGCCATCATTCAGAGGAGTCTCTACACTATGAGGGTCGAGCAGTGGACA
TCACCACGTCCGACCGGGACCGCAGCAAGTACGGCATGCTGGCTCGCCTGGCTGTGGAAGCAGGTTTCGA
CTGGGTCTACTATGAATCCAAAGCTCACATCCACTGTTCTGTGAAAGCAGAGAACTCCGTGGCGGCCAAA
TCCGGCGGCTGTTTCCCGGGATCCGCCACCGTGCACCTGGAGCAGGGCGGCACCAAGCTGGTGAAGGACT
TACGTCCCGGAGACCGCGTGCTGGCGGCTGACGACCAGGGCCGGCTGCTGTACAGCGACTTCCTCACCTT
CCTGGACCGCGACGAAGGCGCCAAGAAGGTCTTCTACGTGATCGAGACGCTGGAGCCGCGCGAGCGCCTG
CTGCTCACCGCCGCGCACCTGCTCTTCGTGGCGCCGCACAACGACTCGGGGCCCACGCCCGGGCCAAGCG
CGCTCTTTGCCAGCCGCGTGCGCCCCGGGCAGCGCGTGTACGTGGTGGCTGAACGCGGCGGGGACCGCCG
GCTGCTGCCCGCCGCGGTGCACAGCGTGACGCTGCGAGAGGAGGAGGCGGGCGCGTACGCGCCGCTCACG
GCGCACGGCACCATTCTCATCAACCGGGTGCTCGCCTCGTGCTACGCTGTCATCGAGGAGCACAGCTGGG
CACACCGGGCCTTCGCGCCTTTCCGCCTGGCGCACGCGCTGCTGGCCGCGCTGGCACCCGCCCGCACGGA
CGGCGGGGGCGGGGGCAGCATCCCTGCAGCGCAATCTGCAACGGAAGCGAGGGGCGCGGAGCCGACTGCG
GGCATCCACTGGTACTCGCAGCTGCTCTACCACATTGGCACCTGGCTGTTGGACAGCGAGACCATGCATC
CCTTGGGAATGGCGGTCAAGTCCAGCTGAAGCCCGACGGGACCGGGCAAGGGGCGGGCGGGGCGGGGAGC
GACTGCGAAATAAGGAACTGATGGGAAAGCGCACGGAAGGAGACTTTTAATTATAAGAATAATTCATAAT
AATAATAATAATGATAATAATAATAATAAGTAGGGCAGTCCAAAGTAGACTATAAGGAAGCAAAAAC
CCCGGGGAGTTCTGTTGTTATGTTTAGTTTATATATTTTTTTTTGAAATTTTTCGTTATTGTCTTATATG
GGTTGTTTTTCTCCTCTCCTGGCTATTTATTTGTTTCGTATGAATAGATGTTTTAAAAATATGAACGGAC
CTTCAAGAGCCTTAACTAGTTTGTGTCTTGGATAATTTATTATTGTGTGAACTGTACTCACAGTGAGGGA
AAGATTATTTTGTGAGGCCAAGCAACCTGCTGAAAGTCTATTTTTCTACATGTCCCTTGTCCTGCGTTTC
AGAAGGCAAACCTCCGCATTCCTCTCCTGCTATGCTCCTGCTTTCCCGCAAGTGTAAACTAAAACCTGCT
CCATGGGGGTCCACAAATTATATTTTTATACACAGAATTGTAAATTAGATTTTTGAGAGATCAATACCTA
ACTGAATGACATTTCATTTTTTGAAAGTGTAAAATATGAAAATATATTATTTTAATTTAACTATTTTCCA
ATGTAATAGCCGTCTTCTGTACTGCCTTCTTGGTTTGTATTTGCTTTGTAACCGCCACTTTGTCATGTTC
TTGGAAACCAAGACTGTTAACGCACACATATACACTTTTTTTTTTGACAGACTGGAAGAACTCTGTTATT
TTTAACTTCAAAGAATTTATTAGAAAATAATATTTTTTAAAAGTGCACCTAGCAGCGAGCCCACGAGGAT
GGAGCCTGTAGTTTGTACAGAGAAAAACAAGGATGTTTTTGCATTAATAAACTGAGAAGTAACTGCTGTA
AATTTACTAAAATGTATTTTTGAATATTTTGTAATAGTTTTATAGAAATAAAGCGTGCCACACACAAAAA
AAAAAAAAAAAAAAAAAAAAAAAAAAAAAAAAAAAAAAAAAAAAAAAAAAAAAAAAAAAAAAAAAAA

Figure 5.4. Shh sequence used to produce the inverted repeats in the pDECAP vector. The sequence was 490 nt in length (pale blue).

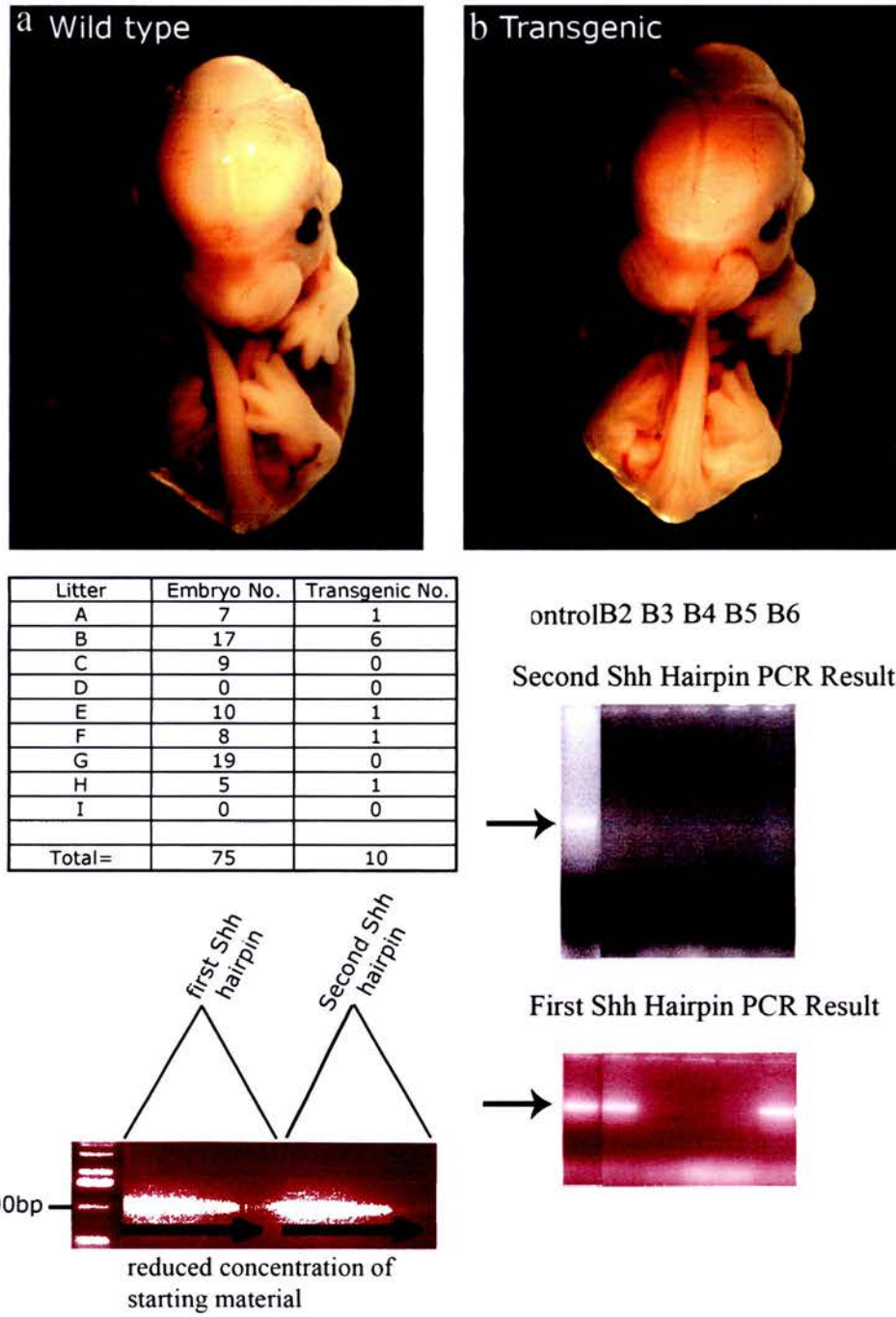

Figure 5.5 Wild type and transgenic mouse embryos had a normal phenotype. Wild-type E13.5 embryo (a) and its transgenic litter mate (b). Both embryos have normal limbs. (c) Table listing the total number of embryos in a litter and the number of transgenics. (di) PCR amplification of the Shh sequence using the sequencing primers on a serial dilution of cDNA (dii) DNA obtained from the amniotic sacs of wild-type control embryos and transgenic litter mates from litter B. Neither of the inverted repeats can be detected in wild type embryos (B3, B4 and B5). In transgenic embryos (B2 and B6) only one of the inverted repeats is detected.

produced by Invitrogen. Therefore, a new primer enabled successful amplification and cloning. This new fragment together with the second fragment successfully cloned into the pDECAP vector between the ribozyme cassette and the MAZ site, forming an inverted repeat sequence.

5.2.2 The generation of transgenic embryos with no discernably abnormal phenotype

A 2.1kb fragment carrying the CMV promoter, ribozyme cassette, Shh inverted repeats and the MAZ sites, was prepared from the pDECAP vector (fig 5.3c). The size and concentration of the fragment was verified using gel electrophoresis and spectrophotometry, respectively, for producing transgenic mice.

All 75 embryos (harvested from 7 litters) generated had wild type phenotypes (fig. 5.5a, 5b). Therefore, it seemed that one of three cases had occurred:

1- The uptake of the fragment had been unsuccessful suggesting that there was a problem with the injection material.
2- Very little siRNA had been produced resulting in a very subtle phenotype that could not be seen with the naked eye.
3- The fragment had been disrupted upon injection and so did not incorporate into the host genome,

Further analysis revealed that 10/75 embryos (fig. 5.5c) were transgenic for one of the Shh repeat fragments, namely the fragment closest to the CMV promoter (fig. 5.5di and dii). The absence of one of fragments meant that double-stranded RNA was not produced to be cut into siRNA, which would otherwise act to knockout Shh functional effect.

After having determined the reason for my failure to knockdown Shh expression I approached a number of other researchers who had recently used the pDECAP construct

to seek their advice. I found that all other researchers had a similar experience, in that one of the hairpin fragments had been frequently lost from the transgenic mice and thus the desired phenotype was not produced. Therefore, I realised that the pDECAP vector system was a highly unreliable vector system for the production of transgenic mice, and that further attempts at producing transgenic mice using this construct would be unwise. Due to time constraints I was unable to pursue other avenues in generating mice with lowered levels of Shh expression, but these avenues have been discussed in section 5.4.

5.3 Discussion

Here I shall discuss the main conclusion that the pDECAP vector is an unreliable system by which to produce transgenic animals. In most cases the inverted-repeat sequence is not integrated into the genome, whether in whole or in part. In cases where it is integrated the phenotype produced does not always correspond to that which is expected.

Other researchers in the unit and I attempted to use the pDECAP vector and we were all unsuccessful in generating transgenic animals with a desired phenotype. In most cases this was because one of either of the inverted repeats were absent in the transgenic mice. For example, Alan Hart (personal communication) was attempting to knockdown a novel gene NM_029537, which harboured a missense mutation in one of his ENU mutants that presented a congenital diaphragmatic hernia (CDH; a recessive lethal condition for the mouse). He was trying to prove that this gene was responsible for the CDH phenotype by knocking down its expression using the pDECAP vector. The gene was relatively small (total coding ~630bp) therefore, he was able to design the pDECAP vector to take 500bp of DNA, which represented the majority of the gene. Upon injection he found that 2 out of the 3 founder lines only had one arm of the inverted repeat hairpin. Thus, the lack of transgenic mice with the complete inverted repeat sequence suggests that when in the oocyte the construct may be digested at the hairpin region prior to integration. Although in my case all transgenics only carried the first hair-pin, in other cases one or the other arm of the inverted repeat sequence was missing. Therefore, I can only speculate that the second Shh fragment was more prone to degradation than the first.

However, there are also examples of transgenic mice that have both inverted repeat sequences but do not have the desired phenotype. For example, Shinagawa and Ishii (2003) generated 13 embryos containing the exogenous pDECAP-Ski DNA fragment. They confirmed integration by Southern blotting and estimated copy number to be 2-12 copies. They also detected si-RNA in transgenic mice using Northern blotting.

Nonetheless, only 5 of the 13 transgenic embryos exhibited neural tube closure. A further example is that of Alan Hart's third founder that harboured both arms of the construct but did not appear to knockdown the NM_029537 gene. In this case, RT-PCR was performed but no major difference in the RT-PCR signal was seen between wild type animals and transgenic animals. It was therefore, not surprising that he did not see any phenotypic difference between the two. However, he did not check copy number and so it may have been very low so that not enough hairpin RNA was made to interfere with endogenous mRNA.

In summary the pDECAP vector system is not an efficient means of knocking out gene expression. In fact it is extremely unreliable and on the whole is unable to produce any discernable phenotype. This is largely due to the fact that one of either of the hair-pin fragments are lost prior to integration and even when both fragments are present a phenotype can not always be seen. Therefore, I would suggest that for the purpose of generating Shh knockdown mice more conventional means be used as discussed in the next chapter.

5.4 Future Work

In 1996 Quinn and associates published a paper in which they had examined the roles for the Pax6 gene in eye and nasal development by producing chimeric mouse embryos composed of a mixture of wildtype and *Sey* mutant cells. The distribution of mutant *Sey* cells was determined by the inclusion of genetic markers. A similar method could be adopted to generate Shh chimeras with different numbers of Shh expressing cells. This would allow us to assess the affects of lowered levels of Shh expression on limb patterning. In this case, Shh mutant strains would be intercrossed to produce eight-cell stage embryos that are all genetically pigmented (C/C), homozygous $Gpi1^{b}$ /$Gpi1^{b}$ but differ at the Shh locus (-/+, -/-, +/+). These would then be aggregated to BALB/c embryos (albino c/c, homozygous $Gpi1^{a}$/ $Gpi1^{a}$, and wildtype for the Shh locus +/+). This should result in embryos that have a limb ZPA composed of different proportions of Shh expressing and non-expressing cells. The cellular compositon of the limb could be quantitatively assessed by DNA in situ hybridisation and by using GPI electrophoretic variants (encoding the ubiquitous enzyme glucose phosphate isomerase e.g. GP1a and GP1b; West and Flockhart, 1994).

This technique should generate some embryos with a large number of wild type cells and a high level of Shh expression and others with few cells and a low level of Shh expression. In theory, visible phenotypic changes in Shh expression levels could range from about 90% - 10% of normal levels of expression from one chimera to the next. In terms of limb patterning this means that different chimeras will have different amounts of Shh expressed from the ZPA and thus have different Shh concentration gradients across the limb bud. Previous research has shown that $Shh^{-/+}$ mutants have normal phenotypes (Chiang et al, 1996), therefore it is proposed that chimeras will have a reduced number of digits if Shh expression is less than 50% of normal expression levels. Furthermore, it is proposed that lower levels of Shh expression will result in more anterior digit identity.

An alternative method that could be used to knock down Shh expression specifically in the limb involves the use of a conditional Cre/loxP system, as described by Kuhn and Torres (2002). The technique involves generating embryos with lox sites at either end of ZRS sequence. Pregnant mothers would then be injected with different levels of tamoxifen at a time when there is no sign of Shh expression in the embryonic limb (Torres, personal communication), such as at day 9 when the hind limb has not yet budded from the flank of the body wall. In essence, higher levels of tamoxifen would cause a greater loss of the ZRS sequence in embryos, resulting in lower levels of Shh expression in the limb and different limb phenotypes. The Cre/loxP conditional knockouts have a benefit over chimeras as Shh expression would only be reduced in the limb and so embryos could be left to develop to term as the phenotype is not embryonic lethal. Further to this, Cre/loxP conditional knockouts are more reproducible and may provide a clearer results in that they can produce invivo tissue combinations where all cells of one tissue, such as the limb mesenchyme, are mutant from particular stages of development, while surrounding tissues would remain wild-type.

Chapter 6 Concluding Remarks

The limb is an excellent model system for understanding developmental processes as both patterning events and mechanical changes can be observed and manipulated easily in this external organ. Moreover, the limb provides both genetic and morphological information pertaining to the evolutionary origins of the tetrapod limb. More than 60 years since the completion of early limb experiments, the scientific community continues to try to unravel the puzzle of how a simple mass of mesenchymal cells develop to form the complicated structure of the limb - a structure containing over 50 muscles, numerous skeletal elements in specific positions connected by tendons and ligaments, infiltrated by nerve and blood supply networks.

The purpose of this thesis was to provide greater insight into the development of the vertebrate limb bud, taking the mouse limb as a model system. Rather than focussing on a single aspect of limb development I have revisited a number of issues in more detail than has been done before by developing and using a variety of techniques and new computational tools. My analysis has allowed me to come to a number of novel conclusions in relation to the development and possible evolution of the vertebrate limb.

In this thesis I have presented work on three main aspects of limb development. Two aspects were fruitful in advancing our understanding of embryonic limb development. These were the analysis of Sox9 expression and, proliferation and cell density studies in the mouse limb. The third, in which we aimed to analyse the patterning effects of reduced levels of endogenous Shh expression, was unsuccessful due to technological failure. However, an alternative approach, as suggested in chapter 5, may be successful in allowing us to meet our aim in the future.

6.1 Scientific and Technological Advances

6.1.1 A comprehensive analysis of Sox9 expression

Numerous gene expression studies have been performed over the past few years and a number of gene expression databases, such as EMAP have been constructed. However, no detailed comprehensive study of Sox9 expression has been published. In this thesis I present the first comprehensive analysis of Sox9 expression patterns in the early mouse limb bud using newly developed OPT software. As shown in this thesis, the new software allows for a more informative analysis to be completed on accumulated data than was previously possible. The data collected spans the point at which Sox9 expression is seen as an amorphous smear until its expression begins to disappear in distal phalangeal regions.

6.1.2 A core dogma about skeletal patterning is not true

In the past many groups have studied the evolutionary development of the limb skeleton with respect to chondrogenic events, such as the appearance of cartilaginous elements (Milaire, 1978; Burke and Alberch, 1985; Hinchcliffe and Vorbeyeva, 1999). These studies did not provide a real insight into early patterning events, rather they could be compared to fossil studies in which conclusions are also derived from a late developmental morphology. In contrast, my study involved the analysis of a slightly earlier stage of chondrogenic development, namely the Sox9 pattern which was considered to be the earliest known marker of chondrogenesis (Chimal-Monroy, 2003).

Studies of late chondrogenic events have led researchers to suggest that a main central axis, otherwise known as the 'metapterygial axis', runs along the ulna/fibula into a 'digital arch' off which digits branch. However, my analysis of the Sox9 expression pattern shows this core dogma to be untrue. The creation of the skeletal pattern in the

mouse limb does not involve all the digits branching off from the digital arch, which is a part of a main central axis (metapterygial axis). Instead I have found that digits arise from both anterior and posterior zeugopodal elements. However, the existence of a 'metapterygial axis' is not completely dismissed as discussed in chapter 2. In this thesis I propose that any such axis passes through the femur, fibula and ends in digital region 4. Other skeletal elements branch off this axis and may further branch into skeletal elements, for example I suggest that the anterior zeugopod branches off the main axis and then further branches into digital regions I, II and III. This model can be seen as an alternative to the digital arch model, or a separate model of an earlier stage of digital deveopment.

6.1.3 Generation of computational tools for the analysis of cellular proliferation and cell density

Early limb proliferation studies have been qualitative in nature. In recent years, Martynoga et al. (2005) developed an IddU/BrdU double labelling technique that allows for the quantification of cell cycle time. In this thesis, I have presented the same technique optimised for limb tissue together with new computational tools that allow for the fast, automatic, and relatively accurate processing of sample images that contain thousands of cells. The tools generate plots of patterns of cell cycle time across a specimen stained with IddU/BrdU and DAPI. The tools were also developed to analyse specimens labelled with phosphohistone H3. Finally, the tools can be used to analyse and generate a plot of patterns of cell density across a section.

6.1.4 Proliferation rates appear to be extremely high

The newly developed proliferation tools were used in the successful analysis of mouse limbs from two developmental stages. The results qualitatively matched those published in the literature. Importantly, at a quantitative level, we have been able to establish that

cell cycle time is high at about 5 hours in both the E10.5 and E11.5 limb bud. Over 24 hours, from E10.5 to E11.5, proliferation does not significantly decrease in certain regions of the limb bud, such as the distal tip. At E10.5 the high rate of proliferation is uniform across the limb bud and at E11.5 the high rate of proliferation is maintained in the distal tip, dorsal and ventral regions of the limb. This is contrary to the findings of Hornbruch and Wolpert (1970), who found that proliferation rates decrease in the distal tip as the age of the limb bud increases. The dfference between the two results may be due species differences as my study was completed on the mouse whereas that of Hornbruch and Wolpert was completed on the chick. Different analysis techniques were also used which may also have affected the results. An IddU/BrdU study completed on the chick limb would clarify the situation and reveal the true nature of proliferation in the limb.

6.1.5 No proximal-distal gradient of proliferation and no "proliferative zone"

The AER is known to be essential to outgrowth of the limb bud and it is assumed that this is achieved through an AER-induced "proliferative zone" located at the distal tip of the limb bud (Niswander, 1993). However, my results show no evidence of a distally localised region of high proliferation in either E10.5 or E11.5 limbs, rather a high region of proliferation runs along the ventral border to the distal tip and on to the dorsal border of the limb. Therefore the results suggest that a "proliferative zone" does not exist. Supporting this conclusion is the fact that there is no general proximal-distal gradient of proliferation, rather lower rates of proliferation are localised to presumptive chondrogenic regions seen only in E11.5 limbs. In these regions proliferation rates go down dramatically from about 5 hours to over 20 hours, which roughly corresponds with condensation events. I suggest that a high rate of proliferation (Tc = 5 hours) exists across the limb bud from E10.5 and it is cellular changes that result in differences in proliferation rates across the limb bud at later stages.

6.1.6 Limb growth is due to the combinatorial effect of a number of factors

In this thesis, I have shown that equivalently high rates of proliferation are found in the ventral, distal and dorsal regions of the limb while limb outgrowth occurs predominantly along the proximal-distal axis. Thus, limb bud outgrowth must be achieved by more than cellular proliferation alone. In 1977 Ede *et al.* suggested that over-all form arises from the pattern of cell division and migration of the mesodermal cells. In contrast, Wolpert (1981) stated that it was much more likely that the form of the limb is determined by the ectodermal jacket; in such a case, growth by cell proliferation is regarded as a space-filling process and the form of the tissue is determined by the jacket. In fact, both of these ideas may be true. Baena-Lopez and associates (2005) have shown that cell divisions are highly orientated in the Drosophila wing in a manner that correlates with the majority of growth occuring along the proximo-distal axis. Furthermore, Li and Muneoka (1999) completed studies which indicate that the AER has a chemoattractive function that directs cell migration towards the distal tip; thus the AER regulates limb outgrowth. Lastly, we have found that limbs grown in culture become malformed if the ectoderm has been damaged and that mesodermal cells spill out from the limb bud, much like a viscous fluid, when the ectodermal jacket has been torn (unpublished results). Thus, limb growth is most likely to be a combinatorial effect of the constraints imposed by the ectoderm, cellular proliferation rates, cell migration and directed cell division.

6.1.7 The threshold effect of Sox9 expression on cellular condensation

An integration of Sox9 expression data with cell condensation data showed that Sox9 expression can be seen prior to cellular condensation, as stated by Chimal-Monroy (2003). However, the analysis of specific levels of Sox9 expression in relation to cellular condensation have revealed that condensation only occurs in regions in which Sox9

expression is high. The results, therefore, suggest that cellular condensation occurs only when Sox9 reaches a threshold concentration.

6.1.8 Phosphohistone H3 labelling is uninformative

I have shown that phosphohistone H3 labelling is not as sensitive as IddU/BrdU labelling. Therefore, the technique can be uninformative with regards to patterns of proliferation. This finding suggest that previous studies which have stated that there is uniform proliferation in a sample may be inaccurate. In summary I suggest that the technique should be avoided for proliferation studies.

6. 2 One small limb for man one giant leap for mankind

Many researchers acknowledge the fact that it is essential to take a holistic perspective when trying to understand development and evolutionary theory. In fact, the literature provides evidence of researchers attempting to put together different pieces of information in order to complete the big picture (Johnson and Tabin, 1997; Schaller et al, 2001; Hinchcliffe 2002; Sanz-Ezquerro and Tickle, 2003). However, we are limited by our own intuition and as such cannot produce a complete picture of development through thought and experimentation alone. Thus, the next step is to integrate the growing mountain of data into a computational framework, such as a model of limb development. Thus, our group aims to integrate the work I have completed during my PhD into a 3D model of gene expression and digital development, and 4D computational model of limb development. However, my data alone will not help to complete the 4D model of limb development; information about cell migration, directed division, gene expression, vasculature formation, to name but a few, are also required. It is my belief that ultimately, only when a limb research consortium is formed and their data is pooled into one computational model can we complete the picture of limb development.

Chapter 7 Materials and Methods

7.1 Manipulation of nucleic acids

7.1.1 General molecular biology reagents

All chemicals were analytical grade and were supplied by Sigma, Roche, Fisher, Invitrogen and BDH. Restriction enzymes were supplied by Roche and New England BioLabs (NEB). Nucleic acid manipulations were performed in 1.5ml centrifuge tubes unless stated otherwise. General solutions were prepared by HGU technical staff, autoclaved and stored at room temperature.

Tris.HCl

Tris base (tris[hydroxymethyl]aminomethane was dissolved in sterile water. HCl was used to adjust the pH to the required value.

EDTA

EDTA (ethyldiaminetetra-acetic acid di-sodium salt) was dissolved in sterile water. The solution was adjusted to pH8.0 by adding solid NaOH.

TE buffer

10mM Tris.HCl (pH7.5); 1mM EDTA.

TBE buffer, 20X stock

Tris base	216g
Boric acid	110g
0.5M EDTA	80ml

Distilled water was added to a final volume of 1 litre. Stock was diluted to 1X with distilled water.

TAE buffer, 50X stock

Tris base	242g
Glacial acetic acid	57.1ml
0.5M EDTA	100ml

Distilled water was added to a final volume of 1 litre. Stock was diluted to 1X with distilled water.

7.1.1.1 DEPC-treatment of solutions

Sterile water (dH_2O), phosphate buffered saline (PBS) was DEPC-treated by the addition of 1µl/ml DEPC (Sigma) followed by gentle mixing using a magnetic stirrer for 1-2 hours. The solution was then allowed to sit in a fumehood at room temperature overnight prior to autoclaving.

7.1.2 Restriction enzyme digestion

Digests were ideally carried out in a large volume (usually 200 µl) to maximise the amount of product obtained. Reaction volume was dictated by the requirement that the total volume of enzyme never exceeded 10% of the total reaction volume, to prevent inhibition of digestion by glycerol. Restriction enzymes were supplied by Roche and New England BioLabs (NEB). Enzyme was added at a concentration of 5-10units/µg DNA, along with appropriate 10x buffer diluted to 1x concentration with dH_2O. The manufacturers guidelines were followed to determine the correct buffer and incubation temperature for each enzyme. Double digests were performed where enzyme buffer and incubation temperature requirements were compatible.

7.1.3 Agarose Gel Electrophoresis

To prepare the gel, the required amount of standard agarose (High Pure, BioGene) or low melting point (LMP; Invitrogen) agarose was dissolved in either 1XTBE or

1XTAE (weight/volume) by heating. Molten agarose was cooled and ethidium bromide added to a final concentration of 50μg/100ml agarose. DNA size markers were run alongside experimental samples to estimate the size and/or amount of DNA in the samples. The size marker used routinely was 1Kb DNA ladder (Invitrogen). Samples were run in 1x loading buffer. The DNA in ethidium bromide stained gels were visualised by UV transillumination using a digital camera.

Solutions

Gel loading Buffer, 10x

Loading buffer was prepared as a 10X stock as detailed below and stored at room temperature.

	Final concentration
Ficoll (Sigma)	15%
Orange G (Sigma)	1%

Made to required volume with TE, pH8.0.

7.1.4 DNA quantification

DNA concentrations were determined in one of two ways: by agarose gel electrophoresis or by measuring DNA absorbance in a spectrophotometer at 260nm (A_{260}). To determine DNA concentration by electrophoresis, several different volumes of the DNA were run alongside DNA ladders (Invitrogen). An estimate of the concentration was made by visual comparison of the samples with the known amounts of DNA under UV illumination.

To determine the concentration by spectrophotometer, the DNA samples were diluted with DEPC-dH_2O. The spectrophotometer was calibrated using a blank sample (dH_2O). The samples were placed in clean cuvettes and the absorbance at

260nm (A_{260}) was measured. The concentration of the original sample in µg/ml was calculated as follows:

Concentration (µg/ml) = A_{260} value x dilution factor x 50µg/ml of DNA.

7.1.5 DNA purification

7.1.5.1 Agarose gel purification

Linearised DNA fragments or PCR products required for further ligation experiments were purified by electrophoresis using standard agarose (High Pure, BioGene) and excised from the gel using a razor blade. DNA was recovered from the excised gel using a Gel Extraction Kit (Qiagen), according to the manufacturers instructions. DNA fragments required for microinjection experiments were purified by electrophoresis using LMP agarose razor excision and the DNA was then recovered using a bio-extraction machine according the manufacturers instructions.

7.1.5.2 Phenol-chloroform purification

For phenol-chloroform extraction of DNA an equal volume of phenol:chloroform:isoamyl alcohol (25:24:1) was added to 250µl of DNA suspended in sterile water. The suspension was vortexed for 30 seconds and centrifuged for 2 minutes at 13,000rpm. The upper phase was transferred to a clean tube and the procedure was repeated. The upper phase was then transferred to a clean tube and the DNA was precipitated through the addition of 1/10 volume 3M sodium acetate and two volumes 100% Ethanol (EtOH) and storage at –20°C for 2 hours. After which, the chilled solution was centrifuged for 15 minutes at 4°C and any supernatant was discarded. The DNA pellet was then washed using 70% EtOH, air dried and resusspended in dH_2O.

7.1.6 Ligations

Fragments with cohesive complementary ends were either ligated overnight at 16°C using T4 DNA ligase and T4 DNA ligation buffer (Rosche) or for 5 minutes at room temperature using T4 DNA ligase quick kit and T4 DNA ligation buffer (Rosche). In order to maximise ligation efficiency, ligations were set up with 1:1 and 1:3 vector:insert molar ratios. Ligation controls lacking either insert or ligase were also included. The amount of vector in each case was approximately 100ng and the total reaction volume was 10µl.

7.2 Microbiology

Aseptic technique was observed for all steps involving the growth of bacterial cells (setting up cultures, pouring agar plates, selecting single colonies and storing bacterial stocks). Liquid cultures were grown with vigorous shaking (220rpm) and dry cultures were grown on inverted agar plates at 37°C overnight.

7.2.1 Growth media for bacterial cultures

HGU technical staff prepared Luria-Bertani broth (L-Broth) and Luria-Bertani agar (L-agar) as detailed below:

<u>L-Broth</u>

Amount per litre:

Tryptone	10.0g
Yeast extract	5.0g
NaCl	10.0g
Glucose	1.0g

<u>L-Agar</u>

Amount per litre:

Tryptone	10.0g
Yeast extract	5.0g
NaCl	10.0g
Agar	15.0g

7.2.1.1 Antibiotic selection

Aliquots of Ampicillin (Invitrogen) 100mg/ml in dH_2O were stored at -20°C. L-Broth and L-Agar which had 100µg/ml were used for the growth and selection of Ampicillin resistant bacterial colonies.

7.2.1.2 Xgal/IPTG indicator plates

When attempting to select for clones carrying pDecap (Shinagawa and Ishii, 2003) or pGEM-Teasy (Promega) plasmids with inserts Xgal and IPTG agar plates were used. Xgal (5-bromo-4-chloro-3-indolyl-b-D-galactoside, Invitrogen) at a final concentration of 40µg/ml and IPTG (isopropyl b-D-thiogalactoside, Invitrogen) at a final concentration of 0.2mM were added to molten L-agar before pouring plates.

7.2.2 Transformations

Library efficiency DH5α *E.coli* competent cells (Invitrogen) were transformed with pGEM T-easy plasmid DNA according to the manufacturers instructions. Transformation controls included puc19, un-ligatted plamids and plasmids without inserts. The amount of plasmid in each case was approximately 10-100ng. Following transformation, 50µl and 100 µl samples of culture were plated in duplicate on LB agar plates with 100µg/ml of ampicillin.

Plasmid vectors (pDECAP) carrying inverted repeats were transformed into SURE 2 supercompetent cells (Stratagene) as the *E.coli* strain lacks components of the pathways that catalyze the rearrangement and deletion of non-standard secondary and tertiary structures, such as inverted repeats. Transformations were performed with and without plasmid DNA using 100 µl aliquot cells and 10pg of pUC18 control DNA according to the manufacturers instructions. The amount of plasmid DNA used was 25-50 ng per aliquot of cells. Following transformation, 5µl, 25µl and 50 µl samples of culture were plated in duplicate on LB agar plates with 100µg/ml of ampicillin.

7.2.3 Isolation of Plasmid DNA

The extraction of small amounts of plasmid DNA (minipreps) from bacterial colonies was accomplished using QIAquick Spin Miniprep Kit (Qiagen). A single colony was selected to inoculate 2ml L-Broth containing a suitable antibiotic for overnight growth at 37°C. The following morning, plasmid DNA was extracted using the kit according to the manufacturers instructions. Plasmid DNA was eluted in either 30µl or 50µl elution buffer. For the extraction of large amounts of plasmid DNA (maxipreps), a 2ml starter culture was established as described previously and incubated at 37°C for 8 hours. The starter culture was then re-suspended in 400ml L-Broth, with antibiotic selection, in a 1 litre conical flask to allow aeration of the bacterial culture, which was incubated overnight at 37°C. Plasmid DNA was extracted the following morning using the QIAquick plasmid maxi kit (Qiagen) according to the manufacturer's instructions. DNA was eluted in 400µl autoclaved TE, pH8.0. DNA concentrations were determined either by agarose gel electrophoresis or by spectrophotometry.

7.3 Polymerase chain reaction (PCR)

7.3.1 Reagents

dNTPs:

dNTPs were purchased from ABgene as stocks of 100mM. Working stocks of 25mM were made by mixing 25µl of each of the dNTPs (dATP, dCTP, dGTP, dTTP) to a final volume of 100µl and stocks were stored at –20°C. dNTPs were used in PCRs at a final concentration of 0.2mM.

Oligonucleotide primers:

PCR primers were designed by selecting a sequence, usually between 20 and 30 nucleotides in length, for which the [G+C]:[A+T] ratio was approximately equal. Care was taken to avoid the likelihood of primers self-annealing or annealing with each other. Primers were purchased from Invitrogen as lyophilized desalted compounds. Stocks were made up at 100µM using sterile dH_2O and primers were used in PCRs at a final concentration of 0.5-1µM.

Primer sequences:

Amplification

A1FShh500: CATGAAGTCGACACATTCTGGTGATCCTTGCTT

A2RShh500: GCATGAGAATTCAGTCGAAACCTGCTTCC

B1FShh500: GATCTAGTCGACGATTTCTGGTGATCCTTGCTTCC

B2RShh500: TACGCATCTAGAAGTCGAAACCTGCTTCC

Sequencing

A1Rseq :ACATTCTGGTGATCCTTGCTTCC

ZRS-F: GTCCAGAACCTCACACATGATC

CMV-For: TGCGGTAGTTTATCACAGTT

B1Fseq: GATTTCTGGTGATCCTTGCTTC

MAZ: CACACCTCCCCCTGAACCT

Myo 1: TTACGTCCATCGTGGACAGC

Myo 2: TGGGCTGGGTGTTAGTCTTA

m13 forward: GTAAAACGACGGCCAGT

m13 reverse: GGAAACAGCTATGACCATG

Additional reagents:

Ampli*Taq* DNA polymerase (5u/µl) (Roche) was used at 0.2µl per 20µl sequencing reaction, and 1µl per 100µl amplification reaction. PCR buffer (Roche) was a 10X stock and therefore diluted 1:10 for reactions. Mg^{2+} (Roche) was used at a final concentration of 2.5mM unless stated otherwise. The reaction was made up to the required volume with sterile dH_2O. PCR amplification required the addition of DMSO (Sigma) at a final concentration of 10% in order to enhance the efficiency of the PCR reaction by decreasing the stability of GC bonds and thus lowering the melting temperature. PCRs were performed in 0.5ml centrifuge tubes in a MJ Research DNA Engine Tetrad.

7.3.2 PCR programmes

Shhfragments (amplifying shh fragments)

94°C for 3 minutes

93°C for 15 seconds

Annealing temperature of 65°C for 20 seconds

72°C for 1 minute per kb of target sequence

Repeat steps 2-4 34 times

72°C for 5 minutes

4 °C for 5 minutes

Shh50C (genotyping mice for shh fragments)

94°C for 3 minutes

94°C for 20 seconds

Annealing temperature of 59°C for 35 seconds

72°C for 1 minute per kb of target sequence

Repeat steps 2-4 50 times

72°C for 5 minutes

4 °C for 5 minutes

Myogenin (internal control genotyping)

94°C for 3 minutes

94°C for 20 seconds

Annealing temperature of 59°C for 30 seconds

72°C for 50 seconds per kb of target sequence

Repeat steps 2-4 34 times

72°C for 5 minutes

4 °C for 5 minutes

Sequencing

96°C for 4 minutes

96°C for 30 seconds

50 °C for 15 seconds

60°C for 4 minutes

Return to step 2 24 times

4°C for 5 minutes

PCR programme	PCR primers
Shhfragments	A1FShh500 & A2RShh500 B1FShh500 & B2RShh500
Shh50C	A1Rseq & ZRS-F A1Rseq & CMV-For B1Fseq & MAZ
Myogenin	Myo 1 & Myo 2
Sequencing	m13 forward & m13 reverse

7.3.3 Molecular cloning

7.3.3.1 Sub-cloning via T-Easy vector (Promega)

Taq DNA polymerase normally adds a single nontemplated nucleotide (nearly always A) to the 3' end of all duplex DNA strands. Accordingly, PCR products were

recovered from an agarose gel (section 7.1.6) and blunt ended DNA was subsequently tailed with dATP's and fragments were ligated to T-Easy vector according to the manufacturer's instructions. The ligated plasmids were transformed into DH5α cells according to the manufacturers instructions.

7.3.3.1.2 Screening for transformants

Cells containing the T-Easy vector were selected for by their acquisition of Ampicillin resistance. Insertion of sequence into the pGEM T-Easy vector results in disruption of the *LacZ* gene, thus transformants were identified as white, as opposed to blue, colonies when plated on IPTG/Xgal indicator plates.

7.3.3.2 Cloning via pDECAP

Fragments initially cloned into the pGEM T-easy vector were cut from the vectors and sequentially added into pDECAP, finally forming an inverted repeat. The first DNA fragment was restricted using EcoRI and SalI and ligated to pDECAP. The pDECAP vector was then transformed into DH5α cells. Fragment carrying clones were determined using enzyme restriction digests. The second DNA fragment was cut from pGEM T-easy using XbaII and SalI and introduced to the pDECAP vector previously carrying a DNA fragment. All ligations were according to the manufacturers instructions. The ligated plasmids were then transformed into SURE 2 supercompetent cells according to the manufacturers instructions.

7.3.3.2.1 Screening for pDECAP vectors with inverted repeats

Cells containing the pDECAP vector were selected for by their acquisition of Ampicillin resistance. The plasmids were extracted from the cells using a quiagen kit. To confirm that the inverted repeat was intact the plasmid clones were digested using SalI and the two DNA fragments were PCR amplified using A1Rseq and CMV-For, and B1Fseq and MAZ.

7.4 Sequencing

Plasmid DNA used for sequencing was prepared using a QIAGEN miniprep kit according to the manufacturer's instructions. DNA was sequenced using the dye-labelled terminator dRhodamine for cycle sequencing. Reagents were thawed on ice and dyes were protected from light as much as possible. Reactions (20µl final volume) were set up in 0.2ml centrifuge tubes as follows:

200-500ng plasmid DNA in dH_2O	11µl
dRhodamine reaction mix	8µl
primer (3.2 pmoles)*	1µl

*The primers used for the sequencing of pGEM T-easy vectors and pDECAP vectors were as follows:

Vector	Sequencing Primers
pGEM T-easy	m13 forward & m13 reverse
pDECAP	A1Rseq & CMV-For B1Fseq & MAZ

Cycle sequencing was performed using an MJ Research DNA Engine Tetrad. Reactions were EtOH precipitated following transfer to a fresh 1.5ml centrifuge tube containing 50µl 100% EtOH and 2µl sodium acetate, pH5.2. Reactions were left on ice for 15 minutes to precipitate, before centrifuging at 13,000rpm for 30 minutes at 4°C. Pellets were washed with 200µl 70% EtOH. The supernatant was removed following a second centrifugation step and pellets were allowed to dry at room temperature for approximately 20 minutes. Samples were submitted to the sequencing service to be run on an ABI machine.

7.5 Animal husbandry

Animals used during transgenic procedures were maintained in a barrier facility and all other animals were maintained in a semi-barrier unit. All experiments were carried out under Home Office licence. Wildtype animals (CD1 and C57BL/6) were obtained from Charles River Laboratories. Embryos for all experiments were generated from timed matings, with the morning of vaginal plug detection being considered as embryonic day 0.5 (E0.5).

7.5.1 Harvesting of postimplantation embryos

Pregnant females were sacrificed by cervical dislocation. The abdominal cavity was opened and uteri were removed to petri dishes containing DEPC-PBS. Embryos were removed from the uteri and freed from extraembryonic membranes using scissors and forceps. Extraembryonic membranes were retained separately to genotype embryos by PCR. Embryos were rinsed in fresh PBS prior to subsequent processing.

7.5.2 Genotyping of transgenic embryos

Transgenic embryos were genotyped by PCR amplification of allelic sequences from genomic DNA extracted from extra-embryonic membranes (yolk sacs). The DNA was extracted from extra-embryonic membranes by incubating the tissue in 50µl of 25mM NaOH, 0.2mM EDTA at 95°C for 20 minutes, followed by vortexing briefly to break up the tissue. The reactions were neutralised by the addition of 50µl of 40mM Tris.HCl. For long-term storage, protein and cell debris were removed by centrifugation and decanting of the supernatant into fresh tubes which were stored at -20°C. 1µl of extracted DNA solution was used in a 20µl genotyping PCR assay. The genotype was determined by agarose gel electrophoresis of the PCR product. Transgenic embryos carrying the Shh inverted repeat were genotyped by PCR amplification using primer sequences A1Rseq and CMV-For, and B1Fseq and MAZ.

7.5.3 Visual assessment of the *Shh* mutation

Wildtype and homozygous mutant *Shh* littermates were visually distinguished owing to gross morphological differences between the embryos. One of the most obvious differences being that Homozygous mutant *Shh* embryos exhibit stunted growth of the forelimbs and hindlimbs and do not develop a hand-plate at later stages.

7.5.4 Staging embryos using a computational staging system

Wild type embryos derived from C57/BL6xC57/BL6 crosses and CD1xCD1 crosses were dissected in DEPC-PBS and their hind-limbs were imaged along the anterior-posterior axis using a Leica MZFLIII stereo-fluorescence microscope, prior to fixation. Staging of the embryos was according to the Theiler staging system (Theiler, 1972, reprinted 1989 with minor changes) as detailed in The Atlas of Mouse Development (Kaufman, 1992).

7.6 Production of transgenic mice

7.6.1 Preparation of linearised recombinant DNA for microinjection into fertilised oocytes

Plasmid DNA harvested from pDECAP vectors identified as containing the desired inverted repeat sequence was cleaved with BamHI and BglII to release the desired sequence (5µg DNA in a 100µl reaction). The digest was electrophoresed on a 0.8% LMP agarose gel in TAE alongside an equivalent amount of undigested DNA to ensure the DNA was completely digested and products were the predicted size. The band containing the desired sequence was then excised from the gel and the sequence was released from the gel into TAE using a bio-extraction machine according to the manufacturer's instructions.

The DNA was precipitated through the addition of 1/10 volume 3M sodium acetate and one volume 100% Isopropanol and storage at –20°C for 3 hours. After which, the chilled solution was centrifuged for 30 minutes at 4°C and any supernatant was discarded. The DNA pellet was washed using 70% EtOH, air dried and resuspended in injection buffer (0.1mM EDTA/10mM Tris pH7.4). The DNA concentration was determined by electrophoresis. DNA was stored at -20°C until the day of microinjection, at which point it was diluted in injection buffer to a final concentration of 2ng/µl and spun through a Spinex 0.22µm column (Costar).

7.6.2 Microinjection of recombinant DNA and oviductal transfers

The microinjections and subsequent oviductal transfers were performed by Paul Devenney as described in MacKenzie *et al.*, 1997. Embryos used for microinjection were derived from CD1 x CD1 F1 matings and were re-implanted into C57BL/6 pseudo-pregnant females.

7.7 Detection of gene expression

7.7.1 RNA *in situ* hybridisation

The fluorescent and non-fluorescent RNA in situ hybridisation experiments were completed using the facilities and resources of the commercial company Bio-Optonics.

7.7.1.1 Preparation of labelled riboprobes

Riboprobes were prepared by staff at MRCT. RNA products were kept on ice as much as possible and gloves were worn at all times to prevent exposure to degradative RNase enzymes. Electrophoresis equipment was treated with RNAse ZAP (Ambion) prior to use in order to destroy RNases.

Either linearised plasmid DNA containing cloned gene fragments, or PCR products amplified from cDNA, constituted templates for *in vitro* synthesis of labelled antisense RNA probes. Plasmid DNA was cleaved at the 5' end of the insert with a suitable restriction endonuclease, whilst the RNA polymerase promoter used for transcription flanked the 3' end of the insert. PCR-generated template DNA was amplified using a primer pair for which a promoter was incorporated into the reverse primer. In each case, the DNA was purified by gel extraction. Template DNA was transcribed using the appropriate RNA polymerase (T3, T7 or SP6) and nucleotides labelled with DIG (digoxigenin) using a DIG RNA labelling kit (Roche) according to the manufacturer's instructions. Template DNA was digested by the addition of 2µl RNase-free DNaseI for 45 minutes at 37°C. Purification of the riboprobe was completed using NucTrap Probe Purification columns (Stratagene) according to the manufacturer's instructions. 2µl RNase inhibitor (Roche) was added to the probe before storage at -20°C. The success of the DIG-labelling reaction was assessed by electrophoresis using a 1% gel run at 120V for 10 minutes.

7.7.1.2 Wholemount NBT/fluorescent in situ hybridisation

Embryos aged between E9.5 and E13.5 were processed for wholemount *in situ* hybridisation. Embryos were dissected in DEPC-PBS and fixed in 4% PFA at 4°C overnight. PFA was removed the following morning and the tissue washed with dPBT twice for 10 minutes each. Tissue not required for immediate use was dehydrated by washing for 5 minutes and then for 25 minutes in increasing concentrations of fresh methanol (MeOH): 25%, 50%, 75% MeOH in dPBT, followed by 3 washes in 100% MeOH before storage in bijou bottles at -20°C. Washing time varied according to the size of the embryo. E13.5 embryos were washed for 5 minutes followed by a wash for 90 minutes in fresh methanol of increasing concentration.

7.7.1.2.1 Solutions for wholemount *in situ* hybridisation

In order to protect the RNA from degradation, solutions were made using DEPC-dH_2O, DEPC-PBS and DEPC-SSC for all steps prior to, and inclusive of, hybridisation.

dPBT

PBT was freshly prepared each time by the addition of 0.5ml 10% Triton X-100 (Sigma) to 50ml DEPC-PBS (final concentration 0.1%).

4% paraformaldehyde (PFA)

4% PFA (Sigma) was freshly prepared in DEPC-PBS.

Pre-hybridisation solution (prehyb)

Compound	Amount added per 50ml	Final concentration
De-ionised formamide (Sigma)	25ml	50%
20XDEPC-SSC	12.5ml	5X
Blocking reagent (Roche)	1g	2%
Triton X-100 (10%) (Sigma)	0.5ml	0.1%
CHAPS (10%) (Sigma)	2.5ml	0.5%
Yeast RNA (50mg/ml) (Sigma)	1ml	1mg/ml
EDTA (0.5M)	0.5ml	5mM
Heparin (10mg/ml) (Sigma)	250µl	50µg/ml

The solution was made up to 50ml with DEPC-dH_2O and all components were dissolved by gentle mixing.

Post-hybridisation solution (posthyb)

Compound	Amount added per 50ml	Final concentration
De-ionised formamide	25ml	50%
20XSSC	12.5ml	5X
Triton X-100 (10%)	0.5ml	0.1%
CHAPS (10%)	2.5ml	0.5%

The solution was made up to 50ml with dH_2O.

TNT

Compound	Amount added per 50ml	Final concentration
TRIS (1M, pH7.5)	2.5ml	50mM
NaCl (5M)	1.5ml	150mM
Triton X-100 (10%)	0.5ml	0.1%

The solution was made up to 50ml with dH_2O.

Blocking solution

Compound	Amount added per 50ml	Final concentration
Sheep serum*	7.5ml	15%
BSA	1g	2%
TRIS (1M, pH7.5)	2.5ml	50mM
NaCl (5M)	1.5ml	150mM
Triton X-100 (10%)	0.5ml	0.1%

*Previously heat inactivated at 50°C for 1 hour. The solution was made up to 50ml with dH_2O.

NMT

Compound	Amount added per 50ml	Final concentration
TRIS (1M, pH9.5)	5ml	0.1M
NaCl (5M)	1ml	0.1M
$MgCl_2$ (1M)	2.5ml	50mM

The solution was made up to 50ml with dH_2O.

7.7.1.2.2 Procedure for wholemount *in situ* hybridisation

Prior to *in situ* hybridisation, dehydrated tissue was first rehydrated through a series of ice-cold MeOH consisting of decreasing concentrations of MeOH in dPBT: 75%, 50% and 25%. Whole embryos were then washed 3 times for 5 minutes in dPBT prior to treatment at room temperature with 10µg/ml proteinase K (Roche) dissolved in dPBT. The treatment time varied according to the size of the tissue: E11.5 and E12.5 embryos were treated for 25 and 30 minutes respectively and treatment times for younger or older tissue were decreased or increased accordingly. Treated embryos were then fixated in 4% PFA for 45 minutes on ice and subsequently washed for 10 minutes in dPBT. Embryos were transferred to 2ml cryotubes or bijou tubes, depending upon the size of the embryo, containing prehyb solution and left at room temperature to equilibrate. This step was carried out twice. Embryos were then incubated in fresh prehyb at 65°C for 1 hour, after refreshing the solution the embryos were incubated at 65°C for a further 2-4 hours, after a final refreshing of the solution the embryos were left in hybridisation solution at at 65°C overnight. Hybridisation solution was made heating 5µl RNA probe in 100µl prehyb to 80°C for 3 minutes, thus denaturing the probe.

The following day, the probe was removed by a series of washes in post-hybridisation washes, each for 10 minutes at 65°C: 100% posthyb, 75% posthyb/25% 2XSSC, 50% posthyb/50% 2XSSC, 25% posthyb/75% 2XSSC. The embryos were then washed twice in 2XSSC/0.1% CHAPS for 30 minutes at 65°C and twice in 0.2XSCC/0.1% CHAPS, also at 65°C for 30 minutes. After 3, 5 minute washes in fresh TNT at room temperature the embryos were placed in blocking solution (pre-filtered using a 0.45µm syringe filter; Millipore) for at least 4 hours (with 3 changes) at 4°C. Embryos were incubated in antibody solution (anti-DIG-AP fab fragment (Roche) at a 1:2000 dilution) with rocking at 4°C overnight.

On the third day, the unbound anti-DIG antibody was removed by completing 5 embryo washes, each for an hour at 4°C in TNT/0.1% BSA (pre-filtered using a 0.45µm syringe filter) with gently rocking. After a further change, embryos were left in TNT/0.1% BSA at 4°C either overnight or up to 2 days.

In preparation for staining, embryos were given 2, 30 minute washes in NMT with 0.1% Triton X-100 and then 3, 10 minute washes in NMT. To visualise the signal, staining solution was prepared by the addition of 3.3µl/ml NBT (100mg/ml in DMF) (Roche) and 3.5µl/ml BCIP (50mg/ml in DMF) (Roche) in NMT. Embryos were stained in the dark and monitored until the stain developed, which usually occurred within 1 to 3 hours, depending upon the probe. The staining reaction was terminated by rinsing the embryos twice in PBS on ice before a final fixation step overnight at 4°C in 4% PFA.

7.7.1.2.3 Solutions for fluorescent *in situ* hybridisation

PBST (0.5% tween)

TBST-T006 (10X)

6% Hydrogen Peroxide-H004

Proteinase K 10mg/ml in PBST (10ml 10mg/ml in 10ml PBST)

Glycine/PBST-G001

Rnase Buffer- R003

Rnase 20mg/ml (200ml 1mg/ml in 10mls) DISPENSE WITH FILTER TIPS ONLY!

SSC/Formamide- (5x SSC/50% Formamide, 0.5% Tween)

1% Roche Block-B009

NTMT –N005

BCIP

NBT

Tyramide Kit

Stop Sol S004

PBS

7.7.1.2.4 Procedure for fluorescent wholemount *in situ* hybridisation

Prior to *in situ* hybridisation, dehydrated embryos were first rehydrated through MeOH series consisting of decreasing concentrations of MeOH in PBST: 75%, 50% and 25%, each step being for 10 minutes on a roller. This was followed by 2, 10 minute washes in PBST. Large embryos, which would not otherwise fit into a 5ml cryotube, were cut in half. Fluorescent wholemount *in situ* hybridisation was completed by the company Bio-Optonics using an InSitu Pro machine. Prior to placing the embryos in the machine the riboprobes were diluted in hyb solution and denatured at 80°C for 7 minutes.

The following protocols (Insitu Pro and Tyramide reaction) was produced by Sarah Wheddon et al, (Bio-Optonics, unpublished).

Insitu Pro

PBST	10min
6% H_2O_2	1 hour
PBST	10min x2
10ug/ml PK see table below for times	
2mg/ml Glycine	5min
PBST	10min x2
50% PBST/ 50% hyb mix	10 min

Following steps at 65°C

Hyb mix	12 min
Hyb mix	90min
Probe (Sox-9 DIG as 1:100)	16hours
Hyb mix	30min x2

Subsequent steps at 37°C

50% Hyb mix/ 50% RNAse Buffer	10min
20ug/ml RNase A	1hour
RNase Buffer	12min
50% RNase buffer/ 50% Formamide/SSC	10min

Following steps at 65°C

Formamide/SSC	30min	x2

Subsequent steps at room temperature

Subsequent steps at Room Temp		
Formamide/SSC	12min	x2
PBST	12min	x3
1% Roche block	1hour	
Sheep Anti DIG-POD at 1:250 (Roche 1 207 733)	8hours	
PBST	12min	
PBST	30min	x12
PBST	60min	x6

Finally remove the embryos from the Insitu Pro machine and tip the embryos into 5ml cryotubes from the Tyramide staining kit (Molecular Probes, Invitrogen Technology).

Proteinase K treatment times:

*** Embryo age**	**P.K. Time**
9.5	4 minutes
10.5	4 minutes
11.5	10 minutes
12.5	11 minutes

Tryramide Reaction.

If the Tryramide_kit is being used for first time, then the Tyramide needs to be resuspended in 150ul DMSO and 30ul dispensed into black 1.5ml tubes. All experiements were completed using Tyramide 568.The hydrogen peroxide must also be diluted in buffer (1:200) in buffer. The reaction buffer must then be made up by adding 1:100 volume of diluted hydrogen peroxide & tyramide 1:200 as required. The reaction buffer is immediately added to the embryos and incubated in the dark for 1 hour, after which embryos are washed in PBS, which is changed every hour. Then wash the embryos in PBS, with shaking at room temperature in the dark. The PBS is changed every hour and finally washed for 2 days in the dark in PBS at 4°C. The embryos can be viewed under a fluorescent microscope the following day.

7.8 Histology

For immunohistochemistry and immunoflurescence, tissues and embryos were processed for embedding in paraffin wax and agarose. Limb tissue was sectioned using either a vibratome or a microtome.

7.8.1Unmounting OPT imaged embryos for histological processing.

Embryos that have been OPT scanned are embedded in 1 % agarose which is not a high enough concentration to allow for successful vibratome sectioning. Further to this embryos are cleared and stored in BABB which is toxic. Therefore, embryos required re-embedding. Throughout the re-embedding of fluorescently stained embryos care needed to be taken to prevent as much light exposure as possible. The first step in the re-embedding process was the removal of BABB through repeated washes of embryos in 100% MeOH, where E9.5 embryos take 24 hours and E13.5 embryos take 72 hours to be washed thoroughly. The embryo is then taken through a series of room temperatur MeOH washes decreasing in concentration of MeOH in dH_2O: 7%, 50%, 30% and 10%, each wash lasting for 2 hours or until the agarose

plug sinks (NB: if the plug has a bubble in it then it will not sink). The final 10% MeOH wash is replaced with room temperature 0.29M sucrose solution and washed for a further 10 minutes. The room temperature 0.29M sucrose solution is then replaced with 0.29M sucrose solution heated to 55°C. The agarose plug is heated at 55°C for 1 hour, after which the embryo can be easily removed from the agarose using a surgical blade (Swann Morton) and tweezers. The sample is then washed for 10 minutes in dH_2O and embedded in 5% agarose.

7.8.1.1 Agarose Embedding

The tissue was first incubated at 55°C in molten 5% agarose for 15 minutes. The molten 5% agarose containing the tissue was then poured into a suitably sized mould and the embryo was orientated under a microscope using a pair of forceps and monitored at room temperature whilst the agarose set. When set, the agarose block containing the tissue was trimmed with a surgical blade (Swann Morton) and glued to the vibratome mount in the desired orientation for sectioning.

7.8.1.2 Vibratome sectioning and immunohistochemistry.

The agarose-embedded embryos were sectioned at 100μm on a vibratome. Each section was carefully lifted from the vibratome waterbath onto a superfrost slide (BDH). A drop of vectashield aqueous mount (Vector labs) carrying the Yo-Pro1 (Molecular Probes) fluorescently labelled antibody was added to the section, which was then covered by a glass coverslip (thickness no.1) (BDH). To further prevent the drying of sections by evaporation, and to protect the tissue, the edges of the coverslip were sealed using nail polish (Rimmel). The mounted sections were stored in the dark at 4°C.

7.8.2 Wax embedding

To facilitate close histological analysis of thin sections of limb tissue, the limbs/embryos were embedded in wax prior to microtome sectioning. Prior to wax

embedding, tissue stored in 100% MeOH was given 2, 10 minute washes in 80 % EtOH/dH_2O followed by 2, 10 minute washes in100% EtOH. This was followed by 3, 15 minute incubations in Xylene, the first of which was at room temperature and the remaining two were at 58°C. The embryo was then incubated in 50% Xylene: 50% wax for 15 minutes, after which it was put through 3, 20 minute incubations in fresh molten wax, at 58°C. The wax containing the specimen was then tipped out into a suitable mould. The embryo was orientated under a microscope using forceps and the wax was left to set. The wax block was then cut into a pentagonal shape conducive for sectioning.

7.8.2.1 Microtome sectioning

Wax embedded samples were sectioned at 7μm on a microtome and ribbons of sections were floated out in a 42°C water bath. The sections were transferred on to Superfrost Plus electrostatically charged slides (BDH)with the aid of a fine-tipped brush. The Slides were air dried and then transferred to a 55°C oven to dry overnight which were then stored at 4°C.

7.8.3 Immunohistochemistry of microtome sections

Dewaxing

2 x 10 minutes Xylene

2 x 3 minutes 100% EtOH

1 x 5 minutes 70% EtOH

1 x 5 minutes 50% EtOH

1 x 5 minutes 30% EtOH

2 x 10 minutes PBS

Antigen Retrieval

Nuclear Antigens are often affected by processing tissue in wax. For effective staining this is countered using an antigen retrieval step. Slides are left to sit at room temperature in 60mM sodium citrate (pH6). The buffer is then boiled in the microwave (900W) for 30 minutes and then allowed to cool for an hour.

Immuno-staining

Slides are removed from the buffer and placed in blocking solution (TBST, 0.05% Triton, 10% heat-inactivated sheep serum) for an hour at room temperature. Sections are then incubated in blocking solution containing rat anti-BrdU (1:100; clone BUI/75 Abecam) and mouse anti-BrdU (1:50; clone B44 from Becton Dickinson). Incubation is completed at room temperature for 30 minutes and then 4 °C overnight, followed by an hours wash in TBST. Sections were incubated with secondary antibodies Cy3 (1:200; ????) and Alexa 488 (1:200; highly cross absorbed goat anti-mouse IgG antibodies) at room temperature for 30 minutes and then 4 °C overnight. Slides were rinsed for an hour using TBST and then mounted using vectashield mounting medium containing DAPI (8ug/ml). Slides were stored in the dark at 4 °C for a maximum of four weeks, after which time the fluorescent signal is lost.

7.9 Optical projection tomography (OPT) analysis

The processing and imaging of OPT samples was done using the facilities and resources of the commercial company Bio-Optonics. The preparation of samples that had been through both fluorescent and non-fluorescent insitu-hybridisation (2.7.3.1)was essentially the same, although the former were kept in the dark at all stages, or as much as possible.

7.9.1 Preparation of samples for OPT scanning

First the tissue is washed 3 times in PBS, each time being for 10 minutes, to wash out excess fixative. It was embedded in 1% LMP agarose made up in sterile dH_2O.

When set, the agarose block was trimmed with a surgical blade, ensuring adequate agarose was left surrounding the tissue, and glued to a cylindrical metal mount in the desired orientation for scanning. The samples were then each placed into a clean glass container (height 5.5cm) and tissue dehydrated at room temperature overnight by the careful addition of 100% MeOH to cover the sample. The following day, 3, 10 minute washes are completed using MeOH, which was then replaced with BABB (1 part Benzyl Alcohol (Sigma) to 2 parts Benzyl Benzoate (Sigma)). With the lid removed, the bijou bottle is allowed to stand overnight at room temperature, in a fume hood, to allow any remaining MeOH. Samples were usually kept in BABB overnight and scanned the following day except in cases of low level or unstable signal: in such cases samples were monitored every 15-30 minutes and scanned by OPT when the tissue reached the desired transparency, so as to preserve the signal as much as possible.

7.9.2 OPT scanning and data analysis

Samples were scanned in a cuvette filled with either BABB or 80% glycerol by both transmission and fluorescence OPT on an OPT scanner developed by Dr. James Sharpe at the MRC Human Genetics Unit, Edinburgh. For further information regarding OPT protocols, please refer to http://genex.hgu.mrc.ac.uk/OPT_Microscopy/. Data reconstructions were performed and 3D rotating movies were produced using scripts written by Dr. James Sharpe.

7.10 Microscopy

7.10.1 Stereo fluorescence microscope

Dissected embryos were imaged with the aid of a Leica MZFLIII stereo fluorescence microscope (Leica Microsystems, Milton Keynes, UK) with 0.5x, 0.63x, 1x, 1.6x objectives, a 100W Hg bulb for fluorescence imaging, and fibre optic cold light source and illuminated base for incident/transmission illumination. Images were captured with a Coolsnap cf colour CCD camera (Photometrics Ltd, Tucson, AZ)

controlled by scripts written (P. Perry) for IPLab Spectrum (Scanalytics Corp, Fairfax, VA).

7.10.2 Two colour confocal microscope

Thick (100μm thick) fluorescently stained sections were imaged using a Zeiss LSM510 confocal microscope comprised of a Zeiss Axiovert 100M microscope with standard laser configuration of Ar and two HeNe lasers giving principle emission lines at 458, 488, 514, 543, and 633 nm. Images were captured using Zeiss imaging software (version 3.1).

7.10.3 Three colour fluorescence microscope

Three colour fluorescent images were captured using an Axioskop II fluorescence microscope with Plan-neofluar objectives, a 100 watt Hg bulb (Carl Zeiss, Welwyn Garden City, UK), Chroma #83000 triple band pass filter set (Chroma Technology Corp., Rockingham, VT) with the excitation filters installed in a motorised filter wheel (Ludl Electronic Products, Hawthorne, NY) and a Photometrics CoolSNAP HQ CCD camera (Photometrics Ltd, Tucson, AZ). High resolution (48 bit) images were automatically captured and saved after manual focussing using a script written (J.Sharpe) for IPLab Spectrum (Scanalytics Corp, Fairfax, VA).

7.11 Statistical Analysis

The data regarding rates of proliferation in the limb were analysed by using ANOVA in Excel (Microsoft XP).

7.12 Programming environments

7.12.1 Hardware and software used for C programming and simulations

OPT software was run on a Linux computer which has two XEON processors, each with a speed of 2.6Ghz, a physical memory of 1Gb and a virtual memory of 4Gb. Hyper-threading was not used as it only increases processing speed by ~5% and has been known to bring about problems during processing.

7.12.2 Hardware and software used for IPLab scripting and simulations

Scripts were written (S.Raja) for IPLab Spectrum (Scanalytics Corp, Fairfax, VA) to locate cells and to record their green, red and blue colour intensities within a text file. The IPLab Spectrum package was run on a Mac OS X.

7.12.3 Hardware and software used for MATLAB programming and simulations

MATLAB programs were used to analyse colour intensity text files generated by IPLab scripts. This information was then used to generate cellular proliferation plots. The MATLAB programs were generated within the MATLAB environment and was run on a PC.

7.13 Bioinformatics

The online bioinformatics programmes and resources used during the course of the PhD research projects are listed below, together with the relevant world-wide web (www) link.

Ensembl	http://www.ensembl.org
NCBI	http://www.ncbi.nlm.nih.gov
BLAST	http://www.ncbi.nlm.nih.gov/BLAST/

Appendix A
Sox9 Expression Patterns

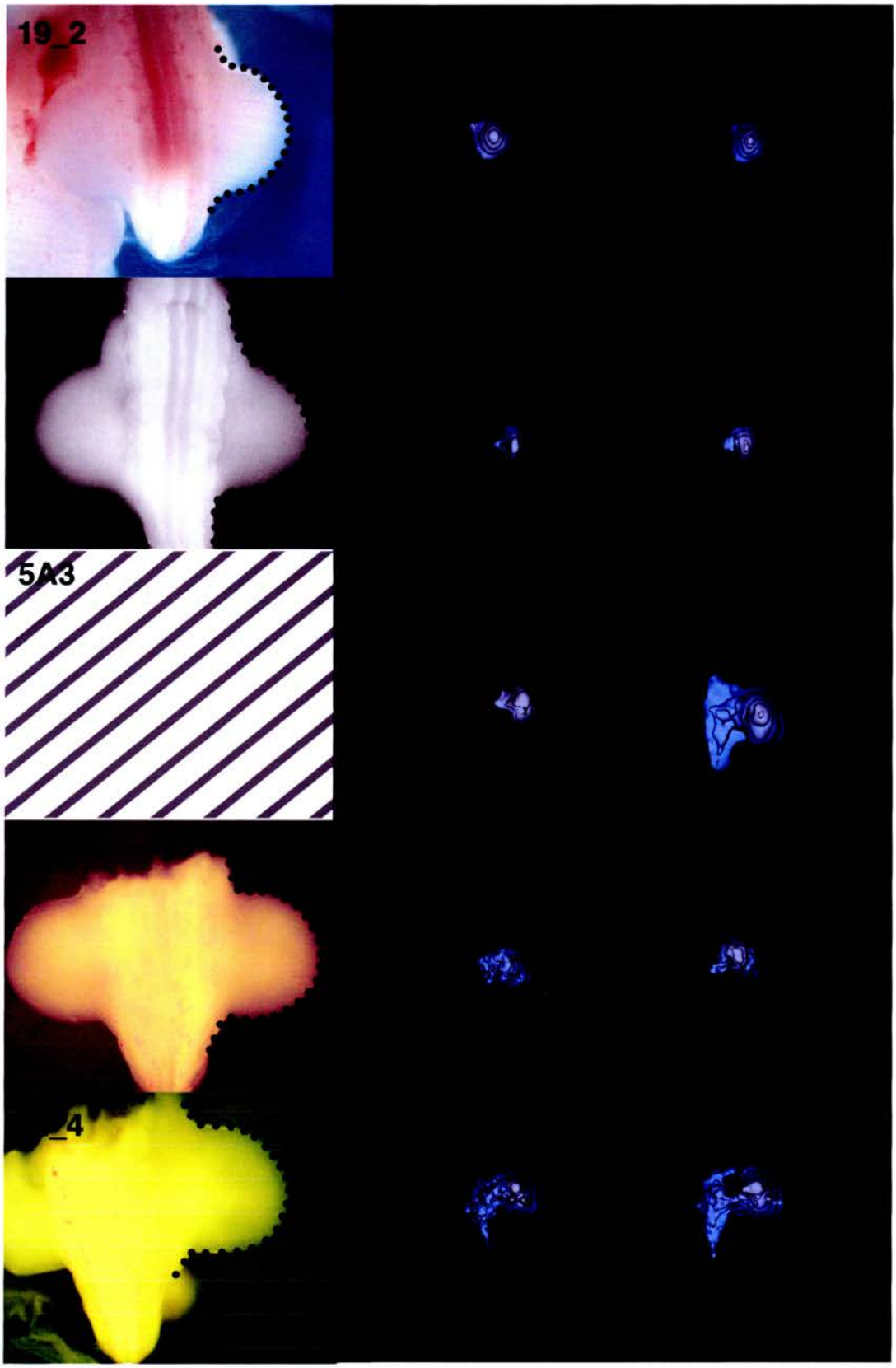
19_2
5A3
_4

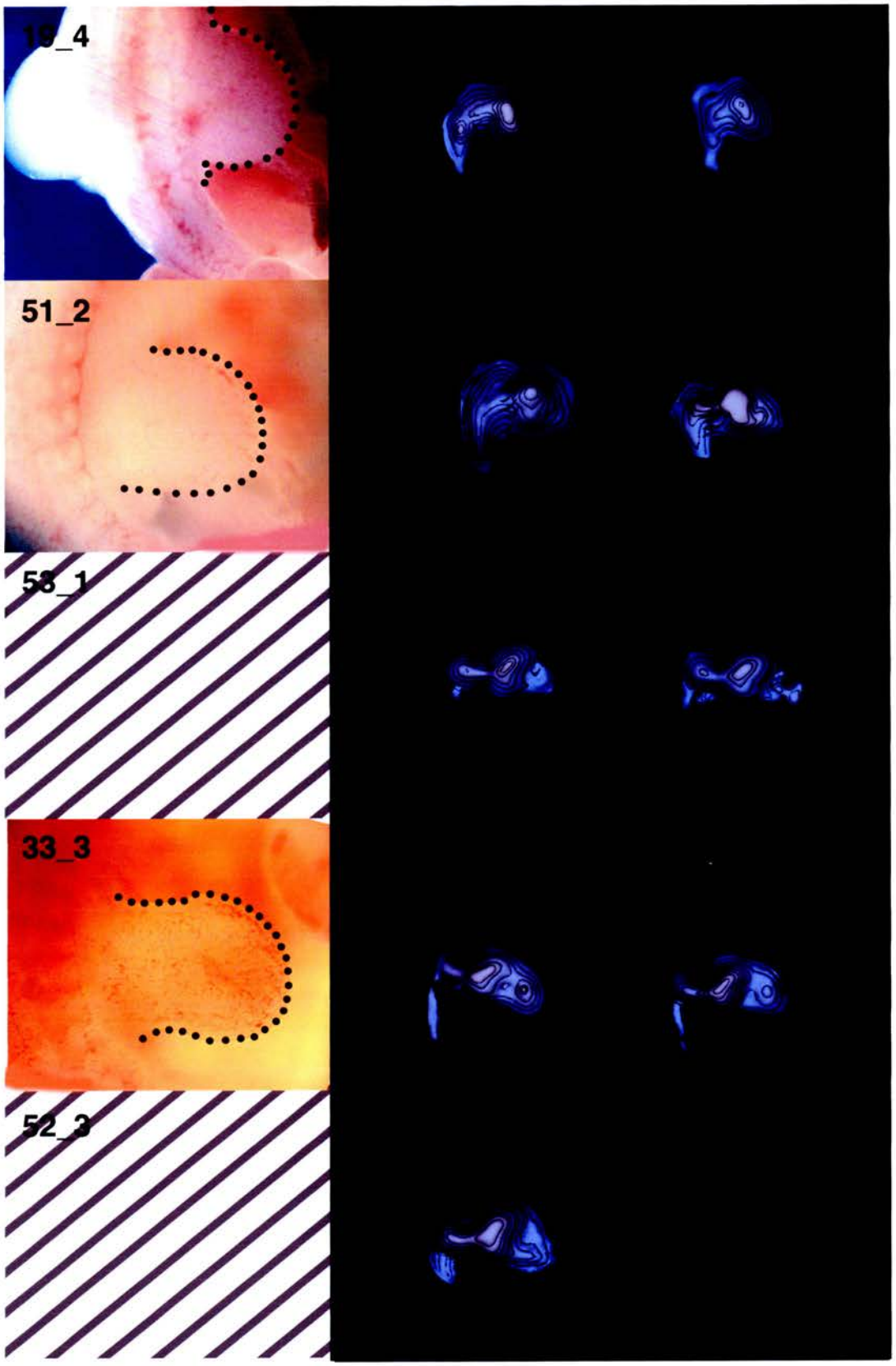
19_4
51_2
58_1
33_3
52_3

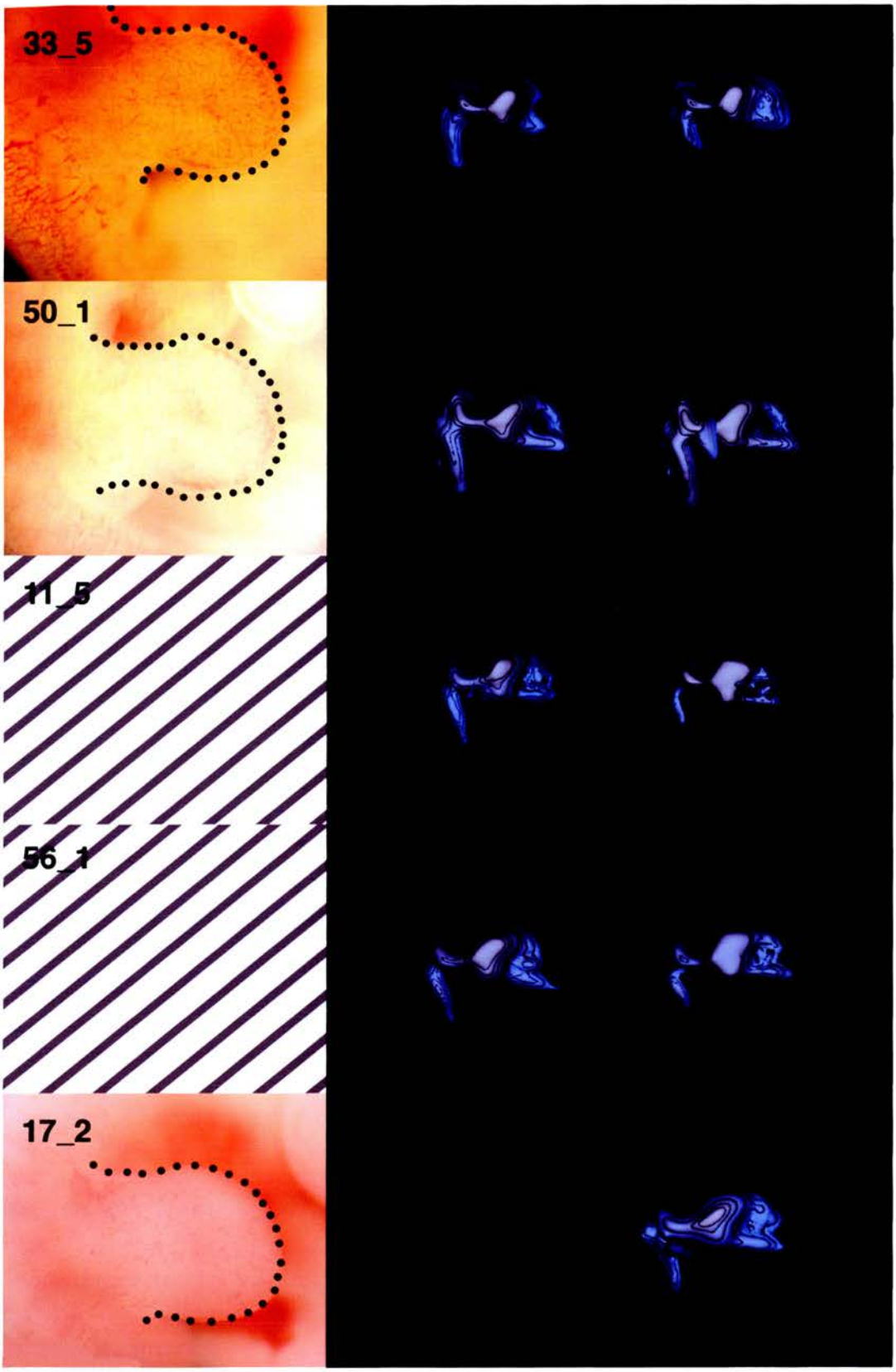
33_5
50_1
11_5
56_1
17_2

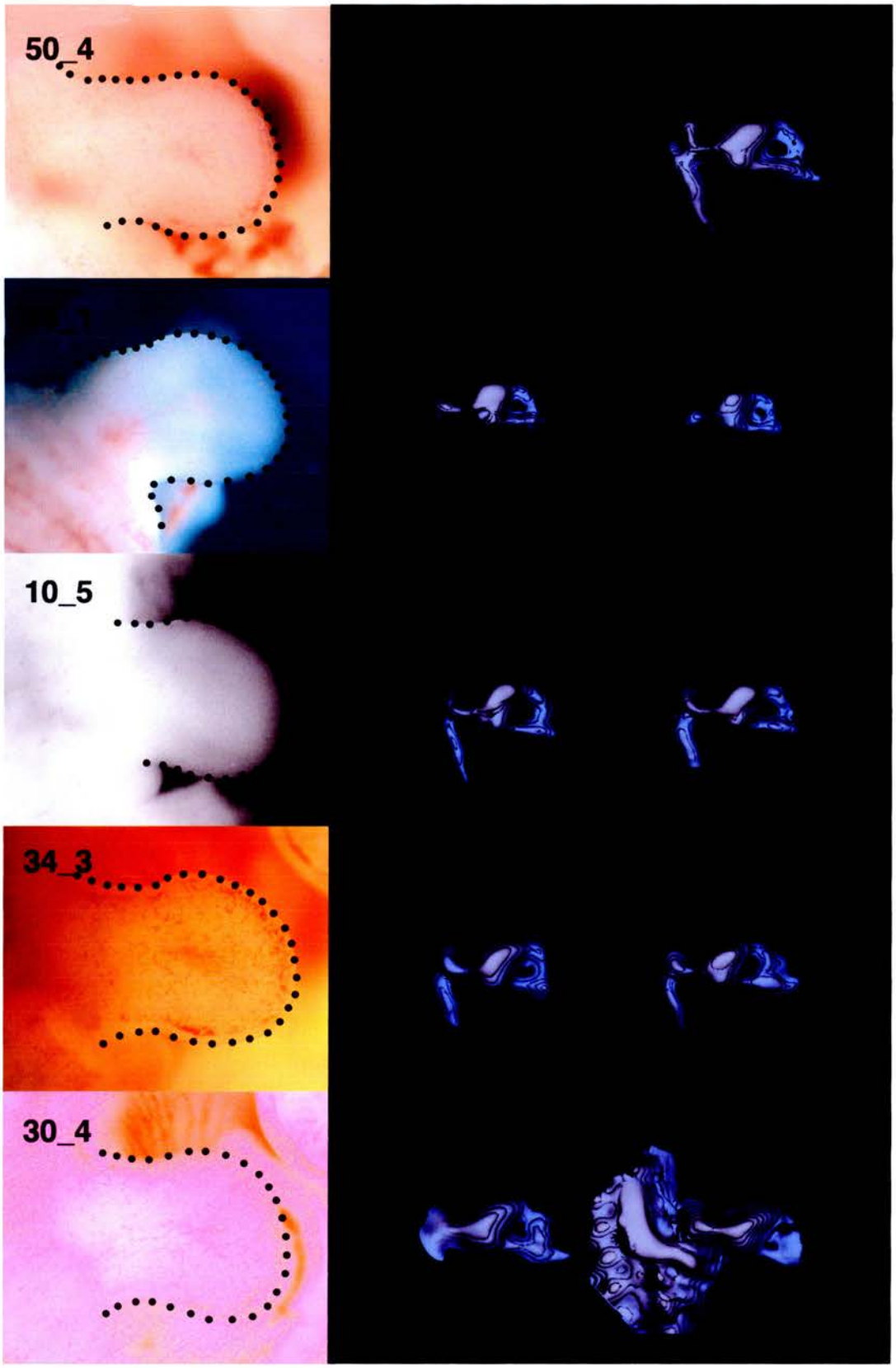
50_4
10_5
34_3
30_4

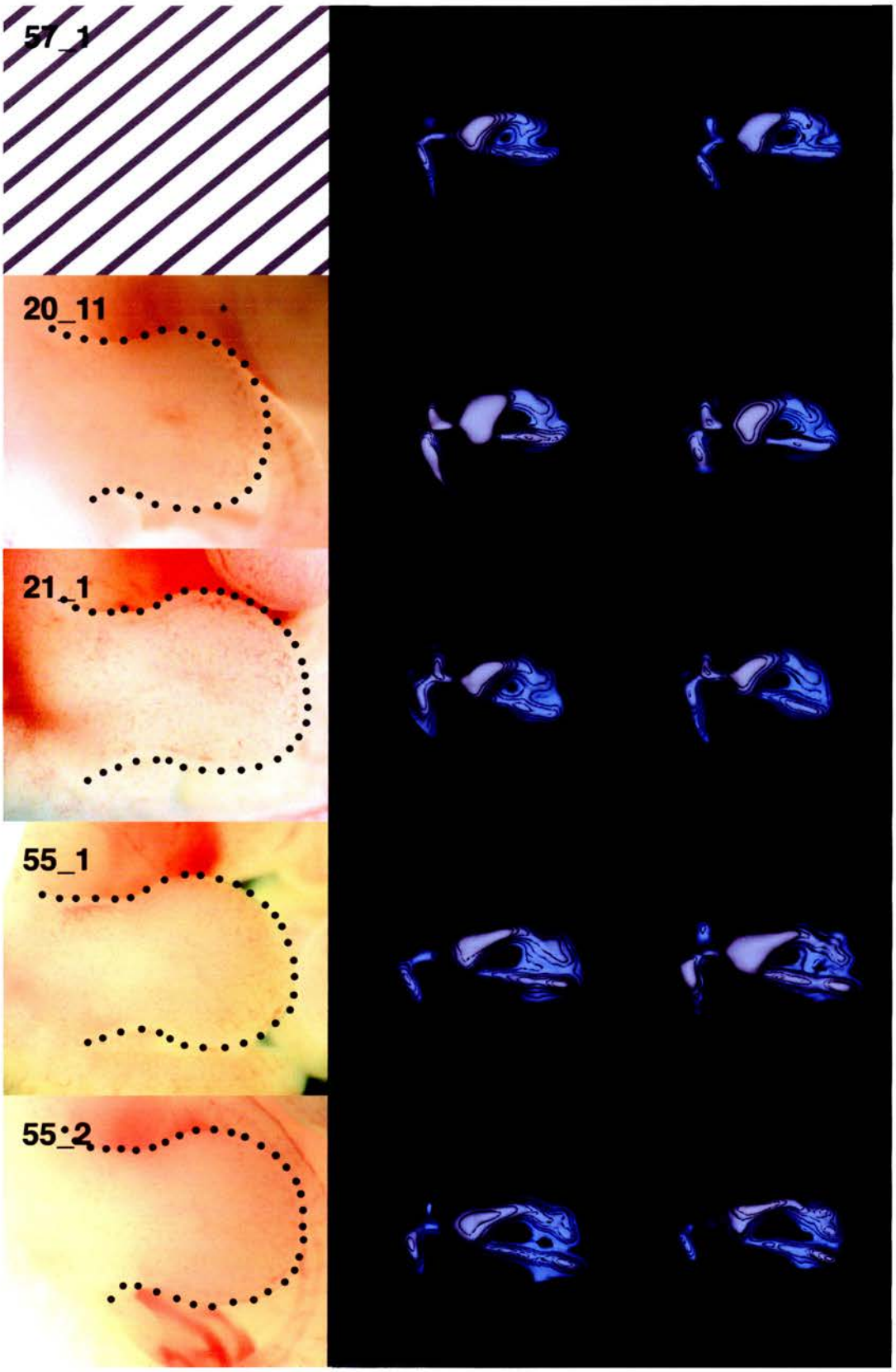
57_1
20_11
21_1
55_1
55_2

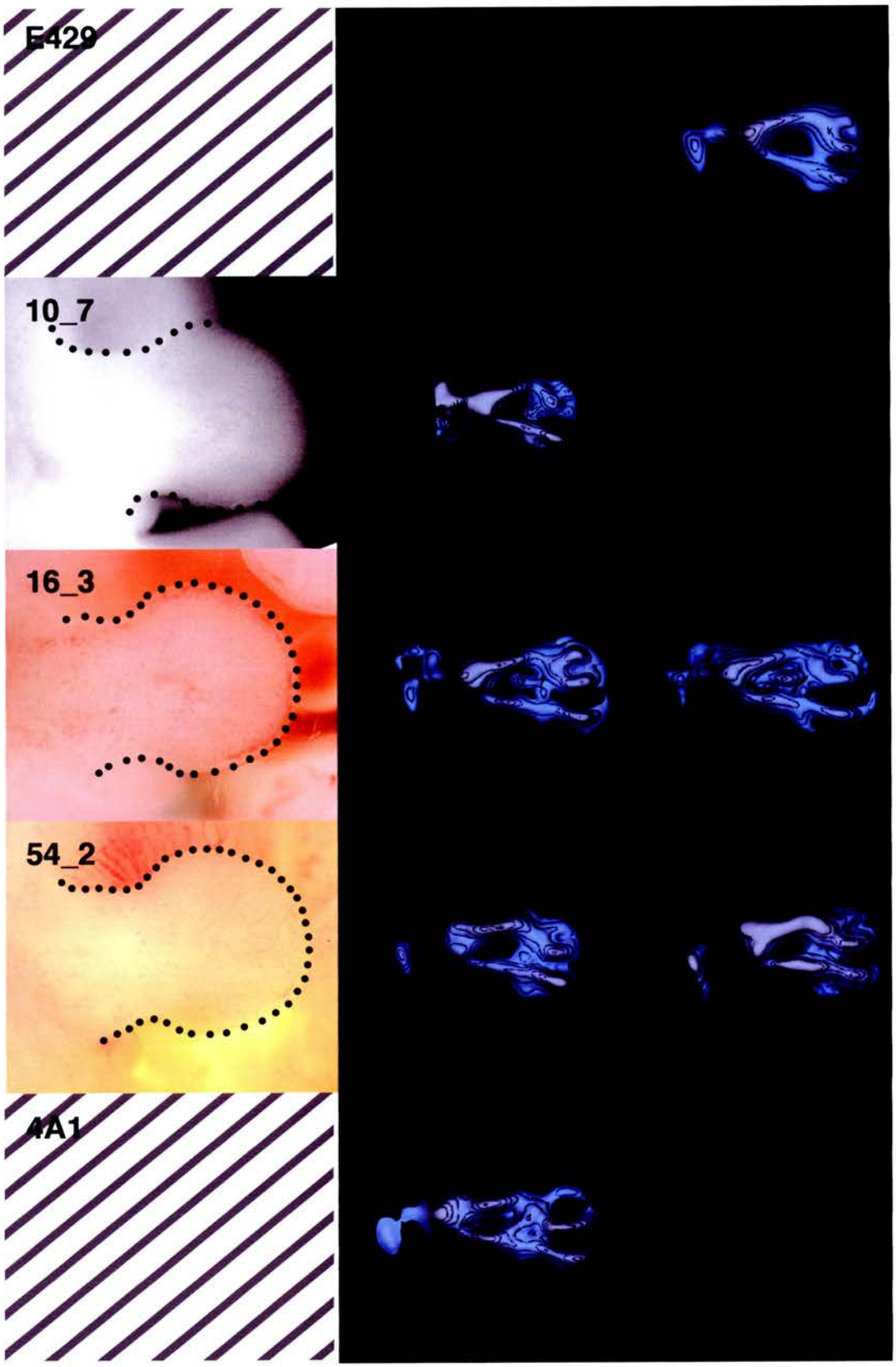
E429
10_7
16_3
54_2
4A1

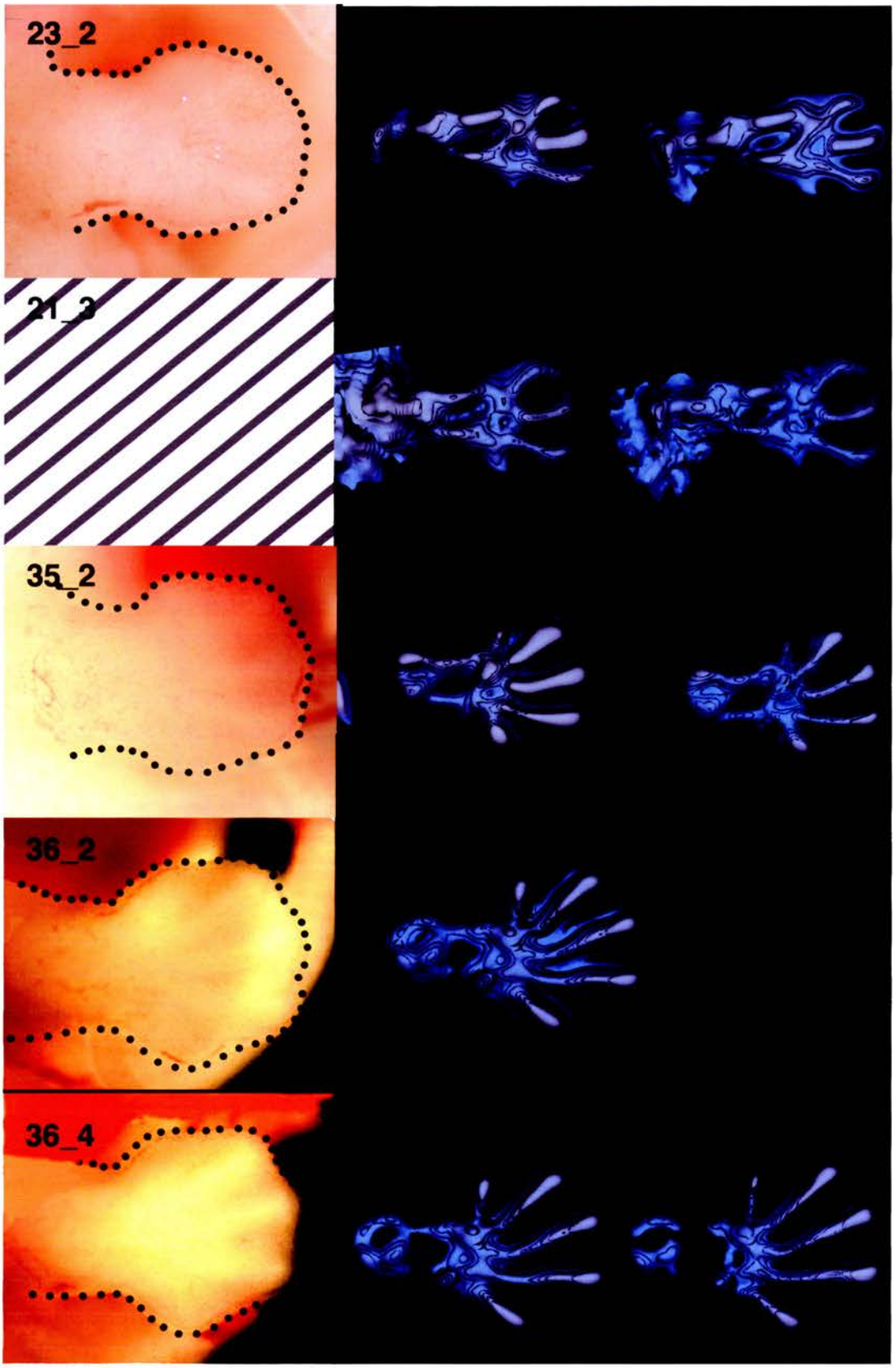
23_2
21_3
35_2
36_2
36_4

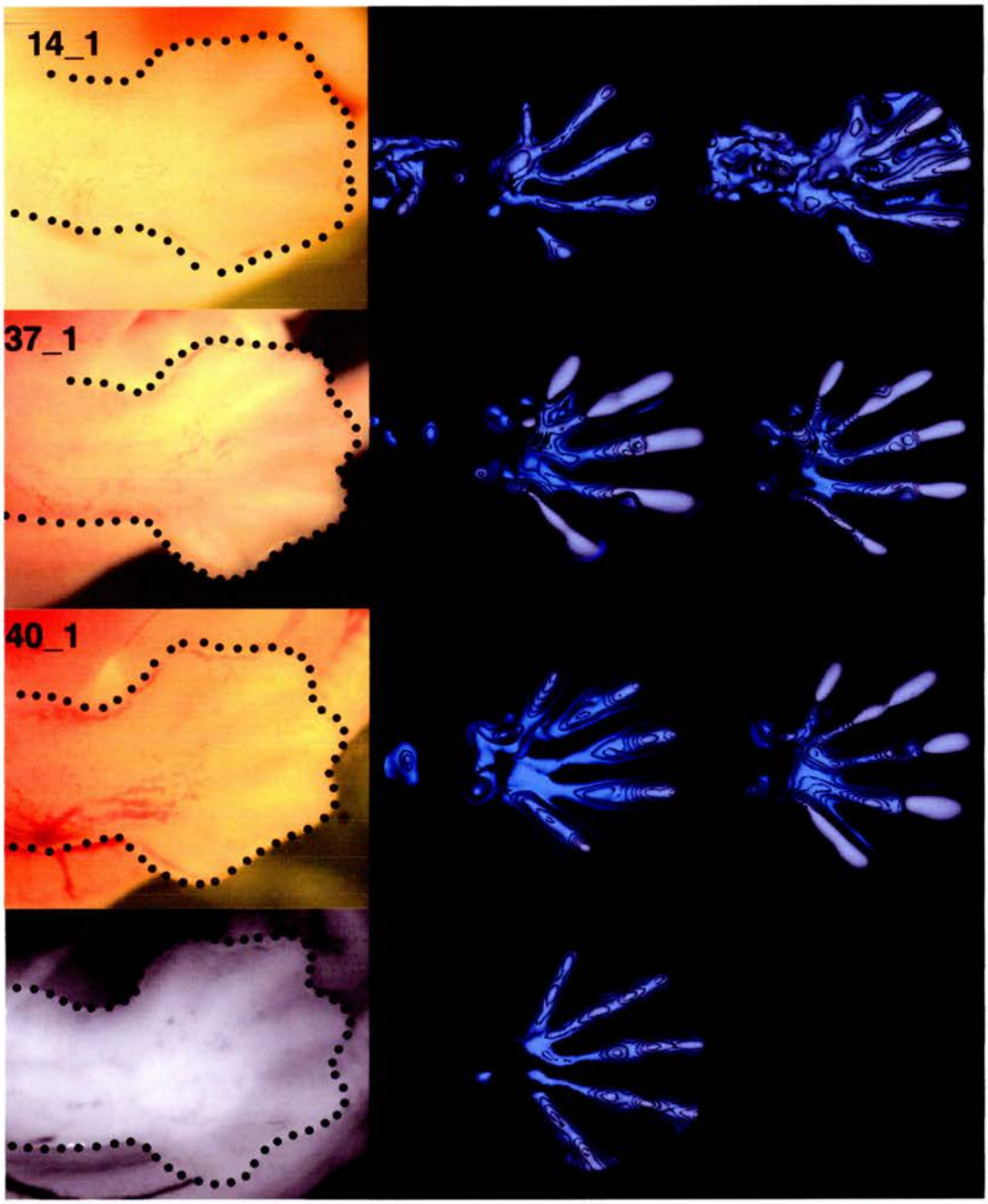
14_1
37_1
40_1

Appendix B
Statistical analysis of proliferation and cell density data from E10.5 and E11.5 limb buds

Density

	proximal	central	distal	dorsal	ventral
E10.5	49	57	58	57	53
	54	54	57	53	55
	52	57	59	55	53
	53	57	60	58	58
	52	54	54	49	50
	53	57	56	61	55
E11.5	68	70	63	56	58
	68	58	60	54	58
	47	51	57	45	53
	54	67	60	60	56
	50	71	58	56	57
	67	61	59	49	58

Tc

	proximal	central	distal	dorsal	ventral
E10.5	5	6	5	7	5
	5	5.5	7.5	6.5	5
	7	6	5.5	7.5	5
	5	5	5.5	5	5
	5.5	5	5	5	5
	5	6	5.5	5	5
E11.5	24	24	4.5	8	7
	20	8	5	5	6.5
	12	8.5	5	5	6.5
	12.5	8	5	5	5
	7.5	7	5	5	5
	12.5	5	5	5.5	5

Proliferation and cell density data was taken for a region from the proximal, central, distal, dorsal and ventral regions, of the three central most sections of embryos. We gathered the data in replicates of 6, so as to reduce the amount of stochastic variation brought about through the use of a small sample group. This data was used to complete Two-way Anova tests and was also used to construct the graphs shown in Figure 4.8.

Anova: Two-Factor With Replication
for Denisty

SUMMARY

						Total
Count	6	6	6	6	6	30
Sum	313	336	344	333	324	1650
Average	52.16666667	56	57.33333333	55.5	54	55
Variance	2.966666667	2.4	4.666666667	17.5	7.2	9.24137931
Count	6	6	6	6	6	30
Sum	354	378	357	320	340	1749
Average	59	63	59.5	53.33333333	56.66666667	58.3
Variance	95.2	60.4	4.3	29.46666667	3.866666667	43.94137931

	Total					
Count	12	12	12	12	12	
Sum	667	714	701	653	664	
Average	55.58333333	59.5	58.41666667	54.41666667	55.33333333	
Variance	57.35606061	41.90909091	5.356060606	22.62878788	6.96969697	

ANOVA

Source of Variation	*SS*	*df*	*MS*	*F*	*P-value*	*F crit*
Rows (Age)	163.35	1	163.35	7.165521275	0.010024611	4.034319545
Columns (Regions)	229.2333333	4	57.30833333	2.51389092	0.053118592	2.557179357
Interaction	173.2333333	4	43.30833333	1.899766048	0.125071096	2.557179357
Within	1139.833333	50	22.79666667			
Total	1705.65	59				

Two-way analysis of collected density data shows that age has a significant effect on density (P = 0.01) as does limb region location (P = 0.05). However, the results do not show significant interaction between age and location, effecting density (P = 0.13).

Anova: Two-Factor With Replication
for Proliferation

SUMMARY

						Total
Count	6	6	6	6	6	30
Sum	32.5	33.5	34	36	30	166
Average	5.416666667	5.583333333	5.666666667	6	5	5.533333333
Variance	0.641666667	0.241666667	0.866666667	1.3	0	0.636781609

Count	6	6	6	6	6	30
Sum	88.5	60.5	29.5	33.5	35	247
Average	14.75	10.08333333	4.916666667	5.583333333	5.833333333	8.233333333
Variance	36.675	48.04166667	0.041666667	1.441666667	0.866666667	29.42643678

	Total					
Count	12	12	12	12	12	
Sum	121	94	63.5	69.5	65	
Average	10.08333333	7.833333333	5.291666667	5.791666667	5.416666667	
Variance	40.71969697	27.46969697	0.566287879	1.293560606	0.583333333	

ANOVA

Source of Variation	*SS*	*df*	*MS*	*F*	*P-value*	*F crit*
Rows (Age)	109.35	1	109.35	12.13427039	0.001038513	4.034319545
Columns (Regions)	204.225	4	51.05625	5.665572406	0.00076889	2.557179357
Interaction	217.025	4	54.25625	6.020667653	0.000491655	2.557179357
Within	450.5833333	50	9.011666667			
Total	981.1833333	59				

Two-way analysis of collected proliferation data shows that age has a significant effect on proliferation (P = 0.001) as does limb region location (P = 0.0008), and interaction between these two factors influences proliferation (P = 0.0005).

References

Ahn, K., Mishina, Y., Hanks, M. C., Behringer, R. R., Crenshaw, E. B., (2001). BMPR-1A signalling is required for the formation of the apical ectodermal ridge and dorsal/ventral patterning of the limb. Development 128: 4449-4461

Akiyama, H., Chaboissier, M. C., Martin, J. F., Schedl, A., and de Crombrugghe, B. (2002). The transcription factor Sox9 has essential roles in successive steps of the chondrocyte differentation pathway and is required for expression of Sox5 and Sox6. Genes Dev. 16: 2813-2828.

Akiyama, H., Furukawa, S., Wakisaka, S and Maeda, T., (2006). Cartducin stimulates mesenchymal chondroprogenitor cell proliferation through both extracellular signal-regulated kinase and phosphatidylinositol 3-kinase/Akt pathways. FEBS J. 273 (10): 2257-

Alberch, P, and Gale, E. (1985). A developmental analysis of an evolutionary trend: digital reduction in amphibians. Evolution, 39: 8-23.

Amprino,R., Camosso,M.E., (1965). Developmental fate of heterotopically grafted proximal pre-axial material of the chick embryo limb bud. Acta Anat. (Basel) 61, 259-288.

Arcuri, P & Murray, J. D. (1986). Pattern sensitivity to boundary and initial conditions in reaction-diffusion models. J. math. Biol. 24, 141-165.

Baena-Lopez LA, Baonza A, Garcia-Bellido A. (2005) The orientation of cell divisions determines the shape of Drosophila organs. Curr Biol. 15(18):1640-4

Baer, K. E. von. 1828. Entwicklungsgeschichte der Thiere: Beobachtung und Reflexion. Bornträger, Königsberg. (translated and cited in Gould, S. J. 1977. Ontogeny and Phylogeny. Harvard University Press, Cambridge.)

Balakier, H. and Pedersen, R. A. (1982). Allocation of cells to inner cell mass and trophectoderm lineage in preimplantation mouse embryos. Dev. Biol. 90:352-362.

Ballard KJ, Holt SJ. (1968). Cytological and cytochemical studies on cell death and digestion in the foetal rat foot: the role of macrophages and hydrolytic enzymes. J Cell Sci., 3(2):245-62.

Barrow, J.R., Thomas, K.R., Boussadia-Zahui, O., Moore, R., Kemler, R., Capecchi, M.R., McMahon, A.P., 2003. Ectoderman Wnt3/-catenin signaling is required for the establishment and maintenance of the apical ectodermal ridge. Genes Dev. 17, 394 – 409.4463– 4474.

Benoît, R., Yvan, L (2006). Anteroposterior patterning in the limb and digit specification: Contribution of mouse genetics. Dev. Dyn., 235: 2337-2352

Bravo,R.; Frank,R.; Blundell,P.A.; Macdonald-Bravo,H. (1987). Cyclin/PCNA is the auxiliary protein of DNA polymerase-delta. Nature. 326: 515-517.

Brickell PM, Tickle C (1989) Morphogens in chick limb development. Bioessays 11, 145–149.

Brunet LJ, McMahon JA, McMahon AP, Harland RM. (1998). Noggin, cartilage morphogenesis, and joint formation in the mammalian skeleton. Science, 280(5368):1455-7.

Bueno D, Skinner J, Abud H, Heath JK. (1996). Spatial and temporal relationships between Shh, Fgf4, and Fgf8 gene expression at diverse signalling centers during mouse development. Dev. Dyn. 207(3):291-9.

Bumcrot, D. A., Takada, R., and McMahon, A. P. (1995). Proteolytic processing yields two secreted forms of sonic hedgehog. Mol. Cell. Biol. 15, 2294-2303.

Burke, A. C. and Feduccia (1997). Developmental patterns and the indentification of homologies in the avian hand. Science, 278: 666-668.

Buscher, D., Bosse, B., Heymer, J. and Ruther, U. (1997). Evidence for genetic control of Sonic hedgehog by Gli3 in mouse limb bud development. Mech. Dev. 62: 175-182.

Buscher, D. and Ruther, U. (1998). Expression rofile of Gli family members and Shh in normal and mutant mouse limb development. Dev. Dyn. 211: 88-96.

Cai, L., Hayes, N. L., and Nowakowski, R. S., (1997). Local Homogeneity of Cell Cycle Length in Developing Mouse Cortex. J of Neurosc.,17(6):2079 –2087

Capecchi, M.R. 1989. Altering the genome by homologous recombina-tion. Science 244: 1288–1292.

Chaplain, M. A. J., Singh, G. D., McLachlan, J. C. (1999). On growth and form: Spatio-temporal pattern formation in biology, Wiley Publishers, 13-29.

Charite,J. de Graaff, W., Shen, S., Deschamps, J. (1994) Ectopic expression of Hoxb-8 causes duplication of the ZPA in the forelimb and homeotic transformation of axial structures. Cell 78, 589-601.

Charite J., McFadden, D. G., and Olson, E. N., (2000). The bHLH transcription factor dHand controls Sonic hedgehog expression and establishment of the zone of polarizing activity during limb development. Development, 127: 2461-2470.

Chen H. and Johnson, R. L., (1999). Dorsoventral patterning of the vertebrate limb: a process governed my multiple events. Cell Tissue Res. 296:67-73.

Chiang, C., Litingtung, Y., Lee, E., Young, K. E., Cordon, J. L., Westphal, H. & Beachy, P. A. (1996). Cyclopia and defective axial patterning in mice lacking Sonic hedgehog gene function. Nature 383, 407-413.

Chiang C, Litingtung Y, Harris MP, Simandl BK, Li Y, Beachy PA, Fallon JF. (2001) Manifestation of the limb prepattern: Limb development in the absence of Sonic Hedgehog function. Dev. Bio. 236: 421-435.

Chimal-Monroy, J., Rodriguez-Leon, J., Montero, J. A., Ganan, Y., Macias, D., Merino, R., Hurle, J. M., (2003). Analysis of the molecular cascade responsible for mesodermal limb chondrogenesis: Sox genes and BMP signalling. Dev. Bio. 257:292-301.

Chuang,P.T.; Kornberg,T.B. (2000). On the range of hedgehog signaling. Curr.Opin.Genet.Dev. 10 (5): 515-522.

Clark, R. M., Marker, P. C., Roessler, E., Dutra, A., Schimenti, J. C., Muenke, M., and Kingsley, D. M. (2001) Reciprocal mouse and human limb pheotypes caused by gain and loss of function mutations affecting Lmbr1. Genetics 159: 715-726.

Coates, M. I., (1994). The origin of vertebrate limbs. Dev. Suppl., 169-180.

Coates, M. I. (1995). Fish fins or tetrapod limbs – a simple twist of fate? Curr Biol 5:844-848.

Cohn, M. J., Patel, K., Krumlauf, R., Wilkinson, D. G, Clarke, J. D. W and Tickle, C. (1997). Hox9 genes and vertebrate limb specification. Nature 387: 97-101

Cohn, M. J. & Tickle, C. (1999). Developmental basis of limblessness and axial patterning in snakes. Nature 399:474-79.

Cohn MJ, Lovejoy CO, Wolpert L, Coates MI. (2002) Branching, segmentation and the metapterygial axis: pattern versus process in the vertebrate limb. BioEssays 24, 460-465.

Cohn, M.J. (2000). Giving limbs a hand. Nature, 406: 953-954.

Colvin, J. S., Green, R. P., Schmahl, J., Capel, B. and Ornitz, D. M (2001) Male to female sex reversal in mice lacking fibroblast growth factor 9. Cell 104: 875-889.

Cooke, J. and D. Summerbell. 1980. Cell cycle and experimental pattern duplication in the chick wing during embryonic development. Nature 287:697-701.

Crampin, E. J., Gaffney, E. A. & Maini, P. K. (1999). Reaction and diffusion on growing domains: Scenarios for robust pattern formation. Bull. Math. Biol. 61, 1093-1120.

Crick, A. P., Babbs, C., Brown, J. M., and Morriss-Kay, G. M. (2003) Developmental mechanisms underlying polydactyly in the mouse mutant Doublefoot . J. Anat. 2002: 21-26.

Cygan, J.A., Johnson, R.L., McMahon, A.P., 1997. Novel regulatory in-teractions revealed by studies of murine limb pattern in Wnt-7a and En-1 mutants. Development 124, 5021–5032.

Davidson D.; Bard J.; Kaufman M.; Baldock R. (2001). The Mouse Atlas Database: a community resource for mouse development. Trends Gen., 17(1): 49-51

Dealy, C. N., Roth A., Ferrari D., Brown A. M., Kosher, R. A., (1993). Wnt-5a and Wnt-7a are expressed in the developing chick limb bud in a manner suggesting roles in pattern formation along the proximodistal and dorsoventral axes. Mech. Dev. 43:175-86.

Deschamps, J., van der Akker E., Forlani, S., De Graff, W., Oosterveen T, et al. (1999). Initiation, establishment and maintenance of Hox gene expression patterns in mouse. Int. J. Dev. Biol. 43:635-50.

Diebold, J., Dopfer, K., Lai, M. & Lohrs, U. (1994) Comparison of different monoclonal antibodies for the immunohistochemical assessment of cell proliferation in routine colorectal biopsy specimens. Scand. J. Gastroenterol. 29(1):47-53.

Doskocil M. (1985). Formation of the femoropatellar part of the human knee joint. Folia Morphol (Praha), 33(1):38-47.

Duboule, D. (1994). Guidebook to the Homeobox Genes. Oxford Univ. Press, Oxford.

Ducy P, Karsenty G.(2000). The family of bone morphogenetic proteins. Kidney Int, 57(6):2207-14. Review.

Dudley, A. T., Ros, M. A., Tabin, C. J., (2002). A re-examination of proximodistal patterning during vertebrate limb development. Nature 418: 539 – 544

Echelard Y, Epstein D. J., St-Jaques B, Shen L, Mohler J, McMahon J. A. et al (1993). Sonic hedgehog, a member of a family of putative signalling molecules, is implicated in the regulation of CNS polarity. Cell 75, 1417-1430.

Ede D.A., Flint O.P., Teague P. (1975) Cell proliferation in the developing wing-bud of normal and talpid3 mutant chick embryos. J Embryol Exp Morphol. 34(3):589-607.

Ede D A, Wilby OKA Colquhoun P (1977) In: Ede D A, Hinchdiffe J R & Balls M, ed. Vertebrate limb and somite morphogenesis, pp. 161-179. Cambridge University Press, Cambridge

Fallon, J. F., Lopez, A., Ros, M. A., Savage, M. P., Olwim, B. B., and Simandl, B. K., (1994). FGF-2: Apical ectodermal growth signal for chick limb development. Science 264: 104-107.

Feduccia A, and Nowicki, J. (2002) The hand of birds revealed by early ostrich embryos. Naturwissenschaften 89:391-393.

Fernandez-Teran M. A., Hinchliffe J. R., Ros M. A. (2006) Birth and death of cells in limb development: a mapping study. Dev Dyn. 235(9):2521-37.

Foster, J. W. et al (1994). Campomelic dysplasia and autosomal sex reversal caused by mutations in an SRY-related gene. Nature, 372: 525-530

Francis-West,P.H.; Robertson,K.E.; Ede,D.A.; Rodriguez,C.; Izpisua-Belmonte,J.C.; Houston,B.; Burt,D.W.; Gribbin,C.; Brickell,P.M.; Tickle,C. (1995) Expression of genes encoding bone morphogenetic proteins and sonic hedgehog in talpid (ta3) limb buds: their relationships in the signalling cascade involved in limb patterning. Dev.Dyn. 203(2):187-197.

Francis-West, P.H, Abde;fattah, A., Chen, P.,Allen, C., Parish, J., Ladher, R., et al (1999a). Mechanisms of GDF-5 action during skeletal development. Development 126, 1305-1315.

Francis-West, P.H, Parish, J., Lee, K., Archer, C.W., (1999b) BMP/GDF signalling interactions during synovial joint development. Cell Tissue Res, 296, 111-119.

Galceran,J., Farinas,I., Depew,M.J., Clevers,H., Grosschedl,R., (1999). $Wnt3a^{-/-}$-like phenotype and limb deficiency in $Lef1^{(-/-)}Tcf1^{(-/-)}$ mice. Genes Dev. 13, 709-717.

Galis, Sinervo and Metz (2002). The Digital Arch Model reconsidered. Trends Eco. Evo. 17(9): 405.

Galis, F. Kundrat, M. and Metz, J. A. J (2005). Hox genes, digit identity and the Theropod/Bird Transition. J. Exp. Zool. (Mol. Dev. Evol.) 304B:198-205.

Geduspan, J. S. and MacCabe, J. A. (1986). Evidence for the transmission of dorsoventral information to the ectoderm during the earliest stages of limb development. Prog Clin Biol Res. 226:115-26.

Geduspan, J. S. and MacCabe, J. A. (1987). The ectodermal control of mesodermal patterns of differentiation in the developing chick wing. Dev Biol. 124, 398-408.

Geduspan, J. S. and MacCabe, J. A. (1989). Transfer of dorsoventral information from the mesoderm to ectoderm at the onset of limb development. Anat. Rec. 224, 79-87.

Gellon, G. and McGinnis, W. (1998). Shaping animal body plans in development and evolution by modulation of Hox expression patterns. BioEssays, 20(2): 116-125.

Gerdes,J.; Lemke,H.; Baisch,H.; Wacker,H.H.; Schwab,U.; Stein,H. (1984). Cell cycle analysis of a cell proliferation-associated human nuclear antigen defined by the monoclonal antibody Ki-67. J.Immunol. 133: 1710-1715.

Goff, D. J. and Tabin, C. J. (1997) Analysis of Hoxd-13 and Hoxd-11 misexpression in chick limb buds reveals that Hox genes affect both bone condensation and growth. Development, 124: 627-636.

Goldring, M. B., Tsuchimochi, K. and Ijiri, K (2006). The control of chondrogenesis. J. Cell. Biochem. 97: 33-44.

Gotz W, Osmers R, Herken R. (1995). Localisation of extracellular matrix components in the embryonic human notochord and axial mesenchyme. J Anat. 186 (Pt 1):111-21.

Gritli-Linde, A; Lewis, P; McMahon, A. P. and Linde, A (2001). The whereabouts of a morphogen: direct evidence for short- and graded long-range activity of Hedgehog Signalling peptides. Dev Bio 236, 364-386.

Hamilton, H. L., (1965), Lillie's Development of the Chick. Holt, Rinehart, and Winston, New York.

Hammond, S.M., Bernstein, E., Beach, D., and Hannon, G.J. 2000. An RNA-directed nuclease mediates post-transcriptional gene silencing in Drosophila cells. Nature 404: 293–296.

Harfe, B. D., Scherz, P. J., Nissim, Tian, S. H., McMahon, A. P. and Tabin, C. J (2004). Evidence for an Expansion-Based Temporal Shh Gradient in Specifying Vertebrate Digit Identities. Cell, Vol. 118, 517–528.

Hayes, N.L. and R.S. Nowakowski (2000) Exploiting the dynamics of S-phase tracers in developing brain: Interkinetic nuclear migration for cells entering vs leaving the S-phase. Dev. Neurosci. 22: 44-55.

Hecht, M. K., and Heebt, B. M. (1994). Conflicting developmental and palaeontological data: The case of the bird manus. Acta Palaeontol. Polonica **38**: 329-338.

Hill RE, Heaney SJ, Lettice LA. (2003) Sonic hedgehog: restricted expression and limb dysmorphologies. J Anat. 202(1):13-20. Review.

Hinchliffe J. R (2002). Developmental basis of limb evolution. Int. J. Dev. Biol. 46:835-845.

Hinchliffe J. R. and Hecht, M. K. (1984) Homology of the bird wing skeleton: Embryological evidence versus palaeontological evidence. Evol. Biol 18: 21-39

Hinchliffe J. R. and Vorobyeva, E. I (1999). Developmental basis of limb homology in urodeles: heterochronic evidence from the primitive hynobiid family.

Holder, N., (1977). An experimental investigation into the early development of the chick elbow joint. J Embryol Exp Morphol. 39:115-27.

Holder, N. (1983). Developmental constraints and the evolution of vertebrate digit patterns. J. Theo. Bio. 104: 451-71

Holmgren, N. (1955). Studies on the phylogeny of birds. Acta Zool. 36: 243-328.

Hornbruch,A., Wolpert,L., (1970). Cell division in the early growth and morphogenesis of the chick limb. Nature 226, 764-766.

Hui EP, Poon TC, Teo PM, Mo F, Zee B, Leung SF, Ho S, Mok TS, Kwan WH, Johnson PJ, Chan AT. (2003). A prospective study of pre-treatment cell kinetics and clinical outcome in nasopharyngeal carcinoma. Radiother Oncol. 69(1):53-62.

Ingham P. W. and McMahon A. P., (2001). Hedgehog singalling in animal development: paradigms and principles. Genes & Dev , 15: 3059-3087.

Janvier, P. (1996). Early vertebrates. Oxford: Clarendon Press.

Johnson, R.L. and Tabin, C.J., (1997). Molecular models for vertebrate limb development, Cell 90:979-990.

Kardong, K. V., (1998). Vertebrates: Comparative anatomy, function, evolution, Second Edition.(WCB/McGraw-Hill) pp 308-310.

Kavanagh E, Abiri M, Bland YS, Ashhurst DE. (2002). Division and death of cells in developing synovial joints and long bones. Cell Biol Int., 26(8):679-88.

Kawakami,Y., Capdevila,J., Buscher,D., Itoh,T., Rodriguez,E.C., Izpisua Belmonte,J.C., (2001). WNT signals control FGF-dependent limb initiation and AER induction in the chick embryo. Cell 104, 891-900.

Kelley, R. O. and J. F. Fallon. 1976. Ultrastructural analysis of the apical ectodermal ridge during vertebrate limb morphogenesis. I. The human forelimb with special reference to gap junctions. Devel. Biol. 51241-256.19:487-507.

Kengaku,M., Capdevila,J., Rodriguez-Esteban,C., De La,P.J., Johnson,R.L., Belmonte,J.C., Tabin,C.J., (1998). Distinct WNT pathways regulating AER formation and dorsoventral polarity in the chick limb bud. Science 280, 1274-1277.

Khan PA, Tsilfidis C, Liversage RA. (1999). Hox C6 expression during development and regeneration of forelimbs in larval Notophthalmus viridescens. Dev. Gen. Evol. 209(6):323-9.

Kimura S, Shiota K. (1996). Sequential changes of programmed cell death in developing fetal mouse limbs and its possible roles in limb morphogenesis. J Morphol., 229(3):337-46.

Kirkwood. J. K., Spratt, D. M and Duignan, P. J. (1989) Patterns of cell proliferation and growth rate in limb bones of the domestic fowl (Gallus domesticus). Res. Ver. Sci 47(2):139 - 147.

Kmita M, Fraudeau N, Herault Y, Duboule D. (2002) Serial deletions and duplications suggest a mechanism for the collinearity of Hoxd genes in limbs. Nature, 420(6912):138-9.

Kmita, M., Tarchini B., Za`ka`ny, J., Logan, M., Tabin, C. J., and Duboule D., (2005). Early developmental arrest of mammalian limbs lacking HoxA/HoxD gene function. Nature, 435: 1113-1116.

Kondo, S & Asai, R. (1995). A reaction-diffusion wave on the skin of marine angelfish Pomacanthus. Nature 376, 765-768.

Kornak,U., Mundlos,S., (2003). Genetic disorders of the skeleton: a developmental approach. Am. J. Hum. Genet. 73, 447-474.

Kostakopoulou, K., Vogel, A., Birckell, P., and Tickle, C (1996). "Regeneration" of wing bud stumps of chick embryos and reactivation of Msx-1 and Shh expression in response to FGF-4 and ridge signals. Mech. Dev. 55, 119-131.

Krauss, S., Concordet, J. P., and Ingham, P.W., (1993) A functionally conserved homolog of the Drosophila segment polarity gene hh is expressed in tissue with polarizing activity in zebrafish embryos. Cell, 75: 1431-1444.

Kraus,P., Fraidenraich,D., Loomis,C.A., (2001). Some distal limb structures develop in mice lacking Sonic hedgehog signaling. Mech. Dev. 100, 45-58.

Kronenberg,H.M., (2003). Developmental regulation of the growth plate. Nature 423, 332-336.

Kubbies M, Schindler D, Hoehn H, Schinzel A, Rabinovitch PS. (1985). Endogenous blockage and delay of the chromosome cycle despite normal recruitment and growth phase explain poor proliferation and frequent edomitosis in Fanconi anemia cells. Am J Hum Genet. 37(5):1022-30

Kuhn, R and R. M. Torres (2002) Transgenesis Techniques, principles and protocols, second edition, Humana Press, pp175-204.

Larsson H. C. E and Wagner, G. P., (2002). Pentadactyl pattern of the avian wing autopodium and pyramid reduction hypothesis. J Exp Zool. (Mol. Dev. Evol.) 294B:146-151.

Laufer, E., Nelson, C. E., Johnson, R. L., Morgan, B. A., Tabin, C. (1994). Sonic hedgehog and Fgf4 act through a signaling cascade and feedback loop to integrate growth and patterning in the developing limb bud. Cell 79, 993-1003.

Lawson, K. A., Meneses, J. J. and Pedersen, R. A. (1986). Cell fate and cell lineage in the endoderm or the presomite mouse embryo, studied with an intracellular tracer. Dev. Biol. 115:325-339

Lawson, K. A., Pedersen, R. A. and Van de Geer (1987). Cell fate, morphogenetic movement and population kinetics of embryonic endoderm at the time of germ layer formation in the mouse. Development 101:627-652.

Lawson, K. A., Meneses, J. J. and Pedersen, R. A. (1991). Clonal analysis of epiblast fate during germ layer formation in the mouse embryo. Development 113: 891-911.

Lee, J. J., Ekker, S. C., von Kessler, D. P., Porter, J. A., Sun, B. I., and Beachy, P. A., (1994). Autoproteolysis in hedgehog protein biogenesis. Science 266, 1528-1537.

Lee, Y., Jeon, K., Lee, J.T., Kim, S., and Kim, V.N. 2002. MicroRNA maturation: Stepwise processing and subcellular localization. EMBO J. 21: 4663–4670.

Lee J, Tickle C. (1985) Retinoic acid and pattern formation in the developing chick wing: SEM and quantitative studies of early effects on the apical ectodermal ridge and bud outgrowth. J Embryol Exp Morphol. 90:139-69.

Lefebvre, V., Li, P., and de Crombrugghe, B. (1998). A new long form of Sox5 (L-Sox5), Sox6 and Sox9 are coexpressed in chondrogenesis and cooperatively activate the type II collagen gene. EMBO J. 17: 2336-2346.

Lettice, L. A., et al. (2002). Disruption of a long-range cis-acting regulator for Shh causes preaxial polydactyly. PNAS 99: 7548-7553.

Lettice LA, Heaney SJ, Purdie LA, Li L, de Beer P, Oostra BA, Goode D, Elgar G, Hill RE, de Graaff E. (2003). A long-range Shh enhancer regulates expression in the developing limb and fin and is associated with preaxial polydactyly. Hum Mol Genet. 12(14):1725-35.

Levin M, Mercola M. (1998). Evolutionary conservation of mechanisms upstream of asymmetric Nodal expression: reconciling chick and Xenopus. Dev Genet. 23(3):185-93.

Lewandoski, M., Sun, X., Martin, G. R (2000). Fgf8 signalling from the AER is essential for normal limb development. Nature Gen. 26: 460-463.

Lewis, P. M., Dunn, M. P., McMahon, J. A., Logan, M, Martin, J. F., St-Jacques, B. and McMahon, A. P.,(2001). Cholesterol modification of Sonic Hedgehog is required for long-range signalling activity and effective modualtion of signalling by Ptc1. Cell 105: 599-612.

Li, S and Muneoka, K (1999). Cell migration and chick limb development: chemotactic action of FGF-4 and the AER. Dev. Bio. 211:335-347.

Liem,K.F.,Jr.; Tremml,G.; Roelink,H.; Jessell,T.M. (1995). Dorsal differentiation of neural plate cells induced by BMP-mediated signals from epidermal ectoderm. Cell 82 (6): 969-979.

Litingtung, Y., Dahn, R. D., Li, Y., Fallon, J. F. and Chiang, C. (2002). Shh and Gli3 are dispensable for limb skeleton formation but regulate digit number and identity. Nature, 418: 979-983.

Lizarraga G, Lichtler A, Upholt WB, Kosher RA. (2002). Studies on the role of Cux1 in regulation of the onset of joint formation in the developing limb. Dev Biol., 243(1):44-54.

Logan, C., Hornbruch, A., Campbell, I., Lumsden, A., (1997) The role of Engrailed in establishing the dorsoventral axis of the chick limb. Development. 124:2317-24.

Logan,M., Simon,H.G., Tabin,C., (1998). Differential regulation of T-box and homeobox transcription factors suggests roles in controlling chick limb-type identity. Development 125, 2825-2835.

Loomis, C. A., Harris, E., Michaud, J., Wurst, W., Hanks M., Joyner, A. L., (1996). The mouse Engrailed-1 gene and ventral limb patterning. Nature, 382: 360-63.

Loomis, C. A., Kimmel, R. A., Tong, C. X., Michaud, J., Joyner, A. L., (1998). Analysis of the genetic pathway leading to formation of ectopic apical ectodermal ridges in mouse Engrailed-1 mutant limbs.
Development, 125:1137-48.

Lopez-Martinez, A., Chang, D. T., Chiang, C. et al. (1995). Limb patterning activity and restricted posterior localization of the amino-terminal product of Sonic-hedgehog cleavage. Curr. Biol. 5, 791-796.

MacCabe A. B., Saunders, J. W. and Picket M. (1973). The control of the anteroposterior and dorsoventral axes in the embryonic chick limbs contructed of dissociated and reaggregated limb-bud mesoderm. Dev. Bio. 31:323-335.

MacCabe, J. A., Errick, J and Saunders, J. W. (1974). Ectodermal control of the dorsoventral axis in the leg bud of the chick embryo. Dev. Biol. 39, 69-82.

Macias,D., Ganan,Y., Sampath,T.K., Piedra,M.E., Ros,M.A., Hurle,J.M., (1997). Role of BMP-2 and OP-1 (BMP-7) in programmed cell death and skeletogenesis during chick limb development. Development 124, 1109-1117.

Mahmood, R., Bresnick, J., Hornbruch, A., Mahony, C., Morton, N., Colquhoun, K., Martin, P., Lumsden, A., Dickson, C., and Mason, I. (1995). A role for FGF-8 in the intiation and maintenance of limb bud outgrowth. Curr Biol. 5: 797-806.

Maini, P. K and Solursh, M (1991) Cellular Mechanisms of pattern formation in the developing limb. Int. Rev. Cyt. 129: 91-133.

Manche, L., Green, S.R., Schmedt, C., and Mathews, M.B. (1992). Interactions between double-stranded RNA regulators and the protein kinase DAI. Mol. Cell. Biol. 12: 5238–5248.

Manouvrier-Hanu,S., Holder-Espinasse,M., Lyonnet,S., (1999). Genetics of limb anomalies in humans. Trends Genet. 15, 409-417.

Mao, X., Fujiwara, Y., and Orkin, S.H. (1999). Improved reporter strain for monitoring Cre recombinase-mediated DNA excisions in mice. Proc. Natl. Acad. Sci. USA 96, 5037–5042.

Marchok, A. C., and Hermann, H. (1967). Studies of muscle development I. Changes in cell proliferation. Dev Biol. 15: 129-155.

Margulies EH, Kardia SL, Innis JW. (2001). A comparative molecular analysis of developing mouse forelimbs and hindlimbs using serial analysis of gene expression (SAGE). Genome Res, 11(10):1686-98.

Mariani,F.V., Martin,G.R., (2003). Deciphering skeletal patterning: clues from the limb. Nature 423, 319-325.

Marigo, V., Johnson, R., Vortkamp, A., and Tabin, C. (1996). Sonic hedgehog differentially regulates expression of Gli and Gli3 during limb development. Dev. Biol. 180: 273–283.

Marshall O.J., Harley V.R. (2000) Molecular Mechanisms of SOX9 Action. Mol. Gen. and Met., 71:455-462.

Marti, E., Takada, R., Bumcrot, D. A., Sasaki, H. & McMahon, A. P. (1995). Distribution of Sonic hedgehog peptides in the developing chick and mouse embryo. Development 121, 2537-2547.

Martin, G. R. (1998) The roles of FGFs in the early development of vertebrate limbs. Genes Dev. 12, 1571-1586.

Martin, P. (1990). Tissue patterning in the developing mouse limb. Int. J. Dev. Biol. 34, 323-336.

Martynoga B. Morrison, H. Price, D. J and Mason, J. O (2005) Foxg1 is required for specification of ventral telencephalon and region-specific regulation of dorsal telencephalic precursor proliferation and apoptosis. Developmental Biology 283: 113-127.

Masuya, H., Sagai, T., Moriwaki, K. and Shiroishi, T. (1997). Multigenic control of the localization of the zone of polarizing activity in limb morphogenesis in the mouse. Dev. Bio. 182: 42-51.

Mauer, A. M and Fisher, V. (1963) In vivo studies of cell kinetics of acute leukaemia. Nature 197:574-576.

Maynard-Smith, J., R. Burian, S. Kauffman, P. Alberch, J. Campell, B. Goodwin, R. Lande, D. Raup and L. Wolpert 1985. Developmental constraints and evolution. Quart. Rev. Biol. 60: 265-287.

McGinnis, W. & Krumlauf, R. (1992). Homeobox genes and axial patterning. Cell 68 (2): 283-302

Mercader,N.; Leonardo,E.; Azpiazu,N.; Serrano,A.; Morata,G.; Martinez,C.; Torres,M. (1999). Conserved regulation of proximodistal limb axis development by Meis1/Hth. Nature, 402 (6760): 425-429.

Merino, R., Macais, D., Gañan, Y., Rodriguez-Leon, J., Economides, A. N., Rodriguez-Esteban, C., Izpisua-Belmonte, J.C. & Hurle, J. M. (1999a). Control of digit formation by activin signalling. Development 126, 2161-2170.

Merino, R., Rodriguez-Leon, J., Macias, D., Gañan, Y., Economides, A. N. & Hurle, J. M. (1999b). The BMP antagonist Gremlin regulates outgrowth, chondrogenesis and programmed cell death in the developing limb. Which journal

Merino, R., Macias, D., Gañan, Y., Economides, A. N., Wang, X., Wu, Q., Stahl, N., Sampath, K.T., Varona P., & Hurle, J. M. (1999c). Expression and function of Gdf-5 during digit skeletogenesis in the embryonic chick leg bud. Dev. Biol. 206, 33-45.

Michaud, J. L., Lapointe, F., Le Douarin N. M., (1997). The dorsoventral polarity of the presumptive limb is determined by signals produced by the somites and by the lateral somatopleure. Development 124: 1453-1463.

Milaire, J. (1978) Etude morphologique, histwhimique. et autoradiographique du developpement du squelette. Arch. Biol. 89:169-216

Miyake,T., Cameron,A.M., Hall,B.K., (1996). Stage-specific onset of condensation and matrix deposition for Meckel's and other first arch cartilages in inbred C57BL/6 mice. J. Craniofac. Genet. Dev. Biol. 16, 32-47.

Moon, A. M. and Capecchi, M. R., (2000) Fgf8 is required for outgrowth and patterning of the limbs. Nature Genet. 26: 455-459.

Morse, E. (1872) Ann. Lyceum Nat . Histor y (New York).

Murray PD, Drachman DB. (1969). The role of movement in the development of joints and related structures: the head and neck in the chick embryo. J Embryol Exp Morphol. 22(3):349-71.

Murray, J. (1990). Discussion: Turing's theory of morphogenesis-its influence on modelling biological pattern and form. Bull. Math. Biol. 52, 119-152.

Nelson, C. E., Morgan , B. A., Burke, A. C., Laufer, E., Dimambro, E., et al (1996). Analysis of hox gene expression in the chick limb bud. Development 122: 1449-1466.

Newman, S. A. & Comper, W. D. (1990). 'Generic' physical mechanisms of morphogenesis and pattern formation. Development 110, 1-18.

Newman, S. A. & Frisch, H. L. (1979). Dynamics of skeletal pattern formation in developing chick limb. Science 205:662-668.

Newman, S. A. and Muller, G. B. (2005). Origination and innovation in the vertebrate limb skeleton: An epigenetic perspective. J. Exp. Zool. (Mol. Dev. Evol.) 304B:593-609.

Ng, L-J. et al. (1997). SOX9 binds DNA, activates transcription, and coexpresses with type II collagen during chondrogenesis in the mouse. Dev. Biol. 183, 108-121.

Niswander, L. (2003). Pattern formation: Old models out on a limb. Nature Gen. 4:133-143.

Niswander, L., Jeffery, S., Martin, G. R. and Tickle, C. (1994). A positive feedback loop coordinates growth and patterning in the vertebrate limb. Nature 371, 609-614.

Niswander, L. and Martin, G. R., (1993). FGF-4 and BMP-2 have opposite effects on limb growth. Nature 371: 609-612.

Niswander, L., Tickle, C., Vogel, A., Booth, I., and Martin, G. R., (1993) FGF-4 replaces the apical ectodermal ridge and directs outgrowth and patterning of the limb. Cell, 75, 579-587.

Nowakowski R. S., Lewin S. B., Miller M. W. (1989) Bromodeoxyuridine immunohistochemical determination of the lengths of the cell cycle and the DNA-synthetic phase for an anatomically defined population. J Neurocytol 18:311–318.

Ohta, Y. and Ichimura, K. (2000). Proliferation markers, proliferating cell nuclear antigen, Ki67, 5-bromo-2'-deoxyuridine, and cyclin D1 in mouse olfactory epithelium. Ann. Otol. Rhinol. Laryngol. 109(11): 1046-1048.

Ohuchi, H., Nakagawa, T., Yamamoto, A., Araga, A., Ohata, T., Ishimaru, Y., Yoshioka, H., Kuwana, T., Nohono, T.,Yamasaki, M.,Itoh, N., and Noji, S. (1997). The mesenchymal factor FGF-10, initiates and maintains the outgrowth of the chick limb bud through interaction with FGF-8, an apical ectodermal factor. Development 124, 2235-2244.

Ohuchi, H., Yoshioka, H., Tanaka, A., Kawakami, Y., Nohno, T., and Noji, S. (1994). Involvement of androgen-induced growth factor (FGF-8) gene in mouse embryogenesis and morphogenesis. Biochem. Biophys. Rec. Comm. 204:882-888.

Olney, P. N., Kean, L. S., Graham, D., Elsas, L. J and May, K. M (1999) Campomelic syndrome and deletion of Sox9. Am. J. Med. Gen. 84: 20-24.

Ormerod, M. G. (2004). Cell-cycle analysis of asynchronous populations. Meth. Mol. Biol. 263, 345-54.

Oster, G. F., Shubin, N. H., Murray, J. D. and Alberch, P. (1988). Morphogenetic rules and evolution. Evolution, 42:862-884.

Ostrom, J. H. (1976) Archaeopteryx and the origin of birds, Biol. J. Linn. Soc. 8: 91-182.

Pacifici M, Koyama E, Iwamoto M, Gentili C. (2000). Development of articular cartilage: what do we know about it and how may it occur? Connect Tissue Res. 41(3):175-84.

Parr, B. A. and McMahon, A. P. (1995) Dorsalizing signal Wnt-7a required for normal polarity of D–V and A–P axes of mouse limb. Nature 374: 350–353.

Parr, B. A., Shae M.J., Vassileva, G., McMahon, A. P. (1993). Mous Wnt genes exhibit discrete domains of expression in the early embryonic CNS and limb buds. Development 119: 247-261.

Pizette, S., Abate-Shen, C., Niswander, L., (2001). BMP controls proximo-distal outgrowth, via induction of the apical ectodermal ridge, and dorsoventral patterning in the vertebrate limb. Development 128, 4463– 4474.

Porter, J. A., von Kessler, D. P., Ekker, S. C., Young, K. E., Lee, J. J., Moses, K., and Beachy, P. A. (1995). The product of hedgehog autoproteolytic cleavage active in local and long-range signalling. Nature, 374, 363-366.

Qu, S., Niswender, K., Ji, Q., van der Meer, R., Keeny, D., Magnuson, M. A., and Wisdom, R. (1997). Polydactyly and ectopic ZPA formation in Alx4 mutant mice. Development 124: 3999-4008.

Qu S., Tucker, S. C., Ehrlich, J. S., Levorse, J. M., Flaherty, L. A., Wisdom, R., and Vogt, T. F., (1998). Mutations in mouse Aristaless-like4 cause Strong's luxoid polydactyly. Development 125: 271-2721.

Quinn JC, West, J. D. and Hill RE, (1996). Multiple functions for Pax6 in mouse eye and nasal development. Genes & Development 10, 435-446.

Rabinovitch PS, Kubbies M, Chen YC, Schindler D, Hoehn H. (1988). Exp. Cell Res. 174(2):309-18.

Reiter, R. S. and Solursh, M. (1982). Mitogenic property of the apical ectodermal ridge. Dev. Biol.93, 28-35.

Richardson M. K., Carl T.F., Hanken J., Elinson R. P., Cope C., Bagley P. (1998). Limb development and evolution: a frog embryo with no apical ectodermal ridge (AER). J Anat. 192 (Pt 3):379-90.

Riddle, R. D., Johnson R. L., Laufer E., Tabin C (1993) Sonic hedgehog mediates the polarizing activity of the ZPA. Cell 75, 1401-1416.

Riddle, R. D., Ensini, M., Nelson, C., Tsuchida T., Jessell T. M., Tabin, C (1995). Induction of the LIM homeobox gene Lmx1 by WNT7a establishes dorsoventral pattern in the vertebrate limb. Cell 83:631-640.

Roberts,D.J.; Johnson,R.L.; Burke,A.C.; Nelson,C.E.; Morgan,B.A.; Tabin,C.(1995). Sonic hedgehog is an endodermal signal inducing Bmp-4 and Hox genes during induction and regionalization of the chick hindgut. Dev. 121(10): 3163-3174.

Rodriguez-Esteban C, Tsukui T, Yonei S, Magallon J, Tamura K, Izpisua Belmonte JC., (1999). The T-box genes Tbx4 and Tbx5 regulate limb outgrowth and identity. Nature, 398(6730):814-8.

Romanoff. A. L., (1960). The Avian Embryo. Macmillan, New York.

Ros, M. A., López-Martinez, A., Simandl, B. K., Rodriguez, C, Belmonte, J. C. I., Dahn, R., Fallon, J. F., (1996). The limb field mesoderm determines initial limb bud anteroposterior asymmetry and budding independent of sonic hedgehog or apical ectodermal gene expressions. Development 122, 2319-2330.

Ros,M.A., Dahn,R.D., Fernandez-Teran,M., Rashka,K., Caruccio,N.C., Hasso,S.M., Bitgood,J.J., Lancman,J.J., Fallon,J.F., (2003). The chick oligozeugodactyly (ozd) mutant lacks sonic hedgehog function in the limb. Development 130, 527-537.

Rubin,L., Saunders,J.W., Jr., (1972). Ectodermal-mesodermal interactions in the growth of limb buds in the chick embryo: constancy and temporal limits of the ectodermal induction. Dev. Biol. 28, 94-112.

Sagai T, Masuya H, Tamura M, Shimizu K, Yada Y, Wakana S, Gondo Y, Noda T, Shiroishi T. (2004) Phylogenetic conservation of a limb-specific, cis-acting regulator of Sonic hedgehog (Shh). Mamm Genome.15(1): 23-34.

Sagai T, Hosoya M, Mizushina Y, Tamura M, Shiroishi T. (2005). Elimination of a long-range cis-regulatory module causes complete loss of limb-specific Shh expression and truncation of the mouse limb. Development 132: 797-803.

Salas-Vidal E, Valencia C, Covarrubias L. (2001). Differential tissue growth and patterns of cell death in mouse limb autopod morphogenesis. Dev Dyn. 220: 295-306.

Salazar-Ciudad, I., Garcia-Fernandez J. & Solé, R.V. (2000). Gene networks capable of pattern formation: from induction to reaction-diffusion. J. Theor. Biol. 205, 1-17.

Santagati F, Abe K, Schmidt V, Schmitt-John T, Suzuki M, Yamamura K, Imai K. (2003). Identification of Cis-regulatory elements in the mouse Pax9/Nkx2-9 genomic region: implication for evolutionary conserved synteny. Genetics, 165(1):235-42.

Sanz-Ezquerro,J.J., Tickle,C., (2003). Digital development and morphogenesis. J. Anat. 202, 51-58.

Saunders, J. W. J. (1948). The proximodistal sequence of the origin of the parts of the chick wing and the role of the ectoderm. J. Exp. Zool. 108, 363-404.

Saunders, J. W. & Gasseling, M. T. (1968). Epithelial-Mesenchymal interactions. Baltimore: Williams & Wilkins. 78-97.

Saunders, J. W., (2002). Is the Progress Zone Model a Victim of Progress? Cell, 110(5): 541-543

Saunders, J. W., Jr and Reuss, C. (1974). Inductive and axial properties of prospective wing-bud mesoderm in the chick embryo. Dev. Biol. 38, 41-50.

Savage, M. P., and Fallon, J. F., (1995). FGF-2 mRNA and its antisense message are expressed in a developmentally specific manner in the chick limb bud and the mesonephros. Dev. Dyn. 202, 343-353.

Scherz, P. J., Harfe, B. D., McMahon, A. P., and Tabin, C. J., (2004) The limb bud Shh-Fgf feedback loop is terminated by expansion of former ZPA cells. Science, 305: 396-399.

Schmidt, E.V., Christoph, G., Zeller, R., and Leder, P. 1990. The cytomegalovirus enhancer: A pan-active control element in transgenic mice. Mol. Cell. Biol. 10: 4406–4411.

Schneider, R. A., Hu D., Helms J. A. (2004). From head to toe: conservation of molecular signals regulating limb and craniofacial morphogenesis. Cell and Tissue Res. 296 (1):103-109

Scott,I.S.; Morris,L.S.; Bird,K.; Davies,R.J.; Vowler,S.L.; Rushbrook,S.M.; Marshall,A.E.; Laskey,R.A.; Miller,R.; Arends,M.J.; Coleman,N. (2003). A novel immunohistochemical method to estimate cell-cycle phase distribution in archival

tissue: implications for the prediction of outcome in colorectal cancer. J. Pathol. 2001:187-197.

Scott MP. (1997). Hox genes, arms and the man.Nat Genet. 15(2):117-8.

Searls, R. L., and Janners, M. Y. (1971). The initiation of limb bud outgrowth in the embryonic chick. Dev. Biol. 24, 198-213.

Sereno, P. C (1993). Shoulder girdle and forelimb of Herrerasaurus. J. Vert. Paleont. 13:425-450.

Sharpe, J., Lettice, L., Hecksher-Sorensen, J., Fox, M., Hill, R., and Krumlauf, R. (1999). Identification of Sonic hedgehog as a candidate gene responsible for the polydactylous mouse mutant Sasquatch. Current Biology 9: 97-100.

Sharpe, J., Ahlgren, U., Perry, P., Hill, B., Ross, A., Hecksher-Sorensen, J., Baldock, R. and Davidson, D (2002). Optical projection tomography as a tool for 3D microscopy and gene expression studies. Science, 296: 541-545.

Shibata, K. and Ajiro, K. (1993) Cell cycle-dependent suppressive effect of histone H1 on mitosis-specific H3 phosphorylation. J Biol Chem 268: 18431-18434.

Shibui,S.; Hoshino,T.; Vanderlaan,M.; Gray,J.W. (1989) Double labeling with iodo- and bromodeoxyuridine for cell kinetics studies. J.Histochem.Cytochem. 37(7):1007-1011.

Shimeld, S. M.,(1999). The evolution of the hedgehog gene family in chordates: insights from amphioxus hedgehog. Dev. Genes Evol., 209: 40-47.

Shinagawa, T. & Ishii, S. (2003). Generation of Ski-knockdown mice by expressing a long double-strand RNA from an RNA polymerase II promoter. Gen. Dev. 17, 1340-1345.

Shubin, N. H., and Alberch, P. (1986). A morphogenetic approach to the origin and basic organisation of the tetrapod limb. In M. K. Hecht, B.Wallace, and G. I. Prance (eds.). Evolutionary Biology. Plenum Press, New York, 319-387.

Shubin, N. Tabin, C. and Carroll, S. (1997). Fossils, genes and the evolution of animal limbs. Nature, 388:639-648.

Smith, J. C (1980). The time required for positional signalling in the chick wing bud. J Embryol Exp Morphol. 60: 321-8.

Smits, P., Li, P., Mandel, J., Zhang, Z., Deng, J. M., Behringer, R. R. de Crombrugghe, B., Lefebvre, V. (2001). The transcription factors L-Sox5 and Sox6 are essential for cartilage formation. Dev. Cell 1: 277-290.

Stark, R. and Searls, R. (1974). The establishment of the cartilage pattern in the embryonic chick wing, and evidence for a role of the dorsal and ventral ectoderm in normal wing development Dev Biol. 38, 51-63.

Stark, G.R., Kerr, I.M., Williams, B.R., Silverman, R.H., and Schreiber, R.D. 1998. How cells respond to interferons. Annu. Rev. Biochem. 67: 227–264.

Stockdale, F. E., and Holtzer, H. (1961). DNA synthesis and myogenesis. Exp. Cell. Res. 24, 508-520.

Storm, E. E., & Kingsley, D. M. (1996). Joint patterning defects caused by single and double mutations in members of the bone morphogenetic protein (BMP) family. Development 122, 3969-3979.

Storm EE, Kingsley DM. (1999). GDF5 coordinates bone and joint formation during digit development. Dev Biol. 209(1):11-27.

Storm EE, Huynh TV, Copeland NG, Jenkins NA, Kingsley DM, Lee SJ. (1994). Limb alterations in brachypodism mice due to mutations in a new member of the TGF beta-superfamily. Nature, 368(6472):639-43.

Sudbeck, P., and G. Scherer. (1997). Two independent nuclear localization signals are present in the DNA-binding high mobility group domains of SRY and SOX9. J. Biol. Chem. 272:27848–27852.

Summerbell, D., and Wolpert, L., (1972). Cell density and cell division in the early morphogenesis of the chick wing. Nature 239, 24-36.

Summerbell, D., Lewis, J. H., and Wolpert, L. (1973). Positional information in chick limb morphogenesis. Nature, 224, 492-496.

Summerbell, D.,(1974). Interaction between the proximo-distal and antero-psterior coordinates of positional value during the specification of positional information in the early development of the chick limb bud. J. Embryol. Exp. Morphol. 32: 227-237.

Summerbell, D. (1977). Reduction of the rate of outgrowth, cell density and cell density, and cell division following removal of the apical ectodermal ridge of the chick limb-bud. J. Embryol. Exp. Morphol. 40:1-21.

Sun X, et al, (2000). Conditional inactivation of Fgf4 reveals complexity of signalling during limb bud development. Nature Gen. 25: 83-86.

Sun X, Mariani FV, Martin GR., (2002). Functions of FGF signalling from the apical ectodermal ridge in limb development. Nature, 418(6897):501-8.

Tabin, C. J. (1991). Retinoids, homeoboxes, and growth factors: toward molecular models for limb development. Cell 66: 199-217.

Tarchini, B., Duboule, D and Kmita, M (2006). Regulatory constraints in the evolution of the tetrapod limb anterior-posterior polarity. Nature 443: 985-988.

Takahashi, T., Nowakowski, R.S., Caviness Jr., V.S., 1992. BUdR as an S- phase marker for quantitative studies of cytokinetic behaviour in the murine cerebral ventricular zone. J. Neurocytol. 21, 185 – 197.

Takahashi, T., Nowakowski, R.S., Caviness Jr., V.S., 1993. Cell cycle parameters and patterns of nuclear movement in the neocortical proliferative zone of the fetal mouse. J. Neurosci. 13, 820 – 833.

Takahashi, M., Tamura, K., Buescher, D., Masuya, H., Yonei-Tamura, S., Matsumoto, K., Naitoh-Matsuo, M., Takeuchi, J., Ogura, K., Shiroishi, T., et al. (1998). The role of Alx-4 in the establishment of anteroposterior polarity during vertebrate limb development. Development, 125: 4417-4425.

Tanaka, M., Münsterberg, A., Anderson, W. G., Prescott, A. R., Hazon, N., Tickle, C., (2002). Fin development in cartilaginous fish and the origin of vertebrate limbs. Nature, 416: 527-531.

Taylor, G., Anderson, R., Reginelli, A. D., and Muneoka, K. (1994) FGF-2 induces regeneration of the chick limb bud. Dev Biol. 163, 282-284.

Theiler, K. (1989). The House Mouse: Atlas of embryonic development. Springer-Verlag, New York.

Thorogood, P. V. & Hinchcliffe, J. R.(1975). An analysis of the condensation process during chondrogenesis in the embryonic chick hindlimb J. Embryol. Exp. Morphol. 33, 581-606.

Tickle, C., Summerbell, D., and Wolpert, L. (1975). Positional signalling and specification of digits in chick limb morphogenesis. Nature 254: 199-202.

Tickle, C. (1981) The number of polarizing region cells required to specify additional digits in the developing chick wing. Nature 289, 295-298.

Todt, W., and Fallon, J. F. (1984). Development of the apical ectodermal ridge in the chick wing bud. J. Embryol. Exp. Morphol. 80, 21-41.

Tsonis, P. A. and Goetinck. P. F (1990) Cell denisty dependent effect of a tumour promoter on proliferation and chondrogenesis of limb bud mesenchymal cells. Exp. Cell. Res. 190(2): 247-253.

Turing, M. A. (1952). The chemical basis of morphogenesis. Phil. Trans. Roy. Soc. Lond. B237, 37-72.

Underwood, G., (1977) Simplification and degeneration in the course of evolution of squamate reptiles, in Mecanismes de la rudimentation des organes chez les embryons de vertebres, pp341-351, Collooques Internationaux CNRS, No266, Paris.

Vargas, A. O and Fallon, J. F (2005). Birds have dinosaur wings: The molecular evidence. J. Exp. Zool. (Mol. Dev. Evol.) 304B:86-90.

Vargesson, N., Clarke, J. D. W., Vincent, K., Coles, C., Wolpert, L.,and Tickle, C. (1997) Cell fate in the chick limb bud and relationship to gene expression. Development, 124: 1909-1918.

Vogel, A., Rodriguez, C., Warnken, W., and Izpisua Belmonte, J.C. (1995). Dorsal cell fate specified by chick Lmx1 during vertebrate limb development. Nature *378*, 716–720.

Vorobyeva, E. I. and Hinchliffe J. R. (1996). Developmental pattern and morphology of Salamandrella keyserlingii limbs (Amphibia, Hynobiidae) including some evolutionary aspects. Russ J. Herpetol 3:68-81.

Wada, N., Kawakami, Y. & Nohno, T. (1999). Sonic hedgehog signalling during digit pattern duplication after application of recombinant protein and expressing cells. Dev. Growth Differ. 41, 567-574.

Wagner,A., (1994). Evolution of gene networks by gene duplications: a mathematical model and its implications on genome organization. Proc. Natl. Acad. Sci. U. S. A 91, 4387-4391.

Wagner, T., et al (1994). Autosomal sex reversal and campomelic dysplasia are caused by mutations in an SRY-related gene SOX9. Cell 79: 1111-1120.

Wagner, G. P. and Chiu, C. (2001). The tetrapod limb: a hypothesis on its origin. J. Exp. Zool. 291: 226-240.

Wanek, N., Muneoka, K., Holler-Dinsmore, G., Burton, R., and Bryant, S. V. (1989). A staging system for mouse limb development. J. Exp. Zool. 249, 41– 49.

Wang, B., Fallon, J. F., and Beachy, P. A. (2000). Hedgehog-regulated processing of Gli3 produces an anterior/posterior repressor gradient in the developing vertebrate limb. Cell 100: 423-434.

Warchol, M. E. (2002). Cell Density and N-Cadherin Interactions Regulate Cell Proliferation in the Sensor y Epithelia of the Inner Ear. J. Neuroscience, 22(7):2607–2616.

Wegner, M. (1999). From head to toes: the multiple facets of Sox proteins. Nucleic Acids Res. 27:1409–1420.

Welscher, P. T., Fernandez-Teran, M., Ros, M. A.,, and Zeller, R. (2002). Mutual genetic antagonism involving Gli3 and dHand prepatterns the vertebrate limb bud mesenchyme prior to Shh signaling. Genes and Dev. 16: 421-426.

Welten, M. C. M., Verbeek, F. J., Meijer, A. H., and Richardson, M. K (2005). Gene expression and digit homology in the chicken embryo wing Evo. Devo. 7(1): 18-28.

West, J. D., and Flockhart, J. H., (1994). Genotypically unbalanced diploid<->diploid foetal mouse chimaeras: Possible relevance to human confined mosaicism. Genet. Res. 63:87-99,

Wolpert, L (1969). Positional information and the spatial pattern of cellular differentiation. J. Theo. Biol. 25, 1-47.

Wolpert, L (1981). Cellular basis of skeletal growth during development. British Medical Bulletin, 37(3): 215-219

Wolpert, L. (1991) in A history of regeneration research (Dinsmore, C., ed.) pp. 201-217, Cambridge University Press.

Wolpert, L (2002) Limb Patterning: Reports of Model's Death Exaggerated. Current Biology, 12: 628-630.

Wolpert, L. et al. (1998). Principles of development. Oxford University Press.

Wolpert, L, Tickle, C and Sampford, M. (1979). The effect of cell killing by X-irradiation on pattern formation in the chick limb. J. Embryol. Exp. Morphol. 50, 175-198.

Wright, E., Hargrave, M. R., Christiansen, J., Cooper, L., Kun, J., Evans, T., Gangadharan, U., Greenfield, A. & Koopman, P. (1995). The Sry-related gene Sox9 is expressed during chondrogenesis in mouse embryos. Nature Genetics 9, 15-20.

Wunderle, V. M., Critcher, R., Hastie, N., Goodfellow, P. N., and Schedl, A. (1998) Deletion of long-range regulatory elements upstream of SOX9 causes campomelic dysplasia. PNAS 95:10649-10654.

Xu, J., Liu, Z. and Ornitz, D. M. (2000). Temporal and spatial gradients of Fgf8 and Fgf17 regulate proliferation and differentiation of midline cerebellar structures. Development 127, 1833-1843.

Yang, Y., Drossopoulou, G., Chuang, P-T et al. (1997). Relationship between dose, distance and time in Sonic-Hedgehog mediated regulation of anteroposterior polarity in the chick limb. Development 124, 4393-4404.

Zakany, J., Kmita, M. & Duboule. D., (2004) A dual role for Hox genes in limb anterior-posterior asymmetry. Science 304, 1669-1672.

Zschabitz,A., (1998). Glycoconjugate expression and cartilage development of the cranial skeleton. Acta Anat. (Basel) 161, 254-274.

Zuniga A, Haramis AP, McMahon AP, Zeller R., (1999). Signal relay by BMP antagonism controls the SHH/FGF4 feedback loop in vertebrate limb buds. Nature, 401(6753):598-602.

Zwilling E. (1955). Ectoderm-mesoderm relationship in the development of the chick embryo limb bud. J. Exp. Zool. 128:423-41.